Experimental studies in jet flows and zero pressure-gradient turbulent boundary layers

by

Ramis Örlü

May 2009
Technical Reports from
Royal Institute of Technology
KTH Mechanics
SE-100 44 Stockholm, Sweden

Akademisk avhandling som med tillstånd av Kungliga Tekniska Högskolan i Stockholm framlägges till offentlig granskning för avläggande av teknologie doktorsexamen den 12 juni 2009 kl 10.15 i sal D3, Lindstedtsvägen 5, Kungliga Tekniska Högskolan, Stockholm.

Universitetsservice US–AB, Stockholm 2009

Ramis Örlü 2009, **Experimental studies in jet flows and zero pressure-gradient turbulent boundary layers**

Linné FLOW Centre, KTH Mechanics, Royal Institute of Technology
SE–100 44 Stockholm, Sweden

Abstract

This thesis deals with the description and development of two classical turbulent shear flows, namely free jet and flat plate turbulent boundary layer flows. In both cases new experimental data has been obtained and in the latter case comparisons are also made with data obtained from data bases, both of experimental and numerical origin.

The jet flow studies comprise three parts, made in three different experimental facilities, each dealing with a specific aspect of jet flows. The first part is devoted to the effect of swirl on the mixing characteristics of a passive scalar in the near-field region of a moderately swirling jet. Instantaneous streamwise and azimuthal velocity components as well as the temperature were simultaneously accessed by means of combined X-wire and cold-wire anemometry. The results indicate a modification of the turbulence structures to that effect that the swirling jet spreads, mixes and evolves faster compared to its non-swirling counterpart. The high correlation between streamwise velocity and temperature fluctuations as well as the streamwise passive scalar flux are even more enhanced due to the addition of swirl, which in turn shortens the distance and hence time needed to mix the jet with the ambient air.

The second jet flow part was set out to test the hypothesis put forward by Talamelli & Gavarini (Flow, Turbul. & Combust. **76**), who proposed that the wake behind a separation wall between two streams of a coaxial jet creates the condition for an absolute instability. The experiments confirm the hypothesis and show that the instability, by means of the induced vortex shedding, provides a continuous forcing mechanism for the control of the flow field. The potential of this passive mechanism as an easy, effective and practical way to control the near-field of interacting shear layers as well as its effect towards increased turbulence activity has been shown.

The third part of the jet flow studies deals with the hypothesis that so called oblique transition may play a role in the breakdown to turbulence for an axisymmetric jet. For wall bounded flows oblique transition gives rise to steady streamwise streaks that break down to turbulence, as for instance documented by Elofsson & Alfredsson (J. Fluid Mech. **358**). The scenario of oblique transition has so far not been considered for jet flows and the aim was to study the effect of two oblique modes on the transition scenario as well as on the flow dynamics. For certain frequencies the turbulence intensity was surprisingly found to be reduced, however it was not possible to detect the presence of streamwise streaks. This aspect must be furher investigated in the future in order to understand the connection between the turbulence reduction and the azimuthal forcing.

The boundary layer part of the thesis is also threefold, and uses both new data as well as data from various data bases to investigate the effect of certain limitations of hot-wire measurements near the wall on the mean velocity but also on the fluctuating streamwise velocity component.

In the first part a new set of experimental data from a zero pressure-gradient turbulent boundary layer, supplemented by direct and independent skin friction measurements, are presented. The Reynolds number range of the data is between 2300 and 18700 when based on the free stream velocity and the momentum loss thickness. Data both for the mean and fluctuating streamwise velocity component are presented. The data are validated against the composite profile by Chauhan et al. (Fluid Dyn. Res. **41**) and are found to fulfil recently established equilibrium criteria.

The problem of accurately locating the wall position of a hot-wire probe and the errors this can result in is thoroughly discussed in part 2 of the boundary layer study. It is shown that the expanded law of the wall to forth and fifth order with calibration constants determined from recent high Reynolds number DNS can be used to fix the wall position to an accuracy of 0.1 and 0.25 ℓ_* (ℓ_* is the viscous length scale) when accurately determined measurements reaching $y^+ = 5$ and 10, respectively, are available. In the absence of data below the above given limits, commonly employed analytical functions and their log law constants, have been found to affect the the determination of wall position to a high degree. It has been shown, that near-wall measurements below $y^+ = 10$ or preferable 5 are essential in order to ensure a correctly measured or deduced absolute wall position. A number of peculiarities in concurrent wall-bounded turbulent flow studies, was found to be associated with a erroneously deduced wall position.

The effect of poor spatial resolution using hot-wire anemometry on the measurements of the streamwise velocity is dealt with in the last part. The viscous scaled hot-wire length, L^+, has been found to exert a strong impact on the probability density distribution (pdf) of the streamwise velocity, and hence its higher order moments, over the entire buffer region and also the lower region of the log region. For varying Reynolds numbers spatial resolution effects act against the trend imposed by the Reynolds number. A systematic reduction of the mean velocity with increasing L^+ over the entire classical buffer region and beyond has been found. A reduction of around 0.3 u_τ, where u_τ is the friction velocity, has been deduced for $L^+ = 60$ compared to $L^+ = 15$. Neglecting this effect can lead to a seemingly Reynolds number dependent buffer or log region. This should be taken into consideration, for instance, in the debate, regarding the prevailing influence of viscosity above the buffer region at high Reynolds numbers. We also conclude that the debate concerning the universality of the pdf within the overlap region has been artificially complicated due to the ignorance of spatial resolution effects beyond the classical buffer region on the velocity fluctuations.

Descriptors: Axisymmetric jet, swirling jet, coaxial jet, heated jet, zero pressure-gradient turbulent boundary layer, wall-bounded turbulent flows, overlap region, passive scalar mixing, hot-wire anemometry, spatial resolution.

Preface

This doctoral thesis is within the area of fluid mechanics and is mainly based on experimental work. The thesis treats both free shear flows, such as axisymmetric, swirling as well as coaxial ones, and canonical wall-bounded turbulent flows, with primary focus on zero pressure-gradient (ZPG) turbulent boundary layers (TBL). The main focus of the thesis is to provide quality experimental data of well-defined character for theoretical work and numerical validation concerning swirling jet and ZPG TBL flows by means of hot-wire anemometry. The thesis is divided into two parts in where the first part, starting with an introductory essay, is an overview and summary of the present contribution to the field of fluid mechanics. The second part consists of six papers, two of them are already published but they are here adjusted to comply with the present thesis format for consistency. In chapter 6 of the first part in the thesis the respondent's contribution to all papers are stated. The thesis is also available as a *PDF* file at the *KTH library* and in that version some figures are in colour.

May 2009, Stockholm
Ramis Örlü

Contents

Part II. Papers

Part I

Overview and summary

CHAPTER 1

Introduction

"Quis leget haec? [Who will read this?]"[1]

Aules Persius Flaccus (34–62)

Nature and that what humankind has established is surrounded by liquids and gases, or for short *fluids*. The discipline which is concerned with the study of the dynamics of these elements is *fluid dynamics*. Most of the naturally occurring, as well as technologically useful flows, are *shear flows*, i.e. inhomogeneous flows with mean velocity gradients. While some of them develop in the presence of boundaries others evolve in their absence. The former type of flows are *wall-bounded shear flows*, while the latter are known as *free shear flows*. The majority of naturally or technologically appearing flows are *turbulent*, a term we are well familiar with, thanks to the stock-market or our last travel by air.[2] These flows are characterised through their rapid changes in time and space, while their less often encountered counterparts, the *laminar* flows, are in the majority of cases sensitive to disturbances and easily turn through various routes (*transition*) into a turbulent state.

So far we have divided *fluid dynamics* into homogeneous and shear flows, laminar, transitional and turbulent flows as well as free and wall-bounded flows. Given the set of the mentioned superficial categories, an attempt can be made to classify the present work, namely, it deals with transitional and turbulent, free and wall-bounded flows. *Jets*, *wakes* and *mixing layers* are classical examples for the former category, while *boundary layer*, *pipe* and *channel flows* are canonical examples of wall-bounded flows. Although it is common to study these types of flows separately in the laboratory, they appear, however, usually simultaneously.

Let's see for instance a passenger airliner. Here large wakes can be easily observed behind it; jets (simple, coaxial and swirled) emanating from the engines can often be heard; channel and pipe flows are present inside the combustion chambers; and finally the effects of the presence of boundary layers are clearly felt when we experience drag.

[1] This is a pledge for the coming footnotes.

[2] Interesting enough, we associate mainly "bad" thoughts with "turbulence", while it is turbulence, that makes living possible, or at least livable.

The flow on the plane surface, while close to the leading edge being laminar, undergoes transition at a certain location and increases drastically the *skin friction* and thereby *drag*, which in turn increases the *fuel consumption*. Boundary layers are present over the entire body of the airplane and it goes without saying that any small reduction in drag will pay off in the long run. This reduction can be performed either by means of *transition delay* or by trying to control directly the turbulent friction. Of course in the latter case a precise knowledge of the flow behaviour in turbulent boundary layers is necessary.

The quest for more *efficient airplanes*, is hence coupled to *drag reduction* and *thrust efficiency*, while the reduction of *noise emissions* is a prescribed goal.

For the focus of the present thesis, a number of topics are readily identifiable, as emphasised throughout the preceding paragraphs, namely the *swirling flow* that leaves the turbofan as a *swirling jet*. The jet on the other hand while passing through the turbofan being set into rotation, gets also divided into a core and bypass flow. The *mixing process* in the combustor, where the fuel gets mixed with the compressed air by means of the coaxial configuration of the turbofan and leaves the turbofan as a *coaxial jet*. *Jet noise* is another arising factor, which has led to high-bypass-ratio turbofans, but also various *active* and *passive flow control* strategies have for decades been tested in order to fulfil more and more stringent requirements.

The next chapters as well as the papers constituting the present thesis, will consider **transitional single** and **coaxial jets** as well as **turbulent swirling jet flows** in the category of free shear flows, whereas in terms of wall-bounded shear flows, **turbulent boundary layers** will be treated. While in the case of the studied turbulent flows, the aim was to provide a quality **experimental data base**, the transitional jets were utilised to study the **underlying physics** as well as to test **control strategies**.

The thesis is organised as follows: Part I, will continue with an essay on axisymmetric, coaxial, and swirling jet flows with different emphasis in chapter 2, while chapter 3 treats turbulent boundary layers, but also deals with the overlap region of wall-bounded turbulent flows in some detail. The experimental facilities in which the mentioned flows were studied as well as the measurement techniques utilised to assess these flows are described in chapter 4. Part I ends with a summary of results and a list of publications as well as describing the authors contribution to the papers in chapter 5 and 6, respectively. Part II on the other hand, contains six papers, one each on the swirling, coaxial and axisymmetric single jet as well as three papers related to the study of wall-bounded turbulent flows.

CHAPTER 2

Jet Flow Studies

"Must we not look upon all [...] jets [...] as musically inclined;"

John Le Conte (1818–1891)

2.1. Axisymmetric transitional single jet flows

The present section will introduce the notation used for the transitional and turbulent jet studies and give a short overview over the common concepts in single and coaxial jet flows.

An axisymmetric jet is produced whenever a fluid is ejected from a round nozzle. Different type of exit velocity profiles can be generated depending on the geometrical characteristics of the nozzle. For instance, if the contraction ratio of the nozzle is large enough the velocity distribution is more or less constant over the cross-section and is commonly denoted as a 'top-hat' profile or a plug flow. Figure 2.1 shows schematically a round jet issuing from a nozzle with diameter D, and its evolution along the streamwise axis, x. Due to the high velocity gradient behind the nozzle lip an axisymmetric shear layer forms and develops between the jet and the ambient air. It is within this region that the velocity of the jet will gradually approach that of the ambient air (moving outwards along the radial axis, r) and where the initial phases of the mixing process occur (for this reason this region is often called mixing layer). The velocity, temperature or density difference between both sides of the shear layer will deeply affect its stability characteristics. The internal and external disturbances present in the jet will trigger the formation of Kelvin-Helmoltz waves that are amplified and grow until they saturate and roll up in discrete vortices undergoing different processes like pairing or tearing until they collapse generating a complete turbulent flow.

The dynamics of these vortical structures strongly affect the downstream increase of the thickness of the shear layer. At a certain downstream location, say 4 to 8 D from the nozzle, the axisymmetric shear layer engulfs the remaining potential region and reaches the centreline. This point is the so-called end of the potential core or cone region, up to which the jet velocity at the centreline has remained at its initial exit velocity, as illustrated through the dashed lines in figure 2.1. The extent of the irrotational core region dependents on

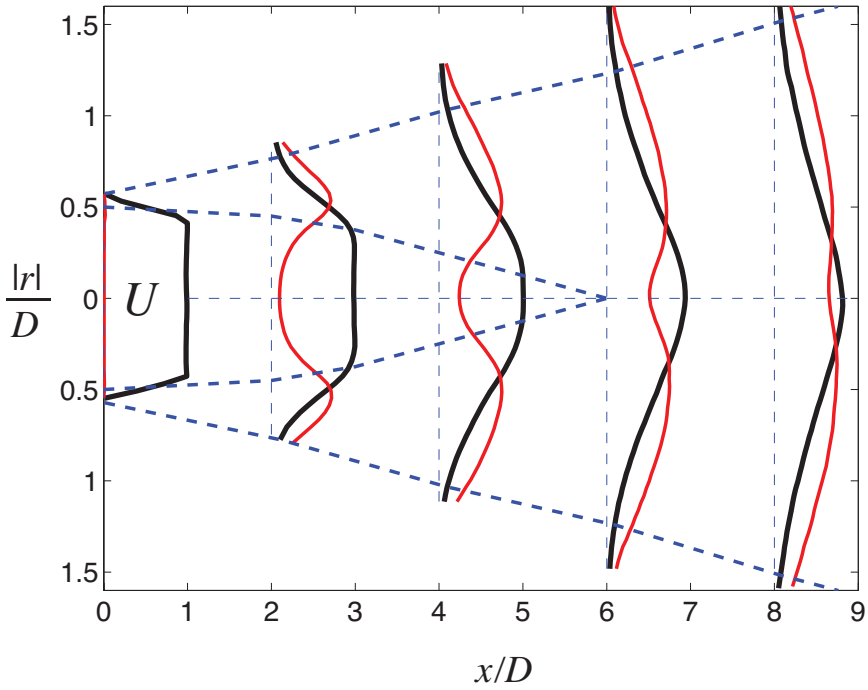

FIGURE 2.1. Near-field region of a single axisymmetric jet. Solid lines indicate measured mean (dark) and turbulence intensity (light) profiles, whereas the turbulence intensity is multiplied by 5 for visibility. Thick dashed lines indicate the potential core and shear layer regions. The profiles are based on measurements in the jet facility at KTH Mechanics at a Reynolds number, Re_D, of around 25000.

the initial and surrounding (ambient) conditions of the jet, and its length is about 6 D for a circular jet with linear spreading and a top-hat velocity profile (Rajaratnam 1976; Lee & Chu 2003). So for instance, a jet in a confined environment is known to spread much faster[1] and the shear layer is found to reach the centreline further downstream than in its unconfined, i.e. free, counterpart (Ashforth-Frost & Jambunathan 1996). Similarly, a jet can issue from a long tube, either laminar or turbulent, where in the latter case, no potential core is present, since the entire jet is rotational already at the orifice exit (Boguslawski & Popiel 1979).

[1]A jet in a diffuser for instance would for certain diffusor angles attach to the wall, due to the Coanda effect.

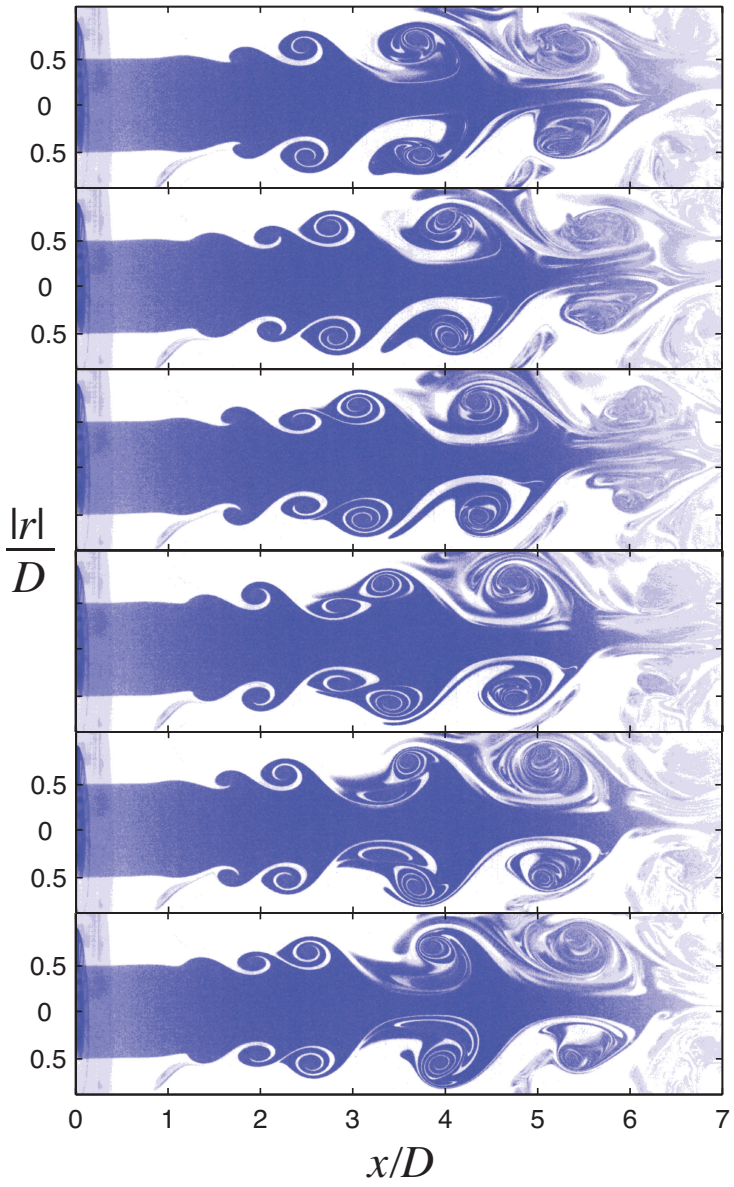

FIGURE 2.2. Flow visualisation of the centreline evolution of an axi-symmetric air jet with $Re_D \approx 5000$ issuing into air at rest. Subsequent snapshots are ordered from top to bottom with a time interval of 5 ms.

Concerning the evolution of the disturbances inside the shear layer, a typical scenario is well represented by the flow visualisation sequences shown in figure 2.2. In this particular case, taking an Eulerian viewpoint at around 1 D downstream, one can observe that the jet appears to "breath". The "remarkable appearance of alternate swellings and contractions described by Savart" (Rayleigh 1879) is the manifestation of the presence of un unstable varicose mode.

Downstream, at about 2 D, the instability saturates and a vortex is fully rolled up. Being conveyed downstream it evolves continuously engulfing the surrounding irrotational fluid, until it finally merges with another vortex (pairing). These processes strongly affect the rate at which the jet spreads (Tritton 1988). The evolution of the aforementioned process is clearly visible in figure 2.2. The sequence of snapshots is taken in an axisymmetric jet facility (cf. section 4.1.1) at a nominal Reynolds number, Re_D, based on the nozzle diameter and centreline velocity, of around 5000. Smoke has been injected at the intake of the fan and the downstream evolution across the centreline has been visualised by "cutting" the vertical plane with a laser sheet.

Close to the jet exit, where the shear layer thickness, θ, is small compared to the diameter of the nozzle, say $\theta/D < 1/50$ (Piquet 1999) the shear layer thickness alone is the fundamental length scale for the instability. Hence, in the vicinity of the jet exit, the shear layer dynamics are similar to that of a plane mixing layer. Further downstream on the other hand, where the shear layer thickness becomes comparable with the nozzle diameter, the latter becomes an important prevailing parameter controlling the dynamics of the flow. With increasing downstream distance the steep gradient between the jet and the ambient fluid smoothes out and ends thereby the similarity to the mixing layer, which on the other hand retains the velocity difference.

The two mentioned length scales are generally used to form two dimensionless time scales characterizing the flow field, viz. the shear layer mode and the jet column or preferred mode. The former is associated with a Strouhal number, St, formed with the shear layer thickness at the nozzle exit, θ_0, and the average velocity between the two streams, U_m, on both sides of the shear layer, $St = f\theta/U_m$, while the latter is based on the nozzle diameter and the centreline velocity, $St_D = fD/U_c$.

The strong velocity gradient between the jet and the ambient fluid is a direct (e.g. for supersonic jets) or indirect (as in the case of subsonic jets) cause of noise, which was one of the main reasons during the 50's that directed the focus towards noise control and control of jets in general (Wooten *et al.* 1972). That flows or flames could be controlled or at least excited was already widely

known[2], however jet turbulence—random in nature and purely statistical treatable at that time—appeared to be a paradox, since the notion of randomness is hardly compatible with the idea of "control".[3] So it is not surprising that jet noise was associated with the intermittent character of the flow, rather then with large scale coherent structures, which only decades later lead to a new focus in turbulence research.

One of the effective ways to reduce the noise level was for instance the employment of weak co-flows. While these have been found to have a negligible effect on the flow dynamics (Pietri *et al.* 2000), their influence becomes more important once the velocity of the co-flow reaches the same order of magnitude as that of the primary jet (Rajaratnam 1976). These flows are known as coaxial or compound jet flows, and will be discussed in the next section.

Although Rayleigh (1878) considered the instability of jets, it was not until Batchelor & Gill (1962), who in an early inviscid linear stability analysis showed, that for a jet with top-hat velocity profile all modes would be unstable. However, the axisymmetric mode, $m = 0$, was found to grow the fastest within the potential core region. Further downstream the profiles approach Gaussian distributions and $m = 0$ becomes stable, whereas higher non-zero azimuthal modes grow the fastest. Using a velocity profile based on an eddy viscosity approximation, the authors concluded, that the helical mode, $m = 1$, was the only unstable azimuthal mode in the far field region. This view, that the jet is characterised by an axisymmetric and helical instability mode in the near-field and far-field, respectively, is—on the whole—the prevailing understanding (see e.g. Lesieur 2008).

The outlined instability modes can visually be interpreted as if the strong vortex rings after some downstream evolution, due to the inherent instabilities in the flow, start to incline with respect to the axis and hence to form oblique or helical modes, i.e. spiral or spinning modes, while being convected

[2]So for instance writes Tyndall (1867) in his classical text book "From a distance of 30 yards I have chirruped to this flame, and caused it to fall and roar. I repeat a passage from Spencer:

> '[...] Sweet words, like dropping honey she did shed;
> And through the pearls and rubies softly brake
> A silver sound, which heavenly music seemed to make.'

The flame picks out certain sounds from my utterance; it notices some by the slightest nod, to others it bows more distinctly, to some its obeisance is very profound, while to many sounds it turns an entirely deaf ear."

[3]It is however interesting to note, that despite the notion of random fields prior to the acceptance of coherent structures within the 70's (Bradshaw 1967; Roshko 1976), Prandtl's mixing length theory (Prandtl 1925) is based on the energy bearing, large scale, actually coherent structures: While Prandtl denoted these structures as "uniformly moving fluid lumps" (Prandtl (1965): "einheitlich bewegte[n] Flüssigkeitsballen"), his students used the term "coherent" (Schlichting & Truckenbrodt (1967): "Es gibt in der turbulenten Strömung Flüssigkeitsballen, die mit einer Eigenbewegung ausgestattet sind und [...] als zusammengehöriges Ganzes unter Beibehaltung ihres x-Impulses bewegen").

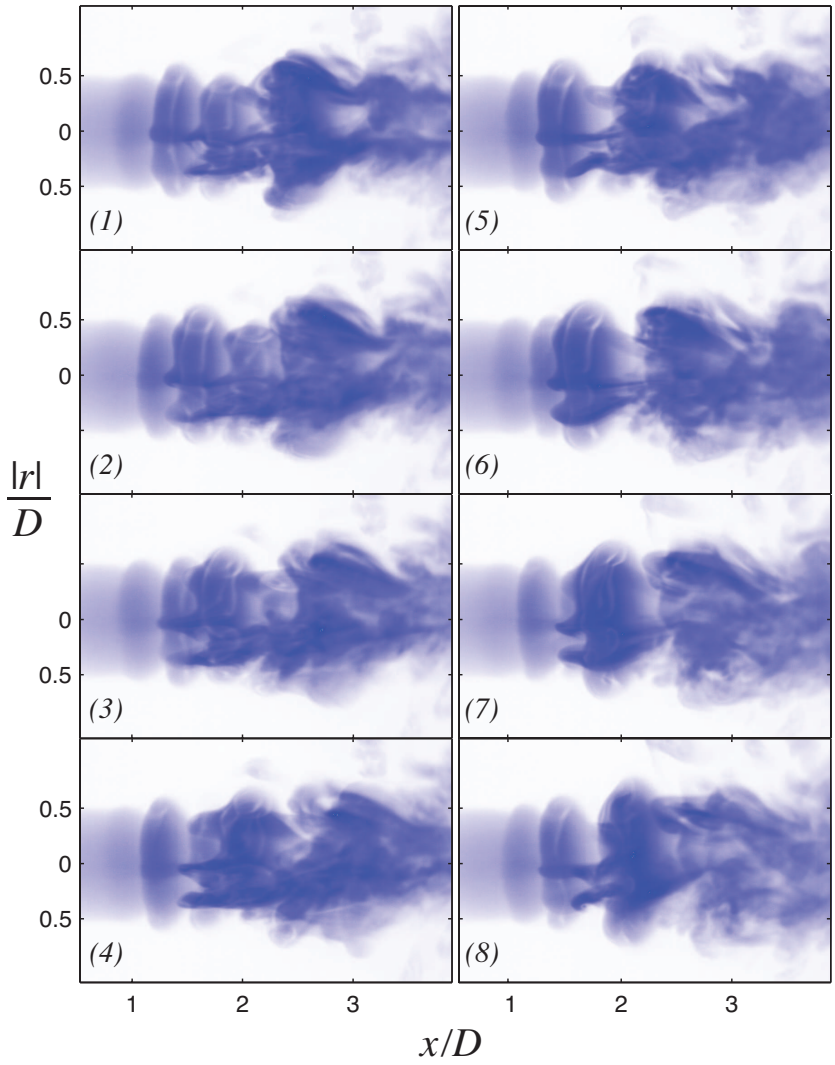

FIGURE 2.3. Smoke flow visualisation of an axisymmetric air jet with $Re_D \approx 8500$ issuing into air at rest. Smoke was injected through the circumference of the stagnation chamber and hence covers only the circumference of the jet, whereas a white light source was used to illuminate the circumference of the jet, that faces the reader. The shown subsequent snapshots are taken with intervals of 2 ms.

from the nozzle exit down to the end of the potential core region. While one of these modes, namely the axisymmetric one, can easily be identified in flow visualisation images focusing on the region where the potential core is present, helical modes are not as easily visible. Figure 2.3 shows smoke flow visualisation pictures from an axisymmetric jet, where the flow was seeded within the stagnation chamber along the walls upstream the contraction nozzle. Due to the circumferential seeding and partial illumination with white light of the side facing the reader, the vortex rings can clearly be captured. Furthermore this kind of visualisation, inspired from the work by Michalke (1964), allows a partial three-dimensional view on the (external) vortex structures.

Particularly the "volcano-like bursting event", an "azimuthally perturbed remnant of a [vortex] ring" described by Citriniti & George (2000), can be associated with the seen structures between 2 and 3 D in figure 2.3. Furthermore, the so called "braid" region, situated between the successive vortex rings (Grinstein *et al.* 1996), is also apparent through the streamwise structures emerging in this region (Liepmann & Gharib 1992; Paschereit *et al.* 1992).

The dominance of mode 1 can even be seen as far downstream as 160 D (Dimotakis *et al.* 1983), also at high Reynolds numbers (Tso & Hussain 1989). The observations made by (Mungal & Hollingsworth 1989) in the exhaust of a TITAN IV rocket motor, at a Reynolds number of around 2 $\times 10^8$, have once and for all established that the described vortical structures are not only a remnant of transitional flows, but are also inherent structural features of fully developed turbulent flows, which goes along with the observations made in mixing layers (Roshko 1976). It is also generally believed that helical structures of both inclination angles occur and are the most dominant ones downstream the potential core (Plaschko 1979; Yoda *et al.* 1992). However, they are not observed to coexist, but rather found to switch in a non-deterministically way from one mode type to the other (Corke *et al.* 1991).

The present picture so far is the classical view, predicted by linear stability theory and confirmed by a large body of experimental works. In short: the ring-like structures, known as the axisymmetric mode is dominant close to the nozzle exit, while towards the end of potential core the inclined or helical structures become important as well and dominate in the far-field of the jet. This view has been widely accepted, however recently it was challenged by George and co-workers (Gamard *et al.* 2002, 2004), namely, by employing proper orthogonal decomposition (POD) on the streamwise velocity component obtained from around 138 hot-wires, they concluded that the double helical mode, $m = 2$, dominates the flow downstream the potential core region in apparent contradiction to the widely held belief that the helical mode, $m = 1$, should be dominant. The contradiction has initiated a number of studies particularly to answer the questions whether the helical mode is indeed the most dominant one in the far field of axisymmetric jets. Despite the overwhelming body of evidence Gamard *et al.* (2004) argued regarding "the earlier experimental results of others", that

"it is likely that the conditional sampling experiments lacked the resolution to measure more than a few azimuthal modes. Since there was no spatial filtering prior to sampling, the unresolved modes were aliased into the lower ones, thereby distorting the low-mode-number energy distribution."[4]

Few recent DNS and noise measurements employing POD seemed initially to support that the double-helical mode is dominant in the far-field, so for instance refers Gamard *et al.* (2004) to Kopiev *et al.* (1999) and Freund & Colonius (2002) to gain support. Having followed the discussion up to this point the idea emerged to set up an axisymmetric jet facility, where the helical mode could be superposed with the axisymmetric one in order to check whether the double-helical mode would emerge due to nonlinear interaction. This was infact observed in wall-bounded flows (Elofsson & Alfredsson 1998, 2000) and was thought to be a possible way to explain the observation of the dominance or at least appearance of $m = 2$ in the far field of jets. The fact that $m = 0$ and 1 are readily present in jets and that disturbances in the stagnation chamber could easily amplify axisymmetric modes was thought to be worth to investigate, as a possible explanation, why the double-helical mode could be observed in experiments.

During the set up of the jet facility, described in section 4.1.1, the work by Iqbal (2005) got published (Iqbal & Thomas 2007), and clarified to a great extent the controversy. By employing a rake of hot-wires and measuring all velocity components they computed the scalar and vector implementation of the POD and found that, while the vector implementation confirmed the large body of previous works, the scalar implementation of the POD on the streamwise velocity fluctuations confirmed the dominance of mode 2. The authors found, that the energy in the radial and azimuthal POD modes are together comparable to the streamwise component and would hence explain why Gamard *et al.* (2004) found the dominance of mode 2. These conclusions were around the same time also confirmed by George and co-workers (Wänström *et al.* 2006) by means of stereo PIV employing the vector implementation of POD.

The aforementioned paragraphs have pointed out that free shear flows are extremely sensitive to external perturbations. In fact, it has been shown by Gutmark & Ho (1983) that the encountered scatter between various experimental investigations regarding the "value of the preferred mode and the spreading rate vary within a range of about 100 %". Particularly, the authors suggest, that "extremely low-level spatially coherent disturbances in individual facilities change the initial conditions of a laminar shear layer". Since a quantitative comparison between various studies is therefore hampered in this respect, it has been common practise to employ periodic excitation of the basic flow at the natural frequency in order to "lock" the evolution of the coherent or organised

[4] Or more generally, the authors believe, that: "Experimentalists appear to have limited their search for alternatives, citing the agreement with theory. Similarly, theoreticians limited the scope of their inquiries because of the apparent agreement with experiment."

structures. This would also help to overcome the difficulty to perform conditionally sampled measurements, due to a natural lack of periodicity, phase jitter or the fact that structures vary in size and shape (Fiedler 1988). Among the most common, and experimentally easily realisable, ways to achieve this goal is acoustic excitation (Hussain & Zaman 1981; Kusek *et al.* 1990; Corke & Kusek 1993). The apparent ease, by which the receptive modes could be "locked" to the excitation frequency, is also exploited in various flow control strategies. Since a considerable fraction of the total turbulent energy, around 10 to 50 % for the far-field and near-field of axisymmetric jets (Fiedler 1988), is inherent in the coherent structures, why a great interest in understanding and figuring out how to control these structures persists. Consequently the study of the underlying physics of coherent structures is not only a fundamental research, but also very applied.

2.2. Transitional coaxial jet studies

We already mentioned the coaxial jet in context of its possibility of jet noise reduction. However, coaxial jet flows, are present in various other technical applications, particularly in combustion devices and chemical engineering systems, due to their known efficiency in mixing. The apparent similarity to the single axisymmetric jet is evident from figure 2.4, where the near-field region of a coaxial jet is depicted. Here U_i and U_o denote the maximum absolute velocity of the inner and outer streams at the nozzle exits, respectively. In fact, it was common to assume, that coaxial jets could be considered as a simple combination of single jets, where the two shear layers originating from the nozzles develop independently from each other (Ko & Kwan 1976; Kwan & Ko 1977).

This convenient view remained until the early 90's, however the scatter between various studies, but particularly the flow visualisation study by Dahm *et al.* (1992) revealed that a multitude of different topological flow regimes can exist, depending on the velocity ratio, $r_u = U_o/U_i$, and Reynolds number. Furthermore the same authors, as well as Wicker & Eaton (1994), found that the vortical motion for $r_u > 1$ is dominated by the vortices emerging in the outer shear layer (cf. figure 2.5(a)). They showed that the evolution of the vortices of the inner shear layer is dictated by the outer vortices and "can be best described as lethargic" (Dahm *et al.* 1992). They are hence trapped in the spaces left free between two consecutive outer shear layers vortices; this scenario became known as the so-called 'locking phenomenon' and describes the observation that the instability, roll-up and vortex interaction processes within each shear layer are strongly coupled. Consequently the vortex passage frequency of the inner shear layer will differ from the one predicted by stability analysis for a single axisymmetric shear layer as shown by Dahm *et al.* (1992) and da Silva *et al.* (2003) by means of flow visualisations and direct numerical simulations, respectively.

A number of excitation studies, similar to those in single jets, has since then been performed. A particular important result was, that of Wicker & Eaton (1994), who concluded that only the outer shear layer is able to significantly control the evolution of the inner shear layer. This view has been widely accepted, as apparent from the focus on control strategies on the outer shear layer (see e.g. Tang & Ko 1994; Angele *et al.* 2006; Kiwata *et al.* 2006).

Recently a number of DNS and LES studies on transitional coaxial jet flows has been performed (da Silva *et al.* 2003; Balarac & Métais 2005; Balarac *et al.* 2007*b*), that confirms that the frequencies of the most amplified modes in the outer and inner shear layer coincide, namely with a Strouhal number that relates to the natural instability predicted by linear stability analysis of the

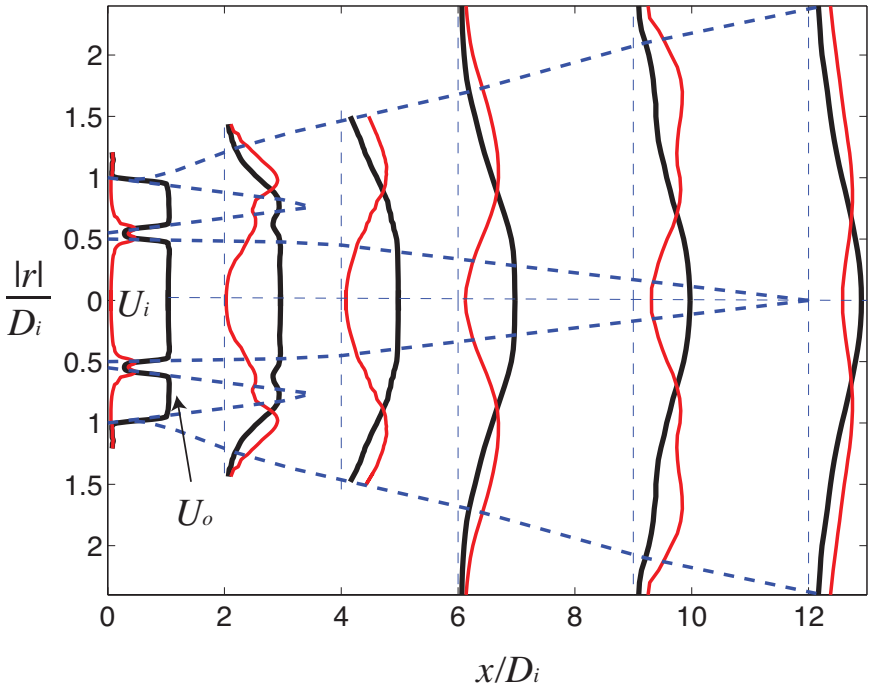

FIGURE 2.4. Near-field region of an axisymmetric coaxial jet. Solid lines indicate measured mean (dark) and turbulence intensity (light) profiles, whereas the turbulence intensity is multiplied by 5 for visibility. The profiles are based on measurements in the coaxial jet facility at the University of Bologna. Thick dashed lines indicate the potential core and shear layer regions.

outer shear layer. Furthermore the effect of axisymmetric and combined axisymmetric and azimuthal excitation on the outer shear layer was investigated in terms of their effect on the dynamics and mixing characteristics (Balarac *et al.* 2007*a*).

The mentioned studies sketch the state of the art understanding of concurrent transitional coaxial jet studies. In short: The coaxial jet can not be considered as a simple combination of single jets. Vortical motion within the near-field is dominated by the vortices emerging from the outer shear layer. The passage frequency of these vortices corresponds to the values predicted by linear stability analysis, i.e. $St_\theta = f\theta/U_o$. The evolution of the inner shear layers vortices is dictated by the outer shear layer (locking phenomenon), i.e. they are trapped in the spaces left free between two consecutive outer shear layer vortices. The literature also indicates that the term "locking" is mainly used to describe the dominance of the outer shear layer over the inner shear layer, which lead experimental and numerical flow control studies to mainly focus on the outer shear layer.

One point left out so far is the geometry of the inner duct wall, the splitter plate in the case of 2D flows. The above mentioned experimental studies had either a thin duct wall or assumed the effect of the thickness to be negligible, while in the mentioned DNS studies the initial momentum loss thicknesses could be varied. Nevertheless, in all mentioned studies the effect of the inner duct wall on the flow dynamics was negligible, i.e. the evolution of the inner shear layers vortices was triggered and dominated by those of the outer shear layer. That the thickness of the inner duct wall plays an important role in the evolution of transitional coaxial jets was experimentally verified by Buresti *et al.* (1994). The authors found, that in the case of a thick blunt separating wall two trains of alternating vortices are shed from both sides of the inner wall with a well-defined frequency, as evident from figure 2.5(b). These were found to scale with the wall thickness and the average velocity of the two streams. Their experimental observation confirmed thereby predictions from linear stability analysis (Wallace & Redekopp 1992), where the wall thickness and the velocity ratio were found to be crucial in determining whether the behaviour in the near-field of coaxial jets could be considered as wake-like or shear-layer-like. Similarly, this effect has been noted in wake flows in general (Huerre & Monkewitz 1990) as for instance in mixing layers (Dziomba & Fiedler 1985; Braud *et al.* 2004).

In a recent study Talamelli & Gavarini (2006) formulated a theoretical background for this experimental finding. They showed, by means of linear stability analysis, that the alternate vortex shedding behind the inner wall can be related to the presence of an absolute instability, that exists for a specific range of velocity ratios and for a finite thickness of the wall separating the two streams. So, for instance, figure 2.5(b) and (c) depict the cases were the absolute stability is predicted to be present and absent, respectively. The

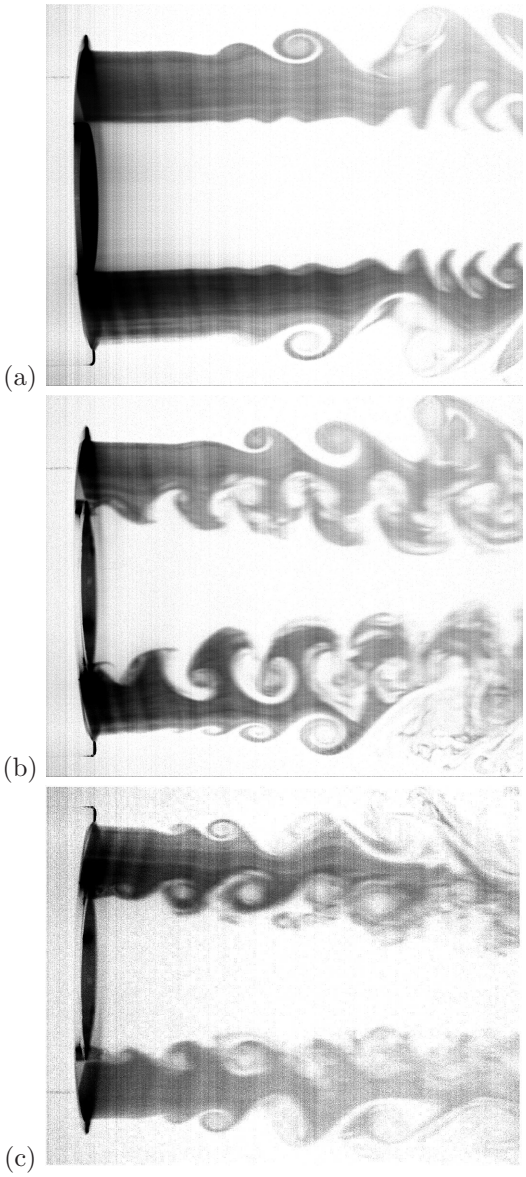

FIGURE 2.5. Smoke flow visualisations with the annular stream seeded. (a) sharp wall, $r_u = 1$ & $U_i = 4$ m/s, (b) thick wall, $r_u = 1$ & $U_i = 4$ m/s, and (c) thick wall, $r_u = 3$ & $U_i = 2$ m/s.

authors proposed that this absolute instability may provide a continuous forcing mechanism for the destabilisation of the whole flow field even if the instability is of limited spatial extent.

One of the studies dealing with coaxial jet flows, described in full length in Örlü *et al.* (2008), aimed at verifying the proposed idea of Talamelli & Gavarini (2006), namely to test if the absolute instability behind an inner wall of a coaxial jet nozzle with finite thickness can be utilised as a continuous forcing mechanism and hence as a passive flow control mechanism for the near-field of coaxial jet flows. The experiments indicate that the vortex shedding behind a thick separating wall can be facilitated as an easily applicable and effective passive control mechanism, however, further studies are needed to verify the parameter range in which the control is applicable as well as to check how robust the control is.

Nevertheless, the experiments by Örlü *et al.* (2008) have so far shown that the trapping of the inner shear layers vortices into the free spaces of the Kelvin-Helmholtz instability of the external shear layer, known as the 'locking phenomenon', is reversible; namely the vortex shedding behind the separating wall with finite thickness was found to dictate the passage frequency of the external shear layers vortices and thereby control the inner and outer shear layers evolution in the whole near-field region. A clear trend towards increased turbulence activity, both within the inner and outer shear layers and thereby the mixing between the two streams of the coaxial jet as well as the outer jet and the ambient surroundings, could be observed. This makes it possible to specifically utilise the geometry of the inner separating wall not only to control the dynamics of the flow, but also to increase the turbulence activity.

2.3. The swirling jet

2.3.1. *Restricting the research area*

The following section deals with turbulent free jets, where an azimuthal velocity is superimposed on the streamwise flow, as depicted in figure 2.6. Turbulent jets with rotation exhibit distinctive characteristics absent in their non-rotating counterparts. A subsonic jet experiences theoretically no static pressure gradient in the axial or radial direction, hence the mechanism for jet spread is dominated by the turbulence mixing at the interface between the jet and the ambient fluid. A swirling jet however, exceeding a certain degree of swirl in the near-field, is affected by the static pressure gradients in both axial and radial direction (Farokhi & Taghavi 1990).

The effect of rotation on jets is well known and for instance exploited in compressible and/or reacting swirling jets in furnace flows and burners as well as in combustion system, due to the increased turbulent mixing of fuel with air. Another phenomenon observed at high swirl intensities is the reverse flow in the vicinity of the orifice, which may lead to vortex breakdown, i.e. an

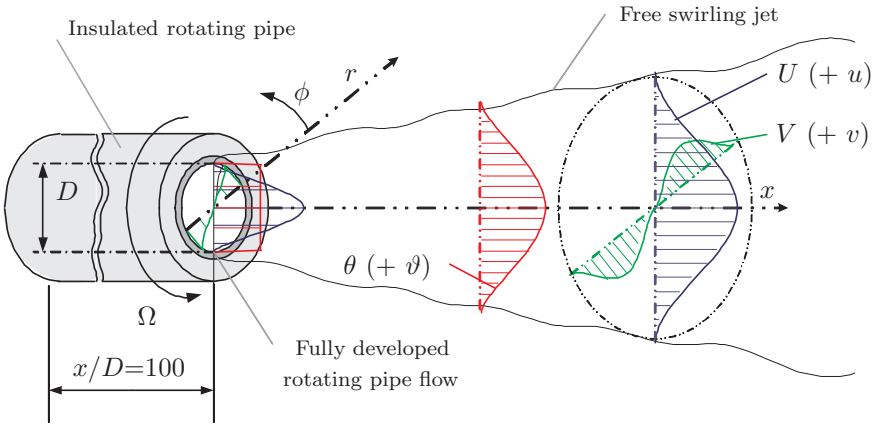

FIGURE 2.6. Schematic of the cylindrical coordinate system of the free developing swirling jet emanating from a fully developed axially rotating pipe flow.

abrupt structural change forming a free stagnation point or recirculation zone on the axis of the mean flow, if a certain swirl strength is exceeded. Although this phenomenon is utilised to stabilise flames in combustion chambers and furnaces, it will not be dealt with in the present investigation, due to our primary interest in low and moderate swirl intensities far below the onset of reverse flow along the centreline and the inaccessibility through the present measurement technique.[5]

To sum up, we restrict ourselves here to incompressible, non-reacting and fully developed turbulent free swirling jets with swirl strengths below the occurrence of reverse flow at the central region of the jet, and refer the interested reader to the review articles of Syred (2006) and Lilley (1977) concerning swirling flows and jets in combustion, to Lucca-Negro & O'Doherty (2001) regarding the vortex breakdown phenomenon in swirling flows and jets and to Billant *et al.* (1998), Loiseleux & Chomaz (2003) and Gallaire & Chomaz (2003) for an account on the instability of swirling jets. A good overview on both theoretical and experimental work is given in the classical textbook by Gupta *et al.* (1985).

Although we have restricted our study to small swirl rates the remaining research field is still of interest for many applications. The addition of mild degrees of swirl to a jet is for instance known to intensify the processes of mass, momentum and heat transfer, to spread, entrain and mix faster and to reduce

[5]Reverse flow itself is an instantaneous phenomenon of turbulent jets issuing into stagnant fluid at the interface between the jet and its irrotational environment. This is one of the major difficulties for the application of stationary *hot-wire anemometry* in the outer edge of the jet.

noise production in the near-field of a jet exhaust. Furthermore swirling jet flows are byproducts of flows through turbomachinery and flows over wings and are utilised in separators. Even though we profit from the mentioned features, for most of the cases we still do not know for sure *why* and *how* swirl embeds all these features. A selection on previous experimental work is given in table 1 evidencing the interest and search for an understanding of the underlying physics.

Before going over to a more detailed review on the results of previous works of interest the parameters defining the swirling jet as well as the techniques to impart the swirl on the axial mean flow will be presented in the next two sections.

2.3.2. *Parameters of a swirling jet*

A free jet emanating in still surrounding is characterised through its Reynolds number and its initial conditions. The latter can be characterised by a large numbers of non-dimensional parameters: the initial mean streamwise velocity profile (and hence the momentum thickness of the inner boundary layer at the exit), its state (laminar or turbulent, as defined by their shape factors and fluctuation intensities), and the spectra (informing about the frequency content of the flow) of the exit jet (see e.g. Buresti *et al.* 1994). For fully developed turbulent conditions at the orifice however, as is the case in the present investigation, the (unforced) free jet is characterised by the Reynolds number and the streamwise velocity profile.

Classical theory (see e.g. Townsend 1976; Pope 2000) assumes that with increasing downstream position a turbulent wake or jet forgets about its origin, so that the actual shape of the orifice and thus the initial velocity profile does not effect the shape of the velocity profile in the far-field if properly scaled. Here we can not contribute on this issue, due to our interest in the near-field evolution, but for the near-field the initial conditions do matter and they even determine the flow field vigourously.

Coming to the swirling jet a third quantity becomes important, namely the swirl, which for instance can be quantified through its swirl number, which will shortly be introduced. However, the exact radial profile of the azimuthal velocity component does have influence (at least) in the near-field of the jet. In the following the three aforementioned parameters will be discussed separately.

2.3.2a. *The Reynolds number.* There are mainly two different characteristic velocities used in the literature to express the Reynolds number, Re, concerning free jets with and without swirl. For swirling jets emanating from rotating pipes one usually selects the cross-sectional mean velocity, the so-called bulk velocity, U_b, at the outlet of the orifice as the characteristic velocity. For all other swirling jet studies, on the other hand, the exit centreline velocity for the non-swirling jet, $U_{0,S=0}$, is usually utilised. As evident from table 1 not much

care was given by the authors to mention the Reynolds number[6], which probably is due to the classical assumption that once the jet is fully turbulent the Reynolds number does not strongly affect the dynamics of the flow. However Pitts (1991) and Richards & Pitts (1993) report that the Reynolds number does matter at least for jets emanating from long pipes below a threshold of approximately $Re = 25000$. Ricou & Spalding (1961) in an early study concerning the entrainment rate of axisymmetric jets have shown that the effect of Reynolds number diminishes for $Re > 25000$. It is worth mentioning that laser-Doppler velocimetry measurements performed by the author along the centreline of the jet in the range of $0 \leqslant x/D \leqslant 10$ showed that at least for the mean axial velocity component as well as its turbulence intensity the flow tends to become independent of the Reynolds number in the higher end of the range from $Re = 6000$ to 34000.

2.3.2b. *The swirl number.* The non-dimensional parameter used to describe the swirl strength in a free jet, but also in internal flows, is the integrated swirl number, $S_{\phi x}$, defined as the ratio between the fluxes of angular momentum and streamwise momentum (see Örlü & Alfredsson 2008, for a full derivation),

$$S_{\phi x} = \frac{\int_0^\infty r^2(UV + \overline{uv})\,dr}{R\int_0^\infty r\left[U^2 + \overline{u^2} - \frac{1}{2}(V^2 + \overline{v^2} + \overline{w^2})\right]\,dr}\,. \tag{2.1}$$

Feyedelem & Sarpkaya (1998), who used three-component laser-Doppler velocimetry, expressed the swirl number though this relation, whereas most of the researchers computed the swirl number without the Reynolds stresses as given, due to the assumed negligible effect of these terms. Furthermore not all investigations provide these components. An additional simplification is often introduced for the far-field of the swirling jet by neglecting the mean azimuthal velocity component in M_x. This simplification is justified for the far-field, since the azimuthal velocity component will quickly reduce to less then 10 % of its initial value just after 6 pipe diameters.

It is obvious that the integral swirl number is a rather difficult to compute quantity, not only for hot-wire measurements, but also for non-intrusive measurement techniques such as LDV and particle image velocimetry (PIV) unless the ambient air is continuously seeded without introducing arbitrary disturbances. Because of these difficulties other measures have been introduced.

Chigier & Chervinsky (1967), who imparted the swirl through tangential slots, showed that for the case of a solid-body rotation plug flow at the orifice a much more convenient swirl number,

[6]The Reynolds numbers reported in table 1 are either the ones mentioned in the respective paper or are recalculated.

$$S_{m_0} = \frac{G/2}{1-(G/2)^2}\,, \tag{2.2}$$

could be introduced, where G is the ratio of maximal angular velocity, V_{m_0}, to maximal axial velocity, U_{m_0}. Good agreement between both swirl numbers were found up to $S_{\phi x} = 0.2$. This definition was for instance used by Toh *et al.* (2005) with a more or less uniform axial velocity profile with solid-body rotation in the core region. Wooten *et al.* (1972) and Samet & Einav (1988), however, used G as their swirl number, whereas Billant *et al.* (1998) employed a more arbitrary swirl number by taking the ratio between the azimuthal velocity at the half radius of their nozzle and the centreline velocity at an axial distance where measurements were possible.

Other frequently used definitions are related to the vane angle when swirl is generated by guide vanes or spirally shaped vanes. Several definitions are mentioned by Bilen *et al.* (2002). However, for jets emanating from long rotating pipes there exist another possibility, namely the ratio between the azimuthal velocity at the wall, V_w, and the bulk velocity, U_b, at the pipe outlet,

$$S = \frac{V_w}{U_b}\,. \tag{2.3}$$

This definition is quite convenient since the wall velocity is directly obtained through the rotational speed of the pipe.

The list of swirl numbers presented here is of course not complete, but it covers all the previous investigations, that will be reviewed in section 2.3.4.

2.3.2c. *The initial boundary conditions.* We already raised the importance of initial conditions and we retain to exclude here the more fundamental quest whether or not turbulent shear flows in the far-field, the region where certain quantities such as mean velocity components or Reynolds stresses, become self-similar when scaled properly. A large variety of mean axial as well as azimuthal velocity profiles, due to different swirl generating methods, can be produced and it is obvious that an integrated quantity like $S_{\phi x}$ will fail to contain all the information which characterises the azimuthal velocity component. Besides S the other introduced swirl numbers have the same shortcoming, because they express only information about the velocity components at a certain radial (and axial) position. Contrary, the fully developed turbulent pipe flow possesses a well-defined axial as well as azimuthal velocity profile making it possible to express the whole flow field at the pipe exit by means of S and Re.

This deficit was recognised right from the beginning (Chigier & Beér 1964; Pratte & Keffer 1972) and was studied by Farokhi *et al.* (1989) and quite recently by Gilchrist & Naughton (2005). The latter study pointed out, that threshold values for the onset of reverse flow or vortex breakdown do not make

sense if decoupled from the exact velocity profiles. This explains why two different types of swirling jet behaviours can exist with both the same swirl number and Reynolds number. In conclusion it becomes clear that besides the Reynolds number and the swirl number also the initial conditions have to be quantified in order to facilitate any comparison between experimental results among themselves or with computations.

2.3.3. *Swirl generating methods*

Throughout the previous sections different methods for introducing the swirl onto the free jet were mentioned without further explanation. We already saw that different swirl generating methods (for a summary of different swirl generating methods see also Facciolo 2006) will most likely lead to different azimuthal, but also axial velocity profiles. Following the description of these methods will be given and the reader is referred to table 1 for a list of previous works and their swirl generating methods.

2.3.3a. *Rotating methods.* In the present investigation the swirling jet emanates from a fully developed axially rotating pipe flow. This method was used by Rose (1962) and Pratte & Keffer (1972) among others and is known to produce well-defined outlet conditions regardless the individual facility provided that the flow is fully developed, i.e. sufficiently high Reynolds number and large enough length-to-diameter ratio. Hence it provides an optimal benchmark for comparisons with turbulence models for the near-field of swirling jets. The length-to-diameter ratio of the pipe used by Pratte & Keffer was just half as large as the one by Rose, hence they implemented a dividing strip of 70 % of the total pipe length into the pipe in order to impart a strong enough azimuthal velocity component. However they had to accept a certain asymmetry in the vicinity of the pipe outlet.

A honeycomb placed inside the rotating pipe may help to overcome this restriction as for instance done by Mehta *et al.* (1991) who placed a honeycomb at the beginning of a rotating pipe (followed by a stationary pipe). A similar technique was employed by Komori & Ueda (1985) who rotated a convergent nozzle producing a rather uniform radial profile of the axial velocity component. Rotating four-bladed paddles upstream of a nozzle were used by Oljaca *et al.* (1998), so that 'top-hat' axial velocity profiles were generated in the absence of swirl, whereas for the swirling case the axial velocity profile became pointed at the centre. A similar behaviour was observed by Billant *et al.* (1998), who used a motor driven rotating honeycomb upstream a nozzle. Gore & Ranz (1964) imparted rotation to axial pipe flow by means of a rotating perforated plate in which holes were drilled.

2.3.3b. *Tangential injection.* Tangential injection methods are widely used in swirling jet experiments and they are known to be capable to generate high

degrees of swirl enabling the study of reverse flow and vortex breakdown along the centreline in the near vicinity of the orifice. Chigier & Chervinsky (1967) injected a portion of the fluid peripherally into a nozzle and controlled the flow field by varying the ratio of axial to tangential air. These axial-plus-tangential entry swirl generators are available in a variety of geometrical shapes changing in the number of supply pipes and tangential inlet slots. A different approach was followed by Ogawa & Hatakeyama (1979) who injected secondary flow into the pipe upstream the output nozzle. Asymmetric azimuthal velocity profiles were observed down to 12 pipe diameters downstream (Ogawa *et al.* 1981). By introducing secondary flow through a large amount of nozzles ordered along circular rings Farokhi *et al.* (1989) and Gilchrist & Naughton (2005) were able to produce different initial swirl distributions.

2.3.3c. *Passive methods.* A rather simple method to deflect the flow into curved streamlines is by means of deflecting or guiding vanes which are mounted upstream the orifice or nozzle. Different sets of shaped profiles were for instance used by Elsner & Kurzak (1987) and Sislian & Cusworth (1986) enabling the study of reverse flow. The necessity of a nozzle downstream the swirl vanes was recognised by Gore & Ranz (1964), who found that the flow was not axisymmetric and in addition to it secondary flows were induced.

Other passive methods to introduce helical streamlines are for instance found in the study of Rahai & Wong (2002) and Wooten *et al.* (1972). The former used coil inserts mounted at the wall while the latter used a circular bundle of soda straws bound together and twisted to a proper angle generating solid-body rotation of the flow.

2.3.4. *Experimental studies on swirling jets*

The first experimental investigation on turbulent swirling jets is probably the one by Rose (1962). By means of hot-wire anemometry he determined radial profiles of all mean velocity components as well as turbulence intensities from the vicinity of the pipe outlet up to 15 diameters downstream. Additionally the centreline decay of the streamwise mean velocity as well as the turbulence intensity up to 70 diameters downstream were determined. One interesting result obtained was, that in the case of a turbulent pipe flow the mean azimuthal velocity—even after 100 pipe diameters—deviates clearly from the solid body rotation, which is observable in laminar pipe flows. He assumed that a solid-body rotation could be obtained with an even longer pipe, but his successors Kikuyama *et al.* (1983) and Imao *et al.* (1996) among others showed experimentally that a fully developed rotating pipe flow has indeed a parabolic profile,

regardless how long the pipe may be.[7] Major features of the addition of rotation to a free jet were observed by him, namely the larger spreading angles, the enhanced entrainment rates, the more rapid decay of the centreline velocity as well as the increased turbulence intensities.

Mean velocity components and static pressure distributions for swirl numbers corresponding to weak, moderate and strong swirl, including the case of the onset of reverse flow in the central region of the jet, were conducted by Chigier & Chervinsky (1967). They found that the swirling motion had more or less completely vanished already at about 10 diameters downstream. For moderate swirl numbers and beyond 4 nozzle diameters downstream their results fitted very well to the integral momentum equations. For high swirl numbers a shift of the mean axial velocity from the centreline outwards is observed. However 10 pipe diameters downstream the peak value moved back to the centreline and from there on the flow could be described by semi-empirical relations, which are based on the aforementioned integral relations.

Pratte & Keffer (1972) investigated the streamwise decay by means of a single hot-wire probe, which could be rotated in order to determine all velocity components.[8] Similar to Chigier & Chervinsky they utilised boundary layer assumptions and self-similarity arguments showing that the maximum axial and swirling velocity components in a region beyond the initial formation region should vary asymptotically as x^{-1} and x^{-2}, respectively. These decay rates were confirmed by their experiments.

Since the invention of the jet engine and the continuously increasing air traffic noise production in turbulent jets became an annoying byproduct. Besides the effect of grids and water droplets to reduce the noise production in the near-field of a jet Wooten *et al.* (1972) investigated the effect of swirl upon the structure of the jet mixing region. Their results indicate that even with a very low degree of swirl ($G = 0.08$) a change in the noise production can be expected. The noise in the initial portion of the jet was higher while noise was substantially reduced in the far-field resulting in an overall noise reduction.

Morse (1980) investigated the near-field of a swirling jet emanating from a short pipe section where the swirl was generated through tangential slots by means of hot-wire anemometry. He provided all mean and Reynolds stress values to validate Reynolds stress closure models (see e.g. Launder & Morse 1979; Gibson & Younis 1986). Although the study by Morse is well known among turbulence modellers and serves as a validation case, the details of the experimental set-up (e.g. swirl generating method or length of the pipe) nor the

[7] Orlandi & Fatica (1997), through direct numerical simulations and Oberlack (1999), by means of theoretical scaling laws fitted to experimental results, confirm the existence of a parabolic profile for the azimuthal velocity component.

[8] Although such routines are common, especially in flows with one main flow direction, it is rather suspicious, how a single wire could be employed in a swirling jet.

measurement technique are accessible from the experimental databases, which makes it rather difficult for turbulence modellers to classify his work.[9]

Fujii *et al.* (1981) applied laser-Doppler velocimetry in the near-field of a swirling jet with reverse flow to acquire all velocity and six Reynolds stress components under isothermal and combustion conditions. They found that the virtual origin of radial spread moves upstream under combustion conditions indicating lesser spread of axial velocity, whereas the turbulence levels where increased as a consequence of combustion.

Other studies in strongly swirling jets with reverse flow were performed by Sislian & Cusworth (1986) and Park & Shin (1993). The latter investigated the entrainment characteristics of the near-field of an isothermal swirling jet for swirl intensities of moderate and strong strength, in which the jet is dominated by the azimuthal component causing up to five times higher entrainment rates. Schlieren flow visualisation was utilised to study the Reynolds number dependence on the entrainment enhancement as well as to explore the role of the *precessing vortex core* (PVC), which induces large-scale periodic motions in the jet boundary regions near the nozzle exit. A Reynolds number dependence was found for swirl intensities causing vortex breakdown, whereas no dependence was found for $S_{\phi x} < 0.6$.

The presence of swirl activates extra production terms in the transport equations causing the shear stresses to be more affected by swirl than the normal stresses as shown by Mehta *et al.* (1991). They report an increase in *all* the peak Reynolds stresses as well as in the shear layer thickness within the mixing layer with increasing swirl number. The otherwise negligible secondary Reynolds shear stresses, $\overline{uv}$ and $\overline{vw}$, reach values around half the value of the primary Reynolds shear stress, $\overline{uw}$.

Feyedelem & Sarpkaya (1998) investigated a swirling jet submerged in water with both a 5-hole pressure tube and three-component laser-Doppler velocimetry. They observed stagnation without vortex breakdown at a critical swirl number of $S_{\phi x} = 0.5$ and vortex breakdown for $S_{\phi x} \geqslant 0.51$. Farokhi *et al.* (1989) detected an even lower value for the occurrence of vortex breakdown ($S_{\phi x} = 0.48$) in their study concerning the effect of initial swirl distributions on the evolution of a turbulent jet. Their unique swirl generator system with 54 elbow nozzles mounted on three concentric rings enabled them to produce different azimuthal velocity profiles by keeping the swirl number constant at $S_{\phi x} = 0.48$. Both of the previous studies query the 'critical value' of $S_{\phi x} = 0.6$ (see e.g. Gupta *et al.* 1985) as a threshold for the occurrence of vortex breakdown and conclude that the characteristics of swirling flows are highly complex

[9]Experimental data of Morse (1980) are for instance available in the *ERCOFTAC "Classical Collection" Database* and in *"Collaborative testing of turbulence models"* funded by AFOSR, Army research office, NASA and ONR (see Bradshaw *et al.* 1996). In the former database, a rather confusing sketch of a rotating pipe, is given, which wrongly implies different initial conditons.

to be described by only the swirl and Reynolds numbers. This is due to the strong influence of the pre-exit history upstream the orifice and the conditions at the orifice itself, which was anticipated already in section 2.3.2c. Using the same experimental setup Taghavi & Farokhi (1988) additionally studied the effect of acoustic excitation as well as the effect of screens upstream the nozzle.[10]

The study of Farokhi *et al.* was recently picked up by Gilchrist & Naughton (2005) who generated swirling jets resembling solid-body and q vortex (solid-body core with a free vortex outer region) type azimuthal velocity components. They found that regardless the swirl generation mechanism, the centreline decay rate seems to be accurately predicted by the swirl number. Contrary as swirl levels sufficient for vortex breakdown are approached, the tangential velocity distribution will play an important role. While Chigier & Chervinsky (1967) believed that the growth rate for low and moderate swirl numbers increases linearly with $S_{\phi x}$, they found enhanced growth rates only when the swirl number exceeded a certain value as did Mehta *et al.* (1991) for the near-field region. Gilchrist & Naughton infers that there appears to be three regions of swirl-enhanced jet growth rates: A region without enhancement effects ($S_{\phi x} < 0.1$), a region were enhancement scales with the swirl number ($0.1 < S_{\phi x} < 0.3$) and a region were the swirl strength is sufficiently high to cause vortex breakdown. This value is however lower than the previously mentioned values of 0.48 and 0.6 by Farokhi *et al.* (1989) and Gupta *et al.* (1985), respectively.

As seen in table 1 most of the early investigations were conducted by means of impact probes, single-wire and/or X-wire probes and were later on supported by one-dimensional laser-Doppler velocimetry. Within the last decade a trend towards 'modern' techniques is recognisable. Oljaca *et al.* (1998) for instance utilises the linear relationship between the Fourier component of the scattered acoustic pressure and the Fourier transform of the vorticity component. They exploited this relationship to compute the power spectra of the pressure field by propagating acoustic waves through a swirling jet and showed the potential of the technique as a non-intrusive spectral probe.

Using X-wire, two-dimensional LDV as well as stereoscopic PIV the near-field of the swirling jet was examined by Facciolo (2006) and the data constitutes a well-defined database for a complex flow field. Besides an encountered counter-rotating core at a downstream position around 6 pipe diameters, which was observed with all measurement techniques involved and through DNS (reported in Facciolo *et al.* 2005), the time resolved PIV measurements show interesting differences between the non-swirling and swirling jet.

Besides the amount of experimental studies on swirling jets generated by different mechanisms few review articles as well as book chapters have been

[10]It is interesting to note that the interest in studying the effect of screens on non-swirling round jets arose much later (Burattini *et al.* 2004).

provided for topics related to combustion and mixing. The review articles by Syred & Beer (1974) and Lilley (1977) give an overview on swirling flows in the field of combustion in general. Rajaratnam (1976) in his book about turbulent jets provides a theoretical background and discusses the turbulence statistics obtained by Chigier & Chervinsky (1967) and Pratte & Keffer (1972). The book chapter by Schetz (1980) briefly reviews the aforementioned works, whereas the classical book by Gupta *et al.* (1985) gives a good overview over experimental as well as theoretical work done on swirling flows in general. A short review over experimental studies in relation to turbulence modelling is given in Piquet (1999).

The above review on previous works on the dynamics of swirling jets shows a wide range of measurement techniques and swirl generating methods, which makes it difficult to compare results in the near-field of the jet. Despite the studies of Rose (1962) and Facciolo (2006) in jets emanating from rotating pipe facilities most of the jets in the near outlet region of the orifice contain traces of the swirl generating method[11] and make it impossible to draw any general conclusion. Most interest has been shown for the recirculation zone, because of its interest for the combustion community and there is less data on nonrecirculating swirling jets. As pointed out by Mehta *et al.* (1991) this complicates the interpretation of the results by the presence of both, a stabilising region around the axis of rotation and an unstable region farther outwards.

The lack on experimental data regarding the passive scalar mixing in swirling jets is even more scarce. Craya & Darrigol (1967) were probably the first ones who determined the mean temperature as well as the root mean square value of the temperature fluctuations with the help of thermocouples and a slightly heated wire.

Using Pitot-tubes and thermistor thermometers the mean dynamic and thermal field of swirling jets for a large variety of Reynolds numbers and swirl numbers were investigated by Ogawa *et al.* (1979, 1981, 1982).

In a rather unique investigation Grandmaison & Becker (1982) used marker nephelometry to study the fluid concentration field of a free swirling turbulent jet with and without internal reverse flow in the self-preserving region up to 60 nozzle diameters downstream including its turbulence intensity. The effect of swirl on the axial decay, the spreading as well as the correlation functions and the spectra of the concentration were accessed. They conclude that the addition of swirl has a small effect on the flow structure, although it increases the rates of entrainment and spreading.

The results by Komori & Ueda (1985) in a weakly heated swirling jet with moderate to strong swirl show that in a strongly swirling jet the ambient fluid is rapidly entrained into the jet in the region near the nozzle exit. They linked the

[11] The study of Pratte & Keffer (1972) is not listed here, due to the asymmetry in the vicinity of the pipe outlet caused by their long dividing strip in the pipe (see section 2.3.3a).

rapid entrainment to the large negative static pressure induced by the strong centrifugal forces. The turbulent kinetic energy was found to exhibit a large peak in the vicinity of the nozzle showing that strong turbulence is generated by the rapid mixing encountered in strongly swirling jets with reverse flow. For a weakly swirling flow the maximum moves further downstream.

The study by Elsner & Kurzak (1987, 1989) extends the work by Komori & Ueda by means of an X-wire, cold-wire and temperature compensated single-wire in a slightly heated swirling jet. All velocity components, Reynolds stresses and heat flux terms were determined giving a full description of the dynamic and thermal flow field.

Qualitative velocity and scalar measurements of the flow flied of low swirl intensity jets were obtained by Toh *et al.* (2005) using multi-grid cross correlation digital particle image velocimetry (MCCDPIV) and planar laser induced fluorescence (PLIF). The findings are consistent with known gross effects of swirl.

Most of the previous studies concerning the concentration or temperature field were restricted to strong swirl intensities, the self-preserving and/or far-field region. Furthermore, they all employed swirl generating methods, which distorted the near field region. Hence, there is clearly a lack of experimental results concerning the effect of rotation on the passive scalar behaviour in the near-field of a free turbulent jet, free of any secondary flows or traces of swirl generating methods, which justifies the need for the present study.

Author(s) (year)	Swirl generator	Measurement technique(s)	Range of $Re \cdot 10^3$	Range of $S_{\phi x}$	Range of x/D	Presented quantities
Rose (1962)	rotating pipe	single hot-wire (SW)		0–0.23	0.235–15	U, V, W & $\overline{u_i u_i}$
Chigier & Beér (1964)	tang. injection	impact probe (IP)		0–0.6	0.39–1.43	U & V
Kerr & Fraser (1965)	passive vanes	impact probe		0–0.72	11.7–19	U, V & W
Chigier & Chervinsky (1967)	tang. injection	impact probe	24–260	0.066–0.64	0.2–15	U, V & P
Pratte & Keffer (1972)	rotating pipe	SW, IP	2.3	0–0.3	1–30	U, V & $\overline{u_i u_j}$
Wooten *et al.* (1972)	straw inserts	X-wire (XW)		(G=)0.08		U, V, u' & v'
Morse (1980)	tang. slots	SW	56	(S=)0.48	0–6	U, V, W & $\overline{u_i u_j}$
Fujii *et al.* (1981)	passive vanes	LDV	100	0.69–1.5	0.5–5	U, V, W & $\overline{u_i u_j}$
Sislian & Cusworth (1986)	passive vanes	LDV	11.5	0.79	0.125–5	U, V, W & $\overline{u_i u_j}$
Samet & Einav (1988)	tang. injection	impact probe		(G=)0–0.49	2–20	U & V
Farokhi *et al.* (1989)	tang. nozzles	IP, SW	375	0.48	0–6	U, V, W, & P
Mehta *et al.* (1991)	rotating honeycomb	SW, XW		0–0.2	0–2.31	U, V & $\overline{u_i u_j}$
Park & Shin (1993)	swirl burner	Schlieren visualization	13–20.5	0–1.87	0–5	images & entrainment rates
Feyedelem & Sarpkaya (1998)	tang. injection	3D-LDV	18	0–0.52	0.14–32	U, V, W & $\overline{u_i u_j}$

TABLE 1. Previous experimental studies on isothermal and heated swirling jets.

Author(s) (year)	Swirl generator	Measurement technique(s)	Range of $Re \cdot 10^3$	Range of $S_{\phi x}$	Range of x/D	Presented quantities
Oljaca *et al.* (1998)	rotating paddle	XW, ultrasound scattering	10	0–0.24	0.25–3	U, V
Gilchrist & Naughton (2005)	tang. injection	impact probe	100	0–0.23	0–20	U, V
Facciolo (2006)	rotating pipe	XW, 2D-LDV, 2D-PIV	12–33.5	(S=)0–0.5	0–8	U, V, W, $\overline{u_i u_i}$ & $\overline{vw}$
Craya & Darrigol (1967)	tang. injection	SW, cold-wire (CW), thermocouple (TC)		0–1.58	1–15	U, V, W, θ, ϑ' & $\overline{u_i u_j}$
Ogawa *et al.* (1979, 1981, 1982)	tang. injection	IP, TC	11.2–105.3	0–0.616	0–20	U, V, P & θ
Grandmaison & Becker (1982)	passive vanes	nephelometry	100	0–0.68	0–60	θ & ϑ'
Komori & Ueda (1985)	rotating nozzle	LDV, CW	4.92	0–0.53	0–10	U, V, W, θ, $\overline{u_i u_i}$, $\overline{uw}$, $\overline{u\vartheta}$ & $\overline{w\vartheta}$
Elsner & Kurzak (1987, 1989)	passive vanes	XW, CW, temp. compensated SW	80	0–0.42	1–15	U, V, W, θ, $\overline{u_i u_j}$ & $\overline{u_i \vartheta}$
Toh *et al.* (2005)	tang. injection	PIV, PLIF	3.9	(S_{m_0}=)0.06–0.15	0–5.8	images
Örlü (2006)	rotating pipe	XW-CW	24	(S=)0–0.5	0–6	U, V, θ, $\overline{u_i u_i}$, $\overline{uv}$, $\overline{u\vartheta}$ & $\overline{v\vartheta}$

CHAPTER 3

Turbulent Boundary layer Flows

"We have found a strange footprint on the shores of the unknown. We have devised profound theories, one after another, to account for its origins. At last, we have succeeded in reconstructing the creature that made the footprint.
And lo! It is our own."

Sir Arthur Eddington (1882 – 1944)

3.1. Preliminaries

The following section will consist of a brief introduction to the common notation in wall-bounded turbulent shear flows, with the main focus on zero pressure-gradient (ZPG) turbulent boundary layer (TBL) flows. However, since ZPG TBL share common features to channel and pipe flows within a region close to the bounding surface, most of the concepts introduced here will also be valid for internal flows. The interested reader is referred to classical and modern textbooks (e.g. Tennekes & Lumley 1972; Pope 2000; Bernard & Wallace 2002), for a more thorough introduction.

For the present chapter, we consider the fully developed turbulent flow along a flat plate under ZPG conditions, i.e. $\partial P/\partial x = 0$, which is equivalent to a constant free stream velocity, U_∞, along the downstream direction. Hereby, x, y, and z, correspond to the streamwise, wall normal and spanwise directions, respectively, with the corresponding mean, i.e. time averaged, velocity components, U, V and W, and the pressure P. The boundary layer thickness, δ, marks the edge of the rotational fluid within the boundary layer in a statistical sense, since the instantaneous demarcation line between the rotational and irrotational fluid is highly corrugated. For the following, and if not otherwise stated, $\delta(x)$ refers to the distance from the wall where the mean velocity is, for instance, within 1 % of the free stream velocity. Since, the latter is an arbitrary measure and poorly conditioned when it comes to both experimentally and numerically obtained velocity profiles, other measures have been devised.

Before we introduce these measures, it is worth to consider the streamwise mean momentum equation, which—for a two-dimensional incompressible steady flow under boundary layer approximations—reads

$$U\frac{\partial U}{\partial x} + V\frac{\mathrm{d}U}{\mathrm{d}y} = -\frac{1}{\rho}\frac{\partial P}{\partial x} + \frac{1}{\rho}\frac{\partial \tau}{\partial y} - \frac{\partial}{\partial x}\left(\overline{u^2} - \overline{v^2}\right), \tag{3.1}$$

where $\overline{u^2}$ and $\overline{v^2}$ denote the Reynolds normal stresses in streamwise and wall normal direction, respectively, and ρ denotes the density of the fluid. The pressure gradient term can furthermore be replaced by means of Bernoulli's equation, and thereby be expressed in terms of the free stream velocity and its gradient in streamwise direction. The mean total shear stress, τ, reads for a turbulent flow,

$$\tau = \rho\nu\frac{\partial U}{\partial y} - \rho\overline{uv}, \tag{3.2}$$

with ν and $-\rho\overline{uv}$ denoting the kinematic viscosity and streamwise-wall normal Reynolds stress, respectively. While under ZPG conditions, the pressure gradient term vanishes, the convective terms as well as the streamwise derivatives of the Reynolds normal stresses are zero for fully developed internal flows, like pipe and channels. Integration of equation (3.1) from the wall to the free stream gives the so called von Kármán integral momentum equation

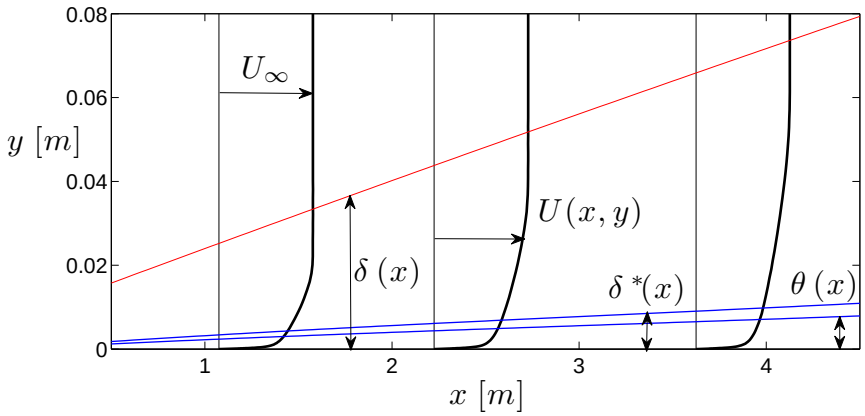

FIGURE 3.1. Turbulent boundary layer profiles evolving along a flat plate under zero pressure-gradient conditions. Profiles and scales correspond to profiles taken from Örlü (2009*a*) at $U_\infty = 13$ m/s. Trends for the boundary layer thickness, δ, displacement thickness, δ^*, and momentum loss thickness, θ, are computed from the experimental data and are extrapolated to a virtual origin.

$$\frac{\tau_w}{\rho} = \frac{\mathrm{d}}{\mathrm{d}x}\left[U_\infty^2 \int_0^\infty \frac{U(x,y)}{U_\infty}\left(1-\frac{U(x,y)}{U_\infty}\right)\mathrm{d}y\right] + U_\infty \frac{\mathrm{dU}_\infty}{\mathrm{d}x}\int_0^\infty \left(1-\frac{U(x,y)}{U_\infty}\right)\mathrm{d}y\ , \tag{3.3}$$

where the contribution from the Reynolds normal stresses was neglected.[1] The wall shear stress is here denoted with τ_w and is a function of x. For a non ZPG flowU_∞ is also a function of x. Introducing, two well defined measures for the boundary layer thickness, viz. the displacement thickness,

$$\delta^*(x) = \int_0^\infty \left(1-\frac{U(x,y)}{U_\infty}\right)\mathrm{d}y \tag{3.4}$$

and the momentum loss thickness,

$$\theta(x) = \int_0^\infty \frac{U(x,y)}{U_\infty}\left(1-\frac{U(x,y)}{U_\infty}\right)\mathrm{d}y\,. \tag{3.5}$$

The ratio of former to the latter is often used as an indicator for the "fullness" of the velocity profile and is hence known as the shape factor, $H_{12} = \delta/\theta$. Utilising the introduced thicknesses, also depicted in figure 3.1, as well as the definition of the skin friction coefficient, c_f, reduces equation (3.3) to

$$c_f = \frac{\tau_w}{\frac{1}{2}\rho U_\infty^2} = 2\frac{\mathrm{d}\theta}{\mathrm{d}x} + \frac{4\theta + 2\delta^*}{U_\infty}\frac{\mathrm{d}U_\infty}{\mathrm{d}x}\,. \tag{3.6}$$

Hence, the skin friction coefficient can be obtained from mean velocity profile measurements at some different downstream positions. For the case, that equation (3.6) is intended to be used, special care should be paid to ensure a well resolved mean velocity profile. In the case of internal flows, as for channel and pipe flows, the streamwise momentum equation, i.e. equation (3.1) or its counterpart in cylindrical coordinates, can readily be used to show, that the wall shear stress is directly related to the pressure drop, i.e.

$$\tau_w = -\delta\frac{\mathrm{d}P_w}{\mathrm{d}x} \qquad \text{and} \qquad \tau_w = -\frac{\delta}{2}\frac{\mathrm{d}P_w}{\mathrm{d}x}\,, \tag{3.7}$$

where δ corresponds to the channel half-width[2], H, and pipe radius, R, respectively, and P_w denotes the mean pressure at the wall. Since the static pressure can easily be obtained by means of pressure taps, the wall shear stress, is from an experimental point easily obtainable. Nevertheless—as will be shown later on—it has instead often been computed by indirect methods. One reason,

[1] The omission of the Reynolds normal stress contribution is justified, since its contribution is less than an order of magnitude than the leading order term. Schlatter *et al.* (2009*a*) shows for instance, that the neglected Reynolds normal stress contribution under ZPG conditions is around 50 times smaller than the leading order term for $Re_\tau \approx 2000$.

[2] Also "channel half-heigth" is the correct geometrical term, it has been common practise to use "channel half-width" synonymously.

which may explain the need to utilise other means than the pressure drop, to compute the wall shear stress, is, that the underlying assumptions are not always fulfilled. So, for instance, are the convective terms for internal flows, only zero under fully developed turbulent conditions, which requires channels and pipes of at least hundred channel heigths or pipe diameters. Another assumption, important for channel flows, is that the two-dimensionality of the flow, is only guaranteed for large aspect ratios, i.e. width-to-height ratios, say, larger than five.[3]

The wall normal momentum equation reveals, that the sum of P and the Reynolds normal stress in wall normal direction, $\overline{v^2}$, is solely a function of the streamwise coordinate. This and equation (3.7) employed in the integration of equation (3.1) for fully developed internal flows yields

$$\tau = \frac{\mathrm{d}P}{\mathrm{d}x}(y-\delta) = \tau_w \left(1 - \frac{y}{\delta}\right) , \tag{3.8}$$

which reveals, that in the vicinity of the wall, i.e. for $y/\delta << 1$, the total shear stress is nearly constant and equal to the wall shear stress. This turns out to be true not only for channel and pipe flows, but also for turbulent boundary layer flows. Consequently, there exists a region in wall-bounded turbulent flows, that is independent of both the dimensions and the geometry of the flow, and is instead characterised through the wall shear stress, τ_w. This fact has brought about the term constant stress layer for the near wall region. Hence, a natural choice for a velocity and length scale within this region, as apparent from equations (3.2) and (3.8), would be

$$u_\tau = \sqrt{\frac{\tau_w}{\rho}} \qquad \text{and} \qquad \ell_* = \frac{\nu}{u_\tau} , \tag{3.9}$$

which are the so-called friction velocity and viscous length scale, respectively. Together with the distance from the wall, these three parameters specify the conditions in the near wall region. More specifically, equation (3.8) can now be rewritten as

$$1 = \frac{\mathrm{d}(U/u_\tau)}{\mathrm{d}(yu_\tau/\nu)} - \frac{\overline{uv}}{u_\tau^2} + \frac{y}{\delta} = \frac{\mathrm{d}U^+}{\mathrm{d}y^+} - \overline{uv}^+ + \frac{y^+}{\delta^+} , \tag{3.10}$$

where the "+" denotes normalisation with viscous/inner/wall units, i.e. u_τ and ℓ_*, and δ^+, is the so-called Kármán number, expressing the ratio between the outer and inner length scale, which is equivalent to the friction Reynolds number, Re_τ. Close to the wall (and to a wider extent, the more the scales are separated), i.e. for $y^+/\delta^+ << 1$, the so-called law of the wall, ascribed to Prandtl (1925) follows from equation (3.10), viz.

[3]The literature is not clear about the value for the length of the pipe or channel as well as the aspect ratio for channels (Doherty *et al.* 2007). Nevertheless, the given values are fairly well accepted (cf. Dean 1978).

$$U^+ = \frac{U}{u_\tau} = f\left(\frac{y}{\ell_*}\right) = f(y^+)\,. \tag{3.11}$$

While the law of the wall is valid in the constant stress layer, further away from the wall, say $y/\delta = \eta = \mathcal{O}(1)$, the dimension of the flow becomes important, and as shown by von Kármán (1930), the deviation from the free stream or centreline velocity can be described by the so-called velocity defect law,

$$U_\infty^+ - U^+ = \frac{U_\infty - U}{u_\tau} = F\left(\frac{y}{\delta}\right) = F(\eta)\,, \tag{3.12}$$

with η being the outer length scale. Following Millikan (1938), the derivates of the law of the wall for $y^+ >> 1$ and the one for the velocity defect law for $\eta << 1$ should overlap (asymptotic matching) within the so-called overlap region, $\ell_* << y << \delta$, yielding

$$y^+\frac{\mathrm{d}f(y^+)}{\mathrm{d}y^+} = \eta\frac{\mathrm{d}F(\eta)}{\mathrm{d}\eta} = \frac{1}{\kappa} = \text{const.} \tag{3.13}$$

In order for the left-hand side to be a function of y^+ and the right-hand side only of η, both sides have to be equal to a constant, which is here introduced as the inverse of κ, the so-called von Kármán constant. Evaluating the resulting equality results in the logarithmic velocity profiles for the law of the wall,

$$U^+ = \frac{1}{\kappa}\ln y^+ + B\,, \tag{3.14}$$

and the velocity defect law,

$$W^+ = U_\infty^+ - U^+ = -\frac{1}{\kappa}\ln\eta + B_o\,, \tag{3.15}$$

respectively, where B and B_o are the integration (additive) constants.

Classical theory considers κ and B to be constants, i.e. independent of Reynolds number and whether pipe, channel or ZPG TBL flows are considered. Although objections to this view have always existed (Simpson 1970; Bradshaw & Huang 1995), they are usually denoted as the universal log law constants. The universality of B_o, on the other hand, has similarly been disputed. So, for instance, is it possible to combine equations (3.14) and (3.15) to express the additive constants as follows,

$$C = B + B_o = U_\infty^+ - \frac{1}{\kappa}\ln\delta^+ = \sqrt{\frac{2}{c_f}} - \frac{1}{\kappa}\ln Re_\tau\,, \tag{3.16}$$

where the equality,

$$c_f = 2\left(\frac{u_\tau}{U_\infty}\right)^2, \tag{3.17}$$

has been utilised. If both, B and B_o, are constants, then c_f should have a specific relationship with Re_τ, viz.

$$c_f = 2\left(\frac{1}{\kappa}\ln Re_\tau + C\right)^{-2}, \tag{3.18}$$

otherwise B_o should bear a Reynolds number dependence if B is as generally assumed a universal constant. Among others, Smith (1994) and Smits & Dussauge (2006) follow the above lines of reasoning and conclude that the employed form of the velocity defect law, i.e. with u_τ as the velocity scale for the outer region, can not be universal. Recent experiments indicate that equation (3.18), the logarithmic skin friction law, can be utilised to describe the directly measured skin friction data over the entire Reynolds number range of practical interest (see e.g. discussion in Nagib *et al.* 2007; Mandal & Dey 2008).[4]

Nevertheless, objections to the choice of u_τ as the appropriate velocity scale for the outer region remain, and a number of alternative scaling laws have within the last decade been proposed for equation (3.12), that consequently lead to different scaling laws for the overlap region. So, for instance, may the free stream velocity, be employed, instead of u_τ, which would yield a power law description for the overlap region in the form (Millikan 1938; George & Castillo 1997),

$$U^+ = \alpha(Re)\,(y^+)^{\beta(Re)}. \tag{3.19}$$

While the above relation is thought to be valid for ZPG TBL flows (George & Castillo 1997) and not for internal flows (Wosnik *et al.* 2000), others suggest its validity also for internal flows (Barenblatt & Chorin 1998*a*), while again others propose its validity in Reynolds number independent form for a somewhat smaller region (Zagarola & Smits 1998*a*; McKeon *et al.* 2004). Another proposed scaling, is the exponential mean velocity profile for the mid-wake region (Oberlack 2001).

Figure 3.2 depicts typical mean streamwise velocity profiles for a low and high Reynolds number in inner and outer scaling together with the classical two layer structure of wall-bounded turbulent flows.[5] While the inner region comprises the viscous sublayer, buffer and overlap region, the outer or wake region consists of the wake/core and overlap region. The former is classically

[4]Nagib *et al.* (2007) points out, that an accuracy of the order of 0.1 % in the skin friction value is needed in order to reliably determine Reynolds number effects over the practical range of Reynolds numbers, which would express itself in a Reynolds number dependence of the additive constants.

[5]The choice for U_∞ for the outer velocity scale in figure 3.2 has solely illustrative reasons, and does not reflect a preference for either of the outer velocity scales.

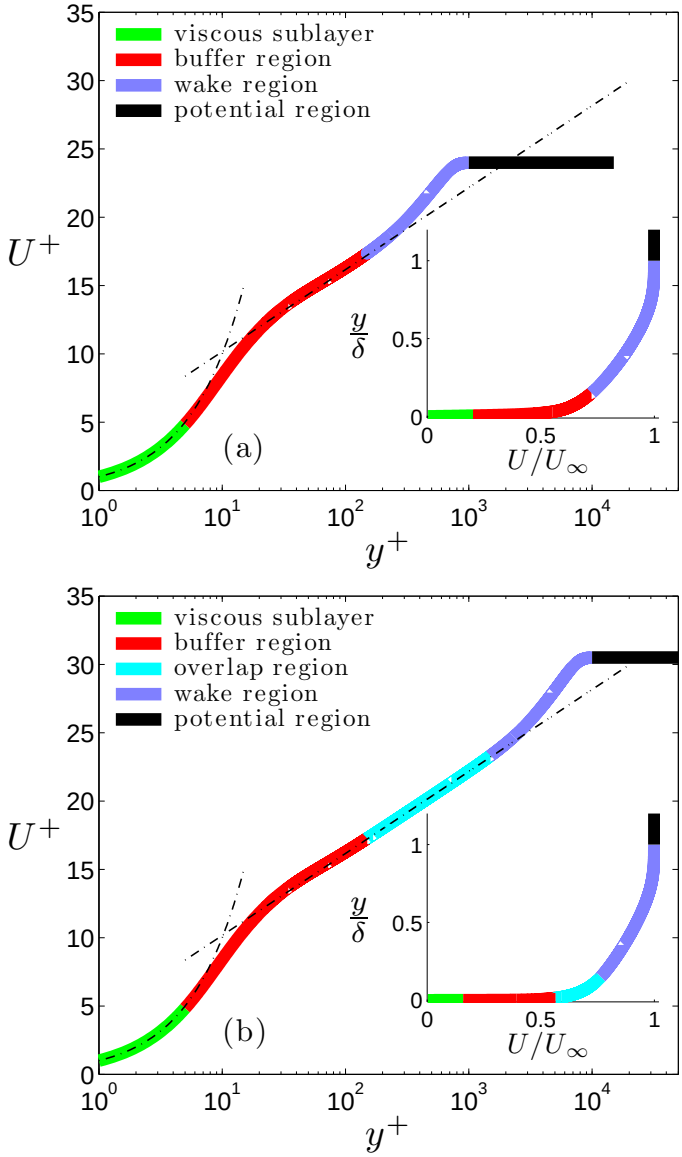

FIGURE 3.2. Typical streamwise mean velocity profile for an equilibrium ZPG TBL flow computed through the composite velocity profile description by Chauhan *et al.* (2009) for Re_τ equal to (a) 1000 and (b) 10000.

considered to be universal, i.e. Reynolds number and flow case independent, whereas the latter depends on both. As anticipated through the asymptotic matching condition, $\ell_* << y << \delta$, the overlap region only appears for high enough Reynolds numbers.

Although Re_τ or δ^+ are well defined parameters in the case of internal flows, for the case of spatially developing flows, a Reynolds number based on the displacement and momentum loss thicknesses, equations (3.4) and (3.5),

$$Re_{\delta^*} = \frac{U_\infty \, \delta^*}{\nu} \qquad \text{and} \qquad Re_\theta = \frac{U_\infty \, \theta}{\nu} \, . \tag{3.20}$$

are more appropriate.

In addition to the functional forms for the law of the wall, equation (3.11), a number of composite velocity profiles has been proposed valid for the entire flow region. Despite the fact, that some of the aforementioned power or log law descriptions were intended to describe the entire velocity profile for internal flows, the need for more appropriate relations has been recognised from Rotta (1950) and onward. One of the first formal descriptions were for instance given by Coles (1956), based on his additional wake function. The composite velocity profile can thus be given as a superposition of the description for the (linear and logarithmic) law of the wall and an additive wake function

$$U^+_{\text{composite}} = U^+_{\text{inner}}(y^+) + \frac{2\Pi}{\kappa} \mathcal{W}\left(\frac{y^+}{\delta^+}\right), \quad 0 \leq y^+ \leq \delta^+ \, , \tag{3.21}$$

where Π and $\mathcal{W}$ are known as the wake parameter and wake function, respectively. A number of wake functions have been developed, of which some have been discussed in Lewkowicz (1982) and Sandham (1991), whereas a summary of more prominent complete analytical expression can be found in appendix E of Örlü (2009*c*).

3.2. The overlap region: Historical account

"Many textbooks will have to be revised" and "Generations of engineers who learned the law will have to abandon it" are some of the catch phrases *Science* (Cipra 1996) used to draw attention to the debate regarding the correct description of the overlap region in wall-bounded turbulent flows.[6] Neither has most textbooks been revised, nor have engineers abandoned "one of [the] few certainties in the difficult field of turbulence" (Cipra 1996). So, what is the debate all about, and what is the essence of it? Well, the story starts some eighty years ago, and calls for a historical excursus.

[6]The quoted phrases are attributed to A. Chorin, but similar phrases can be found in various works by the author, as for instance in Barenblatt & Chorin (1998*a*).

3.2.1. *From the power to the log law*

The early days of wall-bounded (turbulent) flow research were driven forward by Prandtl and his students in Göttingen (see e.g. Eckert 2006), while his former student von Kármán did his best to compete with him,[7] first from Aachen, were von Kármán was Professor and later on from the United States. Studies by Darcy and Stanton (see e.g. Gisonni 2003; Darrigol 2005) on turbulent pipe flow had established a certain understanding on the friction relation in smooth and rough pipe flows. Nonetheless, the first name, which comes to ones mind, when thinking about pipe flows, is Nikuradse, who, in a number of experimental investigations in pipe (Nikuradse 1930), channel (Nikuradse 1929) and flat plate boundary layer (Nikuradse 1942) flows, conducted exhaustive studies. The correlations he provided, and even his data, are still in use, be it for engineering calculations as well as the testing of todays asymptotic theories. In the early 1920's Prandtl and von Kármán extracted the 1/7-power law (based on the data from Blasius 1913), and it was believed to describe the velocity distribution and the friction in pipe flows fairly well over the range of Reynolds numbers investigated so far. However, once Nikuradse reached higher and higher Reynolds numbers in his pipe flow experiments, the data was better fitted to the power law if the exponent was slightly altered. In other words, the 1/7-power law became known as the power law with the Reynolds number dependent exponent, $1/n$, where n increases with increasing Reynolds number. Nevertheless, the power law has since then been considered a fairly accepted formulation for the description of pipe flows (see e.g. Schlichting & Gersten 1979, chap. 20). The advantage of having a description for the velocity profile is, that it can be utilised to derive integral parameters. The fact that the power law was (at that time) a result of extrapolation, neither valid in the vicinity of the wall, nor physical at the centreline of the pipe, was willingly accepted, due to the absence of any better description.

The above mentioned Reynolds number dependence of the exponent in the power law, was a rather annoying fact, and the search for another description challenged both von Kármán as well as Prandtl. Using the published data of Nikuradse, von Kármán was up to something. By starting out from Prandtls mixing length concept (Prandtl 1925) and the experimentally verified fact that the velocity defect in the outer region is independent of the Reynolds number when scaled by the friction velocity (Fritsch 1928), von Kármán, was able to

[7] von Kármán remarks later on (von Kármán 1967, chap. 17), shortly after Prandtl introduced his mixing length concept at the Congress of Applied Mechanics in Zürich (Prandtl 1926): "I suddently felt that Prandtl had won a round, and I came to realize that ever since I had come to Aachen my old professor and I were in a kind of world competition. The competition was gentlemanly, of course. But it was first class rivalry nonetheless, a kind of Olympic Games, between Prandtl and me, and beyond that between Göttingen and Aachen. The 'playing field' was the Congress of Applied Mechanics. Our 'ball' was the search for a universal law of turbulence."

derive a logarithmic relation for both the velocity and friction factor.[8] The excitement of von Kármán when he arrived at the solution, can graspingly be "experienced" in his autobiography (von Kármán 1967, chap. 17). To prove his theory, he however needed experimental data from higher Reynolds numbers, which were readily collected by Nikuradse, but not published so far. Once he obtained the data from his former teacher, he was able to confirm that the logarithmic description resembles the data over the entire Reynolds number range, be it for the mean velocity, or the the friction relation, and hence marks a pivotal point in turbulence research.

3.2.2. *From Stockholm into the world*

Kármáns log law was able to describe both the mean velocity profile as well as the friction relation for the entire Reynolds number range for which data existed, and that independent of the Reynolds number. Although von Kármán planned to present his results at the forthcoming Congress on Applied Mechanics in Stockholm, organised by KTH[9], he felt obliged to inform Prandtl about his new results, since he had obtained and used Nikuradses published and unpublished data. Prandtl invited him thereupon to Göttingen to give a seminar and appreciated the importance of von Kármáns finding, by not giving a talk on fluid dynamics at the meeting in Stockholm. With Prandtls appreciation, expressed through "Kármán did this before I arrived at the result." (von Kármán 1967, chap. 17)[10], von Kármán was ready for Stockholm, where—not knowing whether he would finalise his ideas—only a preliminary title of his talk was printed together with a blank abstract page in the "Abstracts of lectures" (Oseen & Weibull 1930*a*). On August 25, 1930 (cf. figure 3.3) von Kármán gave his legendary lecture on the log law. Since his seminar in Göttingen became only one year later available to the English speaking audience, Stockholm, can be thought as the place, where the log law was first introduced to the turbulence community.

---

[8]Note, that while Schlichting (1965) and George & Castillo (1997), among others, refer to Stanton & Pannell (1914), for the origin of the defect law, Panton (2005) correctly remarks: "This is erroneous. The Stanton reference contains neither velocity profiles nor mention of the defect law." von Kármán (1930), on the other hand, refers to Stanton (1911) for the origin of the defect law, however, remarks in a later publication (loose translation from von Kármán 1932): "Herr Prandtl called my attention to the fact, that, although T. E. Stanton used the relation [...] to depict the velocity distribution in individual cases, he was not aware of its general validity. In point of fact, this was first pronounced in a work by W. Fritsch."

[9]Also the meeting was planned to be held at todays main campus of KTH, it had to be moved, due to the unexpected number of 600 attendees, to the "Swedish House of Lords" (*Riddarhuset*) (Oseen & Weibull 1930*b*).

[10]Prandtl was known for his calmness, especially when it comes to discoveries by von Kármán, so for instance, answered he calmly on an excited von Kármán, when he showed him his results on the (von Kármán) vortex street: "So, you've found something. Very well, write it up, and I will present it." (von Kármán 1967, chap. 7)

It is also important to note, that the constant von Kármán himself extracted for the log law, later on named after him, was 0.36 and 0.38 for the mean velocity and friction relation, respectively (von Kármán 1930).[11] Similar, more general, derivations of the log law followed by Prandtl (1932), Izakson (1937) and Millikan (1938). While the formalism remained the same until today, the constants were continuously reevaluated, over and over again, and varied mostly within the range from 0.36 to 0.44 (Zanoun *et al.* 2003), however with a number of extreme outliers. Based on the extensive reviews by Coles (1956, 1968), the Kármán constant was adapted to 0.4-0.41, which is today widely used (see e.g. Tennekes & Lumley 1972; Schlichting & Gersten 1979; Lesieur 1997).[12]

3.2.3. *Ultimate universality: climax and fall*

The trust in the log law also faded into its constants and since it was widely believed that canonical wall-bounded flows, i.e. channel, pipe and turbulent boundary layers, are similar in the inner region (Ludwieg & Tillmann 1949), the Kármán constant—irrespective of the flow case—was believed to be "a universal constant" (Schlichting & Gersten 2000). Its repetition in classical textbooks (Tennekes & Lumley 1972; Hinze 1975; Tritton 1988, to mention just a few) as well as its seemingly good agreement with various measurements

[11] This fact seems to have fallen in oblivion, so for instance associates Zanoun *et al.* (2003), among others, the value of 0.4 to von Kármán and the year 1930, and the values of 0.36 and 0.38 to Nikuradse. However, von Kármán (1934) himself points out, that "[t]he numerical value found by the author for the universal constant is 0.38" and Nikuradse (1930), in his talk in Stockholm, refers to von Kármán as having mentioned values between 0.36 and 0.38.

[12] This becomes also clear, when going through the ten German editions of Schlichtings reference book, viz. from Schlichting (1951) to Schlichting & Gersten (2006). The Kármán constant remained at 0.41 for over five decades. Furthermore, not even the latest edition, does contain a single reference to the debate log versus power law or revised log law constants.

Författare Verfasser Authors Auteurs	Föredrages av Vorgetragen von Read by Fait par	Ämne Gebiet Subject Sujet	Sektion Section	Dag kl. Zeit Time Heures
KAMPÉ de FÉRIET, J., Prof.		Sur quelques cas d'intégration des équations du mouvement visqueux incompressible.	I —	26/8 11.30.—12. 27/8 15.30.—16.
KARELITZ, G. B., Res. Eng..		Notes on the mechanism of lubrication.	I	29/8 10.—10.30.
v. KÁRMÁN, Th., Prof.		Die Theorie der Turbulenz.	I	25/8 11.30.—12.
KAWADA, S., Dr. Ing.	Shiba	A contribution to the theory of latticed wing.	IV	26/8 16.—16.30.

FIGURE 3.3. Excerpt from the Program of the 3rd International Congress for Applied Mechanics, Royal University of Technology, Stockholm 24–29 August 1930 (Weibull 1930).

stabilised the status of the universal constant(s) of the log law over the years.[13] Based on the gained certainty associated with the log law constants, it was utilised to check the quality of measured profiles and later on exploited to determine the friction velocity from measurements of the mean velocity within the overlap region. A method, introduced by Clauser (1954) (a student of von Kármán), got wide acceptance. Since, the log law with the accepted constants is universal, i.e. Reynolds number and flow case independent, a best fit of a measured velocity profile to the log law determines the only unknown, viz. the friction velocity. It may sound as a surprise, but even there, where the friction velocity could have easily been computed independently of the velocity profile, like in pipe flows (Abell 1974) or where high quality measurements in the viscous sublayer by means of laser Doppler velocimetry (LDV) were available (DeGraaff 1999), the friction velocity was extracted from the so-called Clauser chart method. This, consequently, brought few to coin the described method a measurement technique.[14] Experimental efforts to determine the wall shear stress directly and/or independent of the log law, which showed deviations from the results deduced from the Clauser plot (Karlsson 1980), were not seldom associated with measurement errors (Coles 1968), rather to question the accepted universal constants. Hence, it is of no surprise, that the universal constant(s) got confirmed by a number of experiments, which employed the Clauser method to extract the friction velocity. Using the extracted values to scale the obtained profiles, one seemingly believed to have confirmed the universality of the Kármán constants.

The log law and its universal constants, known as "one of the cornerstorns of fluid dynamics" (Bradshaw & Huang 1995), had thus for over sixty years an undisputed status. At least, that is what *Science* connotes with its popular science account mentioned in the beginning of this review. The power law, in which Prandtl did not believe anymore, started to become of interest again. George & Castillo (1997) and Barenblatt & Chorin (1998*a*), among others, showed that the power law was indeed not only an empirical relation based on an extrapolation, but could—as already demonstrated by Millikan (1938)—be derived in the same manner as the log law, by just interchanging the friction velocity as the velocity scale for the outer region with the centreline or free stream velocity for internal and external flows, respectively. Not only was the Reynolds number independence of the log law constants, and thereby its universality, under attack, but also the log law itself. While Barenblatt & Chorin (1998*a*) abandoned the log law *per se*, George and coworkers (George & Castillo 1997; Wosnik *et al.* 2000) considered the power law appropriate for

[13]The literature is more divergent, when it comes to the universality of the additive constant, however a number of textbooks have contributed to the view, that both constants are universal.

[14]So for instance, states Willmarth & Lu (1972): "The wall shear stress was measured using the Clauser plot".

ZPG TBLs, whereas the log law with Reynolds number dependent constants was found appropriate to describe the overlap region in internal flows. Once, concerns regarding the log law were openly articulated, the discrepancies in the literature, which had always existed[15], became the focus of attention.

Since most of the previous experimental studies had utilised the log law with the classical constants to deduce the skin friction, a need for new measurements supplemented by directly and/or independently determined friction velocities emerged. Furthermore, these had to be acquired at high Reynolds numbers in order to determine the log law constants with certainty and to contribute to the debate log versus power law. A number of experimental facilities was set up, particularly for this purpose, among others the well-known pressurised *Superpipe* at Princeton (Zagarola 1996), which exceeded Nikuradses pipe flow experiments by an order of magnitude in Reynolds number.

While the turbulence community expected answers to the above questions, as soon as the first results from the Superpipe became available, more confusion was added to the controversy. Results apparently indicated, that a Reynolds number independent power law for the region succeeding the buffer region fits the data better, before it merges into a log law much further away from the wall than usually assumed, however with a Kármán constant of 0.436 (Zagarola & Smits 1997, 1998*a*). By admitting a power law below the log law (in terms of y^+), advocates of a so-called mesolayer saw themselves confirmed that the effect of viscosity reaches much further into the classical overlap region (Wosnik *et al.* 2000), whereas others raised doubts on the measured values (Perry *et al.* 2001) as well as the conclusions (Barenblatt 2004). Although, the Princeton group saw a log law in their results (albeit of reduced extent and substantially higher constants), to others the collection of curves appeared "like a collection of power laws" (Barenblatt & Chorin 1998*b*). Hard times had started for a Reynolds number independent log law description for the overlap region in wall-bounded turbulent flows, whereas a Reynolds number dependent power law gained support.

3.2.4. *Back to Stockholm and von Kármáns initial 0.38*

While the power law gained support, due to the results from the Superpipe, new results from experiments in a ZPG flat plate TBL became available from the MTL wind tunnel at KTH (Österlund 1999). Although the Reynolds number range was two orders of magnitude smaller than that in the Superpipe, it provided, contrary to previous ZPG TBL experiments, 70 mean velocity profiles

[15]So for instance, summarises Bradshaw *et al.* (1992): "The actual range—ignoring a few outlying methods—implies a 10 % "uncertainty" in skin friction on a flat plate in a low-speed flow, the simplest of all test cases. We are trying to achieve a consensus!". Similarly Tennekes (1982) proposes, after reviewing reported values for the Kármán constant, that "one should restrain the urge to expound on this issue, and state simply that $\kappa = 0.4 \pm 0.04$ represents the state of the art"

supplemented with independently and directly measured skin friction values by means of oil-film interferometry. The results of this "heroic effort" (George 2006) demonstrated the validity of the log law with Reynolds number independent constants, however above a relatively high threshold Reynolds number as well as an extended buffer region. Furthermore, the extracted Kármán constant did not confirm the classical value of 0.41, but Kármáns initial one of 0.38 (Österlund *et al.* 2000*b*). Although, the conclusions were debated (Barenblatt *et al.* 2000; Österlund *et al.* 2000*a*)[16], further support for the "new" constants came from experiments in channel (Zanoun *et al.* 2003) and ZPG TBL flows (Nagib *et al.* 2004*a*). However the close cooperation between the groups made others doubt the independency of the results.[17] On the other hand, independent confirmation came also from experiments in the atmospheric surface layer (Andreas *et al.* 2006; Zhang *et al.* 2008).

3.3. The overlap region: Status quo

3.3.1. *The quest for higher Reynolds numbers and more data ...*

A number of high Reynolds number experiments have, since the revival of the debate, been performed. Among others DeGraaff & Eaton (2000), Jones *et al.* (2004), Knobloch & Fernholz (2004), Carlier & Stanislas (2005), Nickels *et al.* (2007), and Hutchins & Marusic (2007*b*) in ZPG TBL flows, however, these studies were not supplemented by direct or independent wall shear stress measurements, due to their primary focus on other issues than the scaling of the mean velocity profile. On the other hand, the experiments by Zanoun (2003), Bayoumy (2005), and Monty (2005) in channel and pipe flows, were particularly designed to address the scaling of the mean velocity within the overlap region. Additional measurements from the Superpipe with smaller Pitot tubes, compared to those by Zagarola (1996), were also performed by McKeon (2003).

Despite the mentioned efforts to provide experimental data at high Reynolds numbers, computations by means of direct numerical simulations (DNS), have started to reach Reynolds numbers where a scale separation starts and an

[16]So for instance reports Buschmann & Gad-el-Hak (2003*a*): "The decibel level of a recent shouting match (Barenblatt *et al.* (2000) and Österlund *et al.* (2000*a*)) has been particularly unsettling. Entire sessions during recent AIAA, American Physical Society, and American Society of Mechanical Engineers meetings have been devoted to the controversy. The IUTAM Symposium on Reynolds Number Scaling in Turbulent Flows [...], where a second shouting match took place, has been dominated by the debate.". It is also interesting to note in this context, that it has not always been easy to publish controversial contributions to this debate. So, for instance, added Broberg (2004) an appendix to his paper concerning the morphology of crack propagation, that contained a reevaluation of the database by Österlund advocating the superiority of the power law over the log law description.

[17]So for instance remarks George (2006) regarding the measuements in the NDF tunnel at IIT: "they can hardly be argued to be 'independent' given the close interaction of this group and KTH."

overlap region is established. Starting from the pioneering works by Kim *et al.* (1987), Spalart (1988) and Eggels *et al.* (1994) in channel, ZPG flat plate TBL and pipe flows, respectively, several DNS simulations of canonical wall-bounded turbulent flows have been performed. While in the case of experiments the highest Reynolds numbers reported are from ZPG TBL and pipe flows, the contrary is true for DNS. Here, channel flows have been simulated by a number of groups (Satake *et al.* 2003; Abe *et al.* 2004; Hu *et al.* 2006; Hoyas & Jiménez 2006) with friction Reynolds numbers exceeding one thousand, whereas the highest reported value of Re_τ is 2300 (Iwamoto *et al.* 2005). In the case of ZPG TBL flows the pioneering simulation by Spalart (1988) serves still as the standard reference and validation database for experiments and Large Eddy Simulations (LES) (Hickel & Adams 2008; Pantano *et al.* 2008), respectively.[18] Although, recently others (Khujadze & Oberlack 2004, 2007; Ferrante & Elghobashi 2005; Schlatter *et al.* 2009*b*)[19] have exceeded the Reynolds number by Spalart, these are not available publicly. The highest Reynolds numbers in the case of ZPG TBLs reach around $Re_\theta = 3000$, corresponding to about $Re_\tau = 1000$, and is similar to the highest Reynolds numbers reported in pipe flows (Satake *et al.* 2000; Wu & Moin 2008). Computational simulations will continue to reach for higher Reynolds numbers and one way to speed up the process would be to utilise LES. Such an investigation is currently being undertaken by Schlatter *et al.* (2009*a*,*b*) where DNS and LES simulations are exceeding $Re_\theta = 2500$ and 4000, respectively, and the latter is validated against the former.

3.3.2. *... and what it tells us*

The emergence of the aforementioned efforts to provide the community with high quality numerical and experimental data sets may suggest that the controversy regarding the proper scaling of the mean velocity profile within the overlap region, may have settled. While the emergence of new data sets, has contributed to our understanding regarding the structure of turbulent boundary layers, as well as the scaling of the Reynolds stresses, it has not settled the open issues concerning the simplest measurable quantity, viz. the mean streamwise velocity component. Some of the conclusions from recent investigations were already anticipated in the above review, however, here we will approach the issue more quantitatively. Starting from the first published Superpipe data sets, the evolution of the conclusions and debate—with main focus on the log law—will be presented in the following.

The first Superpipe results indicated that the mean velocity profile within $60 < y^+ < 500$ is best described by a power law, followed by a log law region residing within $600 < y^+ < 0.07\ R^+$ (Zagarola & Smits 1998*b*). Hereby both laws are assumed to be Reynolds number independent, and κ and B are

[18] And this, despite a number of shortcomings, see e.g. Örlü (2009*a*).

[19] The Ekman layer (a pressure-driven three-dimensional boundary layer) simulation of Spalart *et al.* (2008) could also be mentioned in this context.

0.436 ± 0.002 and 6.15 ± 0.08, respectively. Zagarola & Smits (1998*b*) therefore concluded, that the log law is only evident for flows with $Re_\tau > 9000$, which would exclude most of the available data on which the debate has been based so far. The unusual combination of a Reynolds number independent power and a log law with quite high log law constants made Perry *et al.* (2001) reanalyse the data. The authors also hypothesised that roughness effects at the higher Reynolds number end may have influenced the results and thereby the conclusions. In an earlier investigation in sink-flow turbulent boundary layers measured with hot-wires and Pitot tubes, the authors Jones *et al.* (2001) observed, that the Pitot-tube mean profiles display a "slight kick-up from the log-law [with classical values for the constants] which is observed near the buffer region. However this kick-up region is not observed in velocity profiles measured with a normal hot wire." Only, when the MacMillan (1956) and turbulence correction were applied, their Pitot tube measurements agree substantially better with their results from the hot-wire measurements, however the Pitot tube readings were still higher than those from the hot-wire within the buffer region. The reanalysis of the Superpipe data by Perry *et al.* (2001) gave $\kappa = 0.39$ and $B = 4.42$, which came close to the recently published values by Österlund *et al.* (2000*b*) from ZPG TBL experiments at KTH and IIT. The latter authors concluded based on their measurements, that a Reynolds number independent log law in ZPG TBL flows is established for $Re_\theta > 6000$, within $200 < y^+ < 0.15\ \delta^+$ and $\kappa = 0.38$ and $B = 4.1$. Österlund *et al.* (2000*b*) also remark, that a value of 0.41 for κ can be extracted when employing data with $Re_\theta < 6000$ and lowering the beginning of the log law region to $y^+ = 50$. Barenblatt *et al.* (2000) claimed that the "[p]rocessing of the experimental data [...] was incorrect", and "[p]roperly processed" the data would "lead to the opposite conclusion", viz. they would "confirm the Reynolds-number-dependent scaling [power] law and disprove [...] that the intermediate [...] region is Reynolds-number-independent". On the other hand, an independent processing of the Österlund (1999) data by Buschmann & Gad-el-Hak (2003*b*) confirmed the extracted values. The authors, however, also suggest that "neither the log nor the power law is valid throughout the entire overlap region".

A number of open issues regarding the conclusions from the aforementioned Superpipe results were pursued by McKeon (2003), who employed a number of different sized, and particularly smaller, Pitot tubes—in order to reduce the uncertainties due to velocity gradient corrections—and repeated the measurements by Zagarola & Smits (1998*b*). Although the presence of a power law near the wall was confirmed, it was further reduced to be valid within $50 < y^+ < 300$. The log law region, instead, was further extended ($600 < y^+ < 0.12\ R^+$) with modified constants, viz. κ and B were found to be 0.421 ± 0.002 and 5.60 ± 0.08. It was also found that the new and previous Superpipe experiments were not affected by surface roughness. The processing of the acquired data followed the corrections proposed in McKeon *et al.* (2003). One particularly controversial

point in this respect is the fact, that the authors argue that no additional turbulence correction is necessary, once the MacMillan (1956) correction has been applied, since the proposed correction combines that for effects of turbulence and velocity gradients. On the other hand, as pointed out by Monty (2005), MacMillan (1956) states, that: "[a]dditional corrections may also be required to allow for effects of turbulence and of viscosity at zero shear." The importance of corrections in terms of the log law constants—even at high Reynolds numbers—is also emphasised by McKeon *et al.* (2003), where it is found that "there is a difference of greater than 5% in the slope of the logarithmic region between data with and without a wall correction". Similar observations were made by Zanoun (2003) and Monty (2005).

Nagib & Chauhan (2008), recently re-evaluated the Superpipe data and arrived at $\kappa = 0.41$ (by excluding the three highest Reynolds number profiles)[20] for $300 < y^+ < 0.15\ Re_\tau$, when following exactly the same procedure adopted by McKeon (2003). However, they also note that an additional turbulence correction, would lead to a value of around 0.39–0.4. Hence, it becomes clear, that more than a half century after the pioneering work by MacMillan (1956), the turbulence community is not in agreement about Pitot tube corrections. "What is urgently needed" is obviously "an extensive set of mean velocity profiles in a pipe measured with a hot wire", as proposed by Perry *et al.* (2001).

The above call was heard and extensive measurements by means of Pitot tubes and hot-wires in pipe and channel flows followed by Zanoun (2003), Bayoumy (2005) and Monty (2005). The results confirmed the conclusions by Österlund *et al.* (2000*b*), namely that a Reynolds number threshold of around $Re_\tau = 2000$ (which is close to the value of $Re_\theta = 6000$ given by Österlund *et al.* (2000*b*)) is needed in order to establish a log law with Reynolds number independent constants. The extracted log law constants valid for a range between $150 < y^+ < 0.2\ Re_\tau$ were found to be 0.37 ($\approx 1/e$) and 3.7 ($\approx 10/e$). Zanoun *et al.* (2003) also found that the upper limit for the log law varies with Re_τ and extends up to 75 % of the channel half-width for their highest Reynolds number case. Although here, the conclusions were criticised by Buschmann & Gad-El-Hak (2004), since to them it appears more reasonable to allow for Reynolds number dependent variables, instead of adopting "seemingly artificial limits".[21] The region between $30 < y^+ < 150$, where a power law seems to represent their data well, was recently (Zanoun & Durst 2009) associated with the concept of the mesolayer.

The experiments by Monty (2005) in pipe flow revealed for the log law constants evaluated for $100 < y^+ < 0.15\ R^+$, that κ and B are equal to 0.386 and

[20] While it is still controversial whether the highest Reynolds number profiles were effected by roughness, measurements in the Superpipe on rough walls have recently revealed, that at least the highest Reynolds number profile was indeed effected by roughness (Allen *et al.* 2007).

[21] See also the response of Zanoun *et al.* (2004).

4.21 as well as 0.384 and 4.33 for Pitot tube and hot-wire measurements, respectively. Similar values were also extracted for his channel flow experiments, within the same limits for the overlap region, viz. 0.397 and 4.58 as well as 0.389 and 4.23 from Pitot tube and hot-wire measurements, respectively. The comparison between Pitot tube and hot-wire measurements revealed, that the Pitot tube results, viz. the mean velocity readings in the buffer and overlap region and hence κ and B, even after an explicit turbulence correction, are consistently higher then those from hot-wire measurements. Although the differences are small, they were substantially larger when not corrected for the effect of turbulence. Zanoun (2003), who did similar observations, also found that "the larger the Pitot probe the larger the κ-value".

The mentioned experimental results have been re-evaluated by Nagib & Chauhan (2008) in terms of composite profiles, thereby applying the same criteria to all collected data sets. While for ZPG TBL flows they obtain 0.384 for the von Kármán constant, channel flow data (albeit insufficient in Reynolds number) indicate a value of around 0.37.[22] Their extracted value for pipe flows was already mentioned and is around 0.41, however they note that the Superpipe data (despite the issue with the turbulence correction) "is not fully consistent with the trends from the lower Re[ynolds number] results based on other experiments and DNS." Hence, they conclude: "Without the Superpipe data, it may be tempting to conclude for a universal von Kármán constant around 0.38. This would be good news for modeling of turbulence if our only focus is equilibrium flows." This is an important point, since from a theoretical point of view there is reason to admit differences between internal and external flows, not only due to the presence of a (albeit weak) pressure gradient in the former case, but also the fact that TBL flows are spatially developing flows in contrast to the fully developed pipe and channel flows. Similar concerns were already raised by Prandtl (1932), who noted that the log law constants were extracted based on Nikuradses pipe flow experiments, and that a ZPG TBL flow would have an approximately 2 % lower value of the von Kármán constant.[23] Hence, there seems to be no physical argument, to expect why the log law constants should be much different from those of channel and ZPG TBL flows, when the latter two seem to agree closely.[24]

[22]The value extracted for ZPG TBL flows got also unexpected support from (George 2007), who admits, that "theoretical arguments notwithstanding, the log 'law' also appears to apply to developing boundary layers. [...] And to the degree that developing boundary layers can be described this way, the value of κ for them is approximately 0.38."

[23]Based on the experiments in convergent and divergent channels of Nikuradse (1929), Prandtl estimates a value of $\kappa = 1/2.545$ for a ZPG flow, compared to the value of $1/2.495$ extracted for pipe flows.

[24]This is more dramatically expressed in Spalart (2006): "If κ is different in these two flows, I'll quit!"

3.4. The overlap region: Open issues

The review in the previous sections revealed, that the debate is centred around the question whether a log law or a power law description is the appropriate scaling law for the overlap region. Among those, who favour the log law description, the value of the constants is another issue. A more fundamental, and related question is, however, whether the constants are universal, i.e. Reynolds number and flow case independent. In the following some of the open issues—and we will restrain ourselves mainly to the log law—will be summarised and discussed.

3.4.1. *If there is a log law, where is it?*

As apparent from the debate within the last decade, the overlap region, in which scaling laws are thought to be valid, does not have clear boundaries. While the classical log law constants were extracted from fits to the overlap region starting as close to the wall as $y^+ = 30$, this limit has been shifted away from the wall, since the debate arose. Similarly, the upper limit has no fixed value, which brings along a certain subjectivity into the debate regarding the scaling within the overlap region. A survey of classical and new textbooks on turbulence as well as some of the aforementioned research papers reveals the diversity, as apparent from table 1.

A number of terms exists, for one and the same region, therefore it is necessary to explain, how the values in the table come about. Since the overlap layer/region is also denoted as the inertial sublayer, intermediate layer, fully turbulent layer, constant stress layer, logarithmic layer, logarithmic sublayer, and turbulent inner region, the values in table 1 are those which are associated with the region in which a logarithmic description of the mean streamwise velocity component is thought to be situated.[25]

While the beginning of the log law region is given in all references, the upper limit is often not clearly stated and therefore hard to extract. The lower limit for the log law region resides between 30 and 100 wall units, while the upper limit is around 10 and 20 % of the channel height, pipe radius or boundary layer thickness. It is also interesting to note that the German literature, especially those written by students or descendants of Prandtl and Schlichting have a consistently higher lower limit than those in the English literature.[26] Moving over to the more recent research papers, a trend towards higher y^+ values for the beginning of the log region as well as a larger scatter in the upper limit is apparent. This would seemingly support the need for a mesolayer situated

[25] Furthermore, some of the listed references (e.g. Pope 2000) distinguish between the overlap and log law region.

[26] Note that although Rotta is listed as a student of Prandtl, he did not graduate or receive a degree. However, for simplicity he is listed here as a student of him, due to the influence Prandtl had on him. His extraordinary carrier, is probably best illustrated through the fact that his turbulence textbook, is still the only one available in the German language.

Author(s) (Year)	Log-layer		Flow	Remarks
	$y^+ >$	$\eta <$		
Tennekes & Lumley (1972)	30	0.1	G	(a)
Pope (2000)	30	0.1	G	(b)
Bernard & Wallace (2002)	30	0.1	G	
Mathieu & Scott (2000)	30	0.15	G	
White (1991)	30	0.2	G	
McComb (1992)	30	0.2	G	
Kundu & Cohen (2004)	30	0.2	G	
Bradshaw *et al.* (1981)	30–40	0.1–0.2	G	
Piquet (1999)	30–40	0.2	G	
Davidson (2004)	40	0.2	G	
Tietjens (1970)	50	0.1	G	(c)
Cebeci & Cousteix (2005)	50	0.1–0.2	G	(d)
Prandtl (1965)	50–100		G	
Rotta (1962, 1972)	60		G	(c)
Truckenbrodt (2008)	60		G	(e)
Gersten & Herwig (1992)	70		G	(e)
Schlichting & Gersten (2006)	70		G	(f)
Herwig (2008)	70	0.175	G	(g)
Coles (1954)	50	0.2	B	
Perry *et al.* (2001)	100	0.1	P	
Jones *et al.* (2004)	100	0.15	B	
Monty (2005)	100	0.15	C&P	
Zanoun *et al.* (2003)	150	0.15–0.75	C	(h)
Österlund *et al.* (2000*b*)	200	0.15	B	(i)
Nagib *et al.* (2007)	200	0.15	B	
George (2007)	300	0.1	G	(j)
Zanoun *et al.* (2007)	300	0.2	P	
Zagarola & Smits (1998*b*)	600	0.07	P	(k)
McKeon *et al.* (2004)	600	0.12	P	(k)

TABLE 1. Region in which the log law is valid or in which the log law constants are determined—in general (G), for ZPG TBL (B), channel (C) and pipe (P) flows—according to various textbooks and research groups . (a) $\kappa = 0.4$, but asymptotes against 1/3 at high Reynolds number, (b) overlap region: $50 < y^+ < 0.1\ \eta$, (c) student of L. Prandtl, (d) linear sublayer + buffer layer = viscous sublayer, (e) student of H. Schlichting, (f) unchanged since Schlichting (1951), (g) descendant of H. Schlichting, (h) upper limit increases with Re_τ, (i) where η is based on δ_{95}, (j) inertial sublayer described by a power (B) and log law (C&P), (k) with a power law region for $y^+ < 600$.

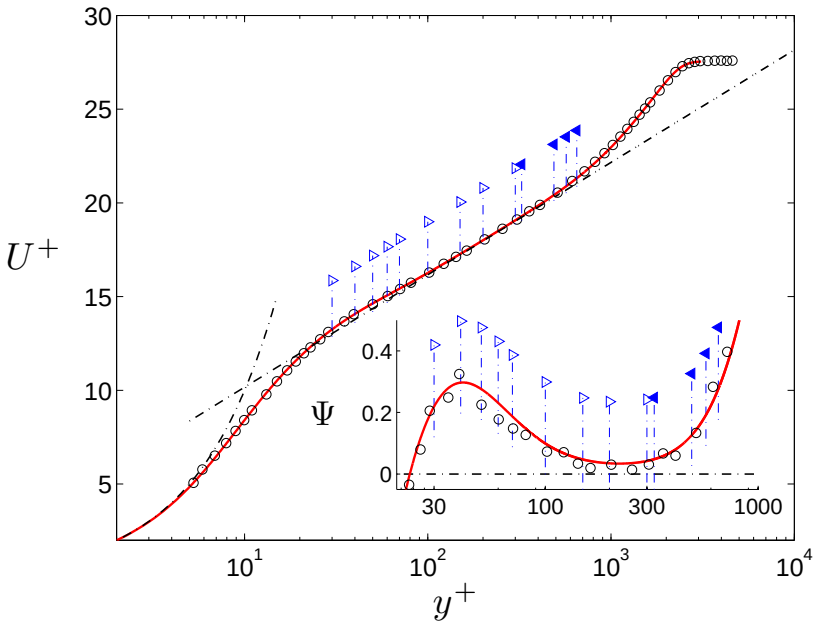

FIGURE 3.4. Schematic of the logarithmic region according to various sources. ○: ZPG TBL experiments by Örlü (2009*a*) at $Re_\theta = 8105$. —: Composite profile by Chauhan *et al.* (2009), ▷ & ◀: begin & end of logarithmic region (cf. table 1). Deviation from the log law, Ψ, is depicted in the insert. The linear and logarithmic profile with $\kappa = 0.384$ and $B = 4.17$ is indicated through the dash-dotted lines.

between the buffer and overlap region, between $30 < y^+ < 300$, in which "the scaled Reynolds stress and mean flow equations retain a Reynolds number dependence" (George & Castillo 1997).[27] Although the mesolayer concept, has not had that much acceptance within the "log law community", some (e.g. Zanoun & Durst 2009) recently used the term mesolayer for the region in which they did not observe a logarithmic scaling, viz. $30 < y^+ < 150$. It should, however, be noted, that Zanoun & Durst (2009) do not ascribe a Reynolds number dependence to their mesolayer region, as it should be, but rather introduce it for practical reasons, viz. in order to avoid the region in which their Pitot tube measurements (despite corrections) overestimate the mean velocity.[28]

[27] "In effect, without admitting it, they [i.e. the log law advocates] have conceded the existence of the mesolayer." (George 2006)

[28] So for instance, notes Zanoun (2003): "However, the fitting process only considered data from $y^+ = 150$ for channel and from $y^+ = 200$ for pipe to avoid the overshoot in U^+".

The different limits for the log law region are illustrated in figure 3.4, where a ZPG TBL at sufficiently high Reynolds number, in order for the log law to be present (at least for most of the given limits), is depicted. The deviation from the log law with $\kappa = 0.384$ and $B = 4.17$ (which is the one given by Chauhan *et al.* (2009) and inherent in the used composite profile) is emphasised in the insert. It goes without saying, that the choice of the log law limits will have a strong influence on the extracted log law constants, as already mentioned by Österlund *et al.* (2000*b*) and demonstrated by Monty (2005). The presence of the overshoot, compared to the log law within the buffer region, which is also present in DNS of channel, pipe and ZPG TBL flows (cf. Örlü 2009*c*), is one of the main reasons why earlier studies had consistently higher log law constants, than those mentioned in the previous section, and why they display a Reynolds number dependence in the log law "constants".

To demonstrate the effect of the listed log law limits on the extracted constants, the profile shown in figure 3.4 as well as the composite profile fit through the experimental data were employed to extract κ and B. The reason to employ the composite profile fit is, that—despite the relatively good resolved profile—the number of measurement points within the overlap region is rather limited, especially for the more narrow limits. Note, however, that many of the earlier investigations had less measurement points, anticipating thereby the inaccuracy in the determined constants. For the following (demonstrative) analysis, the composite profile had around four order of magnitudes more logarithmically spaced "measurement" points than its experimental counterpart, and therefore serves as a check for the sensitivity to the number of measurement points within the overlap region.

Table 2 shows the extracted log law constants depending on their lower and upper limits in which the log law is thought to reside. The values were computed by fitting the inner-scaled log law with variable κ and B in a least-squares method to the data points. As expected, a shift in the lower and upper limits of the log law region away from the wall results in a clear reduction of both constants, and *vice versa*. Hence, depending on where the log law should represent the data well, the coefficients will vary considerably. This explains to a great extent the scatter in the reported log law constants, particularly at low to moderate Reynolds numbers, as already pointed out by von Kármán (1934), who notes "For the velocity distribution near to the wall $\kappa = 0.40$ checks the experiments better, for the velocity distribution in greater distance from the wall $\kappa = 0.38$ fits better".

The extracted values also reveal, that a log law is strictly speaking not present (at least for the profile shown in figure 3.4), since κ and B vary continuously and do not become invariant to the selected overlap region; this suggests a curvature in the semilogarithmic plot. This can also be observed from the insert in figure 3.4, where no horizontal plateau is apparent, needed for a logarithmic region to be present. The reason for this may be, that either the

	$\eta <$	0.1		0.15		0.2	
$y^+ >$		κ	B	κ	B	κ	B
30	EXP	0.403	4.84	0.399	4.73	0.391	4.53
	CP	0.403	4.86	0.394	4.60	0.385	4.32
40	EXP	0.405	4.92	0.399	4.76	0.390	4.49
	CP	0.402	4.84	0.393	4.56	0.383	4.25
50	EXP	0.401	4.79	0.396	4.63	0.386	4.35
	CP	0.400	4.77	0.390	4.47	0.381	4.15
60	EXP	0.399	4.72	0.393	4.55	0.383	4.24
	CP	0.397	4.69	0.388	4.39	0.379	4.06
70	EXP	0.397	4.65	0.391	4.47	0.381	4.13
	CP	0.395	4.60	0.386	4.31	0.377	3.97
100	EXP	0.391	4.44	0.385	4.25	0.373	3.83
	CP	0.389	4.41	0.381	4.12	0.371	3.75
150	EXP	0.383	4.15	0.377	3.94	0.361	3.31
	CP	0.384	4.21	0.376	3.90	0.365	3.46
200	EXP	0.384	4.20	0.375	3.86	0.356	3.04
	CP	0.381	4.08	0.371	3.71	0.359	3.20
300	EXP	–	–	0.369	3.61	0.340	2.25
	CP	0.374	3.83	0.362	3.31	0.348	2.62

TABLE 2. Extracted log law constants depending on the chosen lower and upper limits of the logarithmic region. Values extracted from the experimental data points and composite profile fit, shown in figure 3.4, are indicated through EXP and CP, respectively. CP contains around 10^4 times more data points than EXP, and demonstrates therefore the insensitivity to the number of observations within the selected overlap region.

overlap region is not described by a log law, or the wake part is too strong and consequently penetrates into the overlap region. The latter is supported by the fact that the wake parameter, Π, for the shown profile is higher than its equilibrium value defined by Chauhan *et al.* (2009) (cf. Örlü 2009*a*).

3.4.2. *How to extract the log law constants?*

The notion of universal log law constants brought about, that the skin friction was extracted from a fit to the law of the wall, be it by means of the Clauser

chart method or a Preston tube. Consequently, the extracted friction velocity made the velocity profile seemingly to agree with the log law over the range in which the overlap region was believed to be situated. Since, the revival of the debate, more "sensitive" techniques have been proposed and utilised in order to extract the log law constants or more generally to test whether a power or log law describes the overlap region the best. Nevertheless, it can still be found that the friction velocity is extracted from the log law with classical log law constants, whereupon the obtained inner-scaled velocity profile is utilised to confirm the classical log law coefficients (DeGraaff & Eaton 2000; Knobloch 2008).[29]

Figure 3.5 utilises two velocity profiles, one from a ZPG TBL flow (Österlund *et al.* 2000*b*) and another from a pipe flow experiment (McKeon 2003). While the former has been utilised to confirm the validity of the log law with κ around 0.38 (Österlund *et al.* 2000*b*) for $200 < y^+ < 0.15\ \delta^+$, the latter has been employed to confirm a Reynolds number independent power and log law for $50 < y^+ < 300$ and $600 < y^+ < 0.12\ R^+$, respectively. The three mentioned scaling laws as well as the classical log law (Coles 1968) are given as well and illustrate the close resemblance of the velocity profiles, despite their utilisation for confirming quite differing scaling laws. Furthermore the figure demonstrates, that simple U^+ vs. y^+ plots can not be used to confirm the validity of scaling laws nor to show that certain constants are representing the data well.

A straightforward way to determine the log law constants is the employment of the log law itself, as for instance done by Monty (2005). Similarly, the indicator function, $\Xi = y^+ \mathrm{d}U^+/\mathrm{d}y^+ = 1/\kappa$, can be plotted against y^+, and for the case that a logarithmic velocity profile is present, a constant value, i.e. a horizontal line corresponds to $1/\kappa$ (Österlund *et al.* 2000*b*).[30] Another alternative would be to consider the natural logarithm of the velocity gradient, i.e.

$$\xi = \ln(\mathrm{d}U^+/\mathrm{d}y^+) = \ln(1/\kappa) - \ln y^+ \,,$$

which—when plotted against $\ln y^+$—should follow a straight line from which $1/\kappa$ can be extracted (Zanoun 2003). All three methods have in common, that it has to be decided *a priori* over which range the constants are going to be determined from a fit. While the employment of the log law determines

[29] DeGraaff & Eaton (2000), however, remark that, "[a]lthough it would be circular to attempt to prove the law of the wall with data that is scaled by fitting the law of the wall, there are two independent confirmations which suggest that u_τ is well estimated by the log law fit. [...] [T]he measurements of U^+ vs. y^+ in the sublayer agree very closely with the prediction $U^+ = y^+$." The latter argument—not seldom used—does have a hatch, namely, it presumes, that a wrongly deduced friction velocity would display itself in the viscous sublayer. That this is, in fact not the case, at least when plotted in semi-logarithmic form, can easily be demonstrated (see e.g. Örlü 2009*c*, figure 1(a)).

[30] The same or inverse quantity is also frequently denoted as the "diagnostic function" or the "Kármán measure".

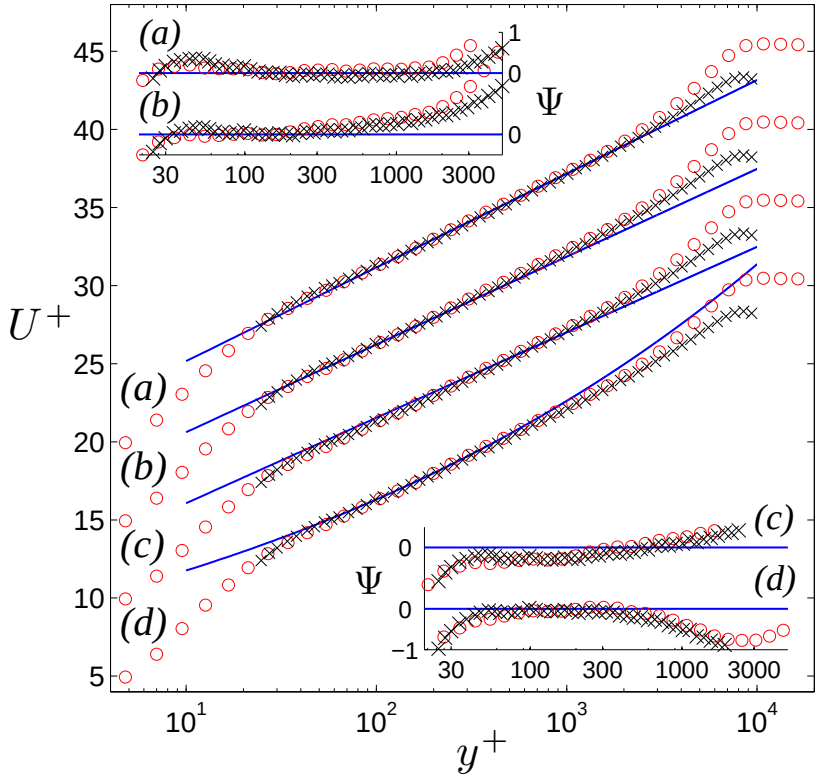

FIGURE 3.5. Comparison of various mean velocity scaling laws demonstrated on ZPG TBL and pipe flow profiles at around $Re_\tau \approx 9000$. ZPG TBL (○) at $Re_\theta = 26612$ (*SW981008A*) from Österlund (1999) and pipe (×) flow at $Re_\tau = 8536$ (*41086E1_SP*) from McKeon (2003). Log law with (a) $\kappa = 0.384$ and $B = 4.17$, (b) $\kappa = 0.41$ and $B = 5.0$, (c) $\kappa = 0.421$ and $B = 5.60$, and (d) power law with $\alpha = 8.48$ and $\beta = 0.142$. The deviation from the respective law is given in the inserts. Respective mean velocity profiles are shifted by 5 u_τ for clarity.

κ and B simultaneously, i.e. in one step, the methods utilising the indicator function as well as the natural logarithm of the velocity gradient, determine κ only. Once, the latter has been determined, the deviation from the log law,

$\Psi = U^+ - 1/\kappa \ln y^+$, can be utilised to extract the additive constant, viz. $\Psi = B$.[31]

Although, theoretically, all three methods are based on the log law, and should hence be identical in their results, they emphasise different parts of the overlap region, which can—due to the discrete and mostly logarithmically spaced experimental data points—lead to different results. To illustrate this, a ZPG TBL profile under equilibrium conditions with $\kappa = 0.384$ and $B = 4.17$ for $Re_\tau = 10000$ has been generated through utilisation of the composite velocity profile by Chauhan *et al.* (2009). For the purpose of demonstrating the effect of various methods as well as numerical schemes to extract the log law constants a random noise with an peak to peak amplitude of $\pm 0.0125\ u_\tau$ was added to the computed logarithmically spaced velocity profile. Figure 3.6 depicts the use of the continuous and (noisy) discrete velocity profile, in order to see the deviation from the log law (a), the indicator function (b), and the natural logarithm of the velocity gradient (c). Also given are their asymptotic values (dashed line).[32]

While in all three methods, the discrete (noisy) velocity profile follows closely the trend of the continuous (exact) profile, the differences between the three methods become apparent. While the region in which the overlap region is to be defined is clearly illustrated in (a) and (b), the double logarithmic plot in (c) makes it difficult to extract this information.

Following the procedure in the preceding section, the log law constants are now extracted for a variety of limits for the overlap region. The results are given in table 3, where κ and B is given as determined from the log law directly, or from the indicator function and the natural logarithm, respectively, together with the deviation from $1/\kappa \ln y^+$, from which the additive constant has been determined. It can clearly be seen that the log law constants are not only dependent on the defined overlap region, but especially on the method used to extract the constants. Various numerical schemes have been tested, e.g. to compute the velocity gradient, or to obtain the fitting parameters, however the trends remained. The results from the final evaluation, those shown in table 3, have been performed as close as possible to the original source, i.e. data sets of ($\ln y+$, U^+) have been used in order to obtain linearly spaced measurement points in $\ln y^+$ (Monty 2005; Spalart *et al.* 2008) and a three point scheme proposed by (Grossmann & Roos 1994) has been used to compute the velocity gradient as done by Buschmann & Gad-el-Hak (2003*a*) and Zanoun (2003).

[31] Similarly κ can be determined from the skin friction relations based on the log law (Österlund *et al.* 2000*b*; Nagib *et al.* 2007), which avoids the necessity to define a overlap region. Consequently, the log law region in the mean velocity profile, can be obtained through κ obtained from the skin friction relation.

[32] Note, that the additive constant approaches its predetermined value in the limit of high Reynolds numbers, which explains the slight deviation in figure 3.6(a) from $\Psi = 4.17$.

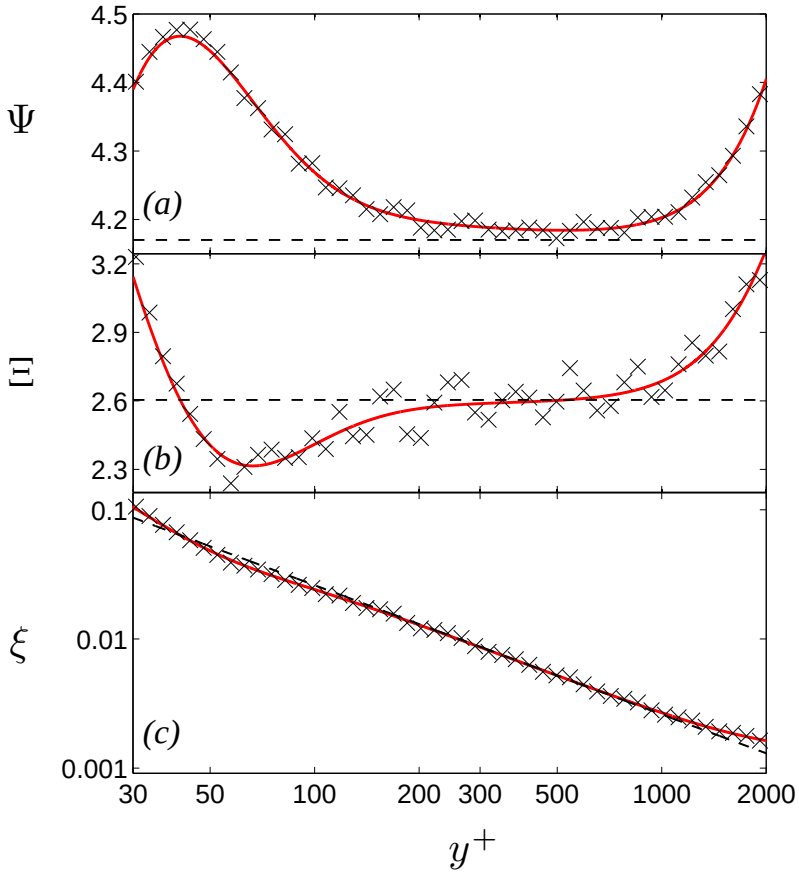

FIGURE 3.6. Comparison between extraction methods to dedude the log law constants. Zero pressure-gradient turbulent boundary layer under equilibrium conditions (with predefined $\kappa = 0.384$ and $B = 4.17$) generated through the composite profile by Chauhan *et al.* (2009) for $Re_\tau = 10000$. Continuous (—) and discrete (×) representation of the composite velocity profile, whereas the latter was superposed with random noise of amplitude $\pm 0.0125\ u_\tau$. (a) Deviation from the log law, Ψ, (b) indicator function, Ξ, and (c) natural logarithm of the velocity gradient, ξ. The asymptotic value of B or $1/\kappa$ is given through the dashed line.

To ensure that the extracted values for the log law constants are self-consistent, the log law in inner scaling, equation 3.14, can easily be transformed to obtain

	$\eta <$	0.1		0.15		0.2	
$y^+ >$		κ	B	κ	B	κ	B
	(a)	0.397	4.72	0.394	4.62	0.391	4.53
30	(b)	0.371	3.78	0.371	3.76	0.371	3.75
	(c)	0.390	4.47	0.387	4.36	0.381	4.17
	(a)	0.395	4.64	0.392	4.53	0.388	4.40
50	(b)	0.416	5.33	0.416	5.37	0.416	5.41
	(c)	0.396	4.65	0.391	4.51	0.385	4.28
	(a)	0.392	4.51	0.389	4.39	0.385	4.27
70	(b)	0.415	5.30	0.415	5.34	0.415	5.38
	(c)	0.393	4.55	0.389	4.40	0.382	4.15
	(a)	0.388	4.36	0.385	4.24	0.381	4.10
100	(b)	0.397	4.70	0.397	4.71	0.397	4.73
	(c)	0.387	4.33	0.383	4.17	0.376	3.89
	(a)	0.385	4.21	0.381	4.05	0.376	3.85
200	(b)	0.386	4.27	0.385	4.25	0.385	4.25
	(c)	0.382	4.12	0.378	3.93	0.370	3.56
	(a)	0.383	4.14	0.378	3.93	0.372	3.66
300	(b)	0.385	4.21	0.383	4.17	0.382	4.14
	(c)	0.381	4.06	0.376	3.83	0.366	3.38

TABLE 3. Extracted log law constants depending on the chosen lower and upper limits of the logarithmic region as determined from the log law (a), the indicator function (b) and the natural logarithm of the velocity gradient (c). Hereby the latter two methods utilised the deviation from $1/\kappa \ln y^+$ to determine B.

$$\kappa = \frac{\ln y^+_{\log}}{U^+_{\log} - B}\,, \tag{3.22}$$

which relates κ to B for a pair of $(y^+_{\log}, U^+_{\log})$ values from the overlap region. Assuming the log law with (κ, B)=(0.384, 4.17) to be valid, a single "measurement" point from the overlap region suffices to obtain a curve on which the extracted κ and B values have to lie. Equation (3.22) is related to the empirical relation given by Nagib & Chauhan (2008), which relates κB to B for various pressure gradient flows, although equation (3.22) gives this relation for any logarithmic region, independent of the pressure gradient. It is surprising that a simple algebraic manipulation, as equation (3.22), can represent the variety

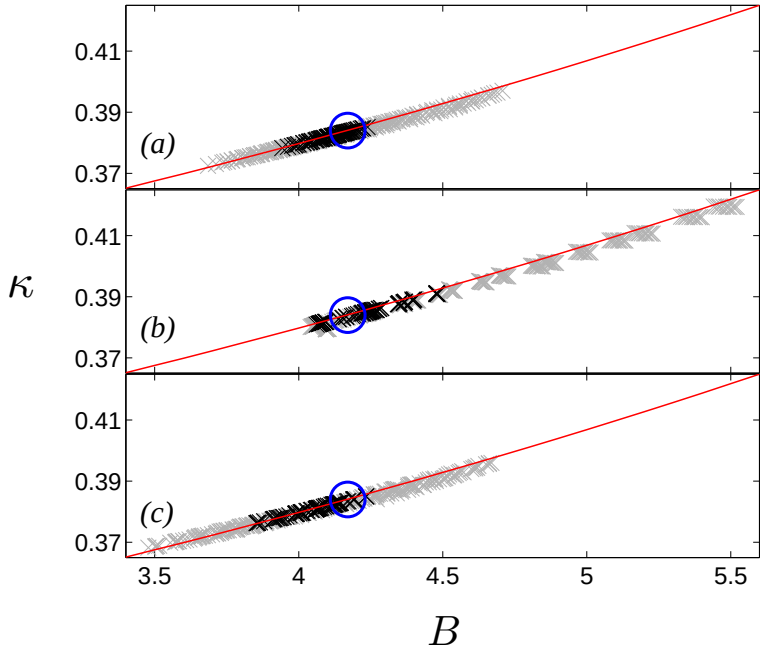

FIGURE 3.7. Consistency check for the extracted log law constants from (a) the log law, (b) the indicator function and the deviation from the log law, and (c) the natural logarithm of the velocity gradient and the deviation from the log law. Constants extracted for 30:10:300 $< y^+ <$ 0.1:0.01:0.2 Re_τ and 150:10:300 $< y^+ <$ 0.15:0.01:0.2 Re_τ are shown through $\times$ and $\times$, respectively, whereas equation (3.22) with $(y^+_{\log}, U^+_{\log}) = (300, 19.02)$ as well as $(\kappa, B) = (0.384, 4.17)$ are given through — and $\circ$, respectively.

of log law constants even for strong pressure gradient flows to an acceptable accuracy.[33]

Figure 3.7 shows the extracted values from the three aforementioned methods, together with the analytical line given through equation (3.22). It is apparent, that while all of the extracted values for the log law constants are fairly consistent with the log law, the extracted constants differ between the three

[33] The empirical correlation given by Nagib & Chauhan (2008) reads $\kappa B = 1.6[\exp(0.1663B) - 1]$ and is fairly well represented by an expression derived from the log law, $\kappa B = B(U^+_{\log} - B)^{-1} \ln y^+_{\log}$.

tested methods. The differences are substantial, when recalling that the statistical uncertainty for κ and B is not seldom given with values below $\pm$ 0.005 and 0.1, respectively. The dark symbols in figure 3.7 are from the overlap region with a lower limit above $y^+ = 150$, and illustrates that even with the more recent lower limit for the log region, a variation between the methods of the order of the mentioned error bars remains. It is also interesting to note, that the method employed by Zanoun *et al.* (2003, 2007), shown in (c), from which the lowest log law constants were reported, gives consistently lower log law constants, particularly when compared with the indicator function, shown in (b).

3.4.3. *What else matters?*

3.4.3a. *The absolute wall position.* It is widely accepted that mean quantities within the inner region of wall-bounded turbulent flows scale on viscous units. Having said that, it consequently follows, that the mean velocity has to be scaled by the friciton velocity and the wall-normal distance by the viscous length scale. While the importance of an independent and/or direct measure of the skin friction has already been discussed, the possibility of a wrongly measured or deduced wall position has not been considered in the literature.

A review on commonly used measurement techniques to determine the wall position in experimental studies, given in Örlü (2009*c*), has shown that the accuracies vary within an order of magnitude. Furthermore, the possibility of deflections of the measurement instruments has generally not been considered. Despite a number of known post-processing methods to deduce (or correct for) the absolute wall position, a number of pecularities has been shown to exist. The linear velocity profile for the streamwise velocity component has, for instance, been applied for wall positions, where it does not even provide an engineering approximation. Similarly, the Taylor expanded linear profile has been calibrated against low Reynolds number DNS and applied to experiments to higher Reynolds numbers. The law of the wall as well as analytical descriptions from the wall to the overlap region or the entire profile have been utilised to determine the friction velocity as well as wall position. Although shifts in the absolute wall position become less important further away from the wall, these have an influence on integral parameters, but also effect the extracted log law constants whenever the lower, i.e. classical, log region limits are used.

3.4.3b. *Spatial resolution issues.* While searching for the best description of the velocity profile (not only its mean quantity) one is confronted with the dilemma that for low Reynolds numbers the overlap region has either not established itself or is too short to determine the scaling law and its constants or parameters without being fouled by the experimental scatter. The need for high Reynolds numbers is hence desirable to ensure a well defined and long

enough overlap region to test the offered and available scaling laws and to determine their constants with high accuracy. The drawback, at least for most laboratory facilities is, however, that with increasing Reynolds number, the viscous scale becomes smaller, which in turn lets the sensing element to appear larger. Only few laboratories can provide both a high Reynolds number and large enough small scales, so that their measurability is ensured or at least that their neglection does not alter the measurements. Promising results, albeit still with large scatter, are becoming available from atmospheric boundary layers, which outreach available laboratory high Reynolds numbers experiments by orders of magnitude. On the other hand joint "gigantic" laboratory experiments are under construction, to allow both, high Reynolds numbers, by keeping the smallest scales large enough so that the measurement sensors are not exceeding them in size by orders of magnitude. For the time being, however, high Reynolds numbers are in most facilities achieved by decreasing the viscous length scale. As long as the scaling of the mean velocity is of interest and not the turbulence intensity or spectral scaling, spatial resolution has generally been disregarded.

However, Örlü (2009*b*) has demonstrated that a careful examination of ZPG TBL flow experiments, reveals a detectable influence of the hot-wire sensor length on the mean streamwise velocity component. Particularly, spatial averaging was found to reduce the mean streamwise velocity over the entire buffer region. Hence, attention should be paid to hot-wire data from high Reynolds number facilities, were the high Reynolds numbers are associated with relatively small viscous length scales. Similarly, conclusions about the influence of viscosity above $y^+ > 30$ (the beginning of the classical overlap region or the mesolayer advocated by others), should bear in mind, that variations in the mean velocity, do not have to be related to Reynolds number effects, but could also be associated to spatial resolution effects. Furthermore, the viscous scaled length of the hot-wire probes, should be given, even if only the mean velocity is reported, in order to enable a distinctions between possible Reynolds number or spatial resolution effects.

3.4.3c. *Pitot-tube corrections.* The previous sections have emphasised that Pitot tubes overestimate the mean velocity, when compared to hot-wire measurements. Although, an explicit turbulence correction, was reported to reduce the overestimated velocity readings, the Pitot tube results are still found to be higher than those from hot-wires. Consequently, the same note on caution as for spatial resolution issues in hot-wire measurements, is also valid for Pitot tube measurements. The effect of the various turbulence corrections on the extracted log law constants is two order of magnitudes higher than the uncertainties given for κ, i.e. while tolerance intervals of the order of ± 0.001 are often given, the effect of an explicit turbulence corrections is on the order of ± 0.1. Unfortunately, despite a number of advances in pressure based velocity measurements

a point raised by von Kármán more than eight decades ago (see Knight *et al.* 1922), is still a challenge for today's turbulence community: "Measuring instruments such as the Pitot tube, should be standardized [...]. Unfortunately [...], the speed [...] measured is not a true expression, depending, as it does, on the magnitude of the vibrations or the so-called degree of turbulence."[34]

3.4.3d. *Canonical flows and their pseudo counterparts.* Scaling laws for mean and Reynolds stress components are primarily tested in canonical wall-bounded turbulent flows, i.e. fully developed internal flows and equilibrium ZPG TBL flows. Although the search for scaling laws for these canonical flows has bothered minds over the last decades, there seems to be no consensus on what requirements have to be fulfilled in order to consider a particular flow as a canonical flow. The development length in pipe and channels, the aspect ratio in channels and the height of the bounding surface (the ceiling) for ZPG TBL flows are only some of the open issues, which are still being under debate. Depending on which criteria one utilises to categorise certain experiments or DNS in channel, pipe and ZPG TBL flows, it is possible to end up with a different set of data for canonical wall-bounded flows. This is particularly true for the equilibrium ZPG TBL, where a number of well-known DNS and experiments, that do not fulfil classical Coles (1968) and/or recent (Chauhan *et al.* 2009) criteria, are still being in use to test scaling laws for canonical flows. Even for the most simulated case, the channel, DNS results differ from each other within the buffer region.

3.4.3e. *Convergence of statistical quantities.* In the case of experiments, it is generally ensured to have a sufficient long sampling time, in terms of large scale turnover times. With the discovery of large and very long structures in wall-bounded turbulent flows, be it in TBL flows (Hutchins & Marusic 2007*a*) or internal flows (Monty *et al.* 2007), the issues of sampling time may need to be revisited. The length of these very long structures varies and values up to 25 channel heights, pipe radii or 20 boundary layer thicknesses have been reported. Whether or not DNS is capable of discovering these very long structures in short simulation boxes is an open issue. Some experiments at high Reynolds numbers are also restricted in time (due to running costs, like the measurements in the DNW tunnel by Fernholz *et al.* 1995) restricting the sampling time by an order of magnitude compared to generally accepted values (Klewicki & Falco 1990), nevertheless these data sets have extensively been used for scaling arguments of mean but also Reynolds stress components.

3.5. The overlap region: Concluding remarks

The mentioned topics have pointed out a number of problems in the debate regarding the proper scaling of the mean velocity profile within the overlap region.

[34] Emphasised by von Kármán.

There is a need for standardisation of methods and evaluation methods, or at least a common language within wall-bounded turbulent flow research, in order to give terms like "sufficient long development length", "sufficient long sampling time", "large enough aspect ratio", "fully developed flow", "equilibrium conditions", "spatial resolution effects are negligible", "turbulence corrections were applied", "near-wall correction were applied", "wall position was accurately measured", "friction velocity was deduced from the Clauser method", "friction velocity was deduced from a fit to the log law within the overlap region", and many more a quantitative meaning (similar efforts have been pursued more than eight decades ago, see e.g. Knight *et al.* 1922). A first step towards this direction is for instance the joint effort around the CICLoPE project (Talamelli *et al.* 2009), where different groups (KTH (Alfredsson), IIT (Nagib), Melbourne (Marusic), Princeton (Smits)) performed measurements in ZPG TBL flows in three different facilities [35] employing a variety of hot-wire probes and anemometers as well as Pitot tubes in order to validate the measurement techniques and facilities.

For the time being, it seems therefore advisable to exclude the region below $y^+ < 150$–200 when considering the scaling within the overlap region for reasons mentioned above (spatial resolution issues, Pitot tube and wall position uncertainties, etc.). The variety of diagnostic tools and numerical methods employed have been shown to have a non negligible effect on the extracted log law constants and should therefore be stated explicitly. The employment of hypothesis tests, extensively used in other branches of natural sciences, does not seem to have found usage in the debate regarding the preference of various scaling laws in wall-bounded turbulent flows. Similar debates are taking place in various areas dealing with empirical data (see e.g. Goldstein *et al.* 2004; Clauset *et al.* 2009), and problems with logarithmically spaced data and least-squares methods seem to have been treated in these areas in a time when the turbulence community confirmed log law constants by looking at mean velocity profiles. It is hence clear, that curve fitting will not suffice and more advanced techniques are needed, at least for the time being until "better", i.e. larger, experimental facilities, like the long pipe at CICLoPE, start to operate.

[35] These are the *Minimum Turbulence Level* (MTL) wind tunnel at KTH in Stockholm, the *National Diagnostic Facilty* (NDF) at IIT in Chicago, and the *High Reynolds Number Boundary Layer Wind Tunnel* (HRNBLWT) at the University of Melbourne.

CHAPTER 4

Experimental set-up and techniques

"A theory is something nobody believes,
except the person who made it.
An experiment is something everybody believes,
except the person who made it."

Albert Einstein (1879–1955)

The following chapter gives a short overview over the experimental facilities and set-ups in which the experiments of the following thesis have been performed together with the experimental techniques employed to study the quantities of interest. Since the relevant details for a particular investigation are given in the respective papers, the following sections will suffice with superficial summaries of the main features of the used experimental rigs and give a reasoning for the choice of the employed measurement techniques.

4.1. Experimental facilities

4.1.1. *Excited Jet facility*

The project related to the study of transitional modes in axisymmetric jets, was a short time one, and that is why most of the equipment has been borrowed from other experimental facilities, and does therefore not necessarily present the best choice. The facility, located at the *Fluid Physics Laboratory* of the *Linné Flow Centre* at *KTH Mechanics* in Stockholm, shown in figure 4.1, consists of a round jet facility and the excitation equipment. The jet rig itself, has been in use as a hot-wire calibration facility for several years (see Facciolo 2003; Örlü 2006, for details). Due to the need to have a disturbance free laminar top-hat profile, the fan was placed 8 m away from the stagnation chamber (**A**), to which it was connected through a plastic pipe. A distribution chamber, situated directly downstream the fan, was interposed in order to reduce the transmission of vibrations generated by the fan. Furthermore, the stagnation chamber was equipped with 7 valves for the fine adjustment of the mass flow through the pipe connected to the stagnation chamber, as well as to vary the turbulence level at the exit of the nozzle. A 1.5 m long glass pipe, in which a honeycomb (**B**), consisting of drinking straws, was placed, ends finally with

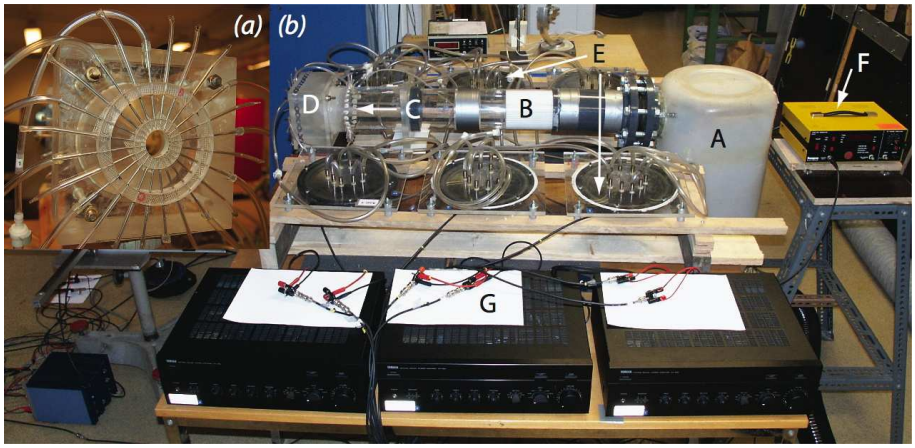

FIGURE 4.1. Excited jet facility. (a) Front view of the nozzle with excitation rig, consisting of 24 equally spaced flush mounted (excitation) holes. (b) Top view of the excited jet facility. **A)** Stagnation chamber, **B)** honeycomb, **C)** 24 equally spaced flush-mounted (excitation) holes, **D)** nozzle, **E)** loudspeakers, **F)** signal generator, and **F)** amplifiers.

a nozzle of contraction ratio of 16:1 (**D**). Screens or sponges, have not been used for the present investigation, since they have been found to increase the turbulence intensity, but also to cause an asymmetry in the the radial velocity component across the nozzle exit.

Preliminary, it was intended to excite the flow upstream the nozzle, i.e. within the straight pipe section, through 24 flush mounted metal tubes **(C)**, however, it was found, that the acceleration through the nozzle contraction was too strong for the disturbances to survive. Nevertheless, the affixed metal tubes were found useful for flow visualisation studies, where only the circumference of the jet was intended to be visualised. Instead, the excitation was imparted to the flow at the nozzle lip, by adding a 10 mm long pipe section to the 25 mm diameter nozzle exit. The short straight plexiglass tube section is equipped with 24 perpendicular aligned metal tubes, that are also flush mounted to the inner pipe surface, as shown in figure 4.1(a).

The excitation has been imparted on the initially laminar flow at the nozzle exit in order to generate two opposite helical modes ($m = \pm 1$) in such a way that a standing wave pattern is formed (Kundu & Cohen 2004, chap. 7). If N acoustic sources are planned to be used, the amplitude of the i:*th* source of the m:*th* mode, A_i^m, can be described as

$$A_i^m(t) = A \sin(\omega_i^m t + \Delta\phi_i^m) , \tag{4.1}$$

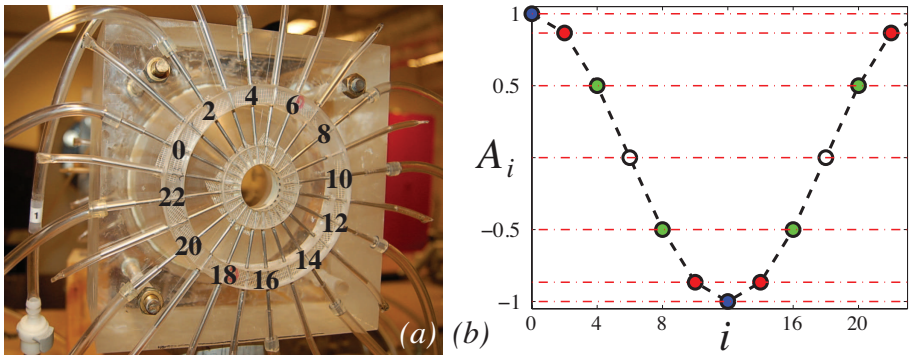

FIGURE 4.2. Excitation scheme. (a) Close up of the excitation rig, together with the hole number, that corresponds to a certain (b) amplitude modulation for the generation of two opposing helical modes, i.e. $m = \pm 1$.

where ω and $\Delta\phi$ denote the angular frequency and phase shift, respectively. With equidistantly arranged excitation sources, the general expression for the combination of two opposite waves is given by a linear superposition of the sources, so that (**?**)

$$A_i = A_i^m(t) + A_i^{-m}(t) = 2A\cos\left(\frac{2\pi m}{N}i\right)\sin(\omega t)\ , \tag{4.2}$$

where the first part of the right-hand side is an amplitude modulation, and the second part represents the temporal variation of the excitation in the i:*th* source. Hence, it is possible to generate a pair of helical modes ($m = \pm 1$) by means of a single signal generator (F), three amplifiers (G), and six loudspeakers (E), when 12 excitation holes are deemed to be sufficient to generate a standing wave pattern of sufficient resolution, as illustrated in figure 4.2.

4.1.2. *Rotating pipe facility*

The passive scalar mixing study in swirling jet flows was performed in the rotating pipe facility located at the *Fluid Physics Laboratory* of the *Linné Flow Centre* at *KTH Mechanics* consists of a 100 pipe diameters long axially rotating pipe. The rotating pipe apparatus, shown in figure 4.3, was designed, built and taken into operation in connection with the work of Facciolo (2006), where the effect of rotation on turbulent pipe and jet flows was investigated. A few modifications on the experimental facility made it possible to extend the focus of investigation from the dynamics of the flow to include the mixing of a passive contaminant.

FIGURE 4.3. Experimental setup showing the pipe mounted within the triangular shaped framework and fed into the stagnation chamber covered by an elastic membrane.

Figure 4.4 shows the modified experimental apparatus schematically. Air at ambient temperature is provided by a centrifugal fan **(A)** with a butterfly valve for flow rate adjustment, which is monitored through the pressure drop across an orifice plate **(B)** inserted in the air supply pipe. A distribution chamber **(D)** to reduce the transmission of vibrations generated by the fan follows. From there the air stream is distributed into three different spiral pipes, which are symmetrically fed into the stagnation chamber **(E)**, consisting of a honeycomb, in order to distribute the air evenly. One end of the cylindrical stagnation chamber is covered with an elastic membrane in order to further reduce the pressure fluctuations as apparent from figure 4.3. A bell mouth shaped entrance first leads the air into a one meter long stationary section, which is connected to the rotating pipe **(K)** through a rotating coupling **(F)**. In the first section of the rotating part of the pipe a 12 cm long honeycomb **(G)**, consisting of drinking straws of a diameter of 5 mm, is mounted which brings the flow into more or less solid body rotation. The inner diameter of the pipe amounts 60 mm whereas the wall thickness is 5 mm. The 6 m long pipe is made of seamless steel and has a honed inner surface with a roughness of less than 5 micron, according to manufacturer specifications. It is supported along its full length by 5 ball bearings **(J)**, which are mounted within a rigid triangular shaped framework. The pipe is belt driven via a feedback controlled DC motor **(H)**, which is capable to run the pipe up to rotational speeds of 2000 rpm. The pipe flow emanates as a free (swirling) jet **(M)** 1.1 m above the floor into the

ambient air at rest. By placing the apparatus in a large laboratory with a large ventilation opening more than 60 pipe diameters downstream of the pipe outlet it is ensured that the jet can develop far away from any physical boundaries. In the present measurements the pipe ends with a 30 cm diameter circular end plate **(L)**.

It is worth mentioning that many previous experimental studies (among others the often cited work by Wygnanski & Fiedler (1969), that became a benchmark and standard reference for both turbulence modellers as well as experimentalists) failed to fulfil the equations believed to govern the flow (see e.g. George 1990). As evinced by Hussein *et al.* (1994) the discrepancies between existing experimental results concerning the far field are more facility-related and not mainly due to the measurement techniques involved. They showed, for instance, that for Wygnanski & Fiedler's data the jet is rather a confined jet in a finite environment, for which conservation of mass demands that a return flow be set up around the outer edge of the facility. The return flow hinders the jet so that the experiment no longer represents a jet in a free environment. Here, however, we are only interested in the near field of the jet, so that despite the moderate distance to the floor ($\sim$ 18 pipe diameters) the jet can be safely considered to be a free jet.

As mentioned above an orifice flow meter is used to monitor the pipe flow rate. The pressure difference across the orifice is measured by a pressure transducer, that was calibrated against hot-wire measurements performed with a single-wire probe in the cold jet at different mass flow rates. Thus the voltage of the pressure transducer is directly related to the axial bulk velocity and hence the Reynolds number, which is based on the bulk velocity and pipe diameter. Such an extensive calibration is not needed for the aim of the investigation presented here, because only measurements at one particular Reynolds number ($Re_D \simeq 24000$) were acquired. Nevertheless it was beneficial to know the deviation from the desired Reynolds number for changes due to variations in the thermophysical quantities. Furthermore the effect of Reynolds number on the axial decay of mean and root mean square values of the streamwise fluctuation was studied by means of LDV (results are not shown here) in collaboration with Facciolo (2006).

To introduce a passive scalar in laboratory shear flows the jet or the pipe wall has to be heated weakly. To heat and maintain a heated rotating pipe at a certain temperature difference above ambient temperature would be an elaborate task. The related boundary conditions of either a uniform surface heat flux or a uniform surface temperature would also yield a 'saddle-back' temperature profile (i.e. the highest temperature would be at the pipe wall rather than in the centre of the pipe) of the jet which is evolving contrary to the streamwise velocity component in the near-field of the jet. Thus it is more advantageous to heat the air before entering the rotating pipe, which is done by placing an electrical heater **(C)** in the flow upstream of the distribution

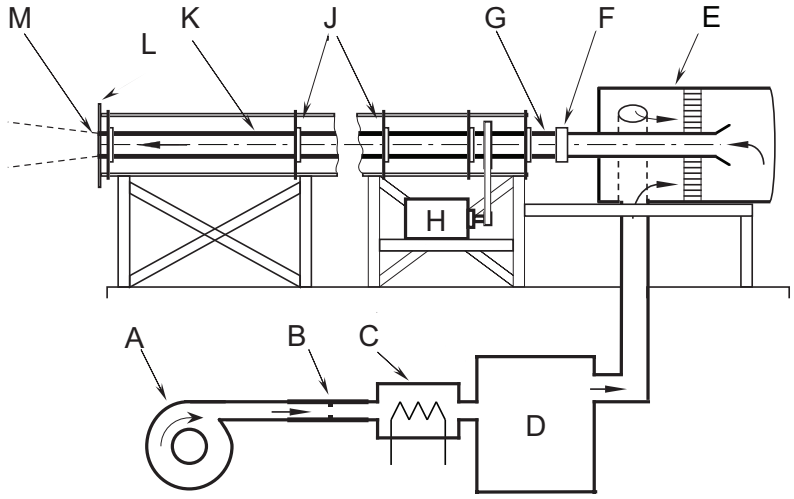

FIGURE 4.4. Schematic of the experimental setup. **A)** Centrifugal fan, **B)** flow meter, **C)** electrical heater, **D)** distribution chamber, **E)** stagnation chamber, **F)** coupling between stationary and rotating pipe, **G)** honeycomb, **H)** DC motor, **J)** ball bearings, **K)** rotating pipe, **L)** circular end plate, and **M)** Pipe outlet.

chamber. The heater power can be regulated and is typically around 800 W, which in consideration of the heat losses determines the temperature at the pipe outlet to be around 12 K above ambient temperature at the pipe outlet. This corresponds to approximately 250 W and the rest is heat losses to the environment. To check furthermore that the installation of the electrical heater does not alter the flow field and its turbulence structure the virtual identity of the power spectral density functions of the streamwise velocity fluctuations were ensured at the pipe outlet.

Preliminary measurements of the temperature profile with thermocouples showed that to reach and maintain a steady temperature difference of 12 K between the flow in the centre of the pipe and the ambient air requires approximately three hours. By insulating the entire outer pipe surface with a 15 mm foam material the time to reach steady state conditions was drastically reduced as can be evinced through figure 4.5, which depicts the temperature evolution in the pipe flow during the heating process. To reduce the time needed to reach the desired operation temperature the heater was operated at 1000 W until the temperature at the centre of the pipe outlet corresponds nearly the desired temperature and then reduced to 800 W, which yields an excess temperature

of approximately 12 K. Due to the ventilation far away from the pipe outlet the ambient temperature remains quite stable. Deviations of the order of 0.1 K occur hardly within an operational time of 24 hours. The temperature evolution at the pipe outlet (solid line) on the other hand clearly emphasises the quality of the experimental setup, i.e. it provides a constant temperature (within the measurement resolution of the thermocouples of 0.1 K) after approximately one hour.

An additional advantage of the insulation is that it flattens the radial temperature profile compared to the uninsulated case and provides a wide area of the pipe outlet with a constant temperature and low temperature fluctuations, which will be exploited as a calibration jet for the temperature sensitive measurement probe.

To ensure that effects due to free convection can safely be neglected the *Grashof* number,

$$Gr_D = \frac{g\beta\theta D^3}{\nu^2} \tag{4.3}$$

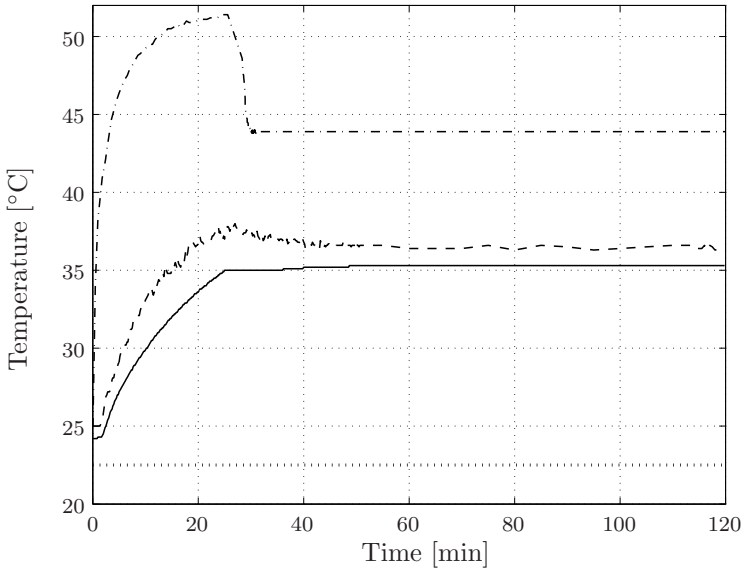

FIGURE 4.5. Thermocouple measurements of the temperature evolution during the heating procedure at different locations for the non-rotating pipe: ambient (dotted line), heater box (dash-dot line), pipe inlet (dashed line) and centre of the pipe outlet (solid line).

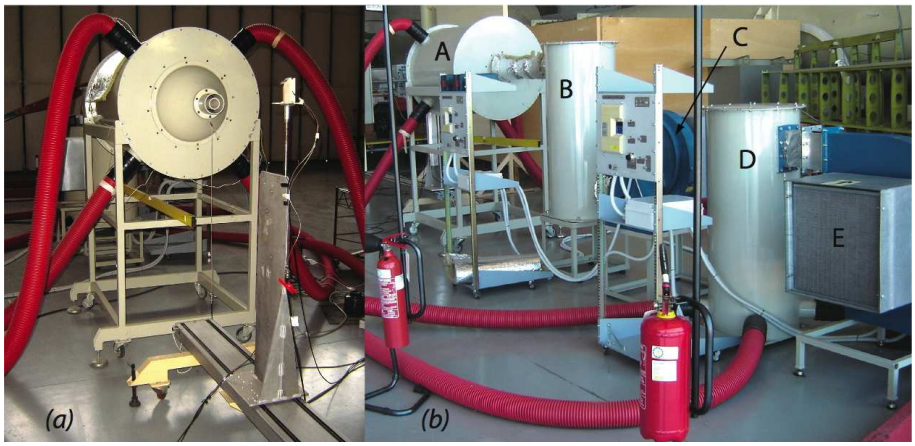

FIGURE 4.6. Coaxial Air Tunnel (CAT) facility at the University of Bologna. (a) Front view of the settling chamber and the used 2D traversing system, (b) Side view of the entire facility. **A)** Settling chamber **B)** inner jet pre-settling chamber, **C)** inner jet blower, **D)** outer jet pre-settling chamber, and **E)** outer jet blower.

indicating the ratio of buoyancy force to the viscous force, has to satisfy the inequality $(Gr_D/Re_D^2) \ll 1$.[1] With a maximal excess temperature of 12 K the left hand side of the inequality is less than 0.01 and hence the temperature can be assumed to act only as a passive contaminant.

4.1.3. *Coaxial jet facility*

The experiments concerning the mixing and passive control of coaxial jet flows were carried out in the *Coaxial Air Tunnel* (CAT) facility in the laboratory of the *Second Faculty of Engineering* at the *University of Bologna* in *Forlí*. The facility, schematically shown in figure 4.6, is composed of two independent centrifugal blowers (**A** and **B**) equipped with three-phase motors. Two pre-settling chambers (**C** and **D**) are placed downstream the blowers to reduce the disturbances from the blowers. Four plastic hoses (**J**) connect the outer jet pre-chamber to the corresponding settling chamber to increase the symmetry of the flow, while a simple diverging pipe (**E**) connects the inner one. Flow conditioning is performed by means of three screens and a honeycomb (**H**)

[1] If density variations are due to temperature variations only, which is assumed in the present case, the volumetric thermal expansion coefficient, β, can—for ideal gases—be expressed as the inverse of the absolute film temperature.

in the inner pipe as well as five screens and a honeycomb on the outer circuit. The inner and outer contraction ratios are 11:1 and 16.5:1, respectively, whereas the inner and outer coaxial nozzles, of exit diameter $D_i = 50$ mm and $D_o = 100$ mm, end with two straight pipes of 100 mm length (**K**). The experimental facility is placed in a large laboratory and the exit of the coaxial jet is far enough from surrounding walls and the floor, ensuring that the experimental results reported here resemble a jet in an infinite environment (cf. appendix B of Hussein *et al.* (1994)).

One of the features of the facility is, that it allows the inner seperating duct to be changed easily. The main investigation was concerned with the possibility to utilise the vortex shedding phenomenon behind a thick inner separating wall to control the near-field of the coaxial jet flow. For that particular reason a 5 mm thick inner duct wall ending in a rectangular shape was employed. The absence of the vortex shedding was instead studied by employing a sharp trailing edge. Additionally, an identical thick separating wall was equipped with cylindrical roughness elements, in order to check whether stable laminar streaks could be generated within the coaxial jet nozzle, which could avoid the vortex shedding at the blunt nozzle exit.

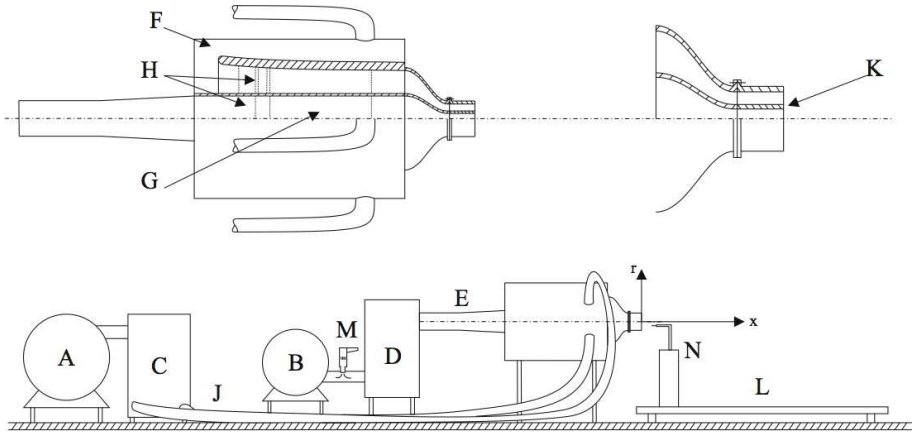

FIGURE 4.7. Schematic of the Coaxial Air Tunnel (CAT) facility at the University of Bologna. **A)** outer jet blower, **B)** inner jet blower, **C)** outer jet pre-settling chamber, **D)** inner jet pre-settling chamber, **E)** inner jet diffuser, **F)** outer jet settling chamber, **G)** inner jet settling chamber, **H)** screens and honeycombs, **J)** outer jet hoses, **K)** close-up of the jet exit with the thick separating wall, **L)** axial traversing, **M)** heat gun, and **N)** radial traversing.

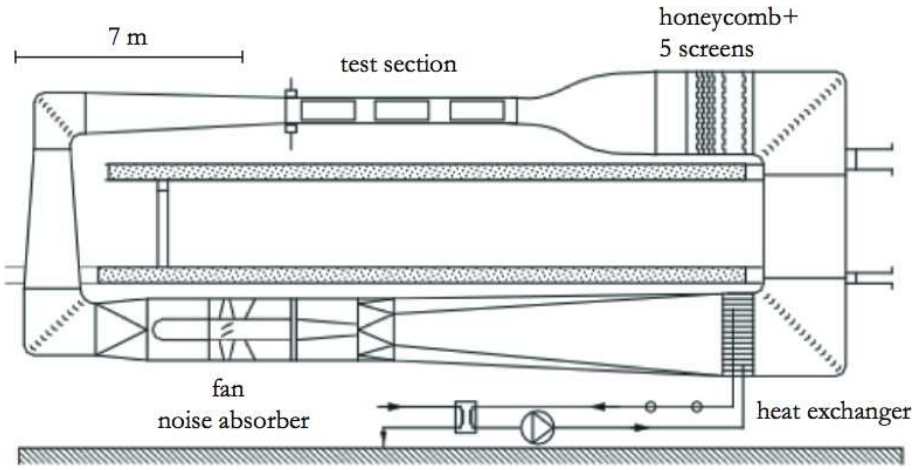

FIGURE 4.8. Schematic of the Minumum Turbulence Level (MTL) wind tunnel at KTH Mechanics. The test section has a cross sectional area of 0.8 m (high) × 1.2 m (wide) and is 7 m long

Another feature of the facility is due to its two separate intakes for the inner and annular jet, thereby enabling independent control of the streams, their flow characteristics as well as temperatures. The temperature difference inside the pre-settling chambers of the inner or outer jet has been introduced by means of a heat gun (**M**) or electrical resistors placed at the inlets of the inner jet pre-settling (**D**) and outer jet settling chamber (**F**), respectively. The amount was kept small in such a way that the temperature can be considered as a passive scalar and is still large enough to ensure a high temperature resolution. A series of experiments have been performed with the inner or outer jet heated in order to study the passive scalar mixing between the two coaxial streams and the annular stream and its surrounding ambient air, respectively.

4.1.4. *MTL wind tunnel*

The flat plate zero pressure-gradient turbulent boundary layer experiments were performed in the *Minumum Turbulence Level* (MTL) windtunnel, schematically shown in figure 4.8, at the *Fluid Physics Laboratory* of the *Linné Flow Centre* at *KTH Mechanics*. The experimental set up is quite similar to the one used by Österlund (1999). Both, the flow quality of the MTL as well as the set up for the ZPG TBL experiments, have been documented previously by Lindgren & Johansson (2002) and Österlund (1999), to which the reader is

referred to. The details of the present set up and a documentation of the flow quality as well as the characteristics of the established equilbrium ZPG TBL is documented in Örlü (2009*a*).

4.2. Measurement techniques

4.2.1. *Hot/Cold-wire anemometry*

While all of the aforementioned experimental facilities were primarily designed to study the dynamics of the particular flow cases, the swirling and coaxial jet flows were also studied regarding their passive scalar mixing characteristics. The instantaneous velocity and temperature signals were thereby of primary importance. The need to resolve the velocity fluctuations temporally and spatially to a high degree leads—despite few alternatives—inevitably to the employment of hot-wire anemometry. As its literal meaning suggests, hot-wire anemometry, refers to the exploitation of an electrically heated wire to measure the speed of wind. In spite of the fact that hot-wire anemometry is mainly dated back to King (1914), many scientists before him were familiar with the fact that a heated wire with temperature dependent resistance exposed in an air flow can be exploited to measure the fluid velocity.[2]

The detecting element of a hot-wire anemometer consists of a tiny tungsten or platinum (or its alloys) wire acting as the fourth arm of a Wheatstone bridge, heated by an electrical current, that responds to changes in velocity and temperature of the fluid around the wire.[3] If the primary interest is the temperature, and not the velocity, it is common to denote the same hot-wire probe, as a cold-wire or resistance wire probe. The first practically functioning hot-wire anemometers consisted of about 10 cm long wires with diameters of a few tenths of a millimetre, whereas today platinum wires down to fractions of a micron in diameter in form of Wollaston wires are available. However due to robustness and operational issues standard probe sizes around 1 mm in length and a few micron in diameter are common in turbulence measurements.

The body on literature is huge[4] and the reader is referred to classical textbooks, like those by Perry (1982), Lomas (1986) or Bruun (1995) or more recent accounts, as that given in Tropea *et al.* (2007), for an account on the operation and limitations of hot-wire anemometry.

[2]According to Comte-Bellot (1976) King himself in a 1915 issued paper mentions preliminary experiments conducted by Shakespear in 1902, whereas Fingerson (1994) refers to a work by Dulong and Petit from 1817 as being the first. However, the latter source, seems rather to deal with the physical mechanism of heat losses from heated bodies, rather than its application as an anemometer.

[3]The influence of humidity on hot-wire measurements can also be explored to measure humidity, which has been exploited in early atmospheric boundary layer studies (see e.g. Paeschke 1935, one of Prandtl's student).

[4]Fingerson & Freymuth (1996) mentions a number of over 2500 publications up to 1992 related to thermal anemometry techniques.

The different time and length scales in the various mentioned flow cases as well as geometrical constraints, besides the different aims in the studies, made it necessary to employ a variety of hot-wire probes. Standard and boundary layer type as well as X-wire probes were built and used for velocity measurements, whereas combined X-wire and cold-wire probes, besides single cold-wires were used for thermal field investigations. While most probes utilised fully etched and soldered wires, partially etched as well as welded ones were utilised as well. Additionally, *DANTEC* single and X-wires were also employed. The design and hot-wire building procedure is to some extent outlined in Örlü (2006), to which the interested reader is referred to.

Depending on the velocity range and importance of the low velocity region, the wires were either calibrated against a Prandtl tube or the static pressure drop of a high contraction ratio nozzle. Single wire probes were either calibrated by means of the standard (Bruun 1995, chap. 4) or modified (Johansson & Alfredsson 1982) King's law, respectively, or higher order polynomial relations (George *et al.* 1989). Regardless of which relation was used, the voltage at zero velocity was always included in the calibration procedure. For X-wire probes, either a tedious look-up table (Österlund 1999) was created or, in the case of robust probes, the modified King's law or a higher order polynomial was used, where in the latter case the yaw response was computed using a sum and difference method (Bruun 1995, chap. 5) with experimentally determined calibration coefficients. All hot-wires were operated in constant temperature anemometry (CTA) mode, either by means of a *DANTEC StreamLine* or an *AA-lab AN-1003* hot-wire anemometry system. While for the jet flow experiments the calibration took place at the exit of a nozzle in a top-hat laminar jet, for the boundary layer experiments the free stream (potential flow) of the wind tunnel was utilised.

Cold-wires were always calibrated against thermistor thermocouples and a linear relationship between the temperature and the signal from the constant current anemometer (CCA) were found to represent the calibration curves over the temperature range of interest. The anemometer used was always an *AA-lab AN-1003* system and details about the CCA settings as well as the temperature compensation scheme utilised can be found in Örlü (2006).

4.2.2. *Oil-film interferometry*

The friction velocity, is one of the most important quantities in wall bounded turbulent shear flows, since it is used to non-dimensionalise the velocities and Reynolds stresses as well as the distance from the wall with it. Consequently most of the observed phenomena in these flows and their associated length, velocity and time scales are often expressed in quantities, which are scaled by the friction velocity, i.e. wall units. This explains the urge to determine this quantity to high accuracy. A number of well-known techniques, have been employed over the last decades, of which some are reviewed in Winter (1977)

and Hanratty & Campbell (1996) and more recently by Naughton & Sheplak (2002), Rüedi *et al.* (2003), and Tropea *et al.* (2007), where the latter mentioned references also treat oil-film interferometry (OFI).

Oil-film interferometry can be described as the utilisation of Fizeau interferometry to measure the mean wall shear stress by means of the thinning rate of an oil film deposited on a surface and subjected to a bounding flow. Compared to other measurement techniques in fluid mechanics OFI has not received the attention it deserves, and this albeit its obvious advantages, viz. its direct and independent character, its low cost and relative simple application and processing. Despite being around for almost three decades, only within the last decade has it been employed in the study of canonical wall-bounded shear flows (Österlund 1999; Zanoun 2003; Nagib *et al.* 2004*a*), and it seems as it will become more accepted within the coming years, since it "is the most reliable method for accurate and direct measurement of mean skin friction" (Nagib *et al.* 2004*b*). The governing equations, a list of references as well as the equipment used in the present thesis can be found in Örlü (2009*a*).

4.2.3. *Flow visualisations*

Flow visualisations can be traced back to Leonardo Da Vinci, whos drawings, not only from an artistic point of view, fascinate (not only) today's fluid dynamicists. Although, in the authors experience, the best visualisations seem to appear after a long trial and error period of mostly random iterative steps, there are guidelines, which could have been read prior to the performed visualisation studies. The interested reader is referred to Merzkirch (1987) and Smits & Lim (2000) for a number helpful guidelines, and especially to the collection of fascinating flow visualisations, presented in Van Dyke (1982) and Samimy *et al.* (2004).[5]

Since all of the studies performed within the scope of this thesis were performed in clean air, i.e. to a great deal dust-free and of low humidity, it was necessary to make the flow visible. Therefore polyethylene glycol was used and evaporated to smoke by means of disco smoke generators. While a white light source is sufficient to visualise the entire flow field, it is common to utilise a laser sheet to "cut" the flow in order to access the plane of interest. A digital camera with a short shutter time, can be utilised to capture the instantaneous vortical structures embedded in the flow (and hence hidden for our eyes), whereas a long shutter time would give a time-averaged picture of the flow. With the emergence of high speed cameras, it is now possible to reveal sequences of snapshots, that let us have part (and joy) in the temporal and spatial evolution of these vortical structures. The extremely short shutter times, however,

[5]What would an experimentalist, who is mainly used to work with hot-wires do without these books, when it comes to illustrate to a nontechnical audience what his or her research is all about. A picture says more than 1000 traces from a hot-wire (at least to a nontechnical audience)!

make it necessary to employ high intensity lasers in order to provide sufficient exposure for the film or nowadays CCD. For the present study, white light and high intensity lasers were utilised in conjunction with high speed cameras. The lasers were either an argon/krypton ion laser (*University of Bologna*) or a dual-head, high-repetition-rate, diode-pumped Nd:YLF Pegasus PIV laser by New Wave (*KTH Mechanics*). The high speed cameras, on the other hand, are a NanoSense MkI camera (*University of Bologna*) and a Photron Fastcam APX RS (*KTH Mechanics*).

CHAPTER 5

Main contribution and Conclusions

The following chapter summarises the main contributions and conclusions the papers constituting Part II of the thesis. For the detailed summaries the reader is referred to the appended papers.

5.1. Mixing in swirling jet flows

- A new set of experimental data for the mixing of a passive scalar in the near-field of a swirling jet has been provided. For the first time can the differences between a swirling jet and its non-rotating counterpart directly and solely be associated to the effect of rotation, rather than the swirl generating methods.
- Addition of a moderate degree of swirl highly modifies the dynamic and thermal flow field of the jet in its near-field region to that effect that the swirling jet in comparison to its non-swirling counterpart spreads and mixes faster as well as increases momentum and heat transport. Albeit known, it can for the first time be associated to the addition of rotation and not only to the various intrusive swirl generators.
- The classical approach to quantify mixing, viz. the axial decay rate of the mean quantity and the turbulence intensity, is not sufficient. Furthermore, neither a high correlation coefficient, nor a high passive scalar flux, are necessarily related to a highly mixed state, since the latter has been found to be related to the engulfment of highly homogeneous "pockets" of ambient air.

5.2. Passive control in coaxial jets flows

- The experimental results confirm the theoretical study by Talamelli & Gavarini (2006), where it was suggested that the self-exciting temporally growing wake instability behind an inner thick wall in coaxial jets, may provide a continuous forcing mechanism for the passive control of the whole flow field.
- The 'locking phenomenon', which commonly is restricted to the dominance of the outer shear layers vortices over the inner ones, is found to be reversible and therefore open doors to apply flow control strategies on the inner nozzle wall.

- The general view that the vortices of the outer shear layer develop with a Strouhal number corresponding to the value predicted by linear stability analysis for the Kelvin-Helmholtz instability, has been revised to that respect, that, particularly in the presence of an absolute instability by means of the vortex shedding mechanism, the vortices of the outer shear layer develop with a Strouhal number corresponding to a value related to the vortex shedding frequency behind the inner separating wall.
- Vortex shedding from blunt coaxial jet inner duct walls can be utilised to increase the turbulence activity in both shear layers and hence the mixing between the two coaxial jet streams as well as the annular jet with the ambient fluid.

5.3. Oblique waves in transitional jets

- A new experimental set-up has been designed, where various types (both the frequency and spanwise periodicity can be varied) of wave disturbances can be generated on an axisymmetric jet.
- The disturbance development was followed through the evolution of the velocity spectra and confirms that the excitation has a strong impact on the evolution of the whole flow field with the imposed periodicity given by the excitation itself.
- For a certain frequency range a pair of oblique waves was found to reduce the turbulence although it was not possible to detect the presence of streamwise streaks that are a prominent feature of the oblique transition scenario in wall-bounded flows.

5.4. Equilibrium turbulent boundary-layer experiments

- A new set of experimental data from a zero pressure-gradient turbulent boundary layer supplemented by direct and independent skin friction measurements has been provided and are found to fulfil recently established equilibrium criteria.

5.5. Wall position in wall-bounded turbulent flows

- The expanded law of the wall to forth and fifth order with calibration constants determined from recent high Reynolds number DNS can determine the wall position to an accuracy of 0.1 and 0.25 ℓ_* when accurately determined measurements reaching $y^+ = 5$ and 10, respectively, are available.
- In the absence of data below the above given limits, commonly employed analytical functions and their log law constants, have been found to effect the determined wall position to a high degree.
- It has been shown, that near-wall measurements below $y^+ = 10$ or preferable 5 are essential in order to ensure a correctly measured or deduced absolute wall position.

- A number of peculiarities in concurrent wall-bounded turbulent flow studies, was found to be associated with a erroneously deduced wall position.
- Utilisation of the linear profile in turbulent flows with upper limits up to 7, 11 and 15, as utilised by a number of authors, overestimates the actual velocity up to 8, 20, and 40 %.
- Contrary to the general assumption, that the limiting behaviour of the relative turbulence intensity in wall-bounded turbulent flows is Reynolds number and flow case independent, both have been found to have an effect on the limiting "constant". For $Re_\tau > 2000$ the value for channel and ZPG TBL flows seem to converge asymptotically to the same value.
- While DNS of pipe, channel and ZPG TBL flows have been found to differ up to 0.5 u_τ as close as $y^+ = 30$ to the wall, a difference of 0.2 u_τ prevails even for channel flow DNS at around the same Reynolds number.
- The method proposed by Kendall & Koochesfahani (2008) to extract the friction velocity and absolute wall position, was found to be accurate within 1.5 % instead of 0.5 % in terms of the friction velocity, but is highly user dependent in the absence of measurement points within the viscous sublayer when it comes to the wall position.

5.6. Spatial resolution using hot-wire anemometry

- The viscous scaled hot-wire length, L^+, has been found to exert a strong impact on the pdf and hence its higher order moments over the entire buffer region and also the lower region of the classical log region. This range extends up to around y^+ of 150 for the range of parameters investigated here. For varying Reynolds numbers spatial resolution effects act against the trends imposed by Reynolds number effects.
- A systematic reduction of the mean velocity as a function of L^+ over the entire classical buffer region and beyond has been found. A reduction of around 0.3 u_τ has been deduced for $L^+ = 60$ compared to $L^+ = 15$. Neglecting this effect can lead to a seemingly Reynolds number dependent buffer or log region. This should be taken into consideration, for instance, in the debate, regarding the prevailing influence of viscosity above the buffer region at high Reynolds numbers.
- The debate concerning the universality of the pdf within the overlap region has been shown to be artificially complicated due to the ignorance of spatial resolution effects beyond the buffer region on the velocity fluctuations, but also due to the unawareness of spatial averaging on the mean velocity component.

CHAPTER 6

Papers and authors contributions

Paper 1

An experimental study of the near-field mixing characteristics of a swirling jet
R. Örlü (RÖ) & P. H. Alfredsson (HAL). *Flow Turbul. Combust.* **80**, 323–350.

This work is of experimental character on swirling jet flows and was published as part of the Licentiate thesis of RÖ. The experiments, the data analysis as well as the writing was done by RÖ with considerable help and supervision by HAL. Parts of these results have been published in:

> *A heated swirling jet emanating from a fully developed turbulent pipe flow*
> R. Örlü, P. H. Alfredsson, N. Tillmark, & A. Talamelli
> **Proc. 6$^{\text{th}}$ World Conference on Experimental Heat Transfer, Fluid Mechanics, and Thermodynamics**,
> 17 – 21 April 2005, *Matsushima, Miyagi, Japan.* (published on CD)

> *Passive scalar flux measurements in the near field of a swirling jet*
> R. Örlü & P. H. Alfredsson
> **Proc. 5$^{\text{th}}$ Baltic Heat Transfer Conference, Vol. 2, pp. 532–540.**
> 19 – 21 September 2007, *St. Petersburg, Russia.*
> Also selected for publication in **Heat Transf. Res. 39**, 597–607.

Paper 2

On the passive control of the near-field of coaxial jets by means of vortex shedding
R. Örlü (RÖ), A. Segalini (AS), P. H. Alfredsson (HAL), & A. Talamelli (AT)
Int. Conf. on Jets, Wakes and Separated Flows, ICJWSF–2, September 16–19, 2008, Technical University of Berlin, Berlin, Germany.

This work is of experimental character on coaxial jet flows and was performed in the *Coaxial Air Tunnel* (CAT) facility in the laboratory of the *Second Faculty of Engineering* at the *University of Bologna* in Forlí. The main part of the experimental work was conducted during a three month stay of RÖ at the *University of Bologna*, whereas the data analysis was performed by RÖ and AS. Supplementary measurements and flow visualisations were performed by AS. The writing was done by RÖ and AS, with comments from AT and HAL. Supplementary material and parts of this work have been published or accepted for publication in:

> *Passive control of mixing in a coaxial jet*
> R. Örlü, A. Segalini, P. H. Alfredsson, & A. Talamelli
> **Proc. 7$^{\text{th}}$ International ERCOFTAC Symposium on Engineering Turbulence Modelling and Measurements, Vol. 2, pp. 450–455.**
> 4 – 6 June 2008, *Limassol, Cyprus.*

> *On the passive control of the near-field of coaxial jets by means of vortex shedding*
> R. Örlü, A. Segalini, P. H. Alfredsson, & A. Talamelli
> **iTi Conference on Turbulence III,**
> 12 – 15 October 2008, *Bertinoro, Italy.* (in press)

> *Experimental study on the use of the wake instability as a passive control in coaxial jet flows*
> R. Örlü, A. Segalini, P. H. Alfredsson, & A. Talamelli
> **7$^{\text{th}}$ IUTAM Symposium on Laminar-Turbulent Transition**,
> 23 – 26 June 2009, *Stockholm, Sweden.* (in preparation)

Paper 3

The effect of oblique waves in transitional jets
R. Örlü, A. Segalini, P. H. Alfredsson, & A. Talamelli
This work is of experimental character on excited jet flows. The experiments and the data analysis were performed by RÖ together with AS, while AS visited *KTH Mechanics*. Supplementary flow visualisations were performed by RÖ. The writing was done by RÖ, with comments from AS, AT and HAL. Parts of these results have been published or accepted for publication in:

> *The effect of oblique waves on jet turbulence*
> A. Segalini, R. Örlü, A. Talamelli, & P. H. Alfredsson
> **iTi Conference on Turbulence III,**
> 12 – 15 October 2008, *Bertinoro, Italy.* (in press)

> *Effect of oblique waves on jet turbulence*
> A. Segalini, R. Örlü, A. Talamelli, & P. H. Alfredsson
> **7$^{\text{th}}$ IUTAM Symposium on Laminar-Turbulent Transition**,
> 23 – 26 June 2009, *Stockholm, Sweden.* (in preparation)

Paper 4

Low Reynolds number Zero Pressure-Gradient Equilibrium Turbulent Boundary-Layer Experiments
R. Örlü (RÖ)

This work is of experimental character on turbulent boundary layer flows. Parts of these results have been published or accepted for publication in:

> *The diagnostic plot — a new way for appraisal of turbulent boundary layer data*
> P. H. Alfredsson, R. Örlü, T. Kurian, J. H. M. Fransson, A. Segalini, J.-D. Rüedi, & A. Talamelli
> **12$^{\text{th}}$ EUROMECH European Turbulence Conference**,
> 7 – 10 September 2009, *Marburg, Germany.* (in press)

> *Turbulent Boundary Layers up to $Re_\theta = 2500$ studied through simulation and experiment*
> P. Schlatter, R. Örlü, Q. Li, G. Brethouwer, J. H. M. Fransson, A. V. Johansson, P. H. Alfredsson, and D. S. Henningson
> accepted for publication in **Phys. Fluids**.

Paper 5

On the determination of the wall position in wall-bounded turbulent flows
R. Örlü (RÖ)

This work is an continuation of Paper 4.

Paper 6

On spatial resolution issues on mean quantities using hot-wire anemometry
R. Örlü (RÖ)

This work is an continuation of Paper 4. Parts of these results have been accepted for publication in:

> *On imperfect hot-wire resolution issues and their effect on mean quantities*
> R. Örlü, J. H. M. Fransson, & P. H. Alfredsson
> **12$^{\text{th}}$ EUROMECH European Turbulence Conference**,
> 7 – 10 September 2009, *Marburg, Germany.* (in press)

Acknowledgements

This work was sponsored by the *Swedish Research Council* (VR) and the *Swedish Energy Agency* (STEM), within its energy related fluid dynamics program, which are both gratefully acknowledged. Furthermore the generous stipends from the *The Swedish Foundation for International Cooperation in Research and Higher Education* (STINT) for my stay at the University of Bologna as well as the travel stipends from the "Erik Petersohns Minne" are acknowledged as well.

The present thesis is the result of my graduate studies at the *Fluid Physics Laboratory* within the *Linné Flow Centre* at *KTH Mechanics*. Hence, the following lines of acknowledgment include not only those who contributed to the work described here, but also those who made the lab my second[1] home and contributed in one or another way to my understanding and development in various technical and non-technical areas.

Given the five years I have been working in the lab it seems impossible to list everyone. I will try anyway and hope that those who I forgot will stay assured that they are not unappreciated.

I would like to start to express my deep and sincere gratitude to my main supervisor, Prof. P. Henrik Alfredsson, for not only accepting me as his graduate student and supervising me over the years as well as sharing his expertise in fluid physics, but also for his cheerful enthusiasm and ever-friendly nature.

My second advisor, Dr. Nils Tillmark, is acknowledged especially for the support during the initial stage of my work and for the smooth handling of all kind of problems.

Thanks to Prof. Alessandro Talamelli, for spending nights with me in the lab solving LabView and hot-wire related issues, but also for making my stay in Italy so effective.

[1] Or "first" according to my family.

Professors Bengt Sunden, Lazlo Fuchs and Yvan Maciel in relation to the swirling jet project and Professors Ivan Marusic and Hassan Nagib as well as their co-workers are acknowledged for making the stay in Melbourne and Chicago from a scientific as well as cultural point of view exciting. Besides them, also Professors Lex Smits, Yoshiyuki Tsuji and Masaharu Matsubara and all co-workers are mentioned here for making the last year an enriching experience in connection with the measurement jamboree. Dr. Jean-Daniel Rüedi is in this context mentioned for interesting discussions regarding OFI and HWA.

Our former and present toolmakers, Marcus Gällstedt, Ulf Landén, Göran Rådberg and Joakim Karlström, deserve a special thank for being there whenever I had problems and giving me free hand in the work shop.

To Antonio Segalini for working side-by-side with me for more than a year and showing me Reggio Emilia. I have only one thing to say: Gracie mille!

My former office mates Luca and Davide, as well as my current one, Thomas, are thanked for making our office a place of positive energy. Also, thank you Thomas for working over months in shifts at the MTL with me and seeing over the mess in our office.

Doctors Fransson and Lundell are acknowledged for various non-technial and—together with Dr. Schlatter—technical discussions.

Many thanks to Bengt, Gabriele, Veronica, Olle (2x), Ola, Outi, Fredrik (2x), Malte and Florian as well as the entire stuff at the Department of Mechanics: *Tack ska ni ha!*

To my parents, brother and sisters: *Hakkinizi helal edin!*

Last but not least there are the ones who waited the most for this day to come: Wera and Bilal: *Was wäre ich ohne euch, eure Liebe, eure Unterstützung, Aufopferung und euer Verständnis!*

References

Abe, H., Kawamura, H. & Matsuo, Y. 2004 Surface heat-flux fluctuations in a turbulent channel flow up to $Re_\tau = 1020$ with $Pr = 0.025$ and 0.71. *Int. J. Heat Fluid Flow* **25**, 404–419.

Abell, C. J. 1974 Scaling laws for pipe flow turbulence. *Ph. D. thesis, University of Melbourne, Australia*.

Allen, J., Shockling, M., Kunkel, G. J. & Smits, A. J. 2007 Turbulent flow in smooth and rough pipes. *Phil. Trans. R. Soc. A* **365**, 699–714.

Andreas, E. L., Claffey, K. J., Jordan, R. E., Fairall, C. W., Guest, P. S., Persson, P. O. G. & Grachev, A. A. 2006 Evaluations of the von Kármán constant in the atmospheric surface layer. *J. Fluid Mech.* **559**, 117–149.

Angele, K., Kurimoto, N., Suzuki, Y. & Kasagi, N. 2006 Evolution of the streamwise vortices in a coaxial jet controlled with micro flap actuators. *J. Turbulence* **7**, 1–19.

Ashforth-Frost, S. & Jambunathan, K. 1996 Effect of nozzle geometry and semi-confinement on the potential core of a turbulent axisymmetric free jet. *Int. Comm. Heat Mass Transfer* **23**, 155–162.

Balarac, G. & Métais, O. 2005 The near field of coaxial jets: A numerical study. *Phys. Fluids* **17**, 065102.

Balarac, G., Métais, O. & Lesieur, M. 2007*a* Mixing enhancement in coaxial jets through inflow forcing: A numerical study. *Phys. Fluids* **19**, 075102.

Balarac, G., Si-Ameur, M., Lesieur, M. & Métais, O. 2007*b* Direct numerical simulations of high velocity ratio coaxial jets: mixing properties and influence of upstream conditions. *J. Turbulence* **8**, 1–27.

Barenblatt, G. I. 2004 Turbulent boundary layers at very large Reynolds numbers. *Russ. Math. Surv.* **59**, 47–64.

Barenblatt, G. I. & Chorin, A. 1998*a* New perspectives in turbulence: Scaling laws, asymptotics, and intermittency. *SIAM Review* **40**, 265–291.

Barenblatt, G. I. & Chorin, A. 1998*b* Scaling of the intermediate region in wall-bounded turbulence: The power law. *Phys. Fluids* **10**, 1043–1044.

Barenblatt, G. I., Chorin, A. & Prostokishin, V. 2000 A note on the intermediate region in turbulent boundary layers. *Phys. Fluids* **12**, 2159.

Batchelor, G. & Gill, A. 1962 Analysis of the stability of axisymmetric jets. *J. Fluid Mech.* **14**, 529–551.

Bayoumy, O. 2005 Fully developed turbulent smooth and rough channel and pipe flows. *Ph. D. thesis, University of Erlangen, Germany*.

Bernard, P. & Wallace, J. 2002 Turbulent flow: Analysis, measurement, and prediction. *Wiley*.

Bilen, K., Bakirci, K., Yapici, S. & Yavuz, T. 2002 Heat transfer from a plate impinging swirl jet. *Int. J. Energy Res.* **26**, 305–320.

Billant, P., Chomaz, J.-M. & Huerre, P. 1998 Experimental study of vortex breakdown in swirling jets. *J. Fluid Mech.* **376**, 183–219.

Blasius, H. 1913 Das Ähnlichkeitsgesetz bei Reibungsvorgängen in Flüssigkeiten. *Forschg. Arb. Ing.-Wesen, Heft 131* .

Boguslawski, L. & Popiel, C. 1979 Flow structure of the free round turbulent jet in the initial region. *J. Fluid Mech.* **90**, 531–539.

Bradshaw, P. 1967 The turbulence structure of equilibrium boundary layers. *J. Fluid Mech.* **29**, 625–645.

Bradshaw, P., Cebeci, T. & Whitelaw, J. H. 1981 Engineering calculation methods for turbulent flow. *Academic Press*.

Bradshaw, P. & Huang, G. 1995 The law of the wall in turbulent flow. *Proc. Math. Phys. Sci.* **451**, 165–188.

Bradshaw, P., Launder, B. E. & Lumley, J. L. 1992 Collaborative testing of turbulence models. *AIAA 1991-0215*.

Bradshaw, P., Launder, B. E. & Lumley, J. L. 1996 Collaborative testing of turbulence models. *J. Fluid Eng.* **118**, 243–247.

Braud, C., Heitz, D., Arroyo, G., Perret, L. & Delville, J. 2004 Low-dimensional analysis, using POD, for two mixing layer-wake interactions. *Int. J. Heat Fluid Flow* **25**, 351–363.

Broberg, K. 2004 Significance of morphology changes at a propagating crack edge. *Int. J. Fracture* **130**, 723–742.

Bruun, H. H. 1995 Hot-wire anemometry: Principles and signal analysis. *Oxford University Press Inc., New York, USA*.

Burattini, P., Antonia, R. A., Rajagopalan, S. & Stephens, M. 2004 Effect of initial conditions on the near-field development of a round jet. *Exp. Fluids* **37**, 56–64.

Buresti, G., Talamelli, A. & Petagna, P. 1994 Experimental characterization of the velocity field of a coaxial jet configuration. *Exp. Thermal Fluid Sci.* **9**, 135–146.

Buschmann, M. H. & Gad-el-Hak, M. 2003*a* Debate concerning the mean-velocity profile of a turbulent boundary layer. *AIAA J.* **41**, 565–572.

Buschmann, M. H. & Gad-el-Hak, M. 2003*b* Generalized logarithmic law and its consequences. *AIAA J.* **41**, 40–48.

Buschmann, M. H. & Gad-El-Hak, M. 2004 Comment on "Evaluating the law of the wall in two-dimensional fully developed turbulent channel" [Phys. Fluids 15, 3079 (2003)]. *Phys. Fluids* **16**, 3507–3508.

Carlier, J. & Stanislas, M. 2005 Experimental study of eddy structures in a

turbulent boundary layer using particle image velocimetry. *J. Fluid Mech.* **535**, 143–188.

Cebeci, T. & Cousteix, J. 2005 Modeling and computation of boundary-layer flows: Laminar, turbulent and transitional boundary layers in incompressible and compressible flows. *Springer, 2nd rev. ed.*

Chauhan, K. A., Monkewitz, P. A. & Nagib, H. M. 2009 Criteria for assessing experiments in zero pressure gradient boundary layers. *Fluid Dyn. Res.* **41**, 021404.

Chigier, N. A. & Beér, J. M. 1964 Velocity and static pressure distributions in swirling air jets issuing from annular and divergent nozzles. *J. Basic Eng.* **86**, 788–798.

Chigier, N. A. & Chervinsky, A. 1967 Experimental investigation of swirling vortex motion in jets. *J. Appl. Mech.* **34**, 443–451.

Cipra, B. 1996 A new theory of turbulence causes stir among experts. *Science* **272**, 951.

Citriniti, J. & George, W. K. 2000 Reconstruction of the global velocity field in the axisymmetric mixing layer utilizing the proper orthogonal decomposition. *J. Fluid Mech.* **418**, 137–166.

Clauser, F. H. 1954 Turbulent boundary layers in adverse pressure gradients. *J. Aero. Sci.* **21**, 91–108.

Clauset, A., Shalizi, C. & Newman, M. 2009 Power-law distributions in empirical data. *SIAM Review* (to appear).

Coles, D. E. 1954 The problem of the turbulent boundary layer. *ZAMP* **5**, 181–203.

Coles, D. E. 1956 The law of the wake in the turbulent boundary layer. *J. Fluid Mech.* **1**, 191–226.

Coles, D. E. 1968 The young person's guide to the data. *AFOSR-IFP-Stanford Conf. on Computation of turbulent boundary layers*, D. E. Coles and E. A. Hirst (Eds.), pp. 1–45.

Comte-Bellot, G. 1976 Hot-wire anemometry. *Annu. Rev. Fluid Mech.* **8**, 209–231.

Corke, T. & Kusek, S. 1993 Resonance in axisymmetric jets with controlled helical-mode input. *J. Fluid Mech.* **249**, 307–336.

Corke, T., Shakib, F. & Nagib, H. M. 1991 Mode selection and resonant phase locking in unstable axisymmetric jets. *J. Fluid Mech.* **223**, 253–311.

Craya, A. & Darrigol, M. 1967 Turbulent swirling jet. *Phys. Fluids* **10**, S197–S199.

Dahm, W., Frieler, C. & Tryggvason, G. 1992 Vortex structure and dynamics in the near field of a coaxial jet. *J. Fluid Mech.* **241**, 371–402.

Darrigol, O. 2005 Worlds of flow: A history of hydrodynamics from the Bernoullis to Prandtl. *Oxford University Press*.

Davidson, P. A. 2004 Turbulence: An introduction for scientists and engineers. *Oxford University Press*.

Dean, R. B. 1978 Reynolds number dependence of skin friction and other bulk flow variables in two-dimensional rectangular duct flow. *J. Fluid Eng.* **100**, 215–223.

DeGraaff, D. B. 1999 Reynolds number scaling of the turbulent boundary layer on

a flat plate and on swept and unswept bumps. *Ph. D. thesis, Stanford University, USA*.

DeGraaff, D. B. & Eaton, J. 2000 Reynolds-number scaling of the flat-plate turbulent boundary layer. *J. Fluid Mech.* **422**, 319–346.

Dimotakis, P. E., Miake-Lye, R. & Papantoniou, D. 1983 Structure and dynamics of round turbulent jets. *Phys. Fluids* **26**, 3185–3192.

Doherty, J., Ngan, P., Monty, J. P. & Chong, M. 2007 The development of turbulent pipe flow. *Proc. 16th Australasian Fluid Mech. Conf., Gold Coast, Queensland, Australia*, pp. 266–270.

Dziomba, B. & Fiedler, H. E. 1985 Effect of initial conditions on two-dimensional free shear layers. *J. Fluid Mech.* **152**, 419–442.

Eckert, M. 2006 The dawn of fluid dynamics: A discipline between science and technology. *WILEY-VCH*.

Eggels, J., Unger, F., Weiss, M. & Westerweel, J. 1994 Fully developed turbulent pipe flow: A comparison between direct numerical simulation and experiment. *J. Fluid Mech.* **268**, 175–209.

Elofsson, P. & Alfredsson, P. H. 1998 An experimental study of oblique transition in plane Poiseuille flow. *J. Fluid Mech.* **358**, 177–202.

Elofsson, P. & Alfredsson, P. H. 2000 An experimental study of oblique transition in a Blasius boundary layer flow. *Eur. J. Mech. B - Fluids* **19**, 615–636.

Elsner, J. & Kurzak, L. 1987 Characteristics of turbulent flow in slightly heated free swirling jets. *J. Fluid Mech.* **180**, 147–189.

Elsner, J. & Kurzak, L. 1989 Semi-preserving development of a slightly heated free swirling jet. *J. Fluid Mech.* **199**, 237–255.

Facciolo, L. 2003 Experimental study of rotating pipe and jet flows. *TeknL thesis, Royal Institute of Technology, Stockholm, Sweden*.

Facciolo, L. 2006 A study on axially rotating pipe and swirling jet flows. *Ph. D. thesis, Royal Institute of Technology, Stockholm, Sweden*.

Facciolo, L., Orlandi, P. & Alfredsson, P. H. 2005 Swirling jet issued from fully developed rotating pipe flow - experiments and numerics. *Proc. 4th Intl Symp. on Turbulence and Shear Flow Phenomena, Williamsburg, USA,* pp. 1243–1248.

Farokhi, S. & Taghavi, R. 1990 Modern developments in shear flow control with swirl. *Tech. Rep. Kansas University Center for Research, USA*, KU-FRL-724-4.

Farokhi, S., Taghavi, R. & Rice, E. 1989 Effect of initial swirl distribution on the evolution of a turbulent jet. *AIAA J.* **27**, 700–706.

Fernholz, H. H., Krause, E., Nockemann, M. & Schober, M. 1995 Comparative measurements in the canonical boundary layer at $Re_{\delta_2} \leqslant 6x10^4$ on the wall of the German–Dutch windtunnel. *Phys. Fluids* **7**, 1275–1281.

Ferrante, A. & Elghobashi, S. E. 2005 Reynolds number effect on drag reduction in a microbubble-laden spatially developing turbulent boundary layer. *J. Fluid Mech.* **543**, 93–106.

Feyedelem, M. & Sarpkaya, T. 1998 Free-and near-free-surface swirling turbulent jets. *AIAA J.* **36**, 359–364.

Fiedler, H. E. 1988 Coherent structures in turbulent flows. *Prog. Aero. Sci* **25**, 231–269.

Fingerson, L. 1994 Thermal anemometry, current state, and future directions. *Rev. Sci. Instrum.* **65**, 285–300.

Fingerson, L. & Freymuth, P. 1996 Thermal anemometers. *Fluid Mechanics Measurements, 2nd ed., R. J. Goldstein (Ed.), pp. 115–173, Taylor & Francis, Washington, USA*.

Freund, J. & Colonius, T. 2002 POD analysis of sound generation by a turbulent jet. *AIAA 2002-0072*.

Fritsch, W. 1928 Der Einfluss der Wandrauhigkeit auf die turbulente Geschwindigkeitsverteilung in Rinnen. *ZAMM* **8**, 199–216.

Fujii, S., Eguchi, K. & Gomi, M. 1981 Swirling jets with and without combustion. *AIAA J.* **19**, 1438–1442.

Gallaire, F. & Chomaz, J.-M. 2003 Mode selection in swirling jet experiments: A linear stability analysis. *J. Fluid Mech.* **494**, 223–253.

Gamard, S., George, W. K., Jung, D. & Woodward, S. 2002 Application of a "slice" proper orthogonal decomposition to the far field of an axisymmetric turbulent jet. *Phys. Fluids* **14**, 2515–2522.

Gamard, S., Jung, D. & George, W. K. 2004 Downstream evolution of the most energetic modes in a turbulent axisymmetric jet at high Reynolds number. Part 2. The far-field region. *J. Fluid Mech.* **514**, 205–230.

George, W. K. 1990 Governing equations, experiments, and the experimentalist. *Exp. Thermal Fluid Sci.* **3**, 557–566.

George, W. K. 2006 Recent advancements toward the understanding of turbulent boundary layers. *AIAA J.* **44**, 2435–2449.

George, W. K. 2007 Is there a universal log law for turbulent wall-bounded flows? *Phil. Trans. R. Soc. A* **365**, 789–806.

George, W. K., Beuther, P. & Shabbir, A. 1989 Polynomial calibrations for hot wires in thermally-varying flows. *Exp. Thermal Fluid Sci.* **2**, 230–235.

George, W. K. & Castillo, L. 1997 Zero-pressure-gradient turbulent boundary layer. *Appl. Mech. Rev.* **50**, 689–730.

Gersten, K. & Herwig, H. 1992 Strömungsmechanik: Grundlagen der Impuls-, Wärme- und Stoffübertragung aus asymptotischer Sicht. *Vieweg Verlag*.

Gibson, M. & Younis, B. 1986 Calculation of swirling jets with a Reynolds stress closure. *Phys. Fluids* **29**, 38–48.

Gilchrist, R. & Naughton, J. 2005 Experimental study of incompressible jets with different initial swirl distributions: Mean results. *AIAA J.* **43**, 741–751.

Gisonni, C. 2003 Henry Darcy and the pipe flow formula. *Henry P.G. Darcy and other pioneers in hydraulics: contributions in celebration of the 200th birthday of Henry Philibert Gaspard Darcy, ASCE Publications,* pp. 24–36.

Goldstein, M., Morris, S. & Yen, G. 2004 Problems with fitting to the power-law distribution. *Eur. Phys. J. B* **41**, 255–258.

Gore, R. & Ranz, W. 1964 Backflows in rotating fluids moving axially through expanding cross sections. *AIChE J.* **10**, 83–88.

Grandmaison, E. & Becker, H. 1982 Turbulent mixing in free swirling jets. *Can. J. Chem. Eng.* **60**, 76–82.

Grinstein, F., Gutmark, E., Parr, T. & Hanson-Parr, D. 1996 Streamwise

and spanwise vortex interaction in an axisymmetric jet. A computational and experimental study. *Phys. Fluids* **8**, 1515–1524.

Grossmann, C. & Roos, H.-G. 1994 Numerik partieller Differentialgleichungen. *B. G. Teubner*.

Gupta, A. K., Lilley, D. G. & Syred, N. 1985 Swirl flows. *ABACUS Press, Cambridge, USA*.

Gutmark, E. & Ho, C. 1983 Preferred modes and the spreading rates of jets. *Phys. Fluids* **26**, 2932–2938.

Hanratty, T. & Campbell, J. 1996 Measurement of wall shear stress. *Fluid Mechanics Measurements, R. J. Goldstein (ed.), Taylor & Francis*, pp. 575–648.

Herwig, H. 2008 Strömungsmechanik. Einführung in die Physik von technischen Strömungen. *Viewig + Teubner*.

Hickel, S. & Adams, N. 2008 Implicit LES applied to zero-pressure-gradient and adverse-pressure-gradient boundary-layer turbulence. *Int. J. Heat Fluid Flow* **29**, 626–639.

Hinze, J. O. 1975 Turbulence. *McGraw-Hill, 2nd. ed.*

Hoyas, S. & Jiménez, J. 2006 Scaling of the velocity fluctuations in turbulent channels up to Re=2003. *Phys. Fluids* **18**, 011702.

Hu, Z. W., Morfey, C. & Sandham, N. D. 2006 Wall pressure and shear stress spectra from direct simulations of channel flow. *AIAA J.* **44**, 1541–1549.

Huerre, P. & Monkewitz, P. 1990 Local and global instabilities in spatially developing flows. *Annu. Rev. Fluid Mech.* **22**, 473–537.

Hussain, A. K. M. F. & Zaman, K. 1981 The 'preferred mode' of the axisymmetric jet. *J. Fluid Mech.* **110**, 39–71.

Hussein, H., Capp, S. & George, W. K. 1994 Velocity measurements in a high-Reynolds-number, momentum-conserving, axisymmetric, turbulent jet. *J. Fluid Mech.* **258**, 31–75.

Hutchins, N. & Marusic, I. 2007*a* Evidence of very long meandering features in the logarithmic region of turbulent boundary layers. *J. Fluid Mech.* **579**, 1–28.

Hutchins, N. & Marusic, I. 2007*b* Large-scale influences in near-wall turbulence. *Phil. Trans. R. Soc. A* **365**, 647–664.

Imao, S., Itoh, M. & Harada, T. 1996 Turbulent characteristics of the flow in an axially rotating pipe. *Int. J. Heat Fluid Flow* **17**, 444–451.

Iqbal, M. 2005 Coherent structure in a turbulent axisymmetric jet via a vector implementation of the proper orthogonal decomposition. *Ph. D. thesis, University of Notre Dame, Indiana, USA*.

Iqbal, M. & Thomas, F. O. 2007 Coherent structure in a turbulent jet via a vector implementation of the proper orthogonal decomposition. *J. Fluid Mech.* **571**, 281–326.

Iwamoto, K., Kasagi, N. & Suzuki, Y. 2005 Direct numerical simulation of turbulent channel flow at $Re_\tau = 2320$. *Proc. 6th Symp. Smart Control of Turbulence*.

Izakson, A. A. 1937 Formula for the velocity distribution near a wall. *Z. Eksp. Teoret. Fiz.* **7**, 919–924.

Johansson, A. V. & Alfredsson, P. H. 1982 On the structure of turbulent channel flow. *J. Fluid Mech.* **122**, 295–314.

Jones, M. B., Marusic, I. & Perry, A. E. 2001 Evolution and structure of sink-flow turbulent boundary layers. *J. Fluid Mech.* **428**, 1–27.

Jones, M. B., Nishizawa, N., Chong, M. S. & Marusic, I. 2004 Scaling of the turbulent boundary layer at high Reynolds numbers. *IUTAM Symposium on Reynolds Number Scaling in Turbulent Flow. A. J. Smiths (Ed.), Kluwer Academic Publisher* pp. 271–278.

Karlsson, R. I. 1980 Studies of skin friction in turbulent boundary layers on smooth and rough walls. *Ph. D. thesis, Chalmers University of Technology, Göteborg, Sweden*.

von Kármán, T. 1930 Mechanische Ähnlichkeit und Turbulenz. *Nachr. Ges. Wiss.* **68**, 58–76.

von Kármán, T. 1932 Theorie des Reibungswiderstandes. *Aus dem Buchwerk der Konferenz über hydromechanische Probleme des Schiffsantriebs, Hamburg* pp. 394–414.

von Kármán, T. 1934 Turbulence and skin friction. *J. Aero. Sci.* **1**, 1–20.

von Kármán, T. 1967 The wind and beyond: Theodore von Kármán. Pioneer in aviation and pathfinder in space. *Little, Brown and Company, Canada*.

Kendall, A. & Koochesfahani, M. 2008 A method for estimating wall friction in turbulent wall-bounded flows. *Exp. Fluids* **44**, 773–780.

Kerr, N. M. & Fraser, D. 1965 Swirl. Part I: Effect of axisymmetrical turbulent jets. *J. Inst. Fuel* **38**, 519–526.

Khujadze, G. & Oberlack, M. 2004 DNS and scaling laws from new symmetry groups of ZPG turbulent boundary layer flow. *Theoret. Comput. Fluid Dynamics* **18**, 391–411.

Khujadze, G. & Oberlack, M. 2007 New scaling laws in ZPG turbulent boundary layer flow. *Proc. 5th Intl Symp. on Turbulence and Shear Flow Phenomena, München, Germany*.

Kikuyama, K., Murakami, M., Nishibori, K. & Maeda, K. 1983 Flow in an axially rotating pipe. *Bull. JSME* **26**, 506–513.

Kim, J., Moin, P. & Moser, R. D. 1987 Turbulence statistics in fully developed channel flow at low Reynolds number. *J. Fluid Mech.* **177**, 133–166.

King, L. 1914 On the convection of heat from small cylinders in a stream of fluid: Determination of the convection constants of small platinum wires with applications to hot-wire anemometry. *Phil. Trans. R. Soc. A* **214A**, 373–432.

Kiwata, T., Ishii, T., Kimura, S., Okajima, A. & Miyazaki, K. 2006 Flow visualization and characteristics of a coaxial jet with a tabbed annular nozzle. *JSME Int. J. Ser. B* **49**, 906–913.

Klewicki, J. C. & Falco, R. 1990 On accurately measuring statistics associated with small-scale structure in turbulent boundary layers using hot-wire probes. *J. Fluid Mech.* **219**, 119–142.

Knight, W., Prandtl, L., von Kármán, T., Costanzi, G., Margoulis, W., Verduzio, R., Katzmayr, R., Wolff, E. B. & Zahm, A. F. 1922 Standardization and aerodynamics. *NACA TN 134* .

Knobloch, K. 2008 Skalierungen und Zweipunkt-Geschwindigkeitskorrelationen in

turbulenten Grenzschichten bei großen Reynoldszahlen. *Ph. D. thesis, Technical University Berlin, Germany*.

Knobloch, K. & Fernholz, H. H. 2004 Statistics, correlations, and scaling in a turbulent boundary layer at $Re_{\delta_2} \leqslant 1.15 \times 10^5$. *IUTAM Symposium on Reynolds Number Scaling in Turbulent Flow. A. J. Smiths (Ed.), Kluwer Academic Publisher* pp. 11–16.

Ko, N. & Kwan, A. 1976 The initial region of subsonic coaxial jets. *J. Fluid Mech.* **73**, 305–332.

Komori, S. & Ueda, H. 1985 Turbulent flow structure in the near field of a swirling round free jet. *Phys. Fluids* **28**, 2075–2082.

Kopiev, V., Zaitsev, M., Chernyshev, S. & Kotova, A. 1999 The role of large-scale vortex in a turbulent jet noise. *AIAA 1999-1839*.

Kundu, P. K. & Cohen, I. C. 2004 Fluid mechanics. *Elsevier, Academic Press, 3rd ed.*

Kusek, S., Corke, T. & Reisenthel, P. 1990 Seeding of helical modes in the initial region of an axisymmetric jet. *Exp. Fluids* **10**, 116–124.

Kwan, A. & Ko, N. 1977 The initial region of subsonic coaxial jets. Part 2. *J. Fluid Mech.* **82**, 273–287.

Launder, B. & Morse, A. 1979 Numerical prediction of axisymmetric free shear flows with a second-order Reynolds stress closure. *Turbulent Shear Flows I, F. Durst et al. (Eds.), Springer-Verlag, Berlin, Germany, pp. 279–294*.

Lee, J. H. W. & Chu, V. H. 2003 Turbulent jets and plumes: A lagrangian approach. *Kluwer Academic Publishers*.

Lesieur, M. 1997 Turbulence in fluids. *Kluwer Academic Publishers, 3rd ed.*

Lesieur, M. 2008 Turbulence in fluids. *Springer*.

Lewkowicz, A. K. 1982 An improved universal wake function for turbulent boundary layers and some of its consequences. *Z. Flugwiss. Weltraumforsch.* **6**, 261–266.

Liepmann, D. & Gharib, M. 1992 The role of streamwise vorticity in the near-field entrainment of round jets. *J. Fluid Mech.* **245**, 643–668.

Lilley, D. G. 1977 Swirl flows in combustion: A review. *AIAA J.* **15**, 1063–1078.

Lindgren, B. & Johansson, A. V. 2002 Evaluation of the flow quality in the MTL wind-tunnel. *Tech. Rep. TRITA-MEK 2002:13, Royal Institute of Technology, Stockholm, Sweden*.

Loiseleux, T. & Chomaz, J. 2003 Breaking of rotational symmetry in a swirling jet experiment. *Phys. Fluids* **15**, 511–523.

Lomas, C. G. 1986 Fundamentals of hot wire anemometry. *Cambridge University Press*.

Lucca-Negro, O. & O'Doherty, T. 2001 Vortex breakdown: a review. *Prog. Energy Combust. Sci.* **27**, 431–481.

Ludwieg, H. & Tillmann, W. 1949 Untersuchungen über die Wandschubspannung in turbulenten Reibungsschichten. *Ing. Arch.* **17**, 288–299.

MacMillan, F. A. 1956 Experiments on Pitot-tubes in shear flow. *Ministry of Supply, Aero. Res. Counc. R. & M. No. 3028*.

Mandal, A. C. & Dey, J. 2008 A Reynolds number independent relation in constant pressure turbulent boundary layers. *Proc. Int. Conf. Aerospace Science and Technology (INCAST), Bangalore, India*.

Mathieu, J. & Scott, J. 2000 An introduction to turbulent flow. *Cambridge University Press*.

McComb, W. D. 1992 The physics of fluid turbulence. *Oxford University Press*.

McKeon, B. 2003 High Reynolds number turbulent pipe flow. *Ph. D. thesis Princeton University, USA*.

McKeon, B., Li, J. D., Jiang, W., Morrison, J. F. & Smits, A. J. 2003 Pitot probe corrections in fully developed turbulent pipe flow. *Meas. Sci. Tech.* **14**, 1449–1458.

McKeon, B., Li, J. D., Jiang, W., Morrison, J. F. & Smits, A. J. 2004 Further observations on the mean velocity distribution in fully developed pipe flow. *J. Fluid Mech.* **501**, 135–147.

Mehta, R., Wood, D. & Clausen, P. 1991 Some effects of swirl on turbulent mixing layer development. *Phys. Fluids* **3**, 2716–2724.

Merzkirch, W. 1987 Flow visualisation. *Academic Press, 2nd. ed.*.

Michalke, A. 1964 Zur Instabilität und nichtlinearen Entwicklung einer gestörten Scherschicht. *Ing. Arch.* **33**, 264–276.

Millikan, C. B. 1938 A critical discussion of turbulent flows in channels and circular tubes. *Proc. 5th International Congress on Applied Mechanics, Cambridge, MA, USA*, pp. 386–392.

Monty, J. P. 2005 Developments in smooth wall turbulent duct flows. *Ph. D. thesis University of Melbourne, Australia*.

Monty, J. P., Stewart, J., Williams, R. & Chong, M. S. 2007 Large-scale features in turbulent pipe and channel flows. *J. Fluid Mech.* **589**, 147–156.

Morse, A. P. 1980 Axisymmetric free shear flows with and without swirl. *Ph. D. thesis University of London, UK*.

Mungal, M. G. & Hollingsworth, D. 1989 Organized motion in a very high Reynolds number jet. *Phys. Fluids* **1**, 1615–1623.

Nagib, H. M. & Chauhan, K. A. 2008 Variations of von Kármán coefficient in canonical flows. *Phys. Fluids* **20**, 101518.

Nagib, H. M., Chauhan, K. A. & Monkewitz, P. A. 2007 Approach to an asymptotic state for zero pressure gradient turbulent boundary layers. *Phil. Trans. R. Soc. A* **365**, 755–770.

Nagib, H. M., Christophorou, C. & Monkewitz, P. A. 2004*a* High Reynolds number turbulent boundary layers subjected to various pressure-gradient conditions. *IUTAM Symposium on one hundred years of boundary layer research, G. E. A. Meier and K. R. Sreenivasan (Eds.), Göttingen, Germany* pp. 383–394.

Nagib, H. M., Christophorou, C., Rüedi, J.-D., Monkewitz, P. A. & Österlund, J. M. 2004*b* Can we ever rely on results from wall-bounded turbulent flows without direct measurements of wall shear stress? *AIAA 2004-2392*.

Naughton, J. & Sheplak, M. 2002 Modern developments in shear-stress measurement. *Prog. Aero. Sci* **38**, 515–570.

Nickels, T. B., Marusic, I., Hafez, S. & Hutchins, N. 2007 Some predictions

of the attached eddy model for a high Reynolds number boundary layer. *Phil. Trans. R. Soc. A* **365**, 807–822.

Nikuradse, J. 1929 Untersuchungen über die Strömungen des Wassers in konvergenten und divergenten Kanälen. *VDI Forschungsheft 289*.

Nikuradse, J. 1930 Widerstandsgesetz und Geschwindigkeitsverteilung von turbulenten Wasserströmungen in glatten und rauhen Rohren. *Proc. 3rd International Congress on Applied Mechanics, Stockholm, Sweden,* pp. 239–248.

Nikuradse, J. 1942 Turbulente Reibungsschichten an der Platte. *ZWB, R. Oldenbourg*.

Oberlack, M. 1999 Similarity in non-rotating and rotating turbulent pipe flows. *J. Fluid Mech.* **379**, 1–22.

Oberlack, M. 2001 A unified approach for symmetries in plane parallel turbulent shear flows. *J. Fluid Mech.* **427**, 299–328.

Ogawa, A. & Hatakeyama, H. 1979 Fluiddynamical characteristics of turbulent straight and rotational jets (1st report). *J. Coll. Engng. Nohon. Univ.* **A-20**, 133–144.

Ogawa, A., Hatakeyama, H. & Fujita, Y. 1981 Fluiddynamical characteristics of turbulent straight and rotational jets (2nd report). *J. Coll. Engng. Nohon. Univ.* **A-22**, 157–170.

Ogawa, A., Hatakeyama, H. & Fujita, Y. 1982 Fluiddynamical characteristics of turbulent straight and rotational jets (3rd report). *J. Coll. Engng. Nohon. Univ.* **A-23**, 89–102.

Oljaca, M., Gu, X., Glezer, A., Baffico, M. & Lund, F. 1998 Ultrasound scattering by a swirling jet. *Phys. Fluids* **10**, 886–898.

Orlandi, P. & Fatica, M. 1997 Direct simulations of turbulent flow in a pipe rotating about its axis. *J. Fluid Mech.* **343**, 43–72.

Örlü, R. 2006 Experimental study of passive scalar mixing in swirling jet flows. *TeknL thesis, Royal Institute of Technology, Stockholm, Sweden*.

Örlü, R. 2009*a* Low Reynolds number zero pressure-gradient equilibrium turbulent boundary-layer experiments. *Ph. D. thesis, Royal Institute of Technology, Stockholm, Paper 4*.

Örlü, R. 2009*b* On spatial resolution issues on mean quantities using hot-wire anemometry. *Ph. D. thesis, Royal Institute of Technology, Stockholm, Paper 6*.

Örlü, R. 2009*c* On the determination of the wall position in wall-bounded turbulent flows. *Ph. D. thesis, Royal Institute of Technology, Stockholm, Paper 5*.

Örlü, R. & Alfredsson, P. H. 2008 An experimental study of the near-field mixing characteristics of a swirling jet. *Flow Turbul. Combust.* **80**, 323–350.

Örlü, R., Segalini, A., Alfredsson, P. H. & Talamelli, A. 2008 On the passive control of the near-field of coaxial jets by means of vortex shedding. *Proc. 2nd Int. Conf. on Jets, Wakes and Separated Flows*.

Oseen, C. W. & Weibull, W. 1930*a* Abstracts of lectures: III International Congress for Applied Mechanics. *Amqvist & Wiksells Boktryckeri AB, Uppsala*.

Oseen, C. W. & Weibull, W. 1930*b* Verhandlungen des 3. Internationalen Kongresses für Technische Mechanik. *A.B. Sveriges Litografiska Tryckerier, Stockholm*.

Österlund, J. M. 1999 Experimental studies of zero pressure-gradient turbulent boundary layer flow. *Ph. D. thesis, Royal Institute of Technology, Stockholm, Sweden*.

Österlund, J. M., Johansson, A. V. & Nagib, H. M. 2000*a* Comment on "A note on the intermediate region in turbulent boundary layers" [Phys. Fluids 12, 2159 (2000)]. *Phys. Fluids* **12**, 2360–2263.

Österlund, J. M., Johansson, A. V., Nagib, H. M. & Hites, M. H. 2000*b* A note on the overlap region in turbulent boundary layers. *Phys. Fluids* **12**, 1–4.

Paeschke, W. 1935 Feuchtigkeitseffekt bei Hitzdrahtmessungen. *Phys. Z.* **36**, 564–565.

Pantano, C., Pullin, D., Dimotakis, P. E. & Matheou, G. 2008 LES approach for high Reynolds number wall-bounded flows with application to turbulent channel flow. *J. Comput. Phys.* **227**, 9271–9291.

Panton, R. L. 2005 Review of wall turbulence as described by composite expansions. *Appl. Mech. Rev.* **58**, 1–36.

Park, S. H. & Shin, D. 1993 Measurements of entrainment characteristics of swirling jets. *Int. J. Heat Mass Transfer* **36**, 4009–4018.

Paschereit, C., Oster, D., Long, T. & Fiedler, H. E. 1992 Flow visualization of interactions among large coherent structures in an axisymmetric jet. *Exp. Fluids* **12**, 189–199.

Perry, A. E. 1982 Hot-wire anemometry. *Clarendon Press*.

Perry, A. E., Hafez, S. & Chong, M. S. 2001 A possible reinterpretation of the Princeton superpipe data. *J. Fluid Mech.* **439**, 395–401.

Pietri, L., Amielh, M. & Anselmet, F. 2000 Simultaneous measurements of temperature and velocity fluctuations in a slightly heated jet combining a cold wire and laser Doppler anemometry. *Int. J. Heat Fluid Flow* **21**, 22–36.

Piquet, J. 1999 Turbulent flows: Models and physics. *Springer-Verlag*.

Pitts, W. 1991 Reynolds number effects on the mixing behavior of axisymmetric turbulent jets. *Exp. Fluids* **11**, 135–141.

Plaschko, P. 1979 Helical instabilities of slowly divergent jets. *J. Fluid Mech.* **92**, 209–215.

Pope, S. 2000 Turbulent flows. *Cambridge University Press*.

Prandtl, L. 1925 Bericht über Untersuchungen zur ausgebildeten Turbulenz. *ZAMM* **5**, 136–139.

Prandtl, L. 1926 Über die ausgebildete Turbulenz. *Verhandlungen des II. Internationalen Kongresses für Technische Mechanik* pp. 62–75.

Prandtl, L. 1932 Zur turbulenten Strömung in Rohren und längs Platten. *Ergebnisse der Aerodynamischen Versuchsanstalt zu Göttingen* **4**, 18–29.

Prandtl, L. 1965 Führer durch die Strömungslehre. *Viewig & Sohn, Braunschweig, 6th ed.*

Pratte, B. & Keffer, J. 1972 The swirling turbulent jet. *J. Basic Eng.* **94**, 739–747.

Rahai, H. & Wong, T. 2002 Velocity field characteristics of turbulent jets from round tubes with coil inserts. *Appl. Thermal Eng.* **22**, 1037–1045.

Rajaratnam, N. 1976 Turbulent jets. *Elsevier, Amsterdam, The Netherlands*.

Rayleigh, L. 1878 On the instability of jets. *Proc. Math. Phys. Sci.* **10**, 4–13.

Rayleigh, L. 1879 On the capillary phenomena of jets. *Proc. R. Soc. London* **29**, 71–97.

Richards, C. & Pitts, W. 1993 Global density effects on the self-preservation behaviour of turbulent free jets. *J. Fluid Mech.* **254**, 417–435.

Ricou, F. & Spalding, D. 1961 Measurements of entrainment by axisymmetrical turbulent jets. *J. Fluid Mech.* **11**, 21–32.

Rose, W. G. 1962 A swirling round turbulent jet; 1 - Mean-flow measurements. *J. Appl. Mech.* **29**, 615–625.

Roshko, A. 1976 Structure of turbulent shear flows: A new look. *AIAA J.* **14**, 1349–1357.

Rotta, J. C. 1950 Das in Wandnähe gültige Geschwindigkeitsgesetz turbulenter Strömungen. *Ing. Arch.* **18**, 277–280.

Rotta, J. C. 1962 Turbulent boundary layers in incompressible flow. *Prog. Aero. Sci* **2**, 1–219.

Rotta, J. C. 1972 Turbulente Strömungen. *B. G. Teubner, Stuttgart*.

Rüedi, J.-D., Nagib, H. M., Österlund, J. M. & Monkewitz, P. A. 2003 Evaluation of three techniques for wall-shear measurements in three-dimensional flows. *Exp. Fluids* **35**, 389–396.

Samet, M. & Einav, S. 1988 Mean value measurements of a turbulent swirling-jet. *AIAA J.* **26**, 619–620.

Samimy, M., Breuer, K., Leal, L. & Steen, P. 2004 A gallery of fluid motion. *Cambridge University Press*.

Sandham, N. D. 1991 An alternative formulation of the outer law of the turbulent boundary layer. *Tech. Rep. No. DLR IB 221-91 A 10, DLR Göttingen*.

Satake, S., Kunugi, T. & Himeno, R. 2000 High Reynolds number computation for turbulent heat transfer in a pipe flow. *Lecture Notes in Computer Science, Springer Berlin / Heidelberg* **1940**, 514–523.

Satake, S., Kunugi, T., Takase, K., Ose, Y. & Naito, N. 2003 Large scale structures of turbulent shear flow via DNS. *Lecture Notes in Computer Science, Springer Berlin / Heidelberg* **2858**, 468–475.

Schetz, J. A. 1980 Injection and mixing in turbulent flow. *AIAA, New York, USA*.

Schlatter, P., Li, Q., Brethouwer, G., Johansson, A. V. & Henningson, D. S. 2009*a* Towards large-eddy simulations of high-Reynolds number turbulent boundary layers. *Proc. 6th Intl Symp. on Turbulence and Shear Flow Phenomena, Seoul, Korea*.

Schlatter, P., Örlü, R., Li, Q., Brethouwer, G., Fransson, J. H. M. H. M., Johansson, A. V., Alfredsson, P. H. & Henningson, D. S. 2009*b* Turbulent boundary layers up to $Re_\theta = 2500$ studied through simulation and experiment. *Phys. Fluids,* (accepted).

Schlichting, H. 1951 Grenzschicht-Theorie. *Verlag G. Braun, Karlsruhe*.

Schlichting, H. 1965 Grenzschicht-Theorie. *Verlag G. Braun, 5th. ed.*

Schlichting, H. & Gersten, K. 1979 Boundary-layer theory. *McGraw-Hill Book Company, 7th ed.*

Schlichting, H. & Gersten, K. 2000 Boundary-layer theory. *Springer, 8th ed.*

Schlichting, H. & Gersten, K. 2006 Grenzschicht-Theorie. *Springer-Verlag, 10th ed.*

Schlichting, H. & Truckenbrodt, E. 1967 Aerodynamik des Flugzeuges. 1. Grundlagen aus der Strömungsmechanik. *Springer*.

da Silva, C., Balarac, G. & Métais, O. 2003 Transition in high velocity ratio coaxial jets an-alysed from direct numerical simulations. *J. Turbulence* **4**, 1—18.

Simpson, R. 1970 Characteristics of turbulent boundary layers at low Reynolds numbers with and without transpiration. *J. Fluid Mech.* **42**, 769–802.

Sislian, J. & Cusworth, R. 1986 Measurements of mean velocity and turbulent intensities in a free isothermal swirling jet. *AIAA J.* **24**, 303–309.

Smith, R. 1994 Effect of Reynolds number on the structure of turbulent boundary layers. *Ph. D. thesis, Princeton University, USA*.

Smits, A. J. & Dussauge, J. 2006 Turbulent shear layers in supersonic flow. *Springer, 2nd ed.*

Smits, A. J. & Lim, T. T. 2000 Flow visualization: Techniques and examples. *Imperial College Press*.

Spalart, P. 1988 Direct simulation of a turbulent boundary layer up to $R_\theta = 1410$. *J. Fluid Mech.* **187**, 61–98.

Spalart, P. 2006 Turbulence: Are we getting smarter? *Fluid Dynamics Award Lecture, 36th Fluid Dynamics Conference and Exhibit, San Francisco, CA, 5-8 June.*

Spalart, P., Coleman, G. & Johnstone, R. 2008 Direct numerical simulation of the Ekman layer: A step in Reynolds number, and cautious support for a log law with a shifted origin. *Phys. Fluids* **20**, 101507.

Stanton, T. 1911 The mechanical viscosity of fluids. *Phil. Trans. R. Soc. A* **85** (579), 366–376.

Stanton, T. & Pannell, J. 1914 Similarity of motion in relation to the surface friction of fluids. *Phil. Trans. R. Soc. A* pp. 199–224.

Syred, N. 2006 A review of oscillation mechanisms and the role of the precessing vortex core (PVC) in swirl combustion systems. *Prog. Energy Combust. Sci.* **32**, 93–161.

Syred, N. & Beer, J. 1974 Combustion in swirling flows-A review. *Combustion and Flame* **23**, 143–201.

Taghavi, R. & Farokhi, S. 1988 Turbulent swirling jets with excitation. *Tech. Rep., Kansas Univ. Center for Research, USA, NASA-CR-180895*.

Talamelli, A. & Gavarini, I. 2006 Linear instability characteristics of incompressible coaxial jets. *Flow Turbul. Combust.* **76**, 221–240.

Talamelli, A., Persiani, F., Fransson, J. H. M. H. M., Alfredsson, P. H., Johansson, A. V., Nagib, H. M., Rüedi, J.-D., Sreenivasan, K. R. & Monkewitz, P. A. 2009 CICLoPE - a response to the need for high Reynolds number experiments. *Fluid Dyn. Res.* **41**, 021407.

Tang, S. & Ko, N. 1994 Experimental investigation of the structure interaction in an excited coaxial jet. *Exp. Thermal Fluid Sci.* **8**, 214–229.

Tennekes, H. 1982 Similarity relations, scaling laws and spectral dynamics. *Atmospheric Turbulence and Air Pollution Modelling. F.T.M. Nieuwstadt and H. Van Dop (Eds.)*, pp. 37–68.

Tennekes, H. & Lumley, J. L. 1972 A first course in turbulence. *MIT Press, Cambridge, Massachusetts*.

Tietjens, O. 1970 Strömungslehre: Bd. 2. Bewegung der Flüssigkeiten und Gase. *Springer*.

Toh, I., Honnery, D. & Soria, J. 2005 Velocity and scalar measurements of a low swirl jet. *Proc. 4th Australian Conf. Laser Diagnostics Fluid Mech. Comb.; The University of Adelaide, South Australia, Australia,* pp. 129–132.

Townsend, A. A. 1976 The structure of turbulent shear flow. *Cambridge University Press, 2nd ed.*

Tritton, D. J. 1988 Physical fluid dynamics. *Oxford University Press*.

Tropea, C., Yarin, A. & Foss, J. 2007 Springer Handbook of Experimental Fluid Mechanics. *Springer-Verlag Berlin Heidelberg*.

Truckenbrodt, E. 2008 Fluidmechanik. *Springer-Verlag Berlin Heidelberg, 4th ed.*

Tso, J. & Hussain, F. 1989 Organized motions in a fully developed turbulent axisymmetric jet. *J. Fluid Mech.* **203**, 425–448.

Tyndall, J. 1867 Sound. A course of eight lectures delivered at the Royal institution of Great Britain. *D. Appleton and Company, New York, USA*.

Van Dyke, M. 1982 An album of fluid motion. *Parabolic Press*.

Wallace, D. & Redekopp, L. 1992 Linear instability characteristics of wake-shear layers. *Phys. Fluids* **4**, 189–191.

Wänström, M., George, W. K. & Meyer, K. E. 2006 Stereoscopic PIV and POD applied to the far turbulent axisymmetric jet. *AIAA 2006-3368*.

Weibull, W. 1930 Program: III International Congress for Applied Mechanics. *Amqvist & Wiksells Boktryckeri AB, Uppsala*.

White, F. 1991 Viscous fluid flow. *McGraw-Hill, 2nd. Ed.*

Wicker, R. & Eaton, J. 1994 Near field of a coaxial jet with and without axial excitation. *AIAA J.* **32**, 542–546.

Willmarth, W. & Lu, S. 1972 Structure of the Reynolds stress near the wall. *J. Fluid Mech.* **55**, 65–92.

Winter, K. G. 1977 An outline of the techniques available for the measurement of skin friction in turbulent boundary layers. *Prog. Aero. Sci* **18**, 1–57.

Wooten, D. C., Wooldridge, C. E. & Amaro, A. J. 1972 The structure of jet turbulence producing jet noise. *Tech. Rep., Stanford Research Institute, California, USA, SRI Project 8139*.

Wosnik, M., Castillo, L. & George, W. K. 2000 A theory for turbulent pipe and channel flows. *J. Fluid Mech.* **421**, 115–145.

Wu, X. & Moin, P. 2008 A direct numerical simulation study on the mean velocity characteristics in turbulent pipe flow. *J. Fluid Mech.* **608**, 81–112.

Wygnanski, I. & Fiedler, H. E. 1969 Some measurements in the self-preserving jet. *J. Fluid Mech.* **38**, 577–612.

Yoda, M., Hesselink, L. & Mungal, M. G. 1992 The evolution and nature of large-scale structures in the turbulent jet. *Phys. Fluids* **4**, 803–811.

Zagarola, M. V. 1996 Mean flow scaling of turbulent pipe flow. *Ph. D. thesis, Princeton University, USA*.

Zagarola, M. V. & Smits, A. J. 1997 Scaling of the mean velocity profile for turbulent pipe flow. *Phys. Rev. Lett.* **78**, 239–242.

Zagarola, M. V. & Smits, A. J. 1998*a* Mean-flow scaling of turbulent pipe flow. *J. Fluid Mech.* **373**, 33–79.

Zagarola, M. V. & Smits, A. J. 1998*b* A new mean velocity scaling for turbulent boundary layers. *Proceedings of FEDSM'98*.

Zanoun, E.-S. 2003 Answers to some open questions in wall bounded laminar and turbulent shear flows. *Ph. D. thesis, University of Erlangen, Germany*.

Zanoun, E.-S. & Durst, F. 2009 Turbulent momentum transport and kinetic energy production in plane-channel flows. *Int. J. Heat Mass Transfer*, (in press).

Zanoun, E.-S., Durst, F., Bayoumy, O. & Al-Salaymeh, A. 2007 Wall skin friction and mean velocity profiles of fully developed turbulent pipe flows. *Exp. Thermal Fluid Sci.* **32**, 249–261.

Zanoun, E.-S., Durst, F. & Nagib, H. M. 2003 Evaluating the law of the wall in two-dimensional fully developed turbulent channel flows. *Phys. Fluids* **15**, 3079–3089.

Zanoun, E.-S., Durst, F. & Nagib, H. M. 2004 Response to "Comment on 'Evaluating the law of the wall in two-dimensional fully developed turbulent channel flows'" [Phys. Fluids 16, 3507 (2004)]. *Phys. Fluids* **16**, 3509–3510.

Zhang, Y., Ma, J. & Cao, Z. 2008 The von Kármán constant retrieved from CASES-97 dataset using a variational method. *Atmos. Chem. Phys.* **8**, 7045–7053.

Part II

Papers

1

Paper 1

"swirl to mix and observe"
"swirl to mix and see if it makes a difference"
"swirl to mix and heat"
"swirl to mix and enjoy"

Excerpts from various ice cream and cake recipes.

An experimental study of the near-field mixing characteristics of a swirling jet

By Ramis Örlü and P. Henrik Alfredsson

Linné Flow Centre, KTH Mechanics, SE-100 44 Stockholm, Sweden

Published in *Flow, Turbul. Combust.* **80**, 51–90, 2008

The present experimental investigation is devoted to the mixing characteristics of a passive scalar in the near-field region of a moderately swirling jet issuing from a fully developed axially rotating pipe flow. Instantaneous streamwise and azimuthal velocity components as well as the temperature were simultaneously accessed by means of a combined X-wire and cold-wire probe. The results indicate a modification of the turbulence structures to that effect that the swirling jet spreads, mixes and evolves faster compared to its non-swirling counterpart. The high correlation between streamwise velocity and temperature fluctuations as well as the streamwise passive scalar flux are even more enhanced due to the addition of swirl, which in turn shortens the distance and hence time needed to mix the jet with the ambient air.

1. Introduction

The addition of an azimuthal velocity component to a free turbulent round jet is well known to entrain more ambient fluid and hence to spread faster than its non-swirling counterpart (Gupta *et al.* 1985; Rajaratnam 1976; Schetz 1980). Especially the formation of a recirculation zone near the orifice at high swirl rates, leading to the vortex breakdown phenomenon (Lucca-Negro & O'Doherty 2001), through which the entrainment rate in the near-field region is drastically increased (Park & Shin 1993), is exploited since the middle of the last century to stabilise and control flames in furnaces and combustion chambers (Kerr & Fraser 1965; Maier 1968; Mathur & MacCallum 1967). Despite the strong focus on combustion conditions (Fujii *et al.* 1981; Lilley 1977; Naughton *et al.* 1997; Syred & Beér 1974), the stability (Billant *et al.* 1998; Gallaire & Chomaz 2003; Loiseleux & Chomaz 2003) or the related recirculation zone in swirling jet flows, the case of the isothermal free jet with swirl strengths below the occurrence of reverse flow on the central axis has also attracted considerable attention (Chigier & Chervinsky 1967; Facciolo *et al.* 2007*b*; Gilchrist & Naughton 2005; Pratte & Keffer 1972; Rose 1962). The addition of mild degrees of swirl to a jet is for instance known to intensify the process of mass, momentum and heat

transport (Elsner & Kurzak 1987; Komori & Ueda 1985), to spread and mix faster (Grandmaison & Becker 1982), and to reduce noise production in the near-field of jet exhausts (Wooten *et al.* 1972).

The vast amount of experimental investigations seemingly suggests that the effect of swirl on free jets is sufficiently studied. This is even supported by the classical view that a swirling jet can be characterised through its Reynolds number and swirl strength. It also is stated that vortex breakdown occurs irrespective of the Reynolds number at an integral swirl number of approximately 0.6 (Gupta *et al.* 1985). Experiments, however, showed that critical swirl numbers as low as 0.51 (Feyedelem & Sarpkaya 1998) or 0.48 (Farokhi *et al.* 1989; Taghavi & Farokhi 1988) were sufficient for the occurrence of the vortex breakdown phenomenon. This and the gross differences between experimental results of investigations with different swirl generating methods revealed that an integral swirl number is not sufficient to describe the dynamics of the flow quantitatively, but also qualitatively in the near-field region (Farokhi *et al.* 1989; Gilchrist & Naughton 2005). For instance the elaborate work by Morse (1980*a*), who provided results for two databases (Bradshaw *et al.* 1996; Morse 1980*b*), does not provide the initial velocity profiles or a description of the swirl generating method. The only provided reference (Gibson & Younis 1986) in the databases does not clarify the situation, although the description can be found in the thesis of Morse (1980*a*).

Databases can serve as a tool for turbulence modellers to evaluate their models. In order for experimental databases to be useful an accurate description of the initial and boundary conditions has to be given. For numerical databases the initial and boundary conditions are well defined per se. Due to the lack of direct numerical simulations (DNS) at a high enough Reynolds number, DNS in the context of swirling jet flows are mainly used for stability considerations (Hu *et al.* 2001). On the other hand large-eddy simulations (LES) showed promising results (McIlwain & Pollard 2002) and are becoming more and more practical for complex geometries (García-Villalba *et al.* 2006).

The short review above suggests that there is a need for experiments with well-defined initial and boundary conditions in order to access the effect of rotation on the free round jet and not the effect of different obstacles upstream the orifice outlet, such as coil inserts (Rahai & Wong 2002) or guiding vanes (Elsner & Kurzak 1987; Sislian & Cusworth 1986). The addition of rotation by means of tangential injection of an azimuthal velocity component removes the inserts, but not the asymmetric velocity profiles, which can persist up to several orifice diameters downstream (Ogawa *et al.* 1981), and hence raises problems for turbulence modellers as well. To obtain symmetric velocity profiles even close to the orifice a large number of nozzles along concentric rings (Farokhi & Taghavi 1990; Gilchrist & Naughton 2005) are needed or one can utilise the flow emanating from a fully developed axially rotating pipe flow (Facciolo 2006; Rose 1962).

By studying the mixing of a passive scalar in the flow field the properties of the turbulent dispersion process can be obtained. Such a knowledge of dispersion is important for instance in heat transfer and mixing processes or in the spreading of pollutants. However, knowledge of the spreading of a passive scalar in swirling jet flows, be it the concentration or temperature field, is even more scarce than its dynamic counterpart. The experimental investigations known to the authors are mainly restricted to the far-field (Grandmaison & Becker 1982), to flow visualisations (Toh *et al.* 2005), the mean values (Kuroda *et al.* 1985; Ogawa *et al.* 1981), to swirling jets with recirculation zones (Craya & Darrigol 1967; Komori & Ueda 1985) or those who are generated by means of passive vanes (Elsner & Kurzak 1987), which distort the flow regime near the outlet. Despite the mentioned experiments no numerical simulations are known to the authors.

The present investigation focuses on the mixing characteristics of a free swirling jet with swirl strength well below reverse flow on the central axis. The jet, emanating from a fully developed axially rotating pipe flow, is slightly heated in order to use the temperature as a passive scalar. Simultaneous measurements of the streamwise and azimuthal velocity component as well as the temperature performed by means of a combined X-wire and cold-wire probe enabled the study of the dynamic and thermal (passive scalar) field in a swirling jet flow free from any traces and asymmetries in the radial distributions. Thereby the observed alterations in the dynamically and thermally axisymmetric flow field could solely be ascribed to the effect of swirl, which in our view is a unique contribution in regards to the passive scalar field in swirling jet flows. Furthermore the measurement technique made it possible to investigate the (joint) probability density distributions of velocity and temperature fluctuations, which – albeit of their potential to describe the mixing of the passive scalar – have not been reported in previous studies.

We restrict ourselves here to the investigation of the passive scalar field, the turbulent heat transport and the mixing processes in a turbulent free swirling jet, whereas the dynamics of the flow in the axially rotating pipe flow as well as the emanating free swirling jet are in good agreement with previous studies in the same experimental facility (Facciolo 2006; Facciolo *et al.* 2007*b*) and do not need to be repeated here.

In the following the governing equations including integral relations are presented together with the characteristic parameters for the turbulent free swirling jet in section 2. After describing the experimental facility and measurement technique in Section 3, the results are presented and discussed in Section 4. Section 5 summarises and concludes the present paper.

2. Theoretical considerations

We are investigating non-isothermal swirling jets and thus, besides the velocity and pressure field, interest in the influence of the turbulence on a scalar quantity, viz. temperature or a concentration, arises. In the following we are restricting ourselves to the investigation of incompressible flows, and at the same time we allow small temperature variations to occur, such that the density and viscosity can still be considered constant, but that variations in the temperature are still large enough to be detected and distinguished from unavoidable deviations in the ambient temperature. As a consequence of this the passive contaminant, i.e. the temperature, has no influence on the dynamics of the flow and we refer to it as a passive scalar, hence it will be considered separately from the velocity field.

2.1. *The velocity field*

The theoretical description of the velocity and pressure field of free swirling jets is based on the incompressible Reynolds-averaged Navier-Stokes equations written for a cylindrical inertial frame of reference under the assumption of a steady and axisymmetric mean flow

$$\frac{1}{r}\frac{\partial}{\partial r}(rW)+\frac{\partial U}{\partial x}=0\,, \tag{1}$$

$$\begin{aligned} W\frac{\partial W}{\partial r}+U\frac{\partial W}{\partial x}+\frac{\partial\overline{w^2}}{\partial r}+\frac{\partial\overline{uw}}{\partial x}-\frac{1}{r}(V^2+\overline{v^2}-\overline{w^2}) \\ =-\frac{1}{\rho}\frac{\partial P}{\partial r}+\frac{1}{r^2}\left[\nu r^3\frac{\partial}{\partial r}\left(\frac{W}{r}\right)\right]\,, \end{aligned} \tag{2}$$

$$\begin{aligned} W\frac{\partial V}{\partial r}+U\frac{\partial V}{\partial x}+\frac{VW}{r}+\frac{\partial\overline{uv}}{\partial x}+\frac{1}{r^2}\frac{\partial}{\partial r}(r^2\overline{vw}) \\ =\frac{1}{r^2}\frac{\partial}{\partial r}\left[\nu r^3\frac{\partial}{\partial r}\left(\frac{V}{r}\right)\right]\,, \end{aligned} \tag{3}$$

$$\begin{aligned} W\frac{\partial U}{\partial r}+U\frac{\partial U}{\partial x}+\frac{\partial\overline{u^2}}{\partial x}+\frac{1}{r}\frac{\partial(r\overline{uw})}{\partial r} \\ =-\frac{1}{\rho}\frac{\partial P}{\partial x}+\frac{1}{r}\frac{\partial}{\partial r}\left[\nu r\frac{\partial U}{\partial r}\right]\,. \end{aligned} \tag{4}$$

Hereby we denote the radial, azimuthal and axial directions with (r, ϕ, x) and the corresponding velocity components with ($W+w$, $V+v$, $U+u$), where capital letters denote the mean components, fluctuating components are expressed by lowercase letters, and the overbar indicates time averaging (see

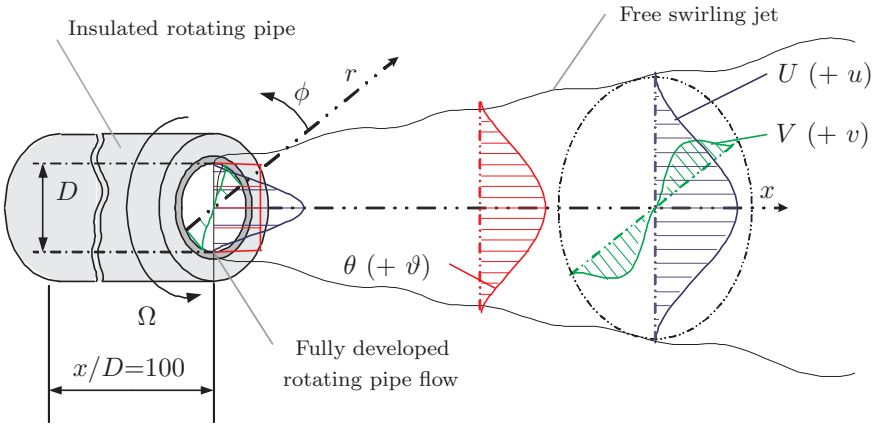

FIGURE 1. Schematic of the cylindrical coordinate system of the free developing swirling jet emanating from a fully developed axially rotating pipe flow.

figure 1). The density, kinematic viscosity and the mean pressure are expressed through ρ, ν and P, respectively.

By following Chigier & Chervinsky (1967) we can simplify the governing equations significantly. Taking advantage of a thin shear layer approximation and assuming a high Reynolds number flow few convective and all viscous terms can be neglected, based on an order of magnitude estimate. In this way equation (2) simplifies to

$$\frac{1}{\rho}\frac{\partial P}{\partial r} = -\frac{\partial \overline{w^2}}{\partial r} + \frac{1}{r}\left(V^2 + \overline{v^2} - \overline{w^2}\right). \tag{5}$$

Neglecting the first term on the right-hand side and anticipating that the azimuthal and radial turbulence intensities are comparable, one can derive the simple radial equilibrium relation (Reynolds 1961),

$$\frac{\partial P}{\partial r} \approx \rho\frac{V^2}{r}. \tag{6}$$

This equation demonstrates the existence of a radial pressure gradient induced by the swirling motion. Multiplying equation (5) with r, integrating it across the jet, i.e. from the centreline ($r = 0$) to a radial position where the presence of the jet is not detectable ($r \to \infty$), and applying the boundary conditions corresponding to a free axisymmetric jet issuing into a quiescent environment at $r = 0$,

$$W = V = 0\,; \quad \frac{\partial U}{\partial r} = 0\,; \quad \frac{\partial \overline{uw}}{\partial r} = \frac{\partial \overline{vw}}{\partial r} = 0\,, \tag{7}$$

and at $r \to \infty$,

$$V = U = 0\,; \quad \overline{uw} = \overline{vw} = 0\,; \quad \frac{\partial U}{\partial r} = \frac{\partial V}{\partial r} = 0\,; \quad \frac{\partial \overline{uw}}{\partial r} = \frac{\partial \overline{vw}}{\partial r} = 0\,, \tag{8}$$

the following relation is obtained

$$\int_0^\infty r(P - P_\infty)\, dr = -\frac{1}{2}\rho \int_0^\infty r \left(V^2 + \overline{v^2} + \overline{w^2}\right) dr\,. \tag{9}$$

In an analogous manner equation (4) can be simplified to obtain

$$\frac{d}{dx}\int_0^\infty r \left[(P - P_\infty) + \rho\left(U^2 + \overline{u^2}\right)\right] dr = 0\,. \tag{10}$$

Substitution of equation (9) into the latter expression the following momentum integral relation can be formulated:

$$\frac{d}{dx}M_x = \frac{d}{dx}\,2\pi\rho \int_0^\infty r \left[U^2 - \frac{V^2}{2} + \overline{u^2} - \frac{\overline{v^2} + \overline{w^2}}{2}\right] dr = 0\,. \tag{11}$$

An integral expression for the conservation of the axial flux of angular (or swirl) momentum can be derived by multiplying equation (3) with $r\,dA$, where $dA = 2\pi r\, dr$, and integrating it under the same conditions as in the previous derivation,

$$\frac{d}{dx}M_\phi = \frac{d}{dx}\,2\pi\rho \int_0^\infty r^2 \left(UV + \overline{uv}\right) dr = 0\,. \tag{12}$$

The ratio of angular momentum, M_ϕ, to the momentum integral expressed through equation (11), M_x, times the radius of the orifice, R, is one of the common ways to quantify the swirl intensity (Gupta *et al.* 1985). Thus an integral swirl number, $S_{\phi x}$, can be defined as

$$S_{\phi x} = \frac{M_\phi}{R M_x}\,. \tag{13}$$

It is common to discuss the integral swirl number in terms of the contribution due to the streamwise and azimuthal mean velocities only. Assuming that the algebraic relation of the squared fluctuating velocity components in equation (11) as well as the turbulent shear stress in the streamwise-azimuthal direction in equation (12) are negligible with respect to the squared mean components the swirl intensity reduces to an expression identical to the one in laminar flow,

$$S_{\phi x} = \left[\int_0^\infty r^2 UV\, dr\right]\left[R\int_0^\infty r\left(U^2 - \frac{1}{2}V^2\right) dr\right]^{-1}. \tag{14}$$

Together with the Reynolds number, defined as

$$Re_D = \frac{U_b D}{\nu}\,, \tag{15}$$

it is often utilised to characterise free swirling jets, although many other initial conditions are important, especially in the near-field region (Buresti *et al.* 1994). However different flow fields can be observed for the same Re_D and $S_{\phi x}$, making it absolutely essential to provide well defined initial conditions to classify the results, which, by the fully developed axially rotating pipe flow, is per se fulfilled. Here the ratio between the azimuthal velocity at the pipe wall, V_w, and the bulk velocity, U_b, can be utilised to form a swirl number,

$$S = V_w/U_b\,, \tag{16}$$

which together with the Reynolds number, Re_D, is sufficient to describe the flow field on its own. The literature is rich on definitions of the swirl number depending on the swirl generating method (Örlü 2006), therefore care is taken in the following to distinguish between them and avoid any confusion. Whereas the integral swirl number, $S_{\phi x}$, although not sufficient to describe the flow, is commonly used to compare different studies (as done in the introductory part), the swirl number for the axially rotating pipe flow, S, will be used throughout this paper, unless otherwise stated.

2.2. *The passive scalar field*

The temperature acts as a passive contaminant and obeys an advection-diffusion relation, which for the mean temperature in steady and axisymmetric flows in cylindrical coordinates leads to the following Reynolds-averaged equation

$$W\frac{\partial\theta}{\partial r} + U\frac{\partial\theta}{\partial x} + \frac{\partial\overline{u\vartheta}}{\partial x} + \frac{1}{r}\frac{\partial(r\overline{w\vartheta})}{\partial r} = \frac{1}{r}\frac{\partial}{\partial r}\left[a\,r\,\frac{\partial\theta}{\partial r}\right]\,. \tag{17}$$

Here the mean and fluctuating temperature are denoted by θ and ϑ, respectively, and a stands for the thermal diffusivity. Similar to the derivation of equations (11) and (12) a conservation equation for the axial heat flux can be derived by multiplying equation (17) with r and integrating it (Elsner & Kurzak 1989):

$$\frac{d}{dx}M_\theta = \frac{d}{dx}\,2\pi\rho\,c_p\int_0^\infty r(U\theta + \overline{u\vartheta})\,dr = 0\,. \tag{18}$$

The counterpart to the Reynolds number for the passive temperature field is the Peclet number, the product of Reynolds and Prandtl number, which appears inversely in the non-dimensionaled passive scalar equation in front of the diffusive term,

$$Pe_D = \frac{U_b D}{a}\,. \tag{19}$$

Both, Re_D and Pe_D, are assumed to be high enough in the present case to neglect the diffusive terms in comparison with the Reynolds stresses and fluxes.

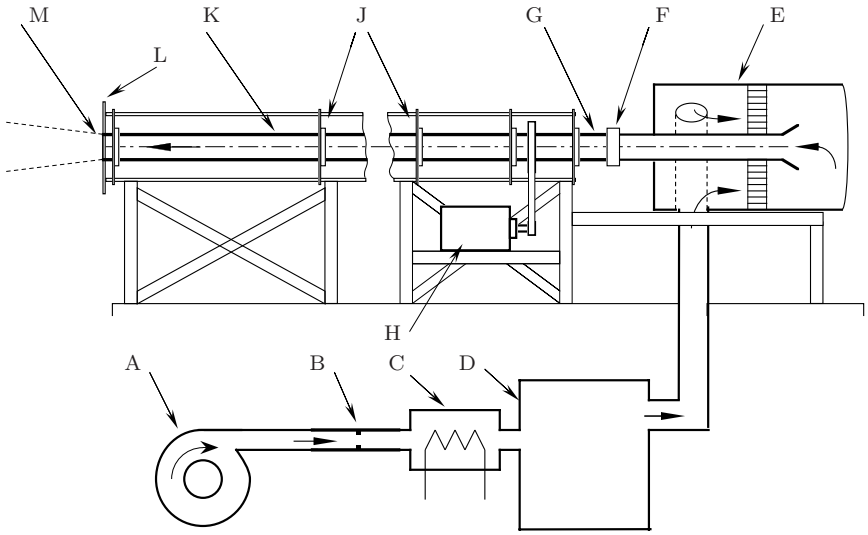

FIGURE 2. Schematic of the experimental setup. A) Centrifugal fan. B) Flow meter, C) Electrical heater, D) Distribution chamber, E) Stagnation chamber, F) Coupling between stationary and rotating pipe, G) Honeycomb, H) DC motor, J) Ball bearings, K) Rotating pipe, L) Circular end plate, M) Pipe outlet.

3. Experimental setup

3.1. *Experimental facility*

The experiments are performed at the *Fluid Physics Laboratory* of *KTH Mechanics* in a specially designed setup, consisting of a 100 pipe diameters long axially rotating pipe as shown in figure 2, which was recently used to study the dynamics of swirling flows in the near-field region (Facciolo *et al.* 2007*b*). The air is provided by a centrifugal fan (A), downstream of which a flow meter (B) monitors the flow rate. After the flow meter a flow distribution chamber (D) distributes the flow into three different pipes, which are symmetrically fed into the stagnation chamber (E). A bell mouth shaped entrance first feeds it into a one meter long stationary section, which is connected to the rotating pipe (K) through a rotating coupling (F). In the first part of the rotating part of the pipe a honeycomb (G) is mounted, which brings the flow into more or less solid body rotation. Thereafter the flow develops along the 6 meter long pipe before it emanates as a free jet (M). The pipe is made of seamless steel and has a honed inner surface. It is supported along its full length by 5 roller bearings (J), which are mounted within a rigid triangular shaped framework, and it is belt driven via a feed back controlled DC motor (H). In the present

measurements the pipe ends with a 30 cm diameter stationary, circular end plate (L), and is placed in a large laboratory with a large ventilation opening far downstream of the pipe outlet in order to prevent the ambient temperature in the laboratory to rise, due to the continuous supply of heated air. The pipe outlet is far enough from the surrounding walls and the floor, ensuring that the experiments reported here resemble a jet in an infinite environment (cf. appendix B of Hussein *et al.* 1994). A heater (C) placed in the flow upstream of the distribution chamber provides the heating of the air. The heater power can be regulated and is typically around 800 W. The outer pipe surface is insulated with a 15 mm thick foam material in order to decrease the heat transfer through the pipe wall and thereby establish a (nearly) constant radial temperature distribution in the pipe. The typical temperature difference between the flow in the pipe and the ambient air is 12 K.

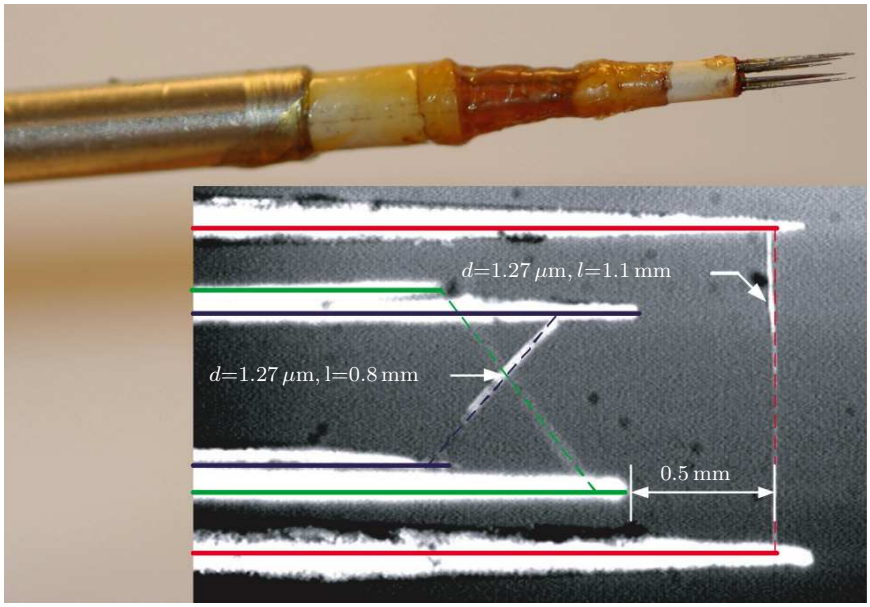

FIGURE 3. Combined X-wire and cold-wire probe with close-up of probe and wire constellation. The picture was taken several months after the performed measurements, which explains the traces of corrosion on the prongs. All wires are soldered to the tip of the prongs, which is not apparent from the two-dimensional microscopic picture.

3.2. *Measurement technique*

In order to get simultaneous acquisition of velocity and temperature, a probe has been designed and built, which consists of a combined X-wire and cold-wire probe operated in the constant temperature (CTA) and constant current (CCA) mode, respectively. The cold-wire consists of a 1.1 mm long wire and is placed 0.5 mm upstream and parallel between the 0.8 mm long hot-wires forming the X-probe in order to minimise the thermal and wake interference, as shown in figure 3. All sensing elements are Platinum wires with a diameter of 1.27 micron. In order to extend the applicability of the combined probe as much as possible into the intermittent region the resistance overheat ratio of the hot-wires and the current through the cold-wire were reduced to 30 % and 0.3 mA, respectively.

The X-probe was calibrated in the potential core of a specially designed contraction jet facility for different velocities and yaw angles at a constant temperature according to the look-up-matrix method (Bruun 1995), whereas the cold-wire was calibrated in the centre of the pipe exit against thermocouples with a measurement resolution of 0.1 K. Due to the small diameter and the low current through the cold-wire the anemometer output becomes a linear function of the fluid temperature and insensitive to velocity, except below velocities of 0.5 m/s. The hot-wire signals on the other hand start even at slightly higher velocities to lie outside the probe acceptance angle. The results presented in the next section do therefore not cover the whole jet cross section.

While the instantaneous temperature can be measured directly by the cold-wire, the voltage output for the hot-wires had to be compensated for changes in the instantaneous fluid temperature. This was accomplished by correcting the measured hot-wire voltages against deviations from the calibration temperature by utilising the well known relation Bruun (1995)

$$E_{\mathrm{out}}(T_{\mathrm{ref}})^2 = E_{\mathrm{out}}(T)^2 \left(\frac{T_h - T_{\mathrm{ref}}}{T_h - T}\right) = E_{\mathrm{out}}(T)^2 \left(1 - \frac{T - T_{\mathrm{ref}}}{a_R/\alpha_{el}}\right)^{-1}, \quad (20)$$

which is derived by considering the heat balance for the hot-wire for both the temperature during the calibration of the X-probe and an elevated temperature to which the probe is exposed in the actual measurements. Hereby $E_{\mathrm{out}}(T_{\mathrm{ref}})$ denotes the hot-wire response obtained for the same velocity under isothermal ($T = T_{\mathrm{ref}}$) conditions, $E_{out}(T)$ is the measured response from the anemometer output, T_h denotes the average temperature of the heated wire, and a_R and α_{el} stand for the resistance overheat ratio and the temperature coefficient of electrical resistivity, respectively. Hence relation (20) provides the anemometer signal which would have been measured if the fluid around the hot-wire would have had the same temperature T_{ref} as during its calibration, whereas in reality it had temperature T.

Instead of utilising a literature or manufacturer value for α_{el}, which in preliminary tests resulted in a too high wire temperature and thereby overcorrected $E_{\text{out}}(T_{\text{ref}})$, here an iterative approach was preferred. Such differences in the value of the temperature coefficient of electrical resistivity have previously be noted (van Dijk & Nieuwstadt 2004) and are probably due to small impurities, which can be found in 'pure Platinum' (Bradbury & Castro 1972) or are caused by tormenting processes during the production of the wire or its soldering (Örlü 2006) or welding (van Dijk 1999) to the prongs. In the evaluation process the coefficient to determine was decreased until the measured streamwise velocity profile of the triple-wire probe coincided with results from single-wire measurements in the cold jet, which are confirmed by results from LDV measurements conducted by Facciolo *et al.* (2007*b*) in the same facility and under the same characteristic parameters. The value for the temperature coefficient of electrical resistivity was tested at different velocities and temperatures and it was confirmed that changes in velocity and temperature in the range of interest are indeed insignificant for the determined value.

The used look-up-matrix method removes several error sources inherent in other X-wire calibration schemes, however, is affected by the out-of-plane velocity-component and rectification error (Bruun 1995). Using the acquired number of samples this error source, viz. the fraction of data points outside the calibration map, can easily be quantified. Table 1 presents the radial positions where approximately 1 % and 4 % of the voltage pairs are outside the calibration domain. The radial positions can be utilised to assess the reliability of the results presented in the next section. The time and spatial resolution of the measuring probe is limited to scales of an order of magnitude smaller than the Taylor microscale (estimated through the method proposed by Hallbäck *et al.* 1989)) and still more than 5 times smaller than these intermediate scales at the pipe outlet from where on the turbulent scales are growing in streamwise and radial direction (Örlü 2006). Although the smallest scales can therefore not be accessed, their effect on the computed quantities is negligible, as can be evinced by the power spectral density of the (joint) fluctuating signals (not shown here). Further details on the measurement technique as well as an assesment of the limitations of the results in the highly intermittent region can be found in Örlü (2006). It is, however, important to note, that despite the limitations of the applied measurement technique in the outer region of the free jet (be it the instantaneous reverse flow for the hot-wires or the velocity sensitivity as well as the traces of the hot wake in case of instantaneous reverse flow for the cold-wire), the combined probe is able to access the probability density distributions in a wide central region, which in the case of external intermittency is quite difficult to obtain with particle tracing techniques like LDV or PIV (Staicu 2002).

The signals from the CTA and CCA channels of an AN-1003 hot-wire anemometry system were offset and amplified through the circuits to match the

fluctuating signal components to the voltage range of the 16-bit A/D converter used, and then digitised on a PC at a sampling frequency of 4 kHz and a sampling duration between 30 s and 60 s depending on the downstream position of the probe.

4. Results and discussion

The results presented here were conducted at a bulk velocity, U_b, of 6 m/s, corresponding to a Reynolds number of around 24000. Previous studies in jets emanating from long pipes (Pitts 1991) as well as nozzles (Ricou & Spalding 1961) report that the effect of the Reynolds number diminishes for $Re > 25000$. To verify this LDV measurements in the non-swirling jet along its centreline were performed in the range of $0 \leqslant x/D \leqslant 10$. Results showed that at least for the mean axial velocity component as well as its turbulence intensity the flow tends to become independent of the Reynolds number in the higher end of the range from $Re = 6000$ to 34000.

The air at the pipe outlet was heated to around 12 K above ambient temperature and it was ensured that the pipe inlet temperature remained unchanged during operation and especially when increasing the rotational speed of the pipe, in order to relate the change in temperature solely to the addition of swirl. The swirling jet results were all acquired at a swirl number of $S = 0.5$ corresponding to an integral swirl number of $S_{\phi x} = 0.15$ at the pipe outlet. Full radial profiles of the axial and azimuthal velocity component as well as the temperature with up to 40 measurement points were acquired from the pipe outlet, $x/D = 0$, to 6 diameters downstream with increments of one diameter.

	r/R			
	$S = 0$		$S = 0.5$	
x/D	1 %	4 %	1 %	4 %
2	1.00	1.20	0.90	1.25
3	0.90	1.30	0.90	1.25
4	1.10	1.30	0.95	1.35
5	0.90	1.40	1.00	1.30
6	1.10	1.40	0.90	1.55

TABLE 1. Radial positions where 1 % and 4 % of the measured voltage pairs are outside the calibration map for the non-swirling and swirling jet.

In the following subsections the results for the mean flow, turbulence as well as their probability density distributions will subsequently be presented and discussed.

4.1. *Mean flow development*

Three-dimensional profiles of the mean axial velocity component and mean temperature are visualised in figures 4 and 5, thus making it possible to follow the evolution of the mean quantities along their radial and axial directions at the same time. The time-averaged values were normalised using the bulk velocity, U_b, and the centreline mean temperature (relative to ambient) at the pipe outlet of the non-swirled jet, θ_0, in order to emphasise the effect of the rotation on both the flow dynamics as well as the passive contaminant. The streamwise and radial coordinates were made non-dimensional by the pipe diameter and radius, respectively. Thick dashed lines are drawn through the centreline values (U^*_{CL} and θ^*_{CL}) as well as through the half-widths (R_U and R_θ) of the streamwise velocity component and temperature, representing the position where the considered quantity reaches half the value of its centreline value. Black lines in the radial direction correspond to the jet with swirl, while grey lines visualise the quantities for the non-swirling jet. The initial conditions for the jet are set by the outlet conditions of the fully developed turbulent pipe flow. This is a streamwise velocity distribution at the pipe outlet coinciding very well with the empirical power-law profile $U/U_0 = (1 - r/R)^{1/7}$ (Schlichting 1979), confirming that the flow upstream the pipe exit resembles a fully developed turbulent pipe flow (Xu & Antonia 2002*a*), as well as a temperature profile resembling a top-hat profile with a maximum deviation from the centreline of 0.03 within a region of $r/R < 0.7$.

The streamwise evolution of the centreline values depicts the axial decay rates and is hence an indication of the mixedness, while the half-widths facilitate the presentation of the spreading of the jet and hence visualises the entrainment rates for both the momentum (black lines) and heat (grey lines), respectively. It is important to note, however, that a faster axial decay is not a sufficient conditions to verify mixing enhancement. A faster axial decay might also be brought about by engulfing more unmixed fluid (e.g. ambient air at rest, colder air or a fluid with a low concentration) appearing or crossing the centreline (Mastorakos *et al.* 1996) as evinced in visualisations of jets with laminar initial conditions (Liepman & Gharib 1992). Hence additional indications from flow visualisations, higher order statistics or probability density distributions have to be consulted.

A recognisable feature of the thermal field is that its centreline value remains almost constant for downstream positions up to 4 D, whereas the centreline streamwise velocity component decreases (weakly) continuously right from the beginning of the pipe outlet. Therefore one could define a thermal potential core extending to 4 D, whereas no dynamic potential core exists by definition,

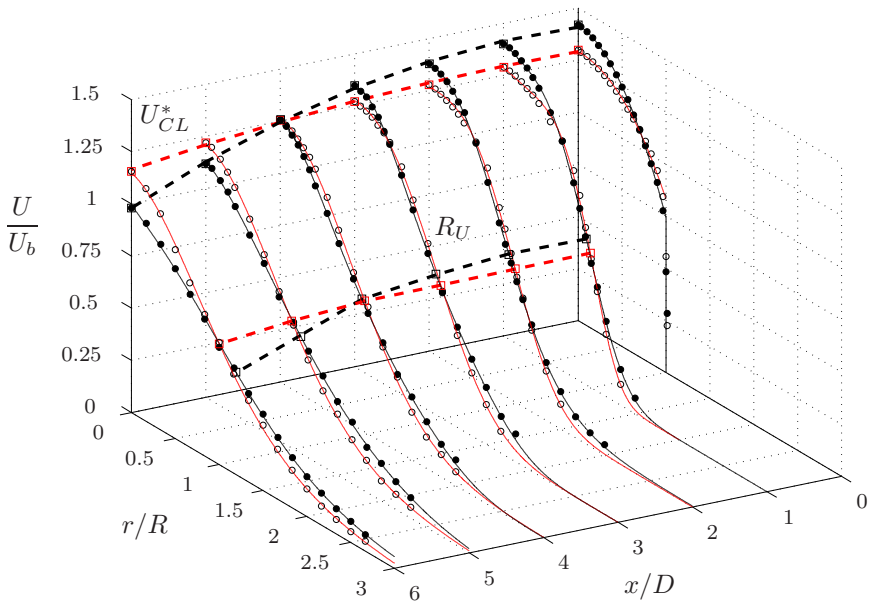

FIGURE 4. Three-dimensional profile of the mean axial velocity for the non-swirled (open markers) and swirled (filled markers) jet. Axial decays (U^*_{CL}) and mean velocity half-widths (R_U) are illustrated through the dashed lines. Full lines are for visual aid only.

although the jet conserves the low turbulence intensity level from the pipe up to 3 D into the jet. The different initial conditions for the temperature and velocity of the jet can be used to explain this behaviour.

It is clearly recognisable that the addition of swirl increases the mean streamwise velocity as well as the mean temperature in a wide central part of the pipe as well as few diameters downstream of the pipe outlet, while in regions beyond three and four diameters downstream the axial velocity component and temperature are overtaken by the non-swirling centreline values, thus indicating the faster axial decay rates through the addition of swirl. The increase of the axial velocity component in a central region of the pipe leads to its decrease close to the wall (cf. figure 6) in order to fulfil mass conservation. This effect results in a decrease of the shear stresses at the wall as can be evidenced by experimental studies (Kikuyama *et al.* 1983) as well as DNS (Satake & Kunugi 2002) and leads to an overall decrease of the pressure-drop. Reynolds analogy demands a proportional decrease in the convective heat transfer at the wall, i.e. the radial temperature gradient at the wall decreases leading to an increase in temperature in a wide central region. Thermocouple measurements at the

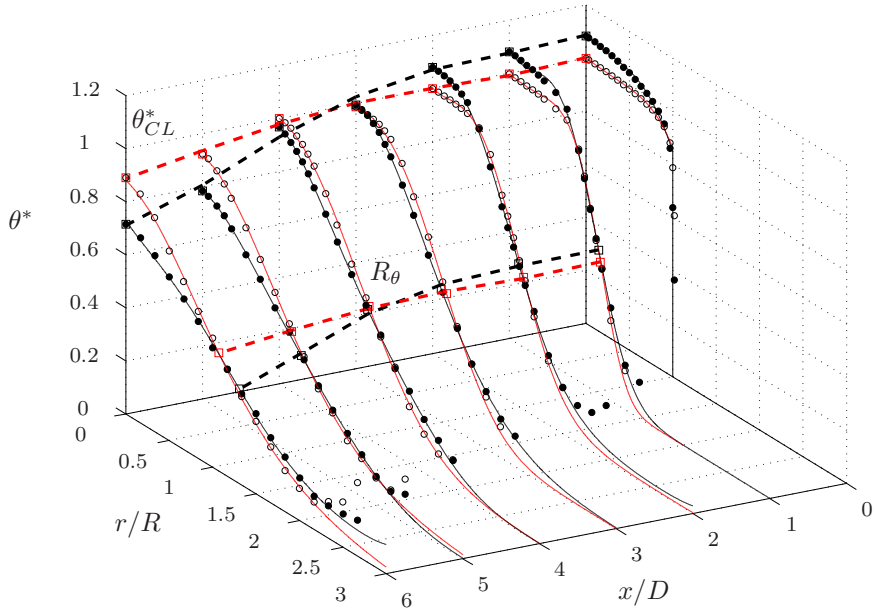

FIGURE 5. Three-dimensional profile of the mean temperature for the non-swirled (open markers) and swirled (filled markers) jet. Axial decays (θ^*_{CL}) and mean temperature half-widths (R_θ) are illustrated through the dashed lines. Full lines are for visual aid only.

pipe inlet ensured that the incoming flow remained at a constant temperature regardless of any change in rotational speed of the pipe. Hence the reduction of the heat transfer towards the pipe wall has to result in an increase of the axial flux of heat. The evaluation of the integral relation governing the passive scalar can be utilised to confirm this conclusion. The same effect, but not as clear, was also observed by Komori & Ueda (1985) in their axially rotating pipe with a divergent pipe exit for moderate swirl numbers. It should be pointed out that the change in the temperature distribution when rotation is induced is almost observed immediately, which shows that this is an effect of the changing dynamics of the flow and not an effect of changed initial and boundary conditions. The strong curvature of the lines representing the half-widths of both the velocity and temperature starting from around 4 D downstream indicates the established experimental fact that rotation increases the spreading rates for momentum as well as heat.

A more precise picture of the initial conditions can be found in figure 6, where the mean axial velocity component and temperature profiles are given for the pipe outlet and 6 diameters downstream. To further access the reliability of

the measurement technique, results from LDV measurements (Facciolo 2006) are shown as well, which were conducted in the same facility and at the same experimental parameters, viz. $Re_D = 24000$ and $S = 0$ as well as $S = 0.5$, albeit in an unheated air flow.

Although the focus of the present study is the mixing of a passive scalar, it is important to present the full set of initial conditions, to which the mean azimuthal velocity profile, shown in figure 7, belongs. As apparent from the value at the pipe outlet the fully developed axially rotating pipe flow exhibits a parabola like profile, which quickly looses its initial strength within the downstream distance under investigation, although the effect on the dynamic (Rose 1962) and thermal (Grandmaison & Becker 1982) flow field persists into the far-field. An interesting feature of the swirling jet emanating from a fully developed axially rotating pipe flow, first observed by Facciolo & Alfredsson (2004), is the counter-rotating core at around 6 diameters downstream, which can clearly be seen in the close-up in figure 7. The zoomed in profile reveals a

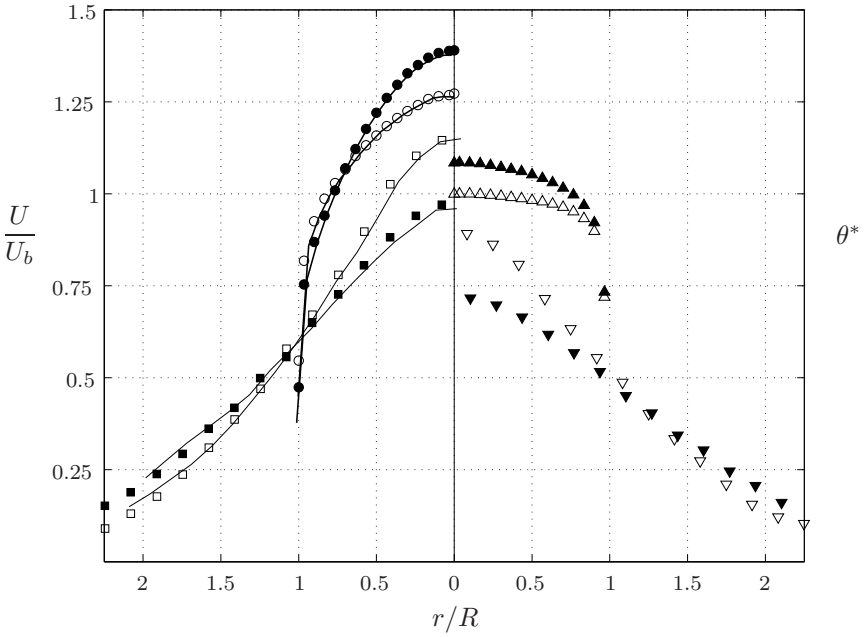

FIGURE 6. Mean axial velocity (left side) and temperature (right side) across the non-swirled (open markers) and swirled (filled markers) jet for two downstream positions: ○ and △: $x/D = 0$, □ and ▽: $x/D = 6$. LDV results for a non-heated jet at the same *Re* from Facciolo (2006) are illustrated through solid lines.

change in sign meaning that in average the jet, in the central region, rotates in a direction, which is opposite to that imposed by the rotating pipe. The azimuthal mean velocity of the counter-rotating core is fairly small, about 2 % of V_w, and it covers a region slightly smaller than the pipe diameter. The counter-rotating region starts between 5–6 D downstream of the pipe outlet, increasing in magnitude and reaching a maximum between 6 and 8 D. This puzzling feature of the swirling jet emanating from an axially rotating pipe flow is assumed to be due to the fact that large-scale turbulent motions, which often lead to strong contributions to the azimuthal-radial Reynolds shear stress, are efficient in transporting mean angular momentum radially outwards (Facciolo *et al.* 2007*a*).

One of the features, which makes the addition of swirl to a turbulent jet profitable, is its enhanced entrainment, as for instance exploited in jet pumps (Guillaume & Judge 2004). The entrainment coefficient, expressed in terms of the ratio of volume flux, Q, and its initial value, Q_0, is shown in figure 8. The jet without rotation reaches twice its mass flow after 6 D, whereas the addition

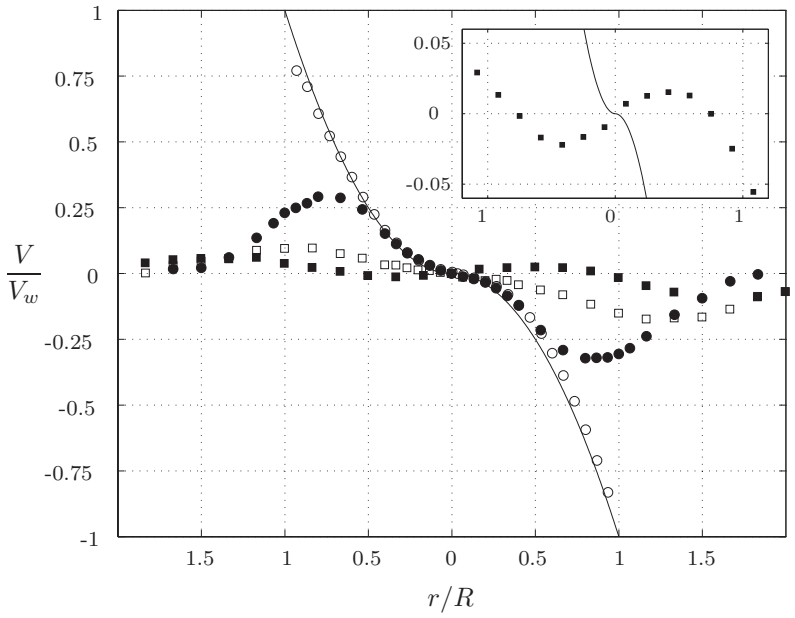

FIGURE 7. Mean azimuthal velocity across the swirled jet for four downstream positions: ○: $x/D = 0$, ●: $x/D = 2$, □: $x/D = 4$, ■: $x/D = 6$. Solid line represents a parabola $(r/R)^2$. Counter-rotating core is enlarged in the close-up.

of swirl reduces the distance needed by 2 D. The results for the non-swirling jet agree very well with results by Boguslawski & Popiel (1979) from a stationary pipe with a length of 50 D presented through a dashed line. Results from a jet emanating from a stationary and rotating pipe flow in the experiments by Rose (1962) show however deviations from the present results, which might be due to the difficulty in acquiring accurate data in the region approaching the still ambient air. The increased volume of the jet is a simple consequence of the intensified radial and axial pressure gradients. Similar observations are made in unbounded and wall-bounded free shear flows, where flow deceleration or an axial adverse pressure gradient increases entrainment as well as mixing (Sreenivas & Prasad 2000).

Another important check of the reliability of the measurement technique is to verify whether the obtained time-averaged quantities fulfil the governing equations. The integral relations expressing the conservation of axial fluxes of momenta, equations (11) and (12), and heat, equation (18), were deduced in section 2 and they are used to explore the consistency of the results. However, one is confronted with the same problems as for the entrainment rate in the low

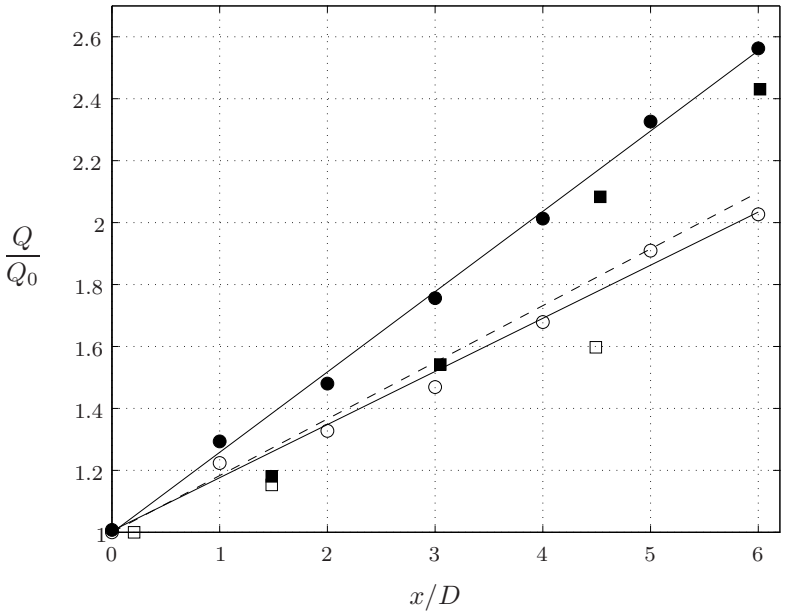

FIGURE 8. Downstream development of the entrainment coefficient for the non-swirled (open symbols) and swirled jet (filled symbols). ○: Present data (full lines are for visual aid only), □: Rose (1962), −−: Boguslawski & Popiel (1979).

	M_x [N]		M_θ [kW]	
x/D	$S = 0$	$S = 0.5$	$S = 0$	$S = 0.5$
0	0.138	0.138	0.230	0.244
2	0.135	0.135	0.220	0.224
4	0.141	0.139	0.226	0.218
6	0.131	0.141	0.205	0.211
mean	0.134	0.139	0.214	0.220
std	0.005	0.003	0.012	0.016

TABLE 2. Axial fluxes of the first-order approximation of the integral expressions of momentum conservation as expressed through equation (11) and (18).

streamwise velocity range for both the axial velocity component and temperature, but especially for the azimuthal velocity component, which – as evident from figure 7 – exhibits very low velocities further downstream and outwards compared to its axial counterpart and is furthermore weighted with the square of the radius (cf. equation (12)) making it difficult to compute an accurate value for the axial conservation of swirl. The integral expressions of momentum conservation as expressed through equations (11) and (18) including the mean and standard deviations of all measured downstream positions is given in table 2. Considering the axial fluxes at the pipe outlet it can be deduced that the axial flux of heat increases with the addition of swirl as already anticipated, contrary to the integral relation for M_x, which remains unchanged for a change in swirl intensity.

4.2. *Turbulence development*

4.2a. *Velocity and temperature fluctuations.* A simultaneous record of the normalised streamwise velocity and temperature fluctuations as well as their product is shown in figure 9 for the non-swirling and swirling jet taken at the centreline for $x/D = 6$. Several interesting features can readily be accessed by examining the figure. Whereas for the non-swirling jet the axial velocity fluctuations are clearly turbulent, the temperature fluctuations seem to be at the edge of the thermal core, where sudden low temperature peaks indicate that unmixed ambient air reaches or crosses the centreline. For the swirling jet, on the other hand, both the velocity and temperature fluctuations are fully turbulent, the fluctuation levels are increased, and the temperature exhibits the

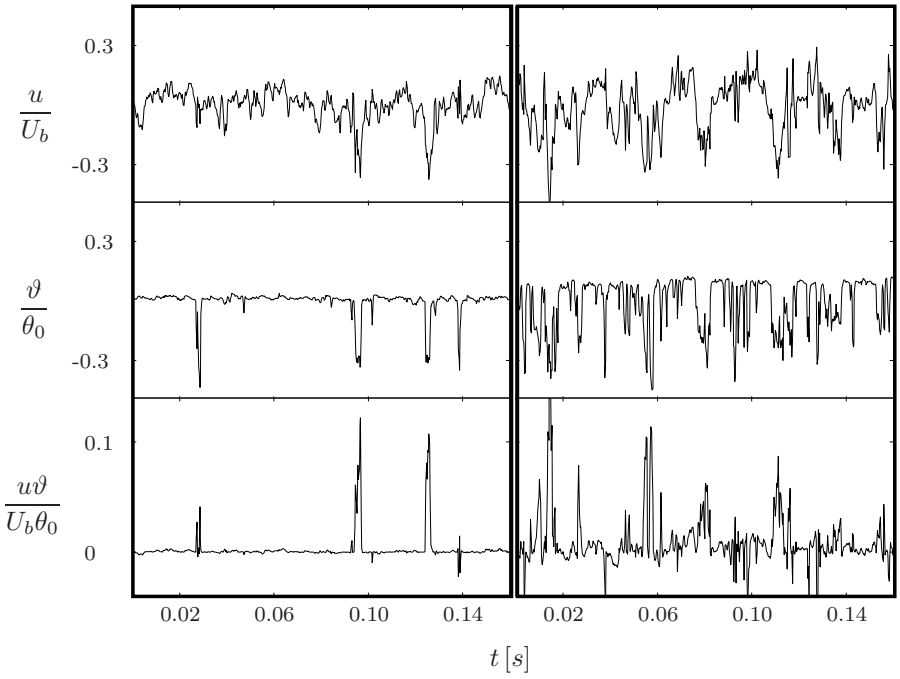

FIGURE 9. Simultaneous record of the normalised streamwise velocity and temperature fluctuations as well as their product at $x/D = 6$ for the non-swirled (left side) and swirled (right side) jet at the centre of the jet.

expected ramp-like structure on which the passive scalar fluctuations are carried (Warhaft 2000). The mentioned upstream displacement of the cold-wire in relation to the position of the X-wire (cf. section 3) is negligible (of the order of 0.1 ms) for all measured values as apparent from the coinciding peaks of low temperature and low streamwise velocities, which are responsible for the large contributions to the passive scalar flux, as the product of u and ϑ anticipates.

4.2b. *Turbulence intensities.* The radial distribution of the root mean square value for the fluctuations in the axial velocity component, u', normalised with U_b as well as the temperature fluctuations, ϑ', normalised with θ_0 are shown in figures 10 and 11 and provide another possibility to analyse the mixing behaviour in the near-field of the jet. As evident from the off-axis peaks and the strong valleys around the centreline for all measured fluctuating components the heated jet fluid is not well mixed with the entrained cold air. The off-axis peaks in the root mean square fluctuations are due to the large radial gradients and can also be attributed to unmixed regions of jet fluid and the

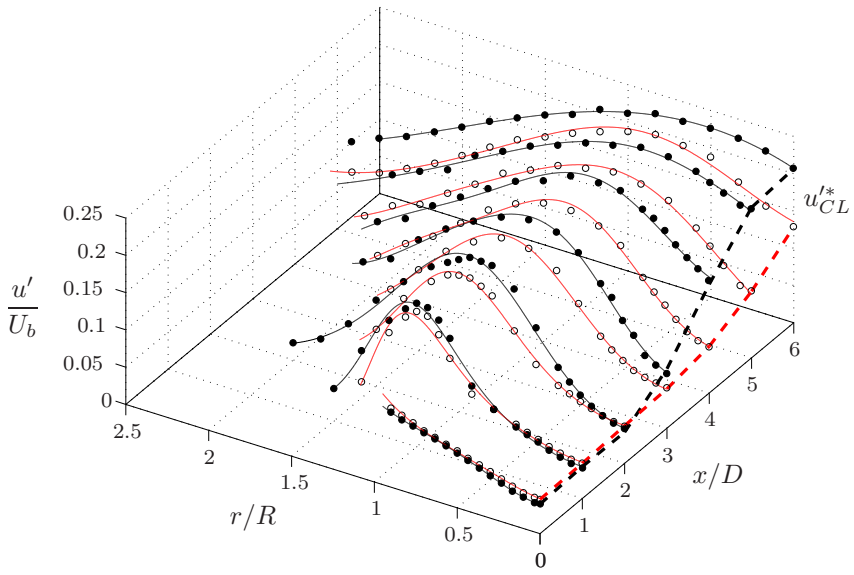

FIGURE 10. Three-dimensional profile of the root mean square value of the axial velocity fluctuations for the non-swirled (open markers) and swirled (filled markers) jet. Their centreline developments (u'^*_{CL}) are illustrated through the dashed lines. Full lines are for visual aid only.

entrained air leading to large-scale variations in the mixing region, whereas the contributions along the centreline are primarily attributed to the small-scale fluctuations (Schefer & Kerstein 1994). However with increasing downstream position the valley looses its extreme difference to the maximum value indicating the transition towards the well mixed and developed jet. The addition of swirl clearly enhances the centreline values (dashed lines) starting from 2–3 D having their largest difference to the non-swirled jet at 4–5 D. The axial trends of the centreline values of the non-swirling (grey dashed lines) and swirling (black dashed line) jet visualise an earlier development of the swirling jet, however the lines converge further downstream due to the restriction of full mixedness.

The U-shaped profile of the temperature fluctuations intensity with its low fluctuating level observed at the pipe outlet is due to the flat mean temperature profile, and diminishes rather quickly adapting the shape of the turbulence intensity profiles for the velocity components in the developing free jet. The measurement results for the root mean square value of the temperature for

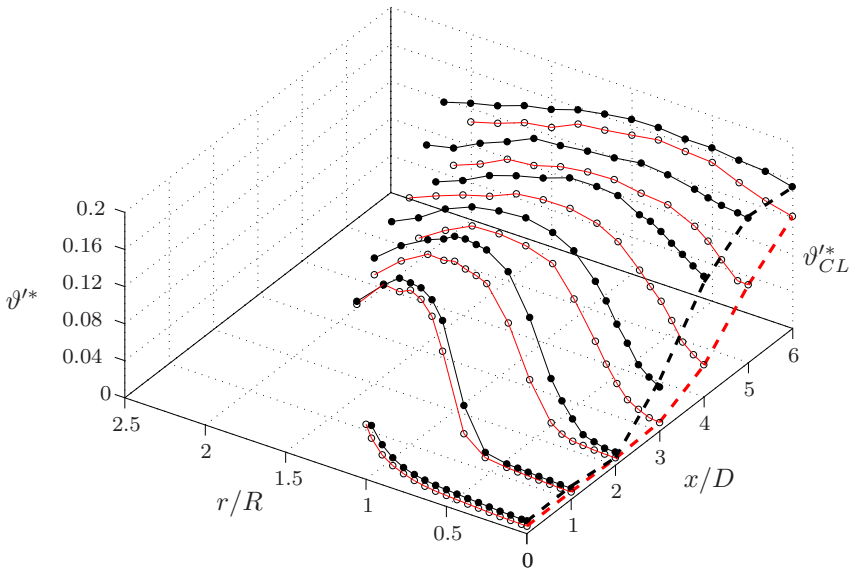

FIGURE 11. Three-dimensional profile of the root mean square value of the temperature fluctuations for the non-swirled (open markers) and swirled (filled markers) jet. Their centreline developments (ϑ'^*_{CL}) are illustrated through the dashed lines. Full lines are for visual aid only.

the non-swirling jet at 3 D downstream agrees very well with the data presented by Xu & Antonia (2002*b*) from an over 100 pipe diameters long pipe at $Re_D = 86000$ and the same excess temperature as in the present case (the effect of the Reynolds number of the scalar field for jets originating from a long pipe is much weaker than compared to jets emanating from nozzles and may be negligible as reported by Pitts (1991)).

Analogous to the mean velocity and temperature profiles in figure 6 a more precise picture of the initial conditions can be found in figure 12, where the root mean square value of the axial velocity and temperature fluctuations across the pipe outlet and 6 diameters downstream are given. The quality of the temperature compensation method can be obtained by comparison with the LDV measurements (Facciolo 2006). The opposite effect of rotation on the variances in the central region of the pipe outlet, viz. a decrease for the axial velocity and an increase for the temperature, can be explained by their initial mean profiles. Whereas the mean axial velocity resembles a fully developed turbulent pipe flow and hence tends to suppress turbulence with increasing

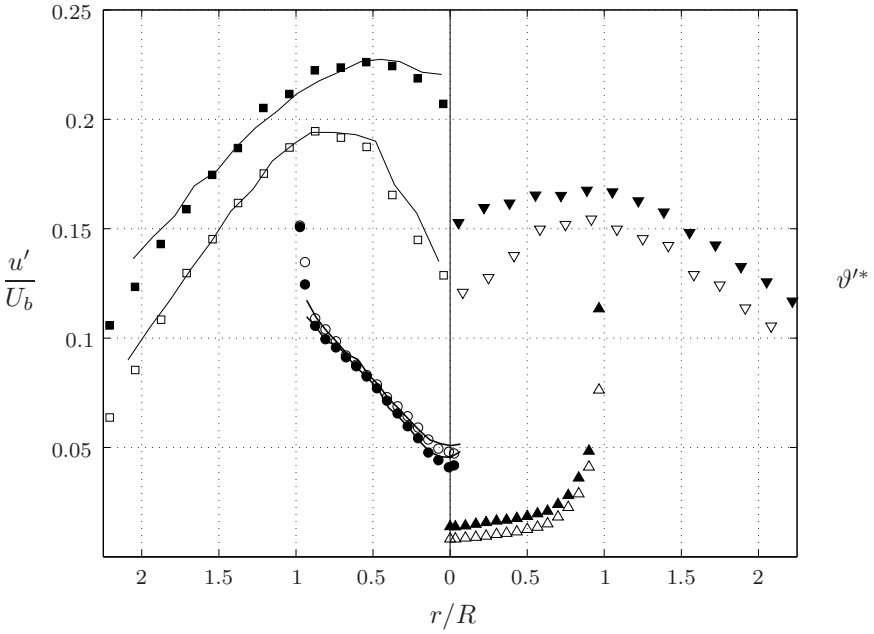

FIGURE 12. Root mean square value of the axial velocity (left side) and temperature (right side) fluctuations across the non-swirled (open markers) and swirled (filled markers) jet for two downstream positions: ○ and △: $x/D = 0$, □ and ▽: $x/D = 6$. LDV results for a non-heated jet at the same Re from Facciolo (2006) are illustrated through solid lines.

rotation (Reich & Beer 1989), the mean temperature profile resembles a top-hat profile, which tends towards a more turbulent one with increasing rotation (Reich *et al.* 1989).

4.2c. *Reynolds shear stress and flux.* Another indication of the effect of rotation on the free jet is apparent from the correlation coefficients, i.e. the cross-variances of the fluctuating components normalised by their appropriate variances. The correlation coefficients of axial velocity and temperature fluctuations, $\rho_{u\vartheta}$, as well as axial and azimuthal velocity fluctuations, ρ_{uv} (due to the change of sign in the azimuthal velocity component around the pipe or jet axis this correlation coefficient exhibits an antisymmetric profile), are visualised for different downstream positions in figures 13 and 14. No differences are detectable between the non-swirling and swirling jet for the fully developed pipe flow as well as for the jet at 6 D downstream, while only marginal differences are observable at $x/D = 2$. In contrast a distinct difference can be found

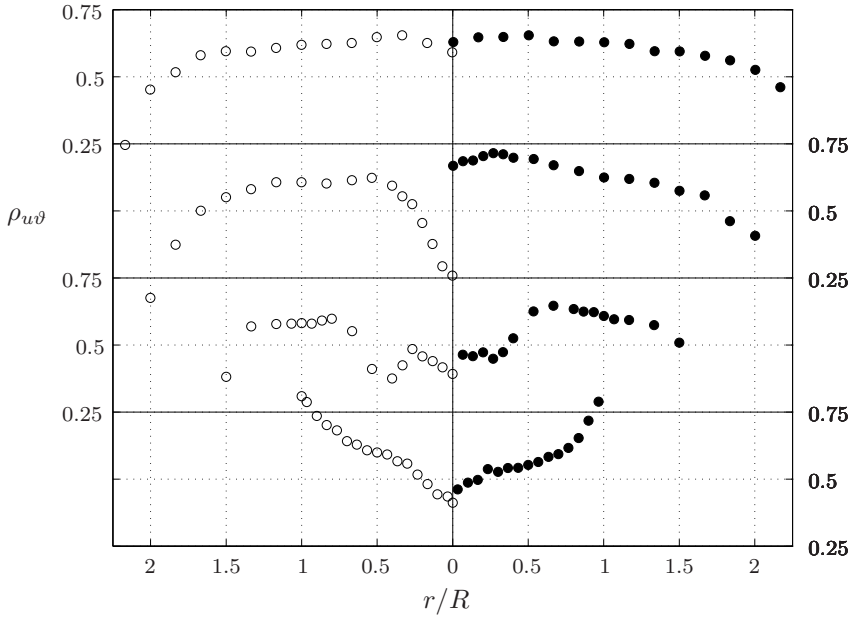

FIGURE 13. Correlation coefficient of axial velocity and temperature fluctuations across the non-swirled (left side, open symbols) and swirled (right side, filled symbols) jet for four downstream positions: from bottom to top corresponding to $x/D = 0$, 2, 4 and 6.

4 D downstream, where the addition of swirl increases the correlation between the instantaneous axial velocity component and the temperature remarkably, which could be anticipated through the increase of the root mean square values of both fluctuating variables (cf. figures 10 and 11) associated with the arrival of the conical shear layer at the jet axis and the end of the thermal potential core.

The maximum value of $\rho_{u\vartheta}$ travels from the pipe outlet to 6 D downstream moving from the pipe wall ($r/R = 1$) to the jet centreline. In contrast, for the swirling jet, the maximum value reaches the centreline 1–2 D earlier. The centreline development shows that for the non-swirling case a minimum is reached around $x/D = 4$ while no minimum is observed for the swirling case. The centreline value remains rather constant right from the pipe outlet up to 3 D downstream. A similar trend is found by Xu & Antonia (2002*b*) where $\rho_{u\vartheta}$ reaches its minimum and maximum value around $x/D = 3$ and 10, respectively. The low values of the correlation coefficient, as e.g. observed around the centreline at $x/D = 4$ in the case of the non-swirling jet, are an indication for

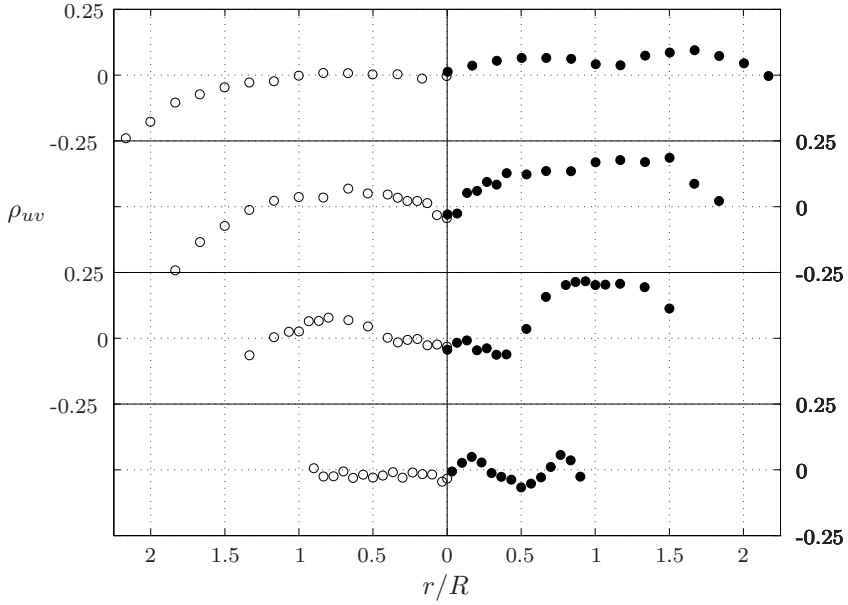

FIGURE 14. Correlation coefficient of axial and azimuthal velocity fluctuations across the non-swirled (left side, open symbols) and swirled (right side, filled symbols) jet for four downstream positions: from bottom to top corresponding to $x/D = 0$, 2, 4 and 6.

the unmixedness of the flow at that particular local position, which is located at the end of the thermal potential core, whereas the axial velocity fluctuations are already fully turbulent.

As expected for the correlation coefficients involving the azimuthal velocity fluctuations ρ_{uv} is zero for the non-swirling pipe flow and remains also zero along the centreline. For the axially rotating pipe flow, on the other hand, two slight peaks are observable, one near the pipe wall and the other near the centreline, which are also seen in DNS studies (Orlandi & Fatica 1997).

To access the physical transport mechanisms quantitatively the turbulent heat flux in the streamwise direction, $\rho\, c_p\, \overline{u\vartheta}$, as well as the axial-azimuthal Reynolds shear stress, $\rho\, \overline{uv}$, are shown non-dimensionalised in figures 15 and 16, respectively. Here the Reynolds flux is non-dimensionalised by $\rho\, c_p\, U_b \theta_0$ and the Reynolds stress by $\rho\, U_b^2$. The addition of rotation shows a drastic increase in the streamwise heat flux, especially 3–5 D downstream along and around the centreline, and remains also over the whole cross-section larger than its non-swirling counterpart. Hence swirl strongly promotes the longitudinal heat flux.

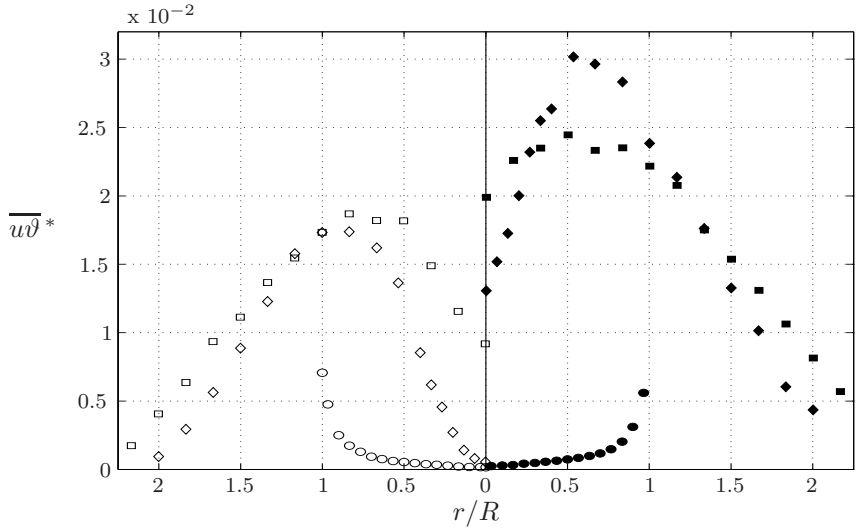

FIGURE 15. Streamwise passive scalar flux across the non-swirled (left side, open symbols) and swirled (right side, filled symbols) jet for three downstream positions: ○: $x/D = 0$, ◇: $x/D = 4$, □: $x/D = 6$.

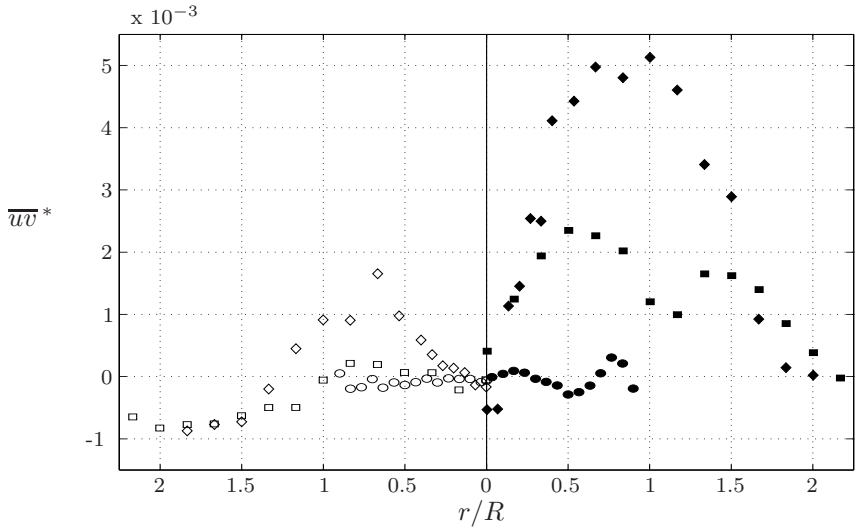

FIGURE 16. Axial-azimuthal Reynolds shear stress across the non-swirled (left side, open symbols) and swirled (right side, filled symbols) jet for three downstream positions: ○: $x/D = 0$, ◇: $x/D = 4$, □: $x/D = 6$.

Due to symmetry reasons $\rho\overline{uv}$ should be zero for the non-swirling case, however with increasing radius the deviation from zero increases. Similar difficulties in measuring the secondary (in magnitude) Reynolds stresses were reported by Mehta *et al.* (1991) and Nayeri (2000). These difficulties are mainly associated with the large instantaneous flow angles and sensitivity to the third velocity component. The error in the measured Reynolds stresses were investigated by Tutu & Chevray (1975) and more recently by Ovink *et al.* (2001). They showed that the Reynolds stresses are underestimated whereas the mean streamwise velocity component is overestimated with increasing local turbulence intensity, i.e. with increasing radial distance from the centreline. The addition of swirl to the developing jet shows a drastic increase on $\rho\overline{uv}$. As pointed out by Launder & Morse (1979) and Gibson & Younis (1986) $\overline{uv}$ exerts a strong influence on $\overline{uw}$, which in turn influences the rate of spread as well as the decay of the axial mean centreline velocity. Hence it is crucial for turbulence models to account for $\overline{uv}$ in the near-field region if an azimuthal velocity component is present.

4.3. *Probability density distributions*

Up to now the development of the measured mean and second order statistics, i.e. Reynolds stresses and fluxes, have been presented and discussed. Although a drastic change due to the addition of swirl could be observed at some centreline locations, there is still some doubt on whether the observed faster axial decay rates of the mean values as well as the increase in the second order statistics are simply a cause of more engulfed unmixed flow appearing or crossing the measurement probe, or whether it is due to higher mixing rates. Therefore the probability density distributions of the axial velocity fluctuations, $p(u)$, the temperature fluctuations, $p(\vartheta)$, their skewness and flatness factors, as well as their joint probability density distributions, $p(u,\vartheta)$, have to be accessed, which to our knowledge has not previously been done in swirling jet studies, despite its advantages to give insight in the state of mixing compared to first and second order statistics. In the following the probability density and joint probability density distributions of the axial velocity and temperature fluctuations will be presented and discussed, whereas the interested reader is referred to Örlü (2006) for an full description of the skewness and flatness factor distributions.

4.3a. *Single probability density distributions.* The single probability density functions (p.d.f.s) of the streamwise velocity fluctuations, $p(u)$, as well as the temperature fluctuations, $p(\vartheta)$, at a downstream position of 6 D are shown in figures 17 and 18, respectively. The quantities on the abscissa were normalised by their root mean square values, whereas the probability density functions were scaled in such a way that the area under each curve is equal to one. The p.d.f.s of three distinct radial positions, corresponding to the centreline ($r/R \simeq 0$), a region of high turbulence intensity ($r/R \simeq 0.6$) and a highly intermittent

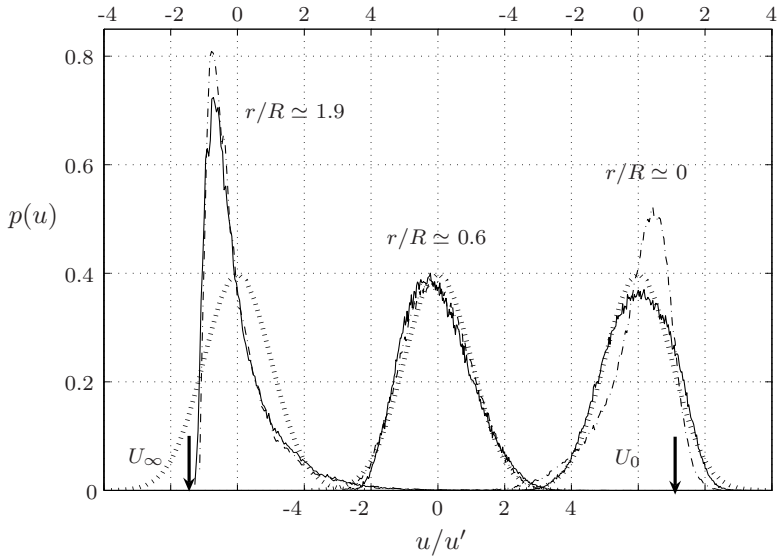

FIGURE 17. Probability density function of the streamwise velocity fluctuations for the non-swirled (dash-dotted line) and swirled jet (solid line) at radial positions corresponding to high intermittency (left), high turbulence intensity (middle) and the centreline (right) at $x/D = 6$. Gaussian distributions are plotted for comparison (dotted).

region ($r/R \simeq 1.9$), are presented for the fluctuating components of both the non-swirling (dash-dotted line) and swirling (solid line) jet. Gaussian distributions are also included as dotted lines for each position for comparison.

By considering $p(u)$ of the non-swirling jet around its axis the information that entrained air (which is initially colder and slower) is not fully mixed with the heated jet emanating from the pipe can be obtained. The measurement probe consequently would experience occasionally air 'blobs' with lower and colder instantaneous streamwise velocities and temperatures, respectively. This can further be affirmed by checking a trace of the axial velocity fluctuations in this region, which exhibit occasionally deep valleys of low fluctuating levels. The position of the mean axial centreline velocity at the pipe outlet for the non-swirling case, U_0, is drawn into the figure to emphasise that instantaneous axial velocities as high as U_0 still occur with a high probability.

Moving radially outwards, towards the position of high turbulence intensity, the shape of the p.d.f. resembles an almost Gaussian distribution indicating the good mixing between the heated jet and the newly entrained cold air. The tail of the jet illustrated in the leftmost side of the figure shows a highly positively

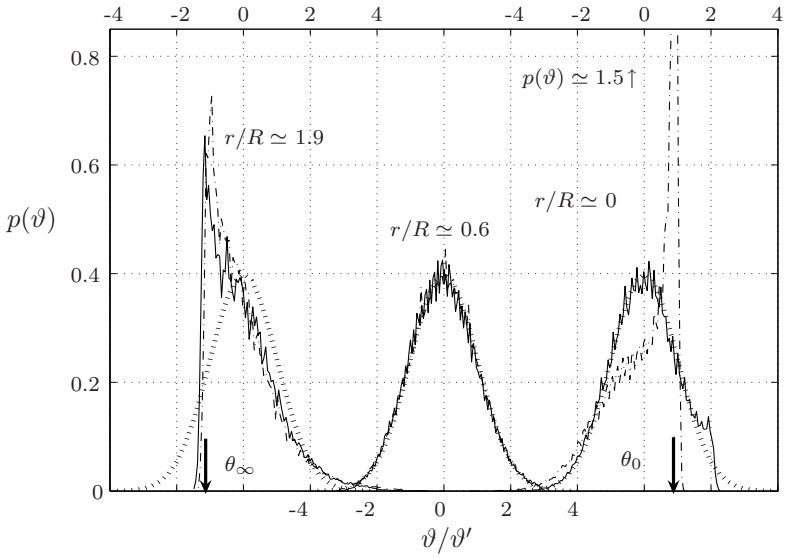

FIGURE 18. Probability density function of the temperature fluctuations for the non-swirled (dash-dotted line) and swirled jet (solid line) at radial positions corresponding to high intermittency (left), high turbulence intensity (middle) and the centreline (right) at $x/D = 6$. Gaussian distributions are plotted for comparison (dotted).

skewed and peaked p.d.f. indicating the occurrence of large-scale intermittent structures of high velocity air. The p.d.f. at this radial position is bounded by the velocity of the ambient air, i.e. air at rest. The inspection of the shape of the p.d.f. leads us to infer that back flow, instantaneous flow in the negative x-direction, might be present for a certain fraction of the time-series of the axial velocity component (around 90 % of the measured samples at this particular location lie within the region of the X-wire calibration plot). Thus the limit of the applied measurement technique is crossed at this radial position (cf. table 1).

The addition of swirl clearly changes the scenario for the jet around its centreline: the initially negatively skewed and peaked p.d.f. follows nearly a Gaussian distribution. On the contrary, no large changes are observable for the two other radial positions. Both radial positions experience approximately the same mean streamwise velocity component as well as turbulence intensity for both the non-swirling and swirling jets. The fluid at the local position corresponding to the region with high turbulence intensity is furthermore already well-mixed with the entrained air, so that the addition of rotation does not show

any further detectable contribution to the mixing process. The faster axial velocity decay and the higher turbulence intensity at the centreline in comparison with its non-swirling counterpart reduces the probability that streamwise velocity fluctuations as high as the initial centreline velocity occur. This indicates that the kinetic energy of the mean flow has mainly been utilised to entrain more irrotational air at ambient temperature and to mix it with the warm and faster mean stream.

A similar interpretation can be obtained from $p(\vartheta)$ for the same radial and axial positions. Here again the non-swirled jet exhibits an even more negatively skewed and highly peaked p.d.f. pointing out the coexistence of 'blobs' of almost unmixed fluid at a temperature close to the initial centreline temperature, θ_0, with 'blobs' of well-mixed fluid. The more skewed and peaked passive scalar p.d.f.s are, however, not surprising if one recalls that the advection-diffusion relation governing the passive scalar does not contain a pressure term. It is known that pressure acts non-local and thus implies that pressure fluctuations (which are directly coupled to the turbulent velocity field) induce far-field pressure forces, which in turn has the consequence that every part of a turbulent flow feels every other part (Davidson 2004). Consequently the pressure field acts as a redistribution process within the velocity field smoothing out much of the intermittent structures. This redistribution process, however, is absent for the passive scalar field, which explains the possibility of occurrence of sharp peaked p.d.f.s. The presence of regions of 'hot' fluid at a temperature very close to θ_0 is attributed to the limited effect of molecular diffusivity on the temperature field (Pietri *et al.* 2000). At the edge of the jet the opposite scenario is present, namely 'blobs' of 'cold' air close to the ambient temperature coexist with well mixed warmer air associated with a more or less Gaussian part along the positive abscissa. This interpretation is supported by the presence of bimodal temperature p.d.f.s at further upstream positions within the conical shear layer (not shown here), which are more pronounced for the non-swirling than the swirling case and smear out further downstream.

The addition of swirl to the jet clearly shows that the highly frequent 'hot' fluid regions in the non-swirling jet do hardly occur in the well mixed swirling jet along the centreline. Hence the probability of intermediate temperatures and consequently mixed fluid increases for the swirling jet when compared to its non-swirling counterpart.

4.3b. *Joint probability density distributions.* The previous paragraph showed, that especially the p.d.f. of the temperature fluctuations is useful in describing the state of mixing, and that the classical approach to analyse the axial decay rates as well as the turbulence intensities is not sufficient and might even give a wrong impression. This will become much clearer when considering the distribution of fluctuations of the streamwise velocity and temperature at the same time by means of joint probability density functions (j.p.d.f.s).

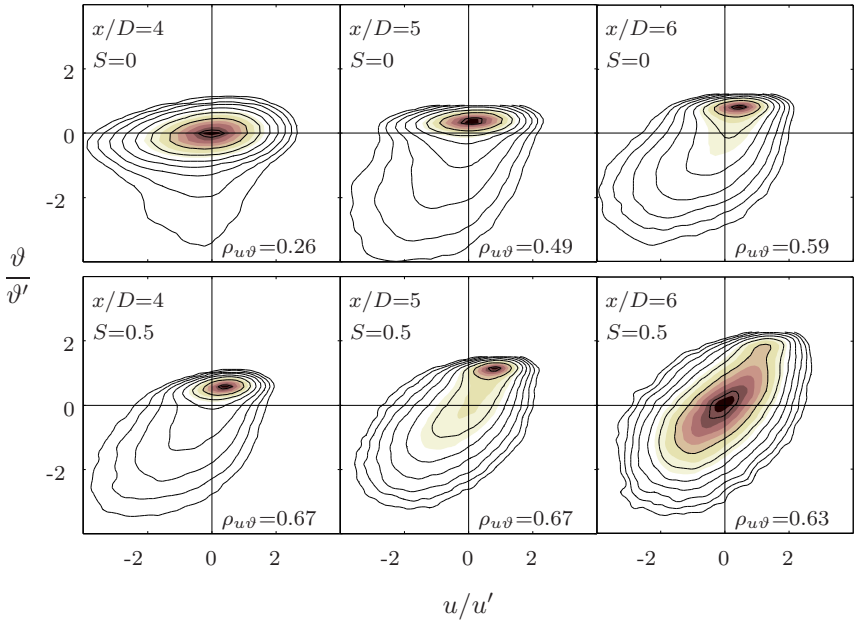

FIGURE 19. Joint probability density distributions of the axial velocity and temperature fluctuations normalised with their own root-mean-square values for $4 \leqslant x/D \leqslant 6$ along the jet centreline for the non-swirled and swirled jet. Black lines and shaded areas denote logarithmically and linearly spaced isodensity loci, respectively.

The j.p.d.f.s of the axial velocity and temperature fluctuations, $p(u, \vartheta)$, normalised with their own root mean square values for the non-swirling and swirling jet at $x/D = 4$, 5, and 6 along the jet centreline and $r/R \approx 0.85$ are shown in figures 19 and 20, respectively. Hereby shaded areas and black curves denote linearly and logarithmically spaced isodensity loci, respectively. While the former visualises the state of mixing, the latter focusses more on the entrainment. The correlation coefficient of both fluctuating components, $\rho_{u\vartheta}$, is additionally given in each subfigure.

Considering the non-swirling jet along its centreline from 4 D to 6 D it can be seen that there exists no dynamic potential core and that the conical shear layer has already reached the centreline, whereas the temperature fluctuations start to increase with downstream evolution indicating the end of the thermal potential core. The clear difference between the linearly and logarithmically spaced isodensity loci clearly exposes that mainly low temperature and low velocity fluid is engulfed and that the newly entrained fluid is highly separated

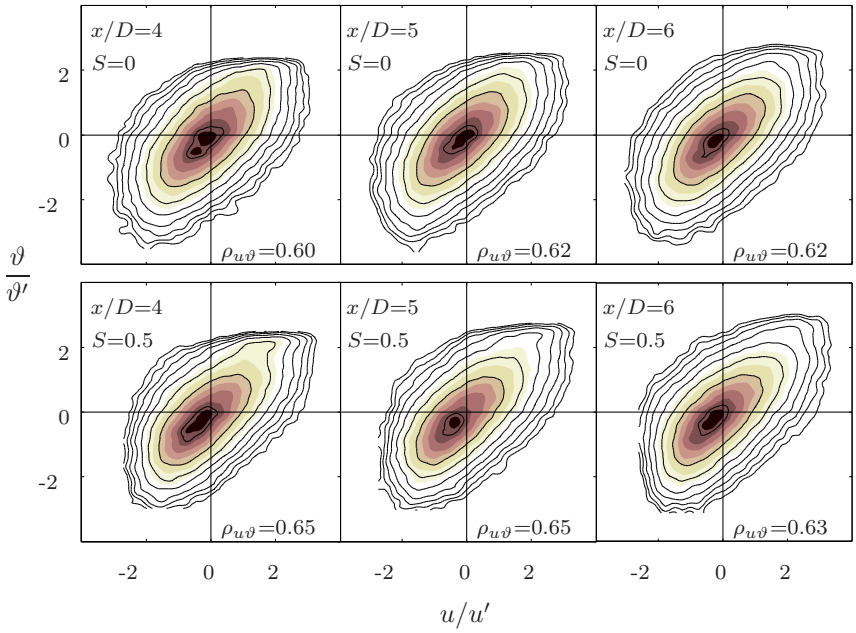

FIGURE 20. Joint probability density distributions of the axial velocity and temperature fluctuations normalised with their own root-mean-square values for $4 \leqslant x/D \leqslant 6$ around $r/R \approx 0.85$ for the non-swirled and swirled jet. Black lines and shaded areas denote logarithmically and linearly spaced isodensity loci, respectively.

from and hence unmixed with the flow issuing from the pipe outlet. In the case of the swirling jet, the entrained flow starts to mix with the initial flow leading to a similar distribution for the linearly and logarithmically spaced isodensity curves. It is interesting to note that the correlation coefficient, does neither indicate the state of mixing nor the amplitude of the streamwise passive scalar flux (cf. figure 15). Furthermore the reported sudden increase in the turbulence intensities and streamwise passive scalar flux, due to the addition of rotation to the jet at the jet axis for $x/D = 4$, can not be associated with a state of higher mixing, which without the (j.)p.d.f.s would have been assumed and is quite common in the literature. Utilising a $u\vartheta$-quadrant analysis (Rajagopalan & Antonia 1982) it can be shown that the main part of the streamwise passive scalar flux is due to the engulfed low speed and cold air for 4 and 6 D downstream for the swirling and non-swirling jet, respectively. Whereas further downstream the first quadrant, i.e. high velocity and high temperature fluctuations, start to contribute as well.

For regions with high turbulence intensities on the other hand, the addition of swirl does not seem to increase the mixing in the region between $4 \leqslant x/D \leqslant 6$ as is evident from figure 20.

5. Summary and conclusion

The effect of rotation on the mixing of a passive scalar in the near-field of a free jet was investigated. The jet emanates from a fully developed turbulent pipe flow and is slightly heated above the ambient temperature, making the temperature act as a passive contaminant. The effect of rotation is studied by rotating the pipe axially which gives rise to a swirling jet at the pipe outlet. In both the non-rotating and rotating cases the pipe flow is fully developed and produces well-defined velocity and temperature profiles.

Several experimental studies concerning the effect of swirl on the mixing characteristics in swirling jets have been reported. A comprehensive and detailed "blueprint" of the near-field of swirling jets has however been hindered due to secondary disturbances and traces induced by swirl generating methods. This also limits the usefulness of previous studies for comparison with numerical simulations and computations. Here however, due to the generation of a swirling jet by an axially rotating pipe (100 pipe diameters long) flow, the observed alterations in the well-defined dynamically and thermally axisymmetric flow field could solely be ascribed to the effect of swirl. In this sense there are no comparable studies concerning the passive scalar mixing in swirling jet flows.

By means of a combined X-wire and cold-wire probe the axial and azimuthal velocity components as well as the temperature were acquired simultaneously making it possible to compensate the hot-wire signals against variations in the temperature. This made it possible to simultaneously access instantaneous velocity and temperature signals, which are viable for mixing studies.

Measurements across the jet from the pipe outlet to 6 D downstream for the heated non-swirled and swirled jet at a Reynolds number of 24000 were performed to study the effect of rotation on the dynamic and thermal flow field, the turbulence (joint) statistics as well as the mixing of a passive scalar in the near-field of the jet.

The addition of a moderate degree of swirl highly modifies the dynamic and thermal flow field of the jet in its near-field region to that effect that the swirling jet in comparison to its non-swirling counterpart spreads and mixes faster as well as increases momentum and heat transport.

Due to the high local turbulence intensity, the high intermittency, the three dimensionality of the mean velocity and the non-isothermal conditions, the heated free swirling jet represents a challenge for any measurement technique. Despite all this it was shown that hot-wire anemometry under the present conditions represents a valuable measurement technique in a wide central region

of the heated swirling jet, when keeping the limitations in mind and accounting for them.

The thereby obtained (joint) probability density distributions evinced that the classical approach to quantify mixing, namely the axial decay rate of the mean quantity and the turbulence intensity, is not sufficient. Furthermore it was shown that neither a high correlation coefficient, nor a high passive scalar flux do indicate a highly mixed state, and that the latter is rather a result of engulfed unmixed ambient air.

Acknowledgments

This work was sponsored by the *Swedish Energy Agency* (STEM), within its fluid dynamics program, as well as the *Swedish Research Council* (VR), which are both gratefully acknowledged. The authors wish to thank Prof. Alessandro Talamelli and Dr. Nils Tillmark for many helpful suggestions and discussions as well as Mr. Marcus Gällstedt and Mr. Ulf Landén for their help in constructing the rotating pipe facility.

References

Billant, P., Chomaz, J. M. & Huerre, P. 1998 Experimental study of vortex breakdown in swirling jets. *J. Fluid Mech.* **376**, 183–219.

Boguslawski, L. & Popiel, C. O. 1979 Flow structure of the free round turbulent jet in the initial region. *J. Fluid Mech.* **90**, 531–539.

Bradbury, L. J. S. & Castro, I. P. 1972 Some comments on heat-transfer laws for fine wires. *J. Fluid Mech.* **51**, 487–495.

Bradshaw, P., Launder, B. E. & Lumley, J. L. 1996 Collaborative testing of turbulence models. *J. Fluid Eng-T ASME* **118**, 243–247.

Bruun, H. H. 1995 *Hot-wire anemometry: Principles and signal analysis*. Oxford University Press Inc., New York, USA.

Buresti, G., Talamelli, A. & Petagna, P. 1994 Experimental characterization of the velocity field of a coaxial jet configuration. *Exp. Thermal Fluid Sci.* **9**, 135–146.

Chigier, N. A. & Chervinsky, A. 1967 Experimental investigation of swirling vortex motion in jets. *J. Appl. Mech.* **34**, 443–451.

Craya, A. & Darrigol, M. 1967 Turbulent swirling jet. *Phys. Fluids* **34**, S197–S199.

Davidson, P. A. 2004 *Turbulence. An introduction for scientists and engineers*. Oxford University Press, Oxford, UK.

van Dijk, A. 1999 Aliasing in one-point turbulence measurements - Theory, DNS and hotwire experiments. PhD thesis, Delft University of Technology, The Netherlands.

van Dijk, A. & Nieuwstadt, F. T. M. 2004 The calibration of (multi-) hot-wire probes. 1. Temperature calibration. *Exp. Fluids* **36**, 540–549.

Elsner, J. W. & Kurzak, L. 1987 Characteristics of turbulent flow in slightly heated free swirling jets. *J. Fluid Mech.* **180**, 147–169.

Elsner, J. W. & Kurzak, L. 1989 Semi-preserving development of a slightly heated free swirling jet. *J. Fluid Mech.* **199**, 237–255.

Facciolo, L. 2006 A study on axially rotating pipe and swirling jet flows. PhD thesis, KTH Mechanics, Stockholm, Sweden, TRITA-MEK Tech. Rep. 2006:02.

Facciolo, L. & Alfredsson, P. H. 2004 The counter-rotating core of a swirling turbulent jet issuing from a rotating pipe flow. *Phys. Fluids* **16**, L71–L73.

Facciolo, L., Alfredsson, P. H. & Maciel, Y. 2007*a* Near-field dynamics of a turbulent round jet with moderate swirl. In *Proc. 5th Int. Symp. Turbulence Shear Flow Phenomena*, pp. 917–922.

Facciolo, L., Tillmark, N., Talamelli, A. & Alfredsson, P. H. 2007*b* A study of swirling turbulent pipe and jet flows. *Phys. Fluids* **19**, 035105.

Farokhi, S. & Taghavi, R. 1990 Modern developments in shear flow control with swirl. *Tech. Rep.*. Kansas Univ. Center for Research, USA, KU-FRL-724-4.

Farokhi, S., Taghavi, R. & Rice, E. J. 1989 Effect of initial swirl distribution on the evolution of a turbulent jet. *AIAA J.* **27**, 700–706.

Feyedelem, M. S. & Sarpkaya, T. 1998 Free- and near-free-surface swirling turbulent jets. *AIAA J.* **36**, 359–364.

Fujii, S., Eguchi, K. & Gomi, M. 1981 Swirling jets with and without combustion. *AIAA J.* **19**, 1438–1442.

Gallaire, F. & Chomaz, J.-M. 2003 Mode selection in swirling jet experiments: A linear stability analysis. *J. Fluid Mech.* **494**, 223–253.

García-Villalba, M., Fröhlich, J. & Rodi, W. 2006 Identification and analysis of coherent structures in the near field of a turbulent unconfined annular swirling jet using large eddy simulation. *Phys. Fluids* **18**, 055103.

Gibson, M. M. & Younis, B. A. 1986 Calculation of swirling jets with a Reynolds stress closure. *Phys. Fluids* **29**, 38–48.

Gilchrist, R. T. & Naughton, J. W. 2005 An experimental study of incompressible jets with different initial swirl profiles: Mean results. *AIAA J.* **43**, 741–751.

Grandmaison, E. W. & Becker, H. A. 1982 Turbulent mixing in free swirling jets. *Can. J. Chem. Eng.* **60**, 76–82.

Guillaume, D. W. & Judge, T. A. 2004 Improving the efficiency of a jet pump using a swirling primary jet. *Rev. Sci. Instrum.* **75**, 553–555.

Gupta, A. K., Lilley, D. G. & Syred, N. 1985 *Swirl flows*. ABACUS Press, Cambridge, USA.

Hallbäck, M., Groth, J. & Johansson, A. V. 1989 A Reynolds stress closure for the dissipation in anisotropic turbulent flows. In *Seventh Symposium on Turbulent Shear Flows* (ed. F. Durst, B. E. Launder & W. C. Reynolds), pp. 17.2.1–17.2.6.

Hu, G. H., Sun, D. J. & Yin, X. Y. 2001 A numerical study of dynamics of a temporally evolving swirling jet. *Phys. Fluids* **13**, 951–965.

Hussein, H. J., Capp, S. P. & George, W. K. 1994 Velocity measurements in a high-Reynolds-number, momentum-conserving, axisymmetric, turbulent jet. *J. Fluid Mech.* **258**, 31–75.

Kerr, N. M. & Fraser, D. 1965 Swirl. Part 1: Effect on axisymmetrical turbulent jets. *J. Inst. Fuel* **38**, 519–526.

Kikuyama, K., Murakami, M., Nishibori, K. & Maeda, K. 1983 Flow in an axially rotating pipe. *Bull. JSME* **26**, 506–513.

Komori, S. & Ueda, H. 1985 Turbulent flow structure in the near field of a swirling round free jet. *Phys. Fluids* **28**, 2075–2082.

Kuroda, C., Ogawa, K. & Inoue, I. 1985 Mixing in swirling jet. *J. Chem. Eng. Jpn.* **18**, 439–445.

Launder, B. E. & Morse, A. P. 1979 Numerical prediction of axisymmetric free shear flows with a Reynolds stress closure. In *Turbulent Shear Flows I* (ed. F. Durst, B. E. Launder, F. W. Schmidt & J. H. Whitelaw), pp. 279–294. Springer-Verlag, Berlin, Germany.

Liepman, D. & Gharib, M. 1992 The role of streamwise vorticity in the near-field of round jets. *J. Fluid Mech.* **245**, 643–668.

Lilley, D. G. 1977 Swirl flows in combustion: A review. *AIAA J.* **15**, 1063–1078.

Loiseleux, T. & Chomaz, J.-M. 2003 Breaking of rotational symmetry in a swirling jet experiment. *Phys. Fluids* **15**, 511–523.

Lucca-Negro, O. & O'Doherty, T. 2001 Vortex breakdown: A review. *Prog. Energy Combust. Sci.* **27**, 431–481.

Maier, P. 1968 Untersuchung isothermer drallbehafteter Freistrahlen. *Forsch. Ingenieurwes.* **34**, 133–140.

Mastorakos, E., Shibasaki, M. & Hishida, K. 1996 Mixing enhancement in axisymmetric turbulent isothermal and buoyant jets. *Exp. Fluids* **20**, 279–290.

Mathur, M. L. & MacCallum, N. R. L. 1967 Swirling air jets issuing from vane swirlers. Part 1: free jets. *J. Inst. Fuel* **214**, 214–225.

McIlwain, S. & Pollard, A. 2002 Large eddy simulation of the effect of mild swirl on the near field of a round free jet. *Phys. Fluids* **14**, 653–661.

Mehta, R. D., Wood, D. H. & Clausen, P. D. 1991 Some effects of swirl on turbulent mixing layer development. *Phys. Fluids* **3**, 2716–2724.

Morse, A. P. 1980*a* Axisymmetyric free shear flows with and without swirl. PhD thesis, University of London.

Morse, A. P. 1980*b* Single-stream swirling jet in still air. ERCOFTAC database, http://www.cfd.me.umist.ac.uk/ercofold/database/test26/test26.html.

Naughton, J. W., Cattafesta, L. N. & Settles, G. S. 1997 An experimental study of compressible turbulent mixing enhancement in swirling jets. *J. Fluid Mech.* **330**, 271–305.

Nayeri, C. 2000 Investigation of the three-dimensional shear layer between confined coaxial jets with swirl. PhD thesis, Technical University of Berlin, Germany.

Ogawa, A., Hatakeyama, H. & Fujita, Y. 1981 Fluiddynamical characteristics of turbulent straight and rotational jets (2nd report). *J. Coll. Engng. Nihon Univ.* **A-22**, 157–170.

Orlandi, P. & Fatica, M. 1997 Direct simulations of turbulent flow in a pipe rotating about its axis. *J. Fluid Mech.* **343**, 43–72.

Örlü, R. 2006 Experimental study of passive scalar mixing in swirling jet flows. *Tech. Rep.*. KTH Mechanics, teknL thesis, TRITA-MEK Tech. Rep. 2006:11; http://www2.mech.kth.se/thesis/2006/lic/lic_2006_ramis_orlu.pdf.

Ovink, R., Lamers, A. P. G. G., Steenhoven, A. A. & Hoeijmakers, H. W. M. 2001 A method of correction for the binormal velocity fluctuation using the look-up inversion method for hot-wire anemometry. *Meas. Sci. Technol.* **12**, 1208–1213.

Park, S. H. & Shin, H. D. 1993 Measurements of entrainment characteristics of swirling jets. *Int. J. Heat Mass Transfer* **36**, 4009–4020.

Pietri, L., Amielh, M. & Anselmet, F. 2000 Simultaneous measurements of temperature and velocity fluctuations in a slightly heated jet combining a cold wire and laser doppler anemometry. *Int. J. Heat Fluid Flow* **21**, 22–36.

Pitts, W. M. 1991 Reynolds number effects on the mixing behaviour of axisymmetric turbulent jets. *Exp. Fluids* **11**, 135–141.

Pratte, B. & Keffer, J. F. 1972 The swirling turbulent jet. *J. Basic Eng.* **94**, 739–747.

Rahai, H. R. & Wong, T. W. 2002 Velocity field characteristics of turbulent jets from round tubes with coil inserts. *Appl. Thermal Eng.* **22**, 1037–1045.

Rajagopalan, S. & Antonia, R. A. 1982 Use of a quadrant analysis technique to identify coherent structures in a turbulent boundary layer. *Phys. Fluids* **25**, 949–956.

Rajaratnam, N. 1976 *Turbulent jets*. Elsevier, Amsterdam, The Netherlands.

Reich, G. & Beer, H. 1989 Fluid flow and heat transfer in an axially rotating pipe. I: Effect of rotation on turbulent pipe flow. *Int. J. Heat Mass Transfer* **32** (3), 551–562.

Reich, G., Weigand, B. & Beer, H. 1989 Fluid flow and heat transfer in an axially rotating pipe. II: Effect of rotation on laminar pipe flow. *Int. J. Heat Mass Transfer* **32** (3), 563–574.

Reynolds, A. 1961 On the dynamics of turbulent vortical flow. *Z. Angew. Math. Phys.* **12**, 149–158.

Ricou, F. P. & Spalding, D. B. 1961 Measurements of entrainment by axisymmetrical turbulent jets. *J. Fluid Mech.* **11**, 21–32.

Rose, W. G. 1962 A swirling round turbulent jet; 1 - Mean-flow measurements. *J. Appl. Mech.* **29**, 615–625.

Satake, S. & Kunugi, T. 2002 Direct numerical simulation of turbulent heat transfer in an axially rotating pipe flow. Reynolds shear stress and scalar flux budgets. *Int. J. Num. Methods Heat Fluid Flow* **12**, 958–1008.

Schefer, R. W. & Kerstein, A. R. 1994 Role of large-scale structure in a nonreacting turbulent CH_4 jet. *Phys. Fluids* **6**, 652–661.

Schetz, J. A. 1980 *Injection and mixing in turbulent flow*. AIAA, New York, USA.

Schlichting, H. 1979 *Boundary-layer theory*, 7th edn. McGraw-Hill, New York, USA.

Sislian, J. P. & Cusworth, R. A. 1986 Measurements of mean velocity and turbulent intensities in a free isothermal swirling jet. *AIAA J.* **24**, 303–309.

Sreenivas, K. R. & Prasad, A. K. 2000 Vortex-dynamics model for entrainment in jets and plumes. *Phys. Fluids* **12**, 2101–2107.

Staicu, A. D. 2002 Intermittency in turbulence. PhD thesis, Eindhoven University of Technology, The Netherlands.

Syred, N. & Beér, J. M. 1974 Combustion in swirling flows: A review. *Combust. Flame* **23**, 143–201.

Taghavi, R. & Farokhi, S. 1988 Turbulent swirling jets with excitation. *Tech. Rep.*. Kansas Univ. Center for Research, USA, NASA-CR-180895.

Toh, I. K., Honnery, D. & Soria, J. 2005 Velocity and scalar measurements of

a low swirl jet. In *Proc. 4th Australian Conf. Laser Diagnostics Fluid Mech. Comb.*, pp. 129–132. The University of Adelaide, South Australia, Australia.

Tutu, N. K. & Chevray, R. 1975 Cross wire anemometry in high intensity turbulence. *J. Fluid Mech.* **71**, 785–800.

Warhaft, Z. 2000 Passive scalars in turbulent flows. *Annu. Rev. Fluid Mech.* **32**, 203–240.

Wooten, D. C., Wooldridge, C. E. & Amaro, A. J. 1972 The structure of jet turbulence producing jet noise. *Tech. Rep.*. Stanford Research Institute, California, USA, SRI Project 8139.

Xu, G. & Antonia, R. A. 2002*a* Effect of different initial conditions on a turbulent round free jet. *Exp. Fluids* **33**, 677–683.

Xu, G. & Antonia, R. A. 2002*b* Effect of initial conditions on the temperature field of a turbulent round free jet. *Int. Comm. Heat Mass Transfer* **29**, 1057–1068.

2

Paper 2

"Every morning as I walked through the laboratory to my work I would pause and ask:
'Herr Hiemenz, it oscillates still?'
He replied sadly: 'Ja. Always it oscillates!' "

Theodore von Kármán (1881–1963)

On the passive control of the near-field of coaxial jets by means of vortex shedding

By Ramis Örlü[1], Antonio Segalini[2], P. Henrik Alfredsson[1], and Alessandro Talamelli[1,2]

[1] Linné Flow Centre, KTH Mechanics, SE-100 44 Stockholm, Sweden
[2] Dept. of Mech. and Aerospace Eng. (DIEM), University of Bologna, I-47100 Forlí, Italy

Published in *Int. Conf. on Jets, Wakes and Separated Flows, ICJWSF–2, September 16–19, 2008, Technical University of Berlin, Berlin, Germany*

The present paper confirms experimentally the theoretical result by Talamelli and Gavarini (Flow, Turbul. & Combust., 2006), who proposed that the wake behind a separation wall between two streams of a coaxial jet creates the condition for an absolute instability. This instability, by means of the induced vortex shedding, provides a continuous forcing mechanism for the control of the flow field. The potential of this passive mechanism as an easy, effective and practical way to control the near-field of interacting shear layers has been demonstrated and its effect towards increased turbulence activity has been shown.

1. Introduction

Flow control in transitional and turbulent flows has become more practical since the recognition of organised motions attributed to coherent structures embedded in the incoherent turbulent background (Roshko 1976; Hussain 1986). Through these coherent structures, which comprise a considerable fraction of the total turbulent energy, ways have been opened to manipulate the dynamics of the flow (Fiedler 1987). In order to highlight the mechanism governing coherent structures and to enhance our understanding of how these can be utilised to control the transport and mixing characteristics, a variety of passive and active flow control mechanisms have been tested and applied within the last decades, principally in single jets (Bradbury & Khadem 1975; Zaman & Hussain 1981; Tong & Warhaft 1994) and other canonical flows (Gad-el-Hak 2000).

In the case of coaxial jets, however, flow control studies have been primarily investigated regarding the receptivity to active flow control strategies (Kiwata *et al.* 2006; Angele *et al.* 2006). Passive strategies, on the other hand, have mainly been disregarded, despite their promising results in other flow cases

(Bradbury & Khadem 1975; Zaman & Hussain 1981; Tong & Warhaft 1994; Gad-el-Hak 2000). One reason for this imbalance might be the fact that a full characterisation of the apparently simple geometry of coaxial jets, depicted in figure 1, is governed by a multitude of parameters (Buresti *et al.* 1994).

The prevailing model for more than a decade, put forward by Ko & Kwan (1976); Kwan & Ko (1977), was that coaxial jets could be considered as a simple combination of single jets, where the two shear layers originating from the nozzles develop independently from each other. This view was modified when Dahm *et al.* (1992) in their flow visualisation study showed the existence of different topological flow regimes for different velocity ratios ($r_u = U_o/U_i$, here U_i and U_o denote the maximum absolute velocity of the inner and outer streams at the nozzle exits, respectively), as well as absolute velocities. Furthermore the same authors, as well as Wicker & Eaton (1994), found that the vortical motion for $r_u > 1$ is dominated by the vortices emerging in the outer shear layer. They showed that the evolution of the vortices of the inner shear layer is dictated by the outer vortices. They are hence trapped in the spaces left free between two consecutive outer shear layers vortices; this scenario became known as the so-called 'locking phenomenon'. Consequently the vortex passage frequency of the inner shear layer will differ from the one predicted by stability

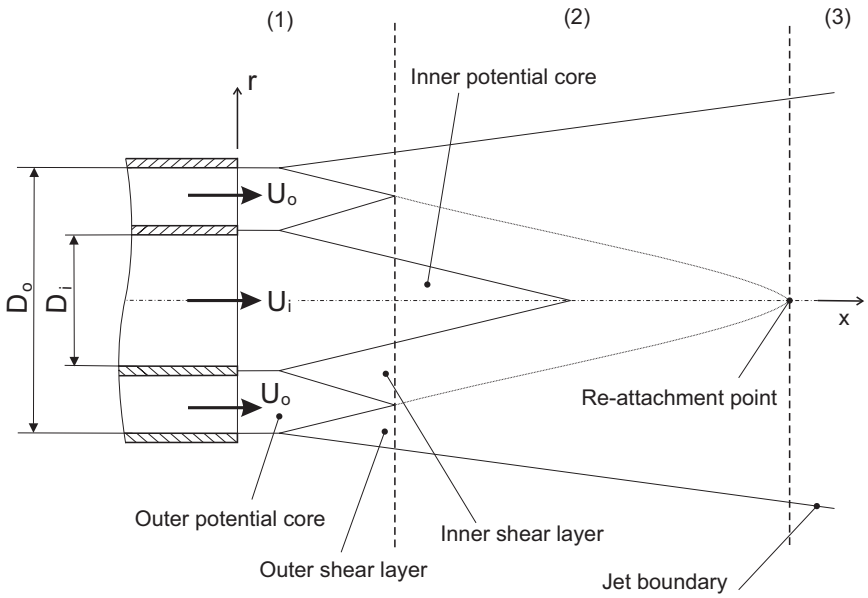

FIGURE 1. Sketch of the flow field of a coaxial jet configuration and its main parameters. (1) Initial merging zone, (2) Intermediate zone, (3) Fully merged zone.

analysis for a single axisymmetric shear layer as shown by Dahm *et al.* (1992) and da Silva *et al.* (2003) by means of flow visualisations and direct numerical simulations, respectively. This finding has led to an increased focus on the control of the outer shear layers' vortices (Angele *et al.* 2006; Balarac *et al.* 2007).

One of the parameters, emphasised by Buresti *et al.* (1994), playing an important role in the evolution of transitional coaxial jets, is the thickness of the (duct) wall, t, separating the two streams from each other. It was shown by the same authors that two trains of alternating vortices are shed from both sides of the inner wall with a well-defined frequency, which scales with the wall thickness and the average velocity of the two streams. In fact both the wall thickness and the velocity ratio were found to be crucial in determining whether the behaviour in the near-field of coaxial jets could be considered as wake-like or shear-layer-like (Dahm *et al.* 1992; Braud *et al.* 2004).

In a recent study Talamelli & Gavarini (2006) formulated a theoretical background for this experimental finding. They showed, by means of linear stability analysis, that the alternate vortex shedding behind the inner wall can be related to the presence of an absolute instability, which exists for a specific range of velocity ratios and for a finite thickness of the wall separating the two streams. The authors proposed that this absolute instability may provide a continuous forcing mechanism for the destabilisation of the whole flow field even if the instability is of limited spatial extent. It is important to point out that this mechanism does not require any external energy input, being considered passive, and therefore is attractive for practical applications.

The present paper aims at verifying the proposed idea of Talamelli & Gavarini (2006), namely to test if the absolute instability behind an inner wall of a coaxial jet nozzle with finite thickness can be utilised as a continuous forcing mechanism and hence as a passive flow control mechanism for the near-field of coaxial jet flows. Furthermore, the experimental results will surpass what linear stability analysis can predict and indicate what the effect of the vortex shedding on the near-field turbulence characteristics is. The experiments show that the vortex shedding behind a thick separating wall can be facilitated as an easily applicable and effective passive control mechanism.

In this context it could be shown that the trapping of the inner shear layers vortices into the free spaces of the Kelvin-Helmholtz instability of the external shear layer, known as the 'locking phenomenon', is indeed reversible; namely we observed that the vortex shedding behind the separating wall with finite thickness dictates the passage frequency of the external shear layers vortices and thereby controls the inner and outer shear layers evolution in the whole near-field region. A clear trend towards increased turbulence activity, both within the inner and outer shear layers and thereby the mixing between the two streams of the coaxial jet as well as the outer jet and the ambient surroundings,

could be observed. This makes it possible to specifically utilise the geometry of the inner separating wall not only to control the dynamics of the flow, but also to increase the turbulence activity, giving the presented passive control mechanism great importance both from a fundamental and applied point of view.

The remainder of the paper is organised as follows: Section 2 describes the coaxial jet facility as well as the measurement technique used. Experimental results showing the viability of the passive control mechanism as well as its effect on the turbulence are presented and discussed in Section 3. The paper finishes with conclusions in Section 4.

2. Experimental set-up and measurement technique

2.1. *The coaxial jet facility*

The experiments were carried out in the *Coaxial Air Tunnel* (CAT) facility in the laboratory of the *Second Faculty of Engineering* at the *University of Bologna* in Forlí. The facility, schematically shown in figure 2, is composed of two independent centrifugal blowers (**A** and **B**) equipped with three-phase motors. Two pre-settling chambers (**C** and **D**) are placed downstream the blowers to reduce the disturbances from the blowers. Four plastic hoses (**J**) connect the outer jet pre-chamber to the corresponding settling chamber to increase the symmetry of the flow, while a simple diverging pipe (**E**) connects the inner

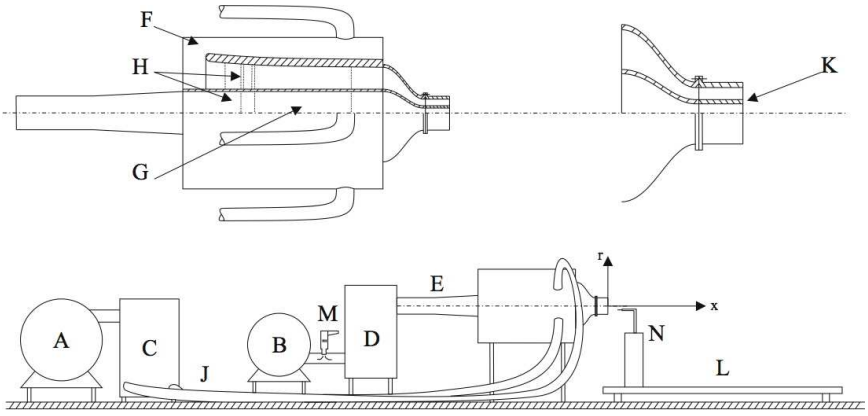

FIGURE 2. Schematic of the coaxial jet facility. **A** outer jet blower, **B** inner jet blower, **C** outer jet pre-settling chamber, **D** inner jet pre-settling chamber, **E** inner jet diffuser, **F** outer jet settling chamber, **G** inner jet settling chamber, **H** screens and honeycombs, **J** outer jet hoses, **K** close-up of the jet exit with the thick separating wall, **L** axial traversing, **M** heat gun, **N** radial traversing.

one. Flow conditioning is performed by means of three screens and a honeycomb (**H**) in the inner pipe as well as five screens and a honeycomb on the outer circuit. The inner and outer contraction ratios are 11:1 and 16.5:1, respectively, whereas the inner and outer coaxial nozzles, of exit diameter $D_i = 50$ mm and $D_o = 100$ mm, end with two straight pipes of 100 mm length (**K**). The experimental facility is placed in a large laboratory and the exit of the coaxial jet is far enough from surrounding walls and the floor, ensuring that the experimental results reported here resemble a jet in an infinite environment (cf. appendix B of Hussein *et al.* 1994).

In the present experiment, two different types of separation walls have been used. The first one has a thickness of $t = 5$ mm and ends in a rectangular geometry, schematically shown in figure 2 (**K**), whereas the second one ends with a sharp trailing edge making the wall thickness negligible ($t \approx 0$ mm) with respect to the sum of the side boundary layers thicknesses. These two separating walls will in the following be denoted as thick and sharp, respectively. The sharp and thick wall cases represent the flow cases in the absence and presence of the vortex shedding phenomenon, respectively, and enable therefore a selective investigation regarding the effect of the absolute instability.

The probe is finally positioned in the flow by means of a motorised traversing system capable to move the probe in the axial (**L**) and radial (**N**) direction. The traversing system and the data acquisition are controlled by a single PC using a *National Instruments* 16-bit PCI-6035E acquisition board.

2.2. *Measurement technique*

For the present investigation a variety of hot-wire probes were used. The characterisation of the boundary layers, upstream the orifice exit and in the vicinity of it, were performed by in-house made long and slender boundary layer probes consisting of 2.5 micron Platinum wires with a length-to-diameter ratio of 400 in order to avoid any blockage effects within the nozzle and reduce near wall effects. All other measurements were performed with a *DANTEC* 55P61 X-wire probe. The hot-wires were operated in the constant temperature (CTA) mode with resistance overheat ratios in the range of 70–80 % either by means of an *DANTEC StreamLine* or an *AA-lab AN-1003* hot-wire anemometry system. The hot-wires were calibrated slightly upstream the inner nozzle against a Prandtl-tube. A modified King's law (Johansson & Alfredsson 1982) was used, where the yaw response was computed using a sum and difference method (Bruun 1995) with experimentally determined calibration coefficients for the wires.

Most of the measurements have been obtained using one point statistics. The measurement set related to the triggering investigation, on the other hand, has been conducted in the cross stream direction and simultaneously behind the inner and outer wall in order to obtain conditional measurements able

to highlight the dynamics of the interacting shear layers. The signals from the CTA channels were offset and amplified through the circuits to match the fluctuating signal components to the voltage range of the 16-bit A/D converter used, and then digitised on a PC at a sampling frequency of 5 kHz (10 kHz for spectral and conditional measurements) and a sampling duration between 10 and 40 seconds depending on the downstream position of the probe.

Additionally a series of flow visualisation photographs were taken for a range of absolute velocities and velocity ratios for both the sharp and thick wall cases. The particles used for the visualisation are small droplets of condensed smoke of polyethylenglycen and were injected at the inlet of the blower for the outer jet. A laser sheet from a 6 W Argon/Krypton Ion laser source was used to illuminate the flow. Images were recorded with a *NanoSense MkI* camera at a sampling frequency of 1 kHz.

3. Results and discussions

In the following three sections results from the sharp and thick wall cases are presented to highlight the effect of the presence of the vortex shedding mechanism on interacting shear layers, section 3.1, its utilisation to control the flow dynamics, section 3.2, as well as its effect on the turbulence activity, section 3.3. The results shown here are all for the case of equal maximum velocities in the inner and annular jet, i.e. $r_u = 1$. The Reynolds numbers investigated range from around 12000 to 100000, based on the inner nozzle diameter, corresponding to absolute velocities from 4 to 32 m/s, respectively. The velocity ratio of unity was selected, because it lies within the range for which an absolute instability behind a thick wall has theoretically been shown to exist (cf. (Talamelli & Gavarini 2006)).

3.1. *Vortex shedding effect on interacting shear layers*

In the case of the sharp wall, the power-spectral density of the fluctuating streamwise velocity component in the inner and outer shear layer as well as a snapshot of a smoke visualisation are shown in figure 3 and 4, respectively. The Kelvin-Helmholtz instability emerging between the annular stream and the ambient is clearly highlighted in the visualisation as well as in the spectral content of the flow ($\sim$ 240 Hz corresponding to a Strouhal number of 0.012 based on the momentum thickness of the external boundary layer, which is related to the 'shear layer mode'; cf. (Zaman & Hussain 1980)). As the snapshot suggest, the flow behind the outer separating wall resembles a picture of a classical Kelvin-Helmholtz instability, whereas the sharp inner separating wall produces a smooth interface between the coflowing jets, being free of any apparent trace of a wake.

For the thick wall, on the other hand, both the smoke visualisation as well as spectral content of the flow, have strong imprints of the vortex shedding

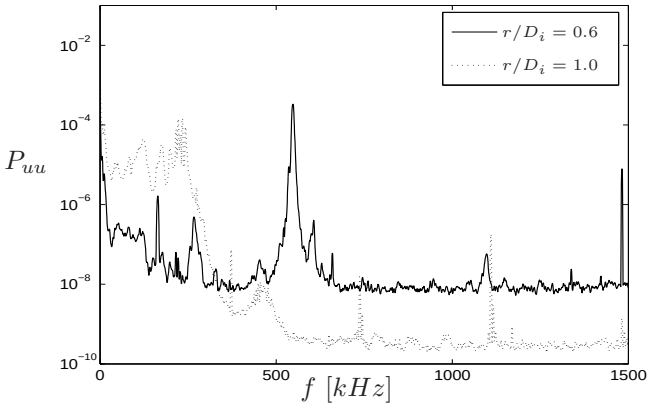

FIGURE 3. Power-spectral density function of the streamwise velocity component measured behind the inner ($r/D_i = 0.6$) and outer ($r/D_i = 1.0$) wall at $U_o = 8$ m/s, $r_u = 1$ and $x/D_i = 0.5$ for the sharp wall.

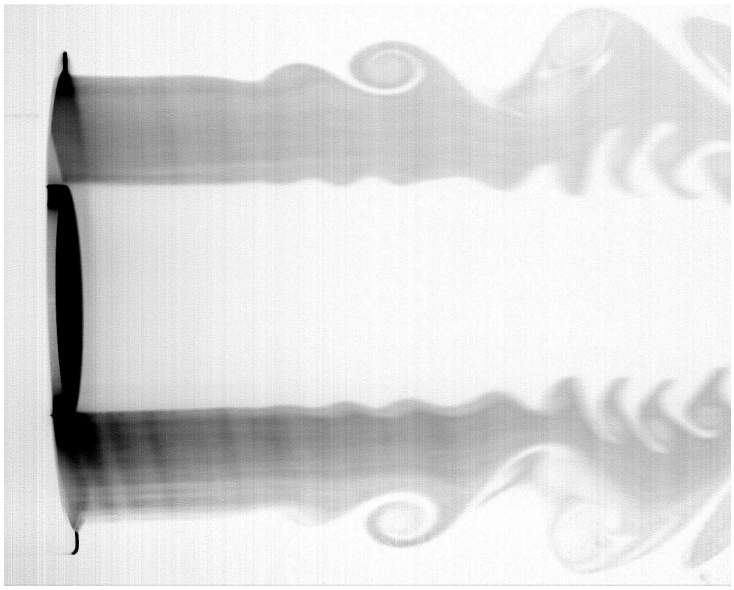

FIGURE 4. Smoke flow visualisation at $U_o = 4$ m/s and $r_u = 1$ for the sharp wall.

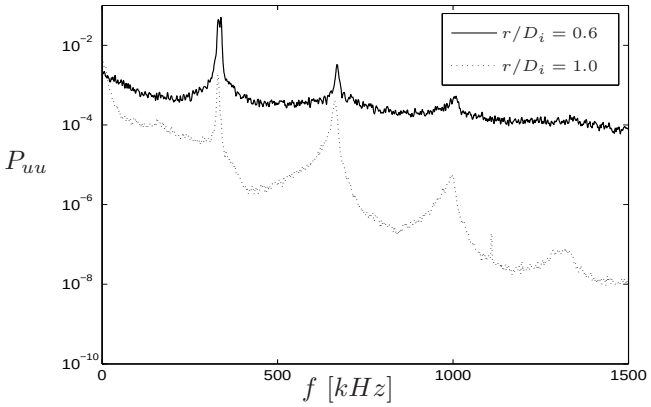

FIGURE 5. Power-spectral density function of the streamwise velocity component measured behind the inner ($r/D_i = 0.6$) and outer ($r/D_i = 1.0$) wall at $U_o = 8$ m/s, $r_u = 1$ and $x/D_i = 0.5$ for the thick wall.

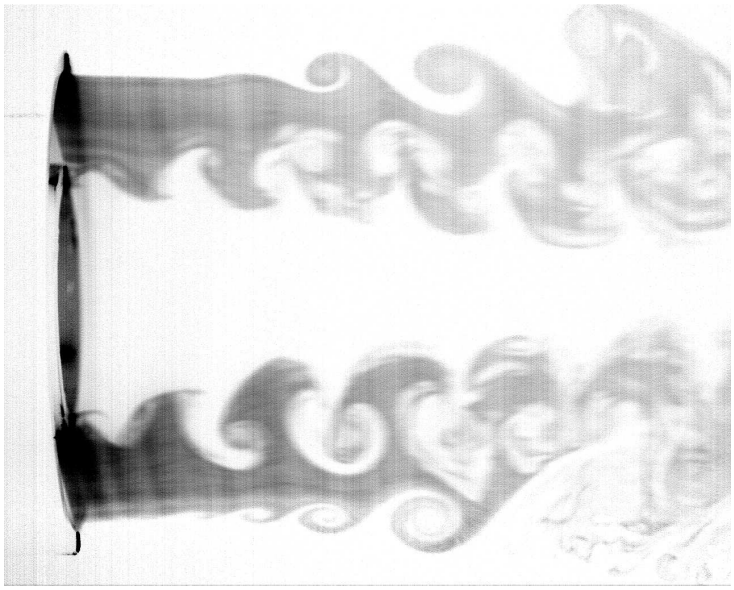

FIGURE 6. Smoke flow visualisation at $U_o = 4$ m/s and $r_u = 1$ for the thick wall.

behind the inner wall. This changes the flow scenario drastically, as evident from figures 5 and 6. In contrast to the sharp wall results the spectral energy is highly concentrated in its fundamental peak and harmonics as well as in the incoherent background fluctuations anticipating an increased turbulence activity as well as the presence of organised structures.

The vortex shedding, starting right behind the inner wall and hence upstream the first emergence of the Kelvin-Helmholtz instability of the outer shear layer in the sharp wall case, traps the outer shear layers vortices into the free spaces left between the ones of the inner shear layer. This increases the coherency between the two shear layers and can further be evinced through figure 7, where a pseudo-flow visualisation has been plotted through a conditional sampling technique. The vortices in the outer shear layer resemble the famous Kelvin's 'cat's eye' pattern predicted by stability analysis (Drazin 2002), whose organisation is strongly coupled to the vortex shedding in the inner shear layer. This again underlines the strong organisation and mutual interaction of the two shear layers in the whole near-field region as could be anticipated from the flow visualisation. An X-wire probe was thereby triggered by the vortex shedding behind the inner separating wall detected by a single hot-wire probe which was placed at the same downstream location, $x/D_i = 0.26$. Figure 8 depicts the instantaneous axial and radial velocities above their mean in the outer shear layer, $r/D_i = 1$, at $x/D_i = 0.26$ from an X-wire probe. The clear cyclical path in the (u, v)-space is a strong indication for the presence of a dominant peak in the outer region, and may also anticipate a formation of larger vortices (Fiedler 1987).

The clear spectral peak of the vortex shedding phenomenon, the pronounced fundamental and its harmonics in the outer shear layer in figure 5, anticipate a clear cyclical path of the streamwise and radial velocity component as found in the conditionally sampled pseudo-flow visualisation. Although the instantaneous smoke visualisation image has been taken at a lower velocity (due to the difficulty to obtain clear images at higher velocities), compared to the presented spectral measurements and pseudo-flow visualisation, its spatial character complements the quantitative time evolution of the two point hot-wire measurements.

These results demonstrate that the recent finding of Balarac & Métais (2005), who stated that (below a critical velocity ratio) the vortices of the outer shear layer develop with a Strouhal number corresponding to the value predicted by linear stability analysis for the Kelvin-Helmholtz instability, is therefore not generally true. This is particularly true for the presence of an absolute instability, which—as shown in figures 5 and 6—dominates the motion of the organised structures.

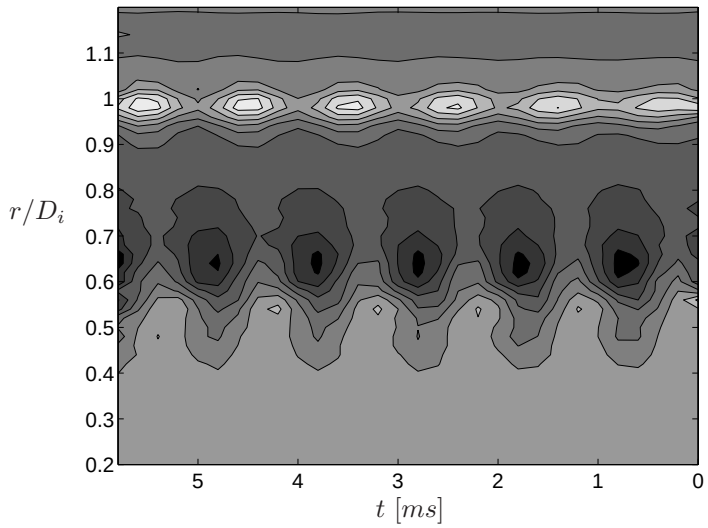

FIGURE 7. Pseudo-flow visualisation by means of conditional sampling technique of the radial velocity component at $U_o = 20$ m/s and $r_u = 1$ for the thick wall. Colormap from white to black corresponding to inflow and outflow conditions, respectively.

3.2. *Vortex shedding as a passive flow control mechanism*

So far we have shown the effect of the vortex shedding on the near-field dynamics of a coaxial jet. The next paragraphs are devoted to the question whether or not the vortex shedding can be used as a viable flow control mechanism and how it affects the turbulence activity. Figure 9 shows the fundamental peak frequency as a function of the absolute velocity for both wall cases. No trend or relationship is observable for the sharp wall case (a) between the vortices in the inner and outer shear layer, whereas the strong controllability of the evolution of the vortices' fundamental frequency in both shear layers is evident from the linear relationship with the absolute velocity in the thick wall (b) case. Hence the absolute instability, by means of the induced vortex shedding behind the inner wall, dictates the evolution of the vortices in both shear layers and hence the whole flow field.

The overlapping at 16 and 20 m/s for the sharp wall in figure 9 could be explained by a whistler tone, which was observed around these absolute velocities (cf. Örlü *et al.* 2008). However, there is no controllability of the fundamental peak, in the sharp wall case, whereas the thick wall presents a

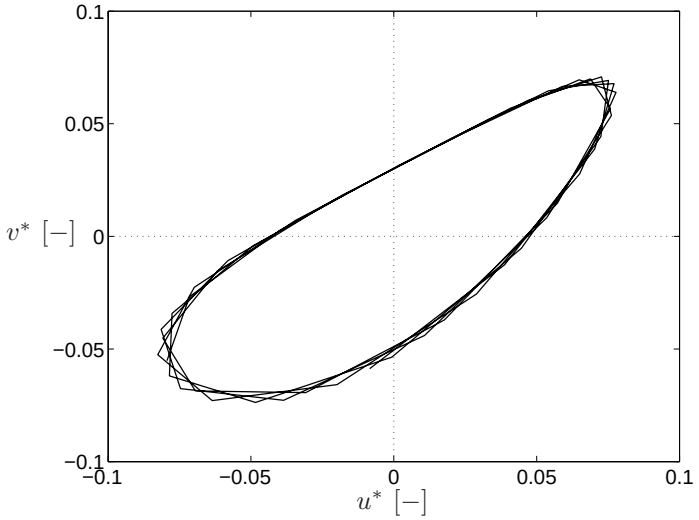

FIGURE 8. Instantaneous streamwise and radial velocity fluctuations plotted in the (u, v)-space above their mean for the thick wall case for $U_o = 20$ m/s at $x/D_i = 0.26$ in the outer shear layer, $r/D_i = 1$.

means to predetermine the evolution of the vortices in the inner and thereby outer shear layer, just by knowing the separating wall thickness, t, and the absolute velocity, U_o, or the average velocity for the case of unequal velocities within the range of the presence of an absolute instability.

3.3. *Vortex shedding effect on the turbulence activity*

In the presence of active excitation, where the amplitude and phase of the excitation signal can be set arbitrarily, an increase in the organisation and formation of larger vortices can result either in a turbulence suppression (Zaman & Hussain 1981; Dahm *et al.* 1992) or an turbulence enhancement (Zaman & Hussain 1980; Crow & Champagne 1971). The power-spectral density functions showed that the energy content of the flow, with the presence of the vortex shedding, is not only brought about by means of the emergence of stronger organised structures, but also by a drastic increase in the incoherent background turbulence. Finally the normalised root mean square values of the radial velocity fluctuations along $r/D_i = 1$ for 4, 8 and 12 m/s are shown in figure 10 for the sharp (a) and thick (b) wall to complete the picture. A clear increase in the rms value of the normalised radial velocity fluctuations can be observed

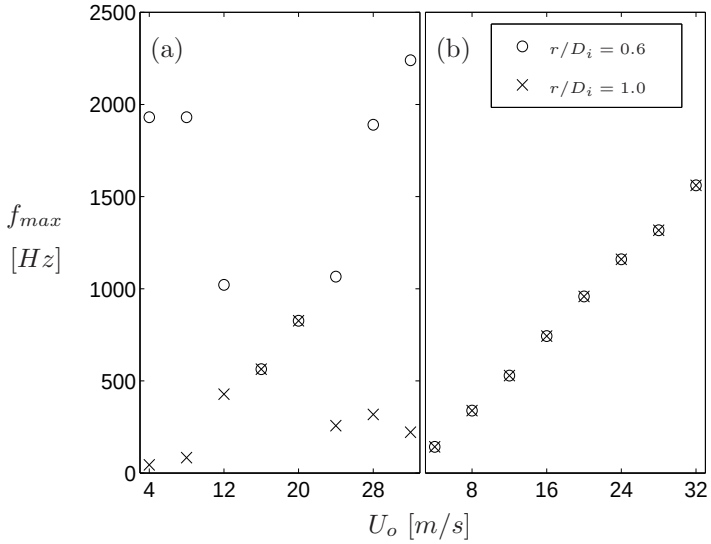

FIGURE 9. Fundamental frequency as function of the outer jet velocity behind the inner and outer wall at $r_u = 1$ and $x/D_i = 0.26$ for the sharp (a) and thick (b) wall.

for all downstream positions as well as absolute velocities. Consequently the thick wall can be used not only to trigger and hence control the evolution of the organised structures, but also—and this is of more practical importance—to increase the turbulence activity within the inner and outer shear layers and thereby the mixing between the two coaxial jets streams as well as the annular jet with the ambient fluid.

A probably larger turbulence enhancement can be obtained if both fluid mechanical and geometrical parameters of the coaxial jet, like momentum thicknesses or the thickness of the separating wall, could be more easily varied.

4. Conclusions

In summary we have presented results from an experimental investigation confirming the theoretical study by Talamelli & Gavarini (2006), where it was suggested that the self-exciting temporally growing wake instability behind an inner thick wall in coaxial jets, may provide a continuous forcing mechanism for the passive control of the whole flow field. The present paper has hence shown, that despite the current trend to utilise mainly active flow control strategies in coaxial jet flows, there are basic flow features, like the vortex shedding behind a thick wall, which—if correctly recognised—can be facilitated to control the flow field without external energy supply.

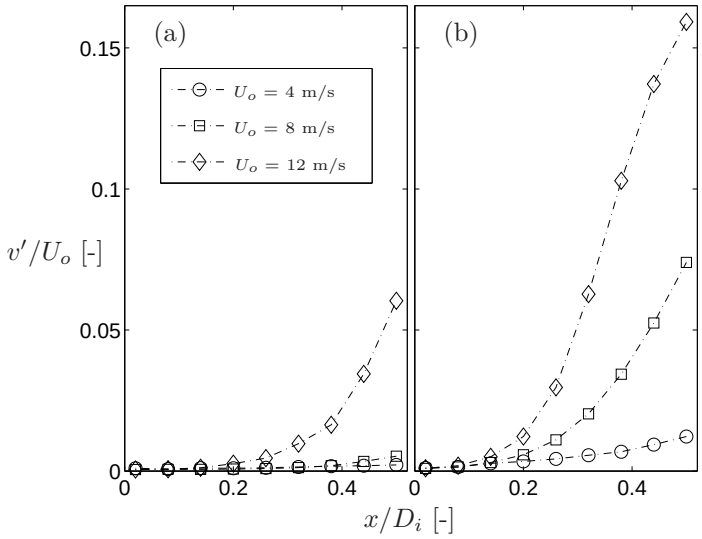

FIGURE 10. Root mean square value of the radial velocity fluctuations along $r/D_i = 1$ at 4, 8 and 12 m/s for the sharp (a) and thick (b) wall.

It was furthermore shown that the 'locking phenomenon', which commonly is restricted to the dominance of the outer shear layers vortices over the inner ones, is reversible and therefore open doors to apply flow control strategies on the inner nozzle wall. This finding also restricts the finding by Balarac & Métais (2005), who showed that (below a critical velocity ratio) the vortices of the outer shear layer develop with a Strouhal number corresponding to the value predicted by linear stability analysis for the Kelvin-Helmholtz instability. It was shown that, particularly in the presence of an absolute instability by means of the vortex shedding mechanism, the vortices of the outer shear layer develop with a Strouhal number corresponding to a value related to the vortex shedding frequency behind the inner separating wall.

The present paper underlines the potential of this passive mechanism as an easy, effective and practical way to control the near-field of interacting shear layers and shows that it can be used to increase the turbulence activity in both shear layers and hence the mixing between the two coaxial jet streams as well as the annular jet with the ambient fluid.

Acknowledgements

RÖ is supported by *The Swedish Research Council* (VR), and the cooperation between *KTH* and the *University of Bologna* is supported by *The Swedish Foundation for International Cooperation in Research and Higher Education*

(STINT), which are both greatly acknowledged. Furthermore Prof. G. Buresti is acknowledged for placing the coaxial jet facility to the disposal of the *Second Faculty of Engineering* of the *University of Bologna* as well as Dr. P. Levoni and Mr. P. Proli for the assistance with the flow visualisations.

References

Angele, K., Kurimoto, N., Suzuki, Y. & Kasagi, N. 2006 Evolution of the streamwise vortices in a coaxial jet controlled with micro flap actuators. *J. Turbulence* **7**, 1—19.

Balarac, G. & Métais, O. 2005 The near field of coaxial jets: A numerical study. *Phys. Fluids* **17**, 065102.

Balarac, G., Métais, O. & Lesieur, M. 2007 Mixing enhancement in coaxial jets through inflow forcing: A numerical study. *Phys. Fluids* **19**, 075102.

Bradbury, L. & Khadem, A. 1975 The distortion of a jet by tabs. *J. Fluid Mech.* **70**, 801—813.

Braud, C., Heitz, D., Arroyo, G., Perret, L. & Delville, J. 2004 Low-dimensional analysis, using POD, for two mixing layer–wake interactions. *Int. J. Heat Fluid Flow* **25**, 351—363.

Bruun, H. H. 1995 Hot-wire anemometry: Principles and signal analysis. *Oxford University Press Inc., New York, USA* .

Buresti, G., Talamelli, A. & Petagna, P. 1994 Experimental characterization of the velocity field of a coaxial jet configuration. *Exp. Thermal Fluid Sci.* **9**, 135—146.

Crow, S. & Champagne, F. 1971 Orderly structure in jet turbulence. *J. Fluid Mech.* **48**, 547—591.

Dahm, W., Frieler, C. & Tryggvason, G. 1992 Vortex structure and dynamics in the near field of a coaxial jet. *J. Fluid Mech.* **241**, 371—402.

Drazin, P. 2002 Introduction to hydrodynamic stability. *Cambridge University Press*.

Fiedler, H. 1987 Coherent structures. *Advances in Turbulence, G. Comte-Bellot and J. Mathieu (Eds.), Springer–Verlag* pp. 320—336.

Gad-el-Hak, M. 2000 Flow control: passive, active, and reactive flow management. *Cambridge University Press*.

Hussain, A. K. M. F. 1986 Coherent structures and turbulence. *J. Fluid Mech.* **173**, 303—356.

Hussein, H., Capp, S. & George, W. K. 1994 Velocity measurements in a high-Reynolds-number, momentum-conserving, axisymmetric, turbulent jet. *J. Fluid Mech.* **258**, 31—75.

Johansson, A. V. & Alfredsson, P. H. 1982 On the structure of turbulent channel flow. *J. Fluid Mech.* **122**, 295—314.

Kiwata, T., Ishii, T., Kimura, S., Okajima, A. & Miyazaki, K. 2006 Flow visualization and characteristics of a coaxial jet with a tabbed annular nozzle. *JSME International Journal Series B* **49**, 906—913.

Ko, N. & Kwan, A. 1976 The initial region of subsonic coaxial jets. *J. Fluid Mech.* **73**, 305—332.

Kwan, A. & Ko, N. 1977 The initial region of subsonic coaxial jets. Part 2. *J. Fluid Mech.* **82**, 273—287.

Örlü, R., Segalini, A., Alfredsson, P. H. & Talamelli, A. 2008 Passive control of mixing in a coaxial jet. *Proc. 7th Int. ERCOFTAC Symp. on Engineering Turbulence Modelling and Measurements (ETMM7)* **2**, 450—455.

Roshko, A. 1976 Structure of turbulent shear flows: A new look. *AIAA J.* **14**, 1349—1357.

da Silva, C., Balarac, G. & Métais, O. 2003 Transition in high velocity ratio coaxial jets analysed from direct numerical simulations. *J. Turbulence* **4**, 1—18.

Talamelli, A. & Gavarini, I. 2006 Linear instability characteristics of incompressible coaxial jets. *Flow Turbul. Combust.* **76**, 221—240.

Tong, C. & Warhaft, Z. 1994 Turbulence suppression in a jet by means of a fine ring. *Phys. Fluids* **6**, 328—333.

Wicker, R. & Eaton, J. 1994 Near field of a coaxial jet with and without axial excitation. *AIAA J.* **32**, 542—546.

Zaman, K. & Hussain, A. K. M. F. 1980 Vortex pairing in a circular jet under controlled excitation. Part 1. General jet response. *J. Fluid Mech.* **101**, 449—491.

Zaman, K. & Hussain, A. K. M. F. 1981 Turbulence suppression in free shear flows by controlled excitation. *J. Fluid Mech.* **103**, 133—159.

Paper 3

3

Professor Tait's plan of exhibiting smoke-rings is as follows:—A large rectangular box, open at one side, has a circular hole [...] in the opposite side. [...] The open side of the box is closed by a stout towel or piece of cloth, or by a sheet of india-rubber stretched across it. A blow on this flexible side causes a circular vortex ring to shoot out from the hole on the other side. The vortex rings thus generated are visible if the box is filled with smoke. [...] A curious and interesting experiment may be made with two boxes thus arranged, and placed either side by side close to one another or facing one another so as to project smoke-rings meeting from opposite directions—or in various relative positions, so as to give smoke-rings proceeding in paths inclined to one another at any angle, and passing one another at various distances.

Lord Kelvin (1824–1907)

Preliminary studies on acoustic excitation in axisymmetric transitional jet flows

By Antonio Segalini, Ramis Örlü, Alessandro Talamelli, and P. Henrik Alfredsson

Linné Flow Centre, KTH Mechanics, SE-100 44 Stockholm, Sweden

The paper describes preliminary experiments on natural and acoustically excited axisymmetric turbulent jet flows. The analysis is based on the hypothesis that so called oblique transition may play a role in the breakdown to turbulence for an axisymmetric jet. For wall bounded flows oblique transition gives rise to steady streamwise streaks that break down to turbulence, as for instance documented by Elofsson & Alfredsson (J. Fluid Mech. **358**). The scenario of oblique transition has so far not been considered for jet flows and the aim was to study the effect of two oblique modes on the transition scenario as well as on the flow dynamics. Even though it is not possible to detect the presence of streamwise streaks, for a certain range of the excitation frequencies, the turbulence intensity, at a fixed streamwise position, seems to be significantly reduced.

1. Introduction

For many years investigations have been conducted in order to understand the flow instabilities that lead to transition in jets. Among the earliest, the inviscid linear stability analysis of Batchelor & Gill (1962) showed that immediately at the jet exit, where the velocity profile has a 'top-hat' behaviour, all the instability modes are able to be exponentially amplified while in the far field region only the helical mode seems to be unstable. The transition between these two different instability regions is still unclear and the analysis is complicated by the presence of several unstable modes embedded in the turbulence background. Therefore, a large number of linear stability analyses (Plaschko 1979), simulations (Danaila *et al.* 1997) and experiments (Corke *et al.* 1991; Zaman & Hussain 1984) have been performed in order to highlight the role and the dynamics of a single or few modes in the evolution of the flow.

Investigations in naturally and artificially excited jets have determined the importance of two instability lengthscales: one associated with the initial shear-layer thickness at the exit of the nozzle (Zaman & Hussain 1981), and the other associated with the jet diameter which governs the shape of the mean

velocity profile at the end of the potential core (Crow & Champagne 1971). The instability modes in the first region develop through continuous and gradual frequency and phase adjustments to produce a smooth merging with the second region.

Axisymmetric excitation by means of acoustic forcing has been able to highlight several important aspects of the complex dynamics involved. So, for instance, have the roles played by the shear layer (Zaman & Hussain 1981) and jet column mode (Crow & Champagne 1971) acting in the near-field region of the jet at the nozzle exit and at the end of the potential core, respectively, been of particular interest. However, fewer works have been devoted to the investigation of higher azimuthal modes, principally, due to the higher complexity of the excitation facility (Cohen & Wygnanski 1987; Corke & Kusek 1993) as well as the insufficiency of hot-wire rakes to resolve higher azimuthal modes, which are known to be affected by spatial aliasing (Citriniti & George 1997).

The motivation of the present work is to investigate the possibility that high order modes can actually be the results of non linear combination of oblique waves, for instance generated by blowing and suction. This implies that oblique transition may play a role in the evolution of the coherent structures until the final breakdown to turbulence also for an axisymmetric jet. For wall bounded flows it was already shown that oblique transition gives rise to steady streamwise streaks that break down to turbulence, as for instance documented by Elofsson & Alfredsson (1998, 2000). The scenario of oblique transition has so far not been considered for jet flows and the aim was to study the effect of two oblique modes on the transition scenario as well as on the flow dynamics.

(a) 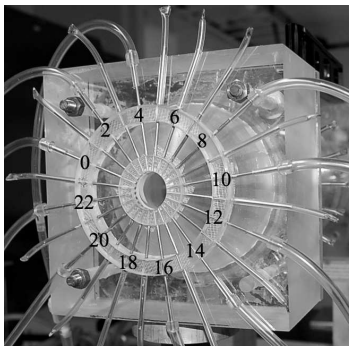

(b) 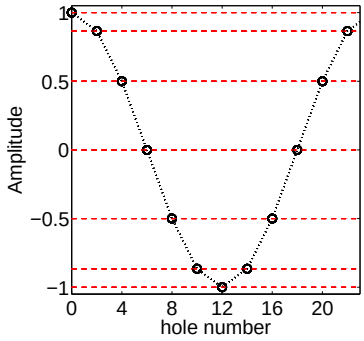

FIGURE 1. Excitation scheme. (a) Close up of the excitation rig, together with the hole number, that corresponds to a certain (b) amplitude modulation for the generation of two opposing helical modes, i.e. $m = \pm 1$.

2. Experimental set-up

The experiments have been carried out in the *Fluid Physics Laboratory* of the *Linné Flow Centre*. The air, driven by a centrifugal fan, passed through a pre-settling chamber placed 3 m downstream in order to reduce the incoming disturbances from the fan. Flow conditioning is performed by means of a honeycomb positioned in the settling chamber after which a plexiglass nozzle with 0.025 m exit diameter is mounted. A short straight plexiglass tube section to provide the acoustic excitation, equipped with 24 perpendicular aligned metal tubes, is fixed to the nozzle exit as shown in figure 1(a).

The excitation has been imparted on the initially laminar flow at the nozzle exit in order to generate two opposite helical modes ($m = \pm 1$) in such a way that a standing wave pattern is formed (Kundu & Cohen 2004, chap. 7). If N acoustic sources are planned to be used, the amplitude of the i:*th* source of the m:*th* mode, A_i^m, can be described as

$$A_i^m(t) = A \sin(\omega_i^m t + \Delta\phi_i^m) , \tag{1}$$

where ω and $\Delta\phi$ denote the angular frequency and phase shift, respectively. With equidistantly arranged excitation sources, the general expression for the combination of two opposite waves is given by a linear superposition of the sources, so that (Elofsson & Alfredsson 2000)

$$A_i = A_i^m(t) + A_i^{-m}(t) = 2A \cos\left(\frac{2\pi m}{N} i\right) \sin(\omega t) , \tag{2}$$

where the first part of the right-hand side is an amplitude modulation, and the second part represents the temporal variation of the excitation in the i:*th* source as depicted in figure 1(b).

Velocity measurements have been performed by means of a X-wire probe using an *A.A. LAB AN-1003* anemometry system in CTA mode. At the beginning of each set of experiments, the amplitude of each loudspeaker has been regulated in such a way that the streamwise velocity rms level around the excitation frequency, measured with a single hot-wire, followed the law depicted in figure 1(b).

3. Results, discussion and conclusions

Figure 2 depicts flow visualisations from both an axisymmetric and oblique excitation. While the axisymmetry prevails for the $m = 0$ excitation, as apparent from figure 2(a) and (b), the $m = \pm 1$ excitation produces a clear helical structure, as would be expected. The presence of a helical mode is also confirmed by means of hot-wire measurements, as shown in figure 3, where conditional sampling combined with a phase averaging technique was used.

An extensive parametric study in terms of frequencies and amplitudes for a selected range of Reynolds numbers was performed in order to focus on the

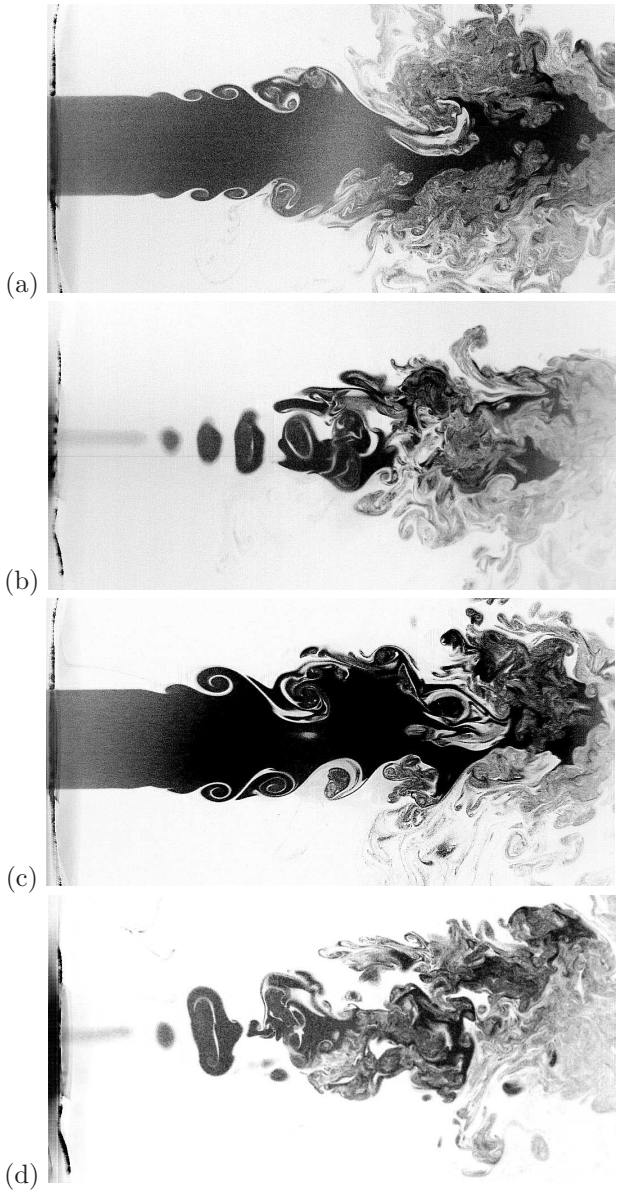

FIGURE 2. Smoke flow visualisations at $Re_D \approx 8500$, based on nozzle diameter and exit velocity: unexcited jet, across $r/D = 0$ (a) and 0.5 (b), excited jet, $St_D = 0.5$ and $m = \pm 1$, across $r/D = 0$ (c) and 0.5 (d).

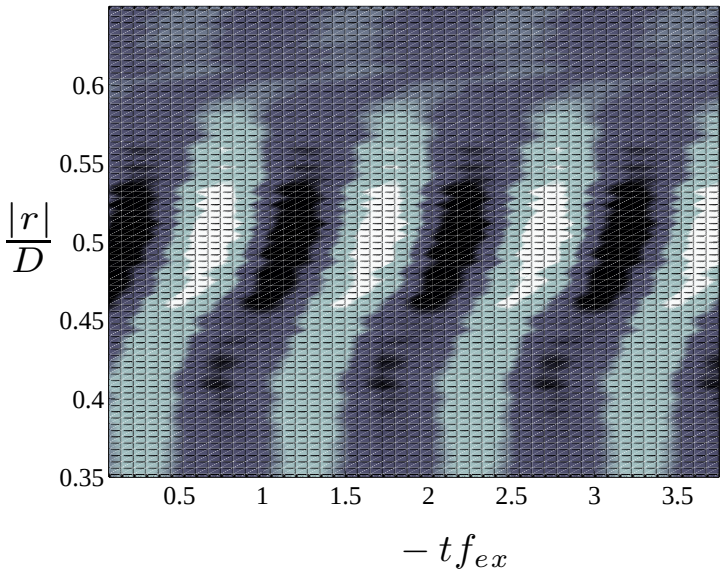

FIGURE 3. Contour of the relative streamwise velocity above its phase average for the excited jet ($m = \pm 1$) for $Re_D \approx 25000$, based on nozzle diameter and exit velocity, at $x/D = 1$ and $St_D = 1.5$. The phase averaged contour are duplicated to better appreciate the helical mode

most influential parameter set. Since the aim of this work was to investigate the flow in the near-field region of the jet, a downstream location of $x/D = 3$ has been chosen to investigate the effect of the excitation on the flow. Several combinations of Reynolds number and excitation frequency have been tested in order to deduce the effect on the streamwise rms level. In figure 4 the relative rms (compared to the unexcited or natural case) as function of the dimensionless frequency, $St_{\theta_0} = f\theta_0/U_c$, is given, where θ_0 is the initial momentum thickness of the boundary layer at the nozzle lip and U_c the jet centreline exit velocity. It must be stated that similar St_{θ_0} have been obtained with different combinations of velocity and excitation frequency which can be the reason for the presence of a non negligible scatter. Due to the latter, a moving average has been performed to clarify the trend. Even though the dispersion is significant, it is interesting to observe that a reduction in the turbulence intensity can be observed around $St_{\theta_0} \simeq 0.012$, which is close to the value found for an axisymmetrically excited jet (Husain & Hussain 1995).

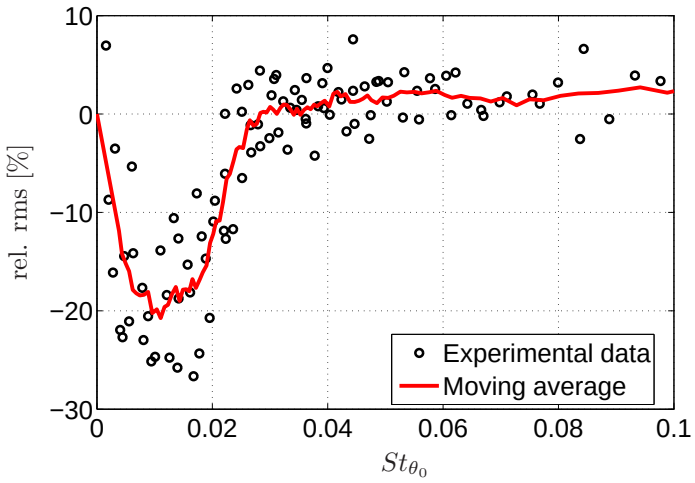

FIGURE 4. Relative change in streamwise velocity rms at x/D =3 between excited and unexcited case for different exit velocities.

In the following, results for a Reynolds number of $Re_D = 25000$ will be presented where a frequency of f_{ex} =1500 Hz was found to show the strongest turbulence reduction at $x = 3D$ and it will be referred to as the "excited case" in contrast to the natural case.

Some important aspects can be deduced from the autocorrelation function or the velocity spectra, reported in figure 5. When the excitation frequency is close to the shear layer mode, several non-linear interactions appear within the first half diameter and then decay further downstream. At $x/D = 2$ the remaining peak is a subharmonic of the excitation frequency, which is somewhat similar to what was observed by Corke & Kusek (1993). It is worthwhile to note that the low frequency energy is lower than in the unexcited case, indicating a strength reduction in the large scales due to the excitation at the jet exit.

The evolution of the power spectral density confirms that the excitation has an impact on the evolution on the whole flow field with the imposed periodicity given by the excitation itself. The scenario seems to be in agreement with the one depicted by Batchelor & Gill (1962) with two unstable oblique modes that will combine to generate several nonlinear interactions. This process saturates most of the energy of the shear layer at the various frequencies and starts to decay faster compared to the natural case, with only some modes that will decay slower than others.

This reduction of turbulence could be connected to the same phenomenon described by Elofsson & Alfredsson (2000) about the effect of oblique waves

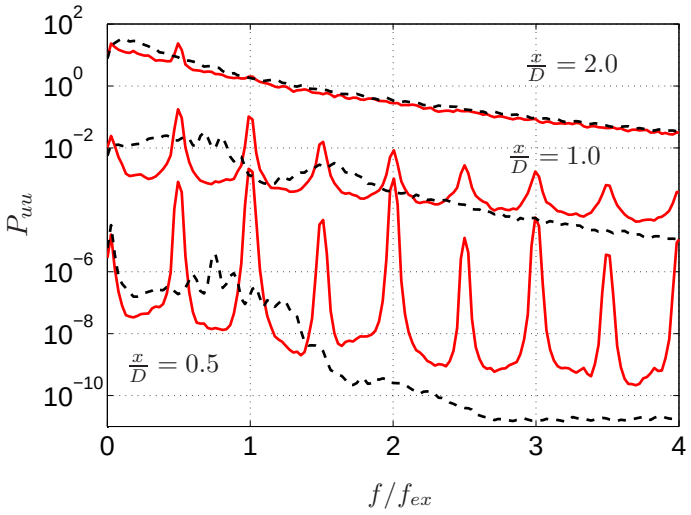

FIGURE 5. Power spectra density distribution in the shear layer region, where the highest turbulence intensity for $Re_D = 25000$ with and without excitation is observed. Excitation at $f = 1500$ Hz (solid line) and natural case (dashed line).

in laminar boundary layers, where the authors showed that the interaction of two waves is able to generate streamwise streaks by means of nonlinear interaction. Unfortunately, in this first investigation it was not possible to detect the presence of such streaks, and this aspect must be furher investigated in the future in order to understand the connection between the turbulence reduction and the azimuthal forcing.

Acknowledgement

The cooperation between *KTH* and the *University of Bologna* is supported by *The Swedish Foundation for International Cooperation in Research and Higher Education* (STINT), which is greatly acknowledged.

References

Batchelor, G. & Gill, A. 1962 Analysis of the stability of axisymmetric jets. *J. Fluid Mech.* **14**, 529–551.

Citriniti, J. & George, W. K. 1997 The reduction of spatial aliasing by long hot-wire anemometer probes. *Exp. Fluids* **23**, 217–224.

Cohen, J. & Wygnanski, I. 1987 The evolution of instabilities in the axisymmetric jet. Part 1. the linear growth of disturbances near the nozzle. *J. Fluid Mech.* **176**, 191–219.

Corke, T. & Kusek, S. 1993 Resonance in axisymmetric jets with controlled helical-mode input. *J. Fluid Mech.* **249**, 307–336.

Corke, T., Shakib, F. & Nagib, H. M. 1991 Mode selection and resonant phase locking in unstable axisymmetric jets. *J. Fluid Mech.* **223**, 253–311.

Crow, S. & Champagne, F. 1971 Orderly structure in jet turbulence. *J. Fluid Mech.* **48**, 547–591.

Danaila, L., Dušek, J. & Anselmet, F. 1997 Coherent structures in a round, spatially evolving, unforced, homogeneous jet at low reynolds numbers. *Phys. Fluids* **9**, 3323–3342.

Elofsson, P. & Alfredsson, P. H. 1998 An experimental study of oblique transition in plane Poiseuille flow. *J. Fluid Mech.* **358**, 177–202.

Elofsson, P. & Alfredsson, P. H. 2000 An experimental study of oblique transition in a Blasius boundary layer flow. *Eur. J. Mech. B - Fluids* **19**, 615–636.

Husain, H. & Hussain, F. 1995 Experiments on subharmonic resonance in a shear layer. *J. Fluid Mech.* **304**, 343–372.

Kundu, P. K. & Cohen, I. C. 2004 Fluid mechanics. *Elsevier, Academic Press, 3rd ed.*

Plaschko, P. 1979 Helical instabilities of slowly divergent jets. *J. Fluid Mech.* **92**, 209–215.

Zaman, K. & Hussain, A. K. M. F. 1981 Turbulence suppression in free shear flows by controlled excitation. *J. Fluid Mech.* **103**, 133–159.

Zaman, K. & Hussain, A. K. M. F. 1984 Natural large-scale structures in the axisymmetric mixing layer. *J. Fluid Mech.* **138**, 325–351.

Paper 4

"The idea is to try to give all the information to help others to judge the value of your contribution; not just the information that leads to judgment in one particular direction or another."

Richard Phillips Feynman (1918 – 1988)

4

Low Reynolds number Zero Pressure-Gradient Equilibrium Turbulent Boundary-Layer Experiments

By Ramis Örlü

Linné Flow Centre, KTH Mechanics, SE-100 44 Stockholm, Sweden

Surveying the large amount of literature regarding low Reynolds number turbulent boundary layer experiments reveals that there is a lack of experimental data, which fulfill equilibrium zero pressure-gradient conditions and is scaled by a directly determined friction velocity. Since direct numerical simulations reach for the lower end of the range of Reynolds numbers where a scale separation starts to establish itself, the need for such experiments is for the purpose of cross-validating both methods, of utmost importance. The present report aims at a detailed documentation of a new set of performed experiments which fulfill the aforementioned requirements.

1. Introduction

1.1. *Justification for the need of new experiments*

The present paper is concerned with experimentally obtained low Reynolds number zero pressure-gradient (ZPG) equilibrium turbulent boundary layers (TBL). During the last decade a large body of experimental data has been obtained with the focus on high Reynolds numbers (see e.g. references given in Fernholz & Finley (1996) or Chauhan *et al.* (2009)). The need for high Reynolds number experiments has been stimulated due to the fact that the classical view on turbulent boundary layers has been challenged from several sides. The "logarithmic law" (or "log law") and its universal constants describing the mean velocity distribution in the overlap region is classically believed to be valid for all wall-bounded turbulent flows with Reynolds number independent constants (including the von Kármán constant, κ) down to the minimum Reynolds number to which a turbulent boundary layer is sustainable (Coles 1962). However, this view has continuously been modified, be it regarding its threshold Reynolds number from where on its constants are to be taken constant (Simpson 1970; Österlund *et al.* 2000), or more substantially, by favoring a power law over the log law (Barenblatt & Chorin 1998; Buschmann 2000). It is generally accepted that high Reynolds numbers are needed in order

to contribute to this debate, due to the scale separation needed to establish a long enough overlap region in which the log law is believed to be situated. This explains the recent emergence of experiments at high Reynolds numbers, among others Hites (1997), Österlund (1999), Nagib *et al.* (2004*a*), Knobloch & Fernholz (2004) and Hutchins & Marusic (2007).

Despite the mentioned efforts to provide experimental data at high Reynolds numbers, computations by means of direct numerical simulations (DNS), have started to reach Reynolds numbers where a scale separation starts to begin and establish an overlap region. Starting from the pioneering work by Spalart (1988) several DNS simulations of turbulent boundary layers have been performed, but just recently has the highest Reynolds number of Spalart been exceeded (Ferrante & Elghobashi 2005). Computational simulations will continue to reach for higher Reynolds numbers and one way to speed up the procedure would be to test various models for Large Eddy Simulations (LES), by accepting a loss in resolution. Such an investigation is currently being undertaken by Schlatter *et al.* (2009*a*,*b*) where the DNS and LES are exceeding Reynolds numbers (we implicitly imply thereby a Reynolds number based on the free stream velocity, U_∞, and the momentum thickness, θ, i.e. Re_θ) of a few thousands. Table 1 lists a selection of physical and computational experiments on turbulent boundary layers, which provide data for the low Reynolds number regime. In the following we loosely use the notion of Erm & Joubert (1991) when referring to low Reynolds number turbulent boundary layer experiments, namely $Re_\theta < 6000$. Table 1 therefore excludes the aforementioned high Reynolds number experiments, as well as those which have focussed on the minimum Reynolds number at which a turbulent boundary layer is sustainable or where a reminiscence of the transition process is probably still observable, as for instance the physical and computational experiments and by Djenidi & Antonia (1993) and Wu & Moin (2008), respectively.

We do not intend here to provide a review of relevant experiments, but rather want to draw the attention to two main issues, which will make the need for the present investigation evident. The most important conclusion from a look at table 1 is that the wall shear stress is in most cases determined through indirect methods, which are usually based on the log law. Only few have quality near-wall data in the viscous sublayer (for instance by using LDV[1]), and not all investigations have profiles at various downstream locations in order to apply the von Kármán momentum integral. The use of Preston or Stanton tubes relies in the same manner on the validity of the law of the wall and does therefore not provide a direct and independent measure of the wall shear stress, which is needed to compare and test various scaling laws. There are, to our knowledge, only two investigations which provide a direct and independent measure of the

[1]As for instance in the case of DeGraaff & Eaton (2000). These authors favored, however, despite their sufficiently resolved near-wall data, a fit to the log law using Coles log law constants.

skin friction in the Reynolds number range of interest, namely that of Osaka *et al.* (1998) and Österlund (1999), who utilised floating elements and the oil-film interferometry technique, respectively. The importance of such direct and independent skin friction measurements has been emphasised in several recent studies, among others, by Nagib *et al.* (2004*b*) and Buschmann & Gad-el-Hak (2006). The absence of direct and independent skin friction measurements partially explains a number of debates and controversies, the already mentioned mean velocity distribution in the overlap region (Monkewitz *et al.* 2008) and the related discussion regarding the universality and Reynolds number dependence of the constants of the laws believed to describe the overlap region (Nagib & Chauhan 2008), the position and value of the maximum in the streamwise velocity fluctuations in wall turbulence (Mochizuki & Nieuwstadt 1996) as well the skin friction relation itself (Nagib *et al.* 2007).

The other issue is the physical state of the turbulent boundary layer itself, which is intended to be an equilibrium zero pressure-gradient one. Whether or not a turbulent boundary layer fulfills the criteria of being an equilibrium one, is more than just a sufficient development length and high enough Reynolds number, rather, as stated in Fernholz & Finley (1996):

> The criteria to be applied must clearly include characteristic quantities observed in the mean velocity profile, such as the Reynolds number [...], shape parameter [...], skin friction coefficient [...], and the strength of the wake component [...].

Furthermore it is supplemented, that:

> Full development also implies that the mean velocity and the turbulence quantities should follow similarity laws valid for both the inner and outer regions.

The quoted criteria are more or less accepted, despite their vagueness when it comes to their practical assessment. While the Reynolds number and shape factor can easily be accessed, the problems start when it comes to the skin friction coefficient and the wake parameter. The former is in most cases not directly measured and sometimes even inferred from various skin friction relations, which in turn can not be used as a criterion sought to be fulfilled, since it is assumed to be valid *a priori*. The scatter between various skin friction relations was recently investigated by Nagib *et al.* (2007), and it was shown that the majority of known relations differs systematically between each other, when used with their original constants. However they can be made to agree fairly well in the range of laboratory experiments, when modified and underpinned by the same directly measured skin friction data. The wake parameter, on the other hand, is commonly determined as the maximum deviation of the wake region from the log law and hence depends strongly on the log law constants and the inferred friction velocity. It is apparent that different physical states can be claimed to be in equilibrium depending on the constants used. The

same vagueness applies for the similarity laws to be fulfilled, which is what is set out to be investigated or proved.

The aforementioned explains why the same set of data can be considered as reliable or not reliable zero pressure-gradient equilibrium data, as is for instance the case of the data by Wieghardt & Tillmann (1951) (cf. discussion in Nagib *et al.* 2005). It is apparent that, for the time being, it does not suffice to state that an equilibrium state has been established, but rather all above mentioned quantities have to be stated not only in their value, but also in the way in which they were determined. Such a detailed description is needed in order to enable an independent and objective assessment of the state of the flow and hence the quality of the data. Most of the mentioned equilibrium criteria discussed here are not always given in the clarity they have to be, which may have contributed to the scatter and controversies we are currently facing in the study of the "simple canonical" flow case of the zero pressure-gradient turbulent boundary layer.

Having said that it becomes clear that, despite a large body of experimental results, of which only a few are given in table 1, there is still a need of experimental data from equilibrium zero pressure-gradient turbulent boundary layers, which fulfill the equilibrium criteria and document them in such a way that they can be accessed objectively. Also a direct and independent measure of the skin friction as part of the equilibrium criteria as well as for the scaling of the data is highly desirable.

Before leaving this section it is also important to comment on the computational experiments mentioned in the beginning. DNS has the general reputation of presenting the exact solution, however due to its tremendous need of computational resources the turbulent boundary layer is in most cases triggered and starts to develop with a certain inflow condition. In order to save computational costs the development length is often very short and also the computational box and grid resolution are restricted in such a way that a solution is within conceivable time. This however brings problems with it, not only are the Reynolds numbers still far away from those needed to conclude the issues currently debated, but the equilibrium conditions are also not fulfilled intrinsically. In fact the pioneering work by Spalart (1988) displays a quite different shape factor from those associated with equilibrium flows (as for instance defined in Chauhan *et al.* (2009)), and they can even display opposite trends from generally accepted views, as for instance the increase in the shape factor with increasing Reynolds number in the simulation by Khujadze (2005) used to test various scaling laws (Khujadze & Oberlack 2004). Only within the last few years have DNS studies exceeded the Reynolds number put forward by Spalart been reported and they do not fulfill the equilibrium criteria *per se*. Laboratory experiments are hence needed to cross-validate physical and computational experiments. LES has become quite prevalent in applied

turbulence studies, however has not yet established itself in the study of computationally high Reynolds number wall-bounded canonical flows, due to their assumption of certain models, which are set out to be confirmed. Nevertheless also they will become important and need validation against experimental data. This again underlines the importance of new experiments focussing on the low Reynolds number region underpinned by independent and direct skin friction measurements.

1.2. *Aim and structure of the paper*

Once the need for new experimental data has become evident from the aforementioned section the aim of the present paper is self-explanatory, namely to document the experimental setup and measurement technique used as well as to provide the necessary details to assure the equilibrium zero pressure-gradient state of the two-dimensional turbulent boundary layer. The experimental set-up and measurement techniques are going to be described in sections 2 and 3, respectively, whereas the parameters describing the experimental dataset are given in section 4. Also the present paper does not aim to discuss the obtained results in detail, the directly measured skin friction, the integral parameters describing the quality of the data as well as statistical quantities will be presented in section 5 for completeness.

2. Experimental set-up

2.1. *Boundary-layer wind tunnel*

The present experimental investigation can be thought as an extension of the extensive experiments performed by Österlund (1999) over a wide range of Reynolds numbers, viz. Re_θ= 2500–27000. Therefore the reader is referred to Österlund (1999) and Lindgren & Johansson (2002) for a description of the Minimum Turbulence Level (MTL[2]) wind tunnel, in which the experiments were performed, and for a more recent quality assessment of its flow quality. The remainder of this section will therefore avoid a repetition of the detailed description given in the above two references of the MTL wind tunnel, the flat-plate, and the traversing system. Only where changes in the set-up, which are coupled to the redefined focus of the present experimental investigation, have been introduced and where a description is needed for clarity and/or completeness details will be given.

A 7 m long aluminium flat plate of 26 mm thickness, designed by Österlund (1999), comprising six 1 m long pieces and a 1.125 m long leading edge part of which the 0.125 m long part is a symmetric and elliptical leading edge, was used for the experiment. The plates are polished before their final arrangement in the tunnel. The plates were placed horizontally near the vertical centre of the test section, and the test plate ends with a 1.5 m long trailing edge. The latter was

[2]Also Mårten Theodore Landahl after its late initiator.

Author(s) (Year)	Reynolds no. $Re_\theta\, x\, 10^{-3}$	Experimental technique(s) velocity profiles	wall shear
Klebanoff & Diehl (1954)	3.6–15.2	HWA	Kármán mom. eq.
Smith & Walker (1959)	2.9–48.3	Pitot	floating element, Preston
Karlsson & Ramnefors (1978)	1.6–11.7	HWA	Coles
Karlsson (1980)	0.8–16.3	Pitot	Preston
Head & Bandyopadhyay (1981)	0.6–16.3	Pitot	Preston
Purtell *et al.* (1981)	0.4–5.1	HWA	wall slope, Kármán mom. eq.
Murlis *et al.* (1982)	0.8–4.8	HWA, Pitot	Preston, Stanton
Smits *et al.* (1983)	0.3–3	Pitot	Preston
Andreopoulos *et al.* (1984)	3.6–15.4	HWA, Pitot	Preston, wall slope
Ahn (1986)	3.3–18.8	HWA	
Spalart (1988)	0.3–1.4	DNS	DNS
Erm (1988); Erm & Joubert (1991)	0.7–2.8	HWA, Pitot	Preston
Wark (1988); Wark & Nagib (1991)	3.2–9.1	HWA	Clauser
Perry & Li (1990)	2.8–11.1	HWA	Preston, Clauser
Naguib (1992)	3.2–8.4	HWA	Clauser
Smith (1994)	4.6–13.1	HWA, Pitot	Preston, Clauser
Warnack (1996)	0.8–4.7	HW	Preston, wall HW
Osaka *et al.* (1998)	0.8–6.1	HWA	floating element
Tsuji (1999); Tsuji & Nakamura (1999)	1.3–4.7	HWA	Clauser
Österlund (1999)	2.3–27.3	HWA	OFI, wall slope
DeGraaff (1999); DeGraaff & Eaton (2000)	1.4–31.7	LDV, HWA	Coles
Ferrante & Elghobashi (2005)	1.4–2.9	DNS	DNS
Khujadze & Oberlack (2004); Khujadze (2005)	0.7–2.5	DNS	DNS
Schlatter *et al.* (2009*b*)	1.4–2.5	DNS	DNS

TABLE 1. Selection of ZPG TBL experiments with data for the low Reynolds number regime, i.e. below Re_θ of 6000. Although given are the velocity measurement techniques used and the method to determine the wall shear. Abbreviations used are: Hot-wire anemometry (HWA), Laser-Doppler Velocimetry (LDV) and Direct Numerical Simulation (DNS) as well as Oil Film Interferometry (OFI).

used to position the stagnation point not at the nose of the leading edge (as was the case for the measurements performed by Österlund) but on the upper part of the flat plate, the hydrodynamically smooth side on which the measurements were performed. The idea behind this and the tripping, to be described in section 2.3, was to ensure that under all measurement conditions, viz. from around 10 to 40 m/s, the stagnation line does not end up at (or even passes) the nose so that it is located underneath the plate and thereby changes the state of the boundary layer from measurement to measurement or even worse, while the measurements for one profile or the skin frcition are undertaken. The optimal arrangement of the trailing flap was tested by checking the difference between two static pressure taps as well as two Pitot tubes (acting as a Preston tube) located in and on the leading edge, respectively. The final iteration step gave an optimum trailing flap angle of 3°.

One flat plate segment is equipped with a cylindrical hole (diameter 160 mm) where a traversing system can be mounted to the plate. In front of that position another circular plug (diameter 100 mm) is mounted. Inside this plug a glass plug (diameter 50 mm) is mounted over which the boundary layer (and also oil-film) measurements are made. For the present measurements this plate was mounted as number 2, giving a measurement distance from the leading edge of 1.625 m.[3] At the inlet of the test section the distance between the tunnel ceiling and the plate is 414 mm and between the plate and the floor 360 mm. The ceiling is adjustable to allow for the growing boundary layers and still obtain a zero pressure gradient. At $x = 1.625$ m the distance is 420 mm between the plate and the ceiling.

Furthermore the gaps between the flat plate and the side walls were sealed along the entire test section length, after having observed that tufts placed within these gaps indicated a flow from above to below the flat plate. Also the slot of 35 mm width on the tunnel roof, for the main traversing system of the MTL was sealed during the adjustments as well as the final measurements. The main traversing system was for all measurements parked at the end of the test section, i.e. around 5 m downstream of the location where the measurements were taken.

2.2. *Traversing system*

The main traversing system of the MTL wind tunnel, i.e. a computer controlled 3D traversing system (in streamwise, spanwise and wall-normal direction) with additional two degrees of freedom, which are able to rotate and pitch the tip of the traversing along its axis and away from the axis of the traversing arm, respectively. However for the present experiments a 1D traversing system

[3]Complementary experiments at 3.625 m downstream, albeit at higher Reynolds numbers, are reported in the appendix. These were collected in the same manner as reported here and are mainly used to check Reynolds number dependencies as well as the effect of spatial resolution.

mounted underneath the flat plate was used. The reason for this was that the main traversing system with its 1.2 m long traversing arm has been observed to vibrate at velocities above 30–40 m/s, but more severely was found to alter the flow field within the lower end of the buffer region when approaching the wall, which could clearly be observed to result in higher shape factors, but especially in the diagnostic plots (cf. section 5.2). This made us disregard a number of measurements taken with the main traverse ranging from $1400 \leqslant Re_\theta \leqslant 5500$ at varying x, which we aimed to provide in addition to the ones measured and presented here with the wall traversing system.[4]

The wall traversing system used and described by Österlund (1999) was used for the experiments in which a single hot-wire probe was held stationary and traversed in the wall normal direction. This traverse was mounted on an instrumentation plug and could be placed in one of the flat plate segments which in turn could be rearranged in the test section to relocate the measurement location in the test section.

The traverse carriage was driven over a maximum displacement of 150 mm by a servo motor with a lead screw equipped with an encoder from which the actual position was read after each movement of the hot-wire probe.

2.3. *Tripping*

In order to reduce the development length to obtain a fully developed turbulent boundary layer and to ensure that repeatable conditions (transition point and hence identical displacement, momentum loss and boundary layer thicknesses) for the turbulent boundary persist for each measurement run it was necessary to trip the boundary layer at the beginning of the plate.

A photograph depicting the tripping tape configurations used during the course of the measurements is shown in figure 1. The tripping consists of 7 DYMO tapes embossed with the letter "V" pointing in the flow direction. Additionally, three, two and one anti-slip tape/s were/was used downstream of the DYMO tapes for T_A, T_B and T_C, respectively. All tapes covered the whole spanwise length of the plate and had a width of 12 and 50 mm for the DYMO and anti-slip tapes, respectively.

Initial measurements were taken with the configuration T_A, which was actually adjusted for measurements at further downstream locations. These caused slightly lower shape factor values than the nominal values for zero pressure-gradient equilibrium turbulent boundary layer, but were still within the tolerances and are therefore reported here as well. By successively reducing the strength of the tripping, T_B and T_C, the shape factor reached the desired equilibrium conditions as will be documented in section 5.3.

[4]The appendix will nevertheless give an overview over the collected data. Although the results will not be discussed here, some of the results may be of use in following papers.

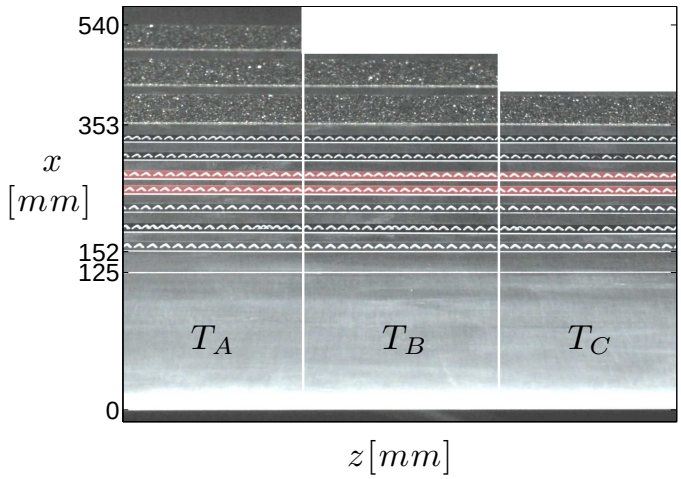

FIGURE 1. Photograph showing the three tripping tape configurations (T_A, T_B and T_C) used. The downstream distance from the leading edge of the set of DYMO and anti-slip tapes is given on the ordinate. Note that the different colours of the DYMO tape they are of the same type and that the scale on the ordinate is distorted due to the camera angle.

2.4. *Pressure gradient*

The upper wall of the tunnel was adjusted in order to achieve a zero pressure-gradient in the streamwise and spanwise direction and thereby ensure the two-dimensionality of the boundary layer. For the initial adjustment a hot-wire probe, placed far into the freestream, was traversed downstream by means of the main traverse and the 48 screws on the upper wall of the tunnel were adjusted iteratively to find the minumum relative streamwise variation. Once this adjustment was completed the relative spanwise variation in the freestream was checked by means of a hot-wire probe mounted on the main traverse as well as on a manual traverse (basically a long stiff cylinder with the hot-wire probe mounted at the centre, which could be moved over the entire spanwise segment of the test section) and iteratively improved upon which the relative streamwise variation was checked again.

The mean streamwise velocity component in the free-stream (at a distance from the plate corresponding to the centre of plate and upper wall), was measured by hot-wire anemometry as well as a Prandtl tube. The hot-wire probe could either be traversed in the streamwise and spanwise direction on the main traverse in the range of $1 \leqslant x \leqslant 5.6$ m and -0.17 $\leqslant z \leqslant$ 0.17 m, respectively, or by means of a manual spanwise traverse in the range -0.5 $\leqslant z \leqslant$ 0.5 m at downstream locations of 1, 3 and 5 m. The Prandtl tube, on the other hand, could

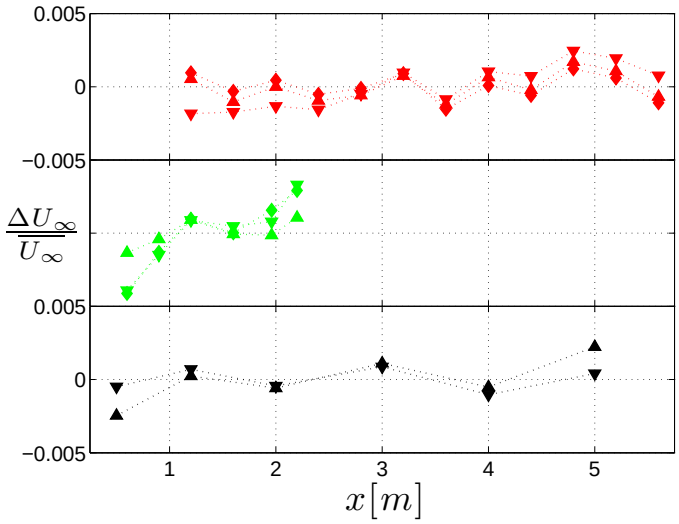

FIGURE 2. Relative streamwise free stream variation for the three tripping tape configurations used. The downstream distance from the leading edge is given in the abscissa, whereas the ordinate denotes the relative mean free stream velocity in regards to the mean over the measured range, ΔU_∞, scaled by the mean over all measured downstream positions, $\overline{U_\infty}$. From top to bottom: T_A (▼: 20 m/s, ♦: 30 m/s, ▲: 40 m/s), T_B (▼: 11.75 m/s, ♦: 16.75 m/s, ▲: 28 m/s) and T_C (▼, 12 m/s, ▲: 17.5 m/s).

manually be positioned at any downstream position between $0.6 \leqslant x \leqslant 6$ m along the slot of the main traversing system.

Both hot-wire and Prandtl tube measurements were carried out with sample times exceeding 60 seconds at each measurement location. The hot-wire was calibrated around the free-stream velocity of interest (20, 30 or 40 m/s), whereas the Prandtl tube was connected to a FC0510 Micromanometer (Furnace Control Limited), from which also the ambient temperature and pressure were obtained.

Figure 2 shows the final free stream variation in streamwise direction for the three tripping configurations obtained by means of the Prandtl tube. While the roof of the tunnel was adjusted in order to obtain zero pressure-gradient conditions for the tripping configuration T_A and T_C, the roof was not adjusted for case T_B. The effect of removing one anti-slip tape can readily be seen by comparing the relative streamwise free stream variation between cases T_A and T_B. While there is no apparent trend for cases T_A and T_C and the variation

appears to be random, the tripping configuration T_B resembles are very weak favorable pressure gradient especially for the two lower velocities measured.

2.5. *Flow stability and quality*

The variation in the free stream velocity was monitored during all measurements by means of a Prandtl tube located at the same downstream position as the hot-wire. From these measurements the variation was found to be around 0.1 % of the free stream velocity for all cases, i.e. 10 to 40 m/s. For the individual cases there is no trend, but a random scatter of the values. During none of the measurements variations in the ambient temperature, measured by means of a Pt-100 at the end of the test section, were observed. The recorded Prandtl tube measurements in the free stream displayed neither a drift nor sudden changes.

3. Measurement techniques

3.1. *Oil-film interferometry*

Oil-film interferometry (OFI) can be described as the utilisation of Fizeau interferometry to measure the mean wall shear stress by means of the thinning rate of an oil film deposited on a surface and subjected to a bounding flow. Compared to other measurement techniques in fluid mechanics OFI has not received the attention it deserves, and this albeit its obvious advantages, viz. its direct and independent character, its low cost and relative simple application and processing. In the following sections a brief overview of the technique, the method used to extract the mean wall shear stress, τ_w, and thereby the friction velocity as well as the necessary oil viscosity determination will be given.

3.1a. *A brief description.* When an oil drop placed on a smooth surface is exposed to a flow it will start to thin due to the surface shear stress excerted on it by the flow. Using a monochromatic light source to illuminate the surface of an oil film, interference patterns, so-called Fizeau fringes, can be observed once the initial oil drop has reduced under a certain thickness. Such an evolution from an initial oil drop, to a thick oil film, towards a thin oil film, is shown in figure 3, where the light reflected from the top and bottom (having travelled twice the local thickness of the thin film) of the oil film brings about the fringe patterns, which become visible between the third and forth image in figure 3. Following Janke (1993) and Brown & Naughton (1999) the height of the k:*th* dark fringe is given as,

$$h_k = h_0 + k\Delta h,\ k = 0, 1, 2, \cdots, \tag{1}$$

where h_0 is the height of the zeroth dark fringe at $k = 0$, i.e. the film edge, and the difference in height between successive dark fringes is given by

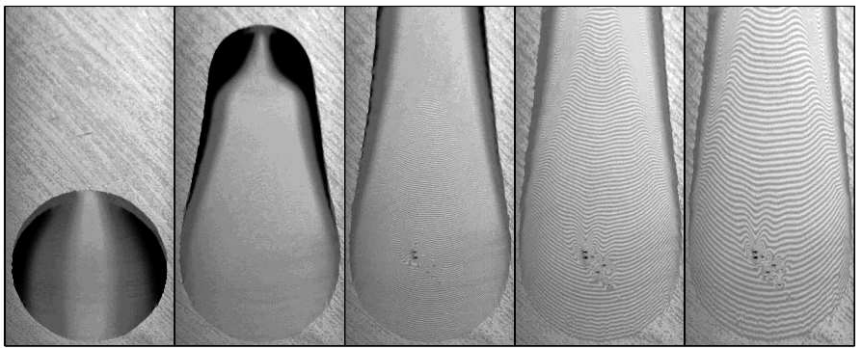

FIGURE 3. Example fringe patterns as derived from oil film light reflections for $U_\infty = 10$ m/s. Flow is from bottom to top and the shown images were taken at $t = 0$, 25, 50, 100 and 150 s after start of the tunnel. Note the dust particles stuck to the lower end of the images and the distortion of the surrounding fringes. The remaining fringe pattern can, however, still be used.

$$\Delta h = \frac{\lambda}{2(n^2 - \sin^2 \alpha)^{1/2}} \,. \tag{2}$$

Once the wavelength of the monochromatic light source, λ, the refractive index of the oil, n, and the viewing angle of the observer, α, are known, the initial and succesive height evolution of the thinning oil film can be computed by means of equations (1) and (2).

Beginning with the pioniering work of Tanner & Blows (1976) several methods have been proposed to solve the thin-oil-film equations, derived by Squire (1961, 1962) in order to extract the mean wall shear stress, of which some are reviewed in Fernholz *et al.* (1996) and Naughton & Sheplak (2002). Following the aforementioned sources the thin-oil-film equation for a two-dimensional flow reduces to

$$\frac{\partial h}{\partial t} = -\frac{1}{2\mu} \frac{\partial(\tau_w h^2)}{\partial x} \,. \tag{3}$$

The most appraised and probably most straightforward method to determine the mean wall shear stress is based on equation (3) and utilises an x-t diagram, extracted by following the Fizeau fringes along one particular line over time. Such an x-t diagram is depicted in figure 4, which readily gives the fringe velocity, u_k, viz.

$$u_k = \left.\frac{\partial x}{\partial t}\right|_{h_k=const}, \tag{4}$$

needed to obtain the mean wall shear stress. Combining the aforementioned equations (1)–(4) one obtains (Janke 1993; Brown & Naughton 1999)

$$\tau_w \left[k + \frac{h_0}{\Delta h}\right] = \mu u_k \frac{2(n^2 - \sin^2\alpha)^{1/2}}{\lambda}. \tag{5}$$

Once the wavelength of the light source, the viewing angle of the camera as well as the index of refraction of the oil are known, the dynamic viscosity remains to be determined (cf. next section) in order to solve equation (5) with the aid of the fringe velocity by means of equation (4). As stated by Rüedi *et al.* (2003), for a number of successive values of k ($k \geqslant 2$), the latter equation represents a linear system from which τ_w and $h_0/\Delta h$ can be determined, for instance, by a least squares method.

In the present evaluation a computer program based on the above description, originally written by Österlund (1999) and further developed by Rüedi *et al.* (2003), was used to determine the last two quantities by locating the fringe centre (the so-called peak gray-scale intensity method). Multiple fringe

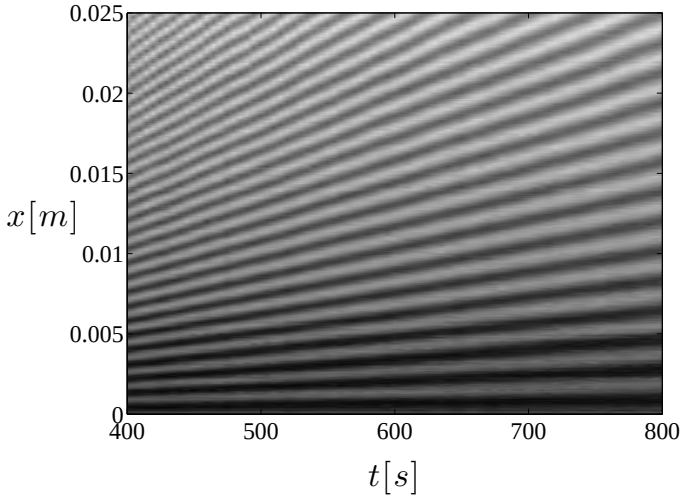

FIGURE 4. x–t diagram as extracted from a time series of fringe pattern images for the case shown in figure 3 after reaching steady conditions. Note that the shown pattern was extracted from a region, where the distortion by dust particles has diminished.

spacing estimates can and were used to obtain statistically robust results (Tropea *et al.* 2007, chap. 12).

For the final post-processing of the recorded images a new technique, developed by Rüedi (2009), which utilises Fourier analysis (similar to the method described by Ng *et al.* (2007)) to determine the fringe spacing, was employed and was found to be a more user independent and robust method compared to the previously used one. However, the results from both techniques showed no systematic differences.

3.1b. *Viscosity determination.* As evident from equation (5) the knowledge of the viscosity is essential in the determination of the absolute value of the wall skin friction. As stated by Naughton & Sheplak (2002) silicon oils have the most suitable properties for oil film interferometry, due to their relatively low temperature dependence. Although the viscosity is given by the supplying company either for a certain reference temperature or through a relation for a certain temperature range, neither the way the viscosity was determined, nor its accuracy, is usually given. The latter is usually provided with an indicated accuracy with at best 1 %. Additionally the density and/or index of refraction of the oil could have been changed over the years, due to exposure to environmental influences (not likely though).

For the present investigation the viscosity was measured by means of a capillary suspended level viscometer[5], which has several advantages compared to other capillary viscometers: independence of the quantity of sample charged into the viscometer, the temperature independence of the viscometer constants, the low susceptibility to errors, due to drainage and alignment, simplicity of operation, and above all an accuracy within ± 0.1 % to mention just a few (Viswanath *et al.* 2006).

The principle of suspended-level (capillary) viscometers is the measurement of the time needed for a sample liquid to fall a predetermined distance (and thereby volume). This process is described by an alterated form of the Hagen-Poiseulle equation formulated by Barr (1931), which reads,

$$\mu = \frac{\pi a^4 \Delta P}{8Q(L+na)} - \frac{m\rho Q}{8\pi(L+na)}\,, \tag{6}$$

where $Q = V/t$ and $\Delta P = \rho g h$ denote the volumetric flow rate and pressure drop along the tube, respectively, a the capillary diameter, and n and m are constants to be determined for corrections of end effects as well as kinetic energy corrections (Tropea *et al.* 2007, chap. 3).[6] Equation (6) can be expressed as

[5]The precise type used here is a BS/IP/SL, Size 2, No 8983 from PSL Poulten Selfe & Lee Ltd.

[6]The correction terms are needed because the Hagen-Poiseuille equation is strickly only valid for parabolic velocity profiles, which is violated at the entrance and exit of the capillary. While the kinetic energy correction accounts for the pressure used in overcoming viscous resistance,

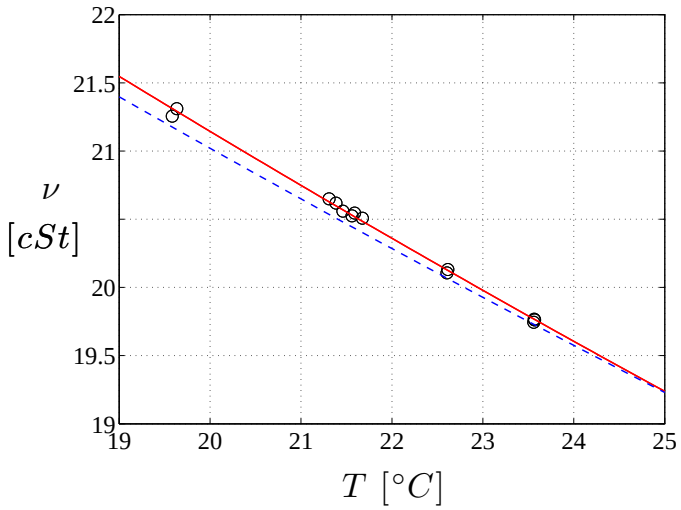

FIGURE 5. Kinematic viscosity of the silicon oil DC200/20 obtained by means of a suspended-level viscometer. ○: Measured values, eq. (8) fitted through the measured values (—) and provided by Österlund (1999) (- -) for the same batch of oil.

$$\mu = c_1 t - \frac{c_2}{t}\,, \tag{7}$$

with c_1 and c_2 determined by calibration with fluids of known viscosity. These are given by the capillary viscometer supplier together with a minimum calibration time to be kept in order to obtain the given accuracy.

For the oil film interferometry measurements presented here, keeping the expected range of the friction velocity in mind, silicon oil with a nominal viscosity of 20 cSt at 25℃ was used[7]. The measured kinematic viscosity for the temperature range of the oil film interferometry measurements is depicted in figure 5 together with a fit through

$$\nu(T) = \nu_{25}\, e^{k(25-T)}\,. \tag{8}$$

Additionally the calibration curve of Österlund (1999) for the same batch of silicon oil is plotted. The calibration constants are given in table 2.

---

the end corrections take the converging and diverging streamlines at the entrance and exit of the capillary into consideration (Viswanath *et al.* 2006).

[7]The precise type of the silicon oil is DOW CORNING 200® Fluid, 20 CST, with a density of $\rho = 949\ kg/m^3$ and a refractive index of 1.400 at 25℃. The latter value was confirmed by an index of refraction meter.

calibration	k	ν_{25} [cSt]
present	1.89e-02	19.24
Österlund (1999)	1.78e-02	19.23

TABLE 2. Silicon oil DC200/20 calibration values obtained by means of a suspended-level viscometer for the same batch of oil.

The plot clearly shows that within a period of more than a decade either the silicon oils viscosity did not change at all for the reference temperature and changed not more than 0.4 % for the lowest measured temperature, or—for the case that the viscosity of the oil did not change—displays the total uncertainty inherent in the technique as well as the user. An even more important message of the plot is that the viscosity given by the supplier is 4 % too high, which in turn would overestimate the wall skin friction by the same amount and the friction velocity by 2 %. This emphasises the importance of an accurate viscosity determination in the range of observed temperatures in order to provide accurate and independent skin friction measurements.

3.1c. *Used equipment and set-up.* The MTL wind tunnel allows primarily two configurations for the use of oil-film interferometry. The tunnel floor has interchangable hatches for which a Plexiglass window exists in order to access the oil-film with both the camera and the light source from underneath. Here, however, a setup similar to the one proposed by Österlund (1999) was adapted, albeit with a number of differences, which are summarised in the following.

To illuminate the oil film a low pressure sodium lamp was used. It had a power of 55 W and a nominal wavelength of 589 nm. The light was mounted horizontally on the roof, alingned along the flow direction and diffused by a white acryl plate. Although the way the sodium bulb is powered is of no particular importance for the results of oil-film interferometry, it may be worth noting that in the present study a new electronic ballast (*EXC 55 SOX 220–240V 50/60Hz*) of 300 grams was used, which replaces the electromagnetic ballast, ignitor and capacitor. The former usually accounts for the main part in terms of mass and size among the other devices used for oil-film interferometry.

The oil-film was monitored by means of a digital single-lens reflex camera (*Nikon D50*) and a telephoto zoom lens (*Nikon Nikkor 200 mm f4*), controlled remotely via a USB cable, which was also used to record the images with a pixel resolution of 3008 x 2000. As may be anticipated from the resolution of figures 3 and 4 the area in focus is not restricted to the oil film alone, but covers

an approximately four times larger area.[8] The camera was mounted upstream the oil-film on the rails of the MTL test section via a custom-made camera stand at an angle of 15° normal to the plate. To allow the monochromatic light as well as the camera to access the oil film the sealing tape of the MTL was hold open at the particular locations. Although these small openings can be considered as leaks, it can safely be assumed that they do not alter the flow. Neither a change in the statistics, nor in the skin friction determined by means of oil-film interferometry was observed between the sealed and non-sealed configuration in a related study.

The oil was deposited on a glass plug on which the camera was focussed. A thermocouple was attached to the bottom side of the plug in order to monitor the surface temperature, whereas a second thermocouple was positioned in the free stream. The two thermocouples used in combination with a handhold digital thermometer (*Fluke*) as well as the Pt-100 connected to the micromanometer and MTL, respectively, were all calibrated against the same reference thermometer, which was used in the water bath in which the oil viscosity was determined. This ensured that all measured temperatures in different steps in the experimental investigation had the same reference temperature. The readings from the Pt-100 thermocouples belonging to the MTL wind tunnel and used to control and monitor the tunnel ambient conditions were, however, not used for the oil-film evaluation, due to the slow responce time of these devices. A fast enough responce time was needed, particularly for the oil-film measurements, recalling that the free stream velocity had to reach the desired speed after having placed the oil drop on the glass plug and the tunnel was started. Too long run times would thin the oil film too quickly (for the selected oil viscosity) and the fringes would start to distort.

3.2. *Hot-wire anemometry*

Due to its intrusive character the geometry and dimension of the hot-wire probe has to be adjusted for the particular flow case and the purpose of the study. Some of these design rules for hot-wire probes can be found in reference literature (Sandborn 1972; Strickert 1974; Lomas 1986; Bruun 1995), others are still being debated or have just not got the attention they may deserve. Some of these design rules are summarised in the following and are intended to reason the selection of the probe used for the present investigation.

All experiments present here and listed in table 3, were performed with the same hot-wire probe (including wire), probe holder and traversing system. Additionally, the operational conditions for the hot-wire were kept identical throughout all measurements, i.e. the overheat ratio, the analog low-pass filter, the calibration procedure, in order not to introduce any systematic differences

[8]This could be further improved by the use of bellows, however image distortion could be introduced and has to be accounted for.

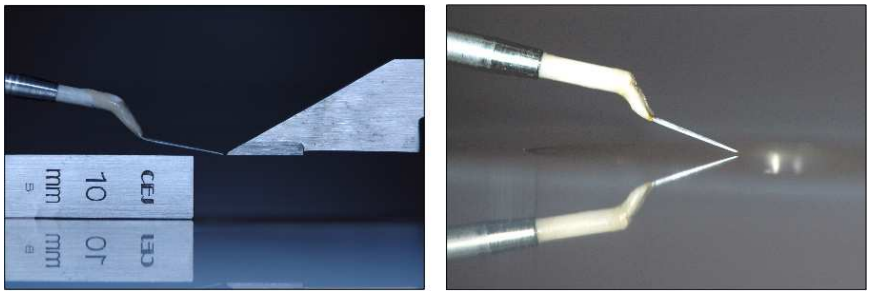

FIGURE 6. Photograph showing the boundary layer type probe during the wall position determination using physical methods, viz. by means of (a) a precision gauge block and a vernier height gauge and (b) the mirrored image. The probe displayed in (b) is the one used for the measurements reported here.

in the acquired and processed signals. Although the aforementioned precautions may sound trivial, they are particularly important in wall bounded flows, and may explain some of the differences observed in the literature, where such an approach is not necessarily followed or aspired.

For the outer region of turbulent boundary layers different hot-wire probes, but also Pitot tubes in size and dimension, are supposed to give non-distinguishable results. On the other hand, quite different results - not only in second and higher order central moments in the case of hot-wires, but even in the mean velocity - can be obtained within the viscous sublayer, buffer region, where the largest velocity fluctuations are found, and the lower end of the logarithmic region.[9] For that particular reason the documentation of the characteristics and operational conditions of the hot-wire probe will become of great importance when interpreting and comparing the results.

The hot-wire probe used for the present measurements is a boundary layer type probe with steel prongs of 0.5 mm diameter etched to give a conical tip with a diameter of around 30 micron. The shape of the prongs resembles a standard Dantec boundary layer probe, viz. a 55P15, however with longer prongs as suggested by Comte-Bellot *et al.* (1971) in order to reduce aerodynamic perturbations. Also the probe was tilted towards the flat plate, as depicted in figure 2, to reduce the aerodynamic blockage caused by the probe body when approaching the wall. The hot-wire itself is a Platinum wire and has a nominal diameter of 2.54 micron. Its length is 470 micron and it is soldered to the end of the tip of the prongs, which faces the flat plate. The 2.54 micron wire diameter is a compromise between the more robust 5 micron wires and the

[9]For the effect of spatial resolution on the mean streamwise velocity component see Örlü (2009*a*).

even smaller wires, which are more fragile and more easily observed to have drift problems[10], despite their ability to resolve higher frequencies and give less biased higher order moments, due to the resulting shorter wire length. Spatial averaging is known to reduce the measured turbulence intensity (Ligrani & Bradshaw 1987), but also falsify higher order moments, as the skewness and flatness factors, as well as reduce the frequency of detected burst events as documented by Johansson & Alfredsson (1983).

Platinum wires were in this study preferred due to mainly two reasons. Although tungsten[11] wires are known for their higher tensile strength, they can (usually) not be soldered to the prongs. The usual process of spot welding makes it however necessary to have a blunt prongs tip, which is bigger than the present prongs. Another reason has recently been demonstrated by Li *et al.* (2004), namely that the usual minimum length to diameter ratio for hot-wires of 200 given for instance in Ligrani & Bradshaw (1987) refers only to the use of platinum wires. For tungsten wires they state that this ratio should be increased to about 270 in order to have the same fraction of heat loss by conduction to the prongs.

3.2a. *Calibration procedure.* The hot-wire, mounted on the wall traversing system, was moved as far out as possible into the free stream to about 120 mm from the plate, where it was calibrated *in situ* in the free-stream against a Prandtl tube. A Micromanometer of type FC0510 (Furnace Control Limited), from which also the ambient temperature and pressure were obtained, was used to read the dynamic pressure from the Prandtl tube. Calibration curves were taken at the beginning and end of each set of measurements as well as between almost each new profile to be measured. The calibration was performed at the temperature at which the actual measurements were planned and consisted of around 20 calibration points. This enabled us to relate at least two calibration curves to each boundary layer measurement, but also few preceding and succeeding calibration curves could be utilised without any deviation for velocities above 3 m/s. The turbulent boundary layer measurements at the lowest free stream velocities however made it necessary to calibrate down to even lower velocities. Therefore calibration points down to 0.5 m/s were acquired, which made it necessary that each calibration exceeded easily the time of the actual measurement, viz. more then one hour, in order to obtain a stable velocity at the desired temperature. Additionally the voltage under no flow conditions, E_0, was recorded before and after each calibration and measurement.

The MTL wind tunnel could maintain steady temperature conditions down to velocities of 2–3 m/s without any observable temperature change measured

[10]Such problems were for instance noted while experimenting with 1.27 micron wires. Similar observations have been reported by Hites (1997) among others.

[11]From Swedish: tung "heavy" + sten "stone". Its other common name is Wolfram. See Goya & Roman (2005) for an account on the traces for both names.

by a Pt-100 located downstream of the test section. However when further reducing the fan speed down to around 0.5 m/s, the temperature could not be kept constant anymore and deviations in the measured temperature could occur with a maximum of up to 0.3 K. A temperature compensation (as described in Örlü (2006)) was applied for these few low speed calibration points, however with no discernible effect on the diagnostic plot (to be introduced in section 5.2) and hence mean and second order terms.

Figure 7 shows three typical calibration curves used for measurements with a free stream velocity of about 12 m/s. Due to the extensive use of the same hot-wire the calibration curves display marginally no apparent drift for velocities above 2 m/s, whereas below this value a small drift can be observed (shown in the insert). The drift may be brought about due to the aging of the hot-wire, which is unlikely due to the long aging and operating time the hot-wire already experienced, drift in the electronic components over several hours, or - which seems to be most likely the case - due to the uncertainty of the pressure measurements at such low velocities. However, a small change in the voltage at zero velocity is present, indicating that not only an increased uncertainty of the pressure transducer, but that also a change in the hot-wire reading is present. During the calibration most of the target velocities were set by the fan speed, hence it was possible to check whether for the same set points of fan speeds the scatter in the pressure measurement or the hot-wire voltage was increased at the lowest speed. However, no conclusion of the drift could be drawn from the inspection of the calibration curves.

A typical mean streamwise velocity profile plotted in inner-scaled variables is show in figure 8, where additionally the (approximate) physical units are given on the opposite axes. The dashed lines indicate the lowest and highest measured velocity fluctuations and emphasize that, particularly in the case of unphysical calibration relations, the hot-wire has to be calibrated from 80 % below the lowest mean velocity measured in the viscous sublayer, up to at least 10 % above[12] the free stream velocity. A simple extension from a slightly higher velocity above the lowest measured velocity by means of any relation without any liable calibration points can easily alter the obtained near-wall quantities below 0.4 U_∞, i.e. the region around the near-wall peak in the streamwise turbulence intensity. This will be further discussed in section 5.2.

A calibration was deemed to be sufficiently stable if the change in free stream velocity before and after the boundary layer measurement was less than 0.5 %. Such a discrepancy did, however, not occur for the measurements presented here.

3.2b. *Data processing and evaluation.* For all of the calibrations and measurements presented here the hot-wire was operated in constant temperature mode

[12]Even higher values may be necessary in the case of higher free stream turbulence levels.

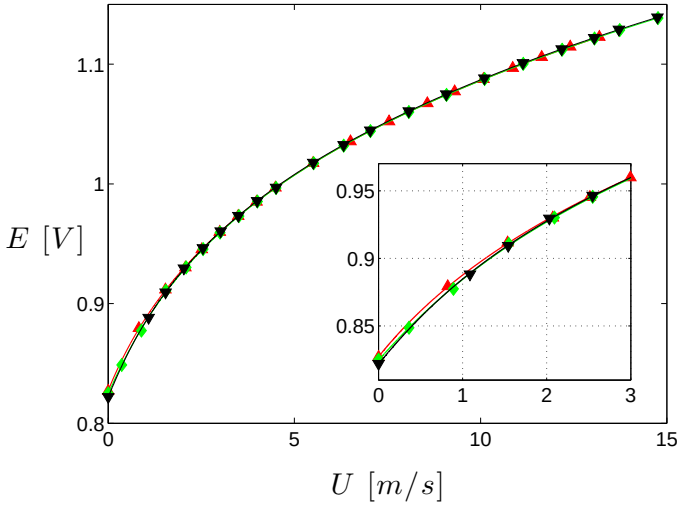

FIGURE 7. Three typical calibration curves for measurements with U_∞ around 12 m/s. The insert shows the low velocity region including the voltage output from the hot-wire anemometer at zero velocity. The solid lines represent a forth order polynomial fitted through the calibration points including the voltage at zero velocity.

at an resistance overheat of 80 %.[13] The hot-wire anemometer system used is a Dantec StreamLine 90N10 frame in conjunction with a 90C10 constant temperature anemometer module. An offset and gain was applied to the top of the bridge voltage in order to match the voltage range of the 16-bit A/D converter used. The square wave test gave a frequency responce of around 35 and 65 kHz for velocities of 0 and 40 m/s, respectively. In order to avoid any aliasing at the higher velocities an analog low pass filter with 30 kHz cut-off frequency was used prior to the data acquisition. The filter was chosen in such a way that the sampling frequency of 60 kHz would be of the order of the viscous time scale, in order to allow sufficiently resolved time signals for spectral analysis. This was for most of the experiments fulfilled (cf. table 3 in section 4, where the sample interval in viscous time units is given for all measurements).

The above settings were not altered throughout the course of the experiments. After completition of a calibration, the hot-wire was moved successively closer to the wall until the measured velocity was close to a fifth of the free

[13] Preliminary measurements with 50, 70, 80 and 150 % overheat in a related study showed that there is virtually no difference between the 80 and 150 % overheat measurements, whereas the nearwall peak in the streamwise turbulence intensity was underestimated with 50 and also slighlty with 70 % overheat.

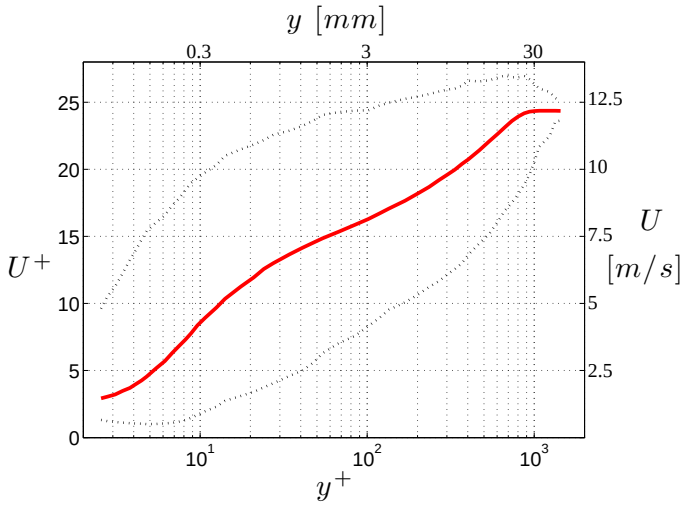

FIGURE 8. Mean streamwise velocity profile in inner law scaling for $Re_\theta = 2532$. Additionally the physical wall position and mean streamwise velocity in physical units is given (rounded off order to match the inner-scaled grid). The region of lowest and highest measured fluctuating velocities is indicated through the dashed line.

stream velocity, so that the near-wall peak in the streamwise turbulence intensity could be captured. From this position on, 50 to 60 measurement points, logarithmically spaced, were traversed and data was sampled for 30 to 45 seconds, giving outer-scaled boundary layer turnover times between 10 000 and 40 000, which ensured converged statistics up to the forth order moments.[14] During the course of the measurements, as during the calibration, the ambient pressure and temperature as well as the free stream velocity measured by means of the Prandtl tube was monitored and recorded. No drifts or jumps were observed for any of the presented measurements here.

3.3. *Determination of the physical wall position*

As simple and trivial the subject, the determination of the wall position, may sound, it remains an important and difficult task in laboratory experiments with consequences not directly obvious.

[14] Tests with sampling times up to 180 seconds indicated that there was marginally no apparent improvement in terms of convergence when increasing the sampling time from 30 to 180 seconds. In fact the mentioned turnover times are of the same order of other reported high quality turbulent boundary layer measurements and are higher than reported limits to achieve converged statistics for all higher order moments and other statistical quantities (see e.g. Klewicki & Falco 1990).

The optical measurement of the distance between the sensing probe, be it a hot-wire or a Pitot tube, can be obtained by means of a highly magnifying microscope. Such measurements are, however, mainly possible under no flow conditions, i.e. the sensing probe and its support is not exposed to any force acting upon it. Pitot tubes and hot-wire probes will, however, be exposed to a force falsifying the measured distance as soon as the flow acts on the probe stem and the traversing system, but also the surface on which the boundary layer is to be measured. Although these deflections are hardly seen they can be detected by online monitoring of the probe and surface position, by means of laser distance meters, as for instance used by Österlund (1999), focussed on the hot-wire (while the probe is not in operation) or the prongs. Another possibility is to use a cameras with a telephoto zoom lens able to resolve the prongs position with enough pixel resolution to detect displacements of the order of microns (depending on the boundary layer thickness). Other mechanical techniques are reported and have shown that it is almost unrealisable to avoid deflections of the probe, therefore, correction methods have to be used to compensate for these effects. Depending on the stiffness and geometry of the probe and its support as well as the the traversing arm or the slackness of connections the actual distance between the probe and wall surface has to be accounted for. Hites (1997) reports for instance in his well documented turbulent boundary layer experiments deflections up to 100 microns at a free stream velocity of 40 m/s.

The application of the mentioned physical measurement techniques does not guarantee the detection of the actual wall position (relative to the hot-wire position) under operating conditions as has been observed by the author. One reason for this dilemma is for instance the assumption that the surface on which the boundary layer evolves, e.g. a flat plate mounted in a wind-tunnel, is fixed. Depending on the pressure distribution underneath and on the flat plate (e.g. caused by the trailing flap angle) the plate may experience a lift force changing its surface position relative to the probe position. A system with few degrees of freedom is hence given depending on how the plate, the traversing, the probe and the measuring instrument is fixed in the tunnel and relative to each other. It is apparent that accuracies of the order of fractions of one viscous unit are needed to resolve the viscous sublayer. This becomes clear when considering figure 9, where the viscous length scale is computed as function of the free stream velocity with Reynolds number as a parameter. Here, as in most other experimental studies, the Reynolds number is increased by an increase in the free stream velocity, which causes a reduction in the viscous length scale and hence lets the sensing length of the hot-wire to appear longer and in the same time request higher accuracies in the determined wall position.

Despite the aforementioned reservations regarding the distance measurement at no flow condition, a method anticipated in figure 2, was tried to measure the absolute distance from the wall. Preliminary measurements showed,

however, that – as anticipated in the previous paragraph – the probe could further be moved "into" the flat plate if the distance measured at no-flow condition would been taken valid also for the case under flow conditions. Nevertheless the attempted measurements enabled us to check whether the traversing systems readings could be corrected for. Therefore the probe was traversed to wall-normal positions of 5, 35, 65, 95 and 125 mm from the wall and high resolution pictures were taken from the probe and the traversing arm at 0, 20, 30 and 40 m/s. The evaluation of these images showed that the probe deflects around 40, 70 and 85 micron away from the wall for 20, 30 and 40 m/s, respectively, compared to its position at no flow. More importantly, no change in these values could be observed for different heights of the traversing arm, which goes along with the observations made by Hites (1997) and means that the correct position can be retrieved by shifting the whole profile by means of common position correction methods.

During the processing of the measurements the final position was obtained by fitting the full mean streamwise velocity profile excluding the points affected by the presence of the wall to the composite profile of Chauhan *et al.* (2009). Different correction methods have been tested and discussed in Örlü (2009*b*) to which the reader is referred to and the above method has been selected

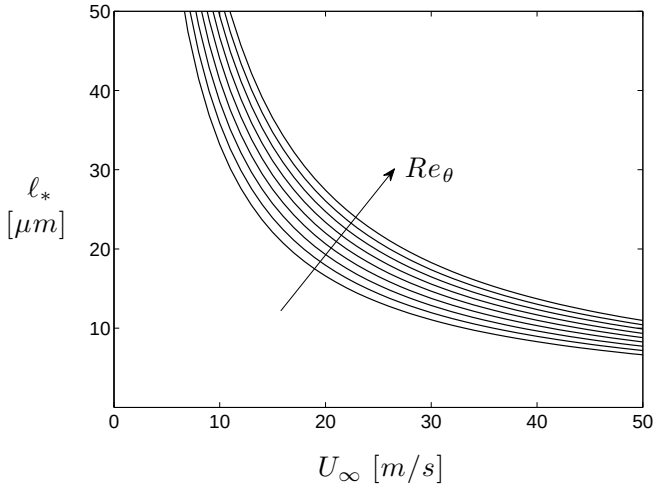

FIGURE 9. Variation in the viscous length scale, ℓ_*, as function of the free stream velocity, U_∞, for various Reynolds numbers. The functional relationship between all three quantities was computed using the Coles-Fernholz relation, eq. (13). (cf. section 5.1), with the constants established by Nagib *et al.* (2007). The Reynolds number shown represent $Re_\theta \times 10^{-3}$ =1, 2, 4, ..., 256.

for reasons of consistency due to its applicability to profiles with and without near-wall data.

4. Measurement matrix

The full range of experimental conditions and sensor geometries is given in table 3. The experiments are grouped according to their tripping configuration and their respective pressure gradient condition can be inferred from figure 2. The free stream velocity, U_∞, is given as the ensemble average of the measurement points in the free stream. The displacement and momentum thickness, δ^* and θ, are computed by means of a trapezoidal integration of the measurement points. The no-slip condition was used as the lower integration limit and the maximum velocity as the upper limit.[15] No additional points were interpolated between the wall and the first measured point nor was any predefined turbulent boundary layer profile fitted through the data and instead used to extract this quantity. This point should be emphasised here and in other studies, because the available literature is vague regarding this point and if the actual data is not provided it will be hard to assess the shape factor or other integral parameters, needed to check the state of the turbulent boundary layer, afterwards.

The boundary layer thickness, δ, is a theoretical construct indicating the wall distance where the velocity exactly equals the free stream velocity. Since it "can hardly be exactly defined" (Rotta 1950), it is often approximated by δ_{99} or $\delta_{99.5}$, however, in the present case, δ will be determined by fitting the composite profile of Chauhan *et al.* (2009) to the data. The Reynolds number based on the free stream velocity and momentum thickness as well as the friction velocity and the boundary layer thickness, the so called Kármán number (δ^+) or friction Reynolds number, are denoted as Re_θ and Re_τ, respectively. The length of the hot-wire is given in viscous-scaled units, $L^+ = L/\ell_*$, where L is the dimensional hot-wire length and ℓ_* represents the viscous length scale, and can hence directly be used to estimate the effect of spatial resolution. The sample interval is given in viscous time units, $\Delta t^+ = \Delta t u_\tau^2/\nu$, where $\Delta t = 1/f_s$ with f_s being the sampling frequency. Finally, total sampling length is expressed in outer-scaled boundary layer turnover times, TU_∞/δ, which according to Klewicki & Falco (1990) should exceed several thousands in order to obtain converged statistics for higher order moments.

[15] The linear extension of the profile towards the wall by use of the no-slip conditions is not an *ad hoc* solution, but rather a physical one whenever the first measurement point lies within the viscous sublayer. See also Örlü (2009*b*) for an account on the error of missing near-wall points on the obtained integral quantities.

Case	U_∞ [ms^{-1}]	Re_θ [-]	Re_τ [-]	δ [mm]	δ^* [mm]	θ [mm]	ℓ_* [μm]	L^+ [-]	Δt^+ [-]	TU_∞/δ [-]
T_A:1	19.93	4 408	1 827	35.8	4.59	3.34	19.6	24.0	0.66	16 700
T_A:2	24.98	5 449	2 237	35.7	4.48	3.30	15.9	29.5	0.99	21 000
T_A:3	26.41	5 806	2 370	35.9	4.50	3.32	15.2	31.0	1.10	22 050
T_A:4	29.93	6 429	2 709	36.5	4.38	3.24	13.5	34.9	1.39	24 600
T_A:5	39.97	8 745	3 663	38.0	4.40	3.30	10.4	45.4	2.34	31 600
T_A:6	40.14	8 792	3 706	38.2	4.41	3.31	10.3	45.5	2.36	31 500
T_B:1	11.52	2 331	1 007	32.1	4.32	3.08	31.9	14.7	0.25	10 500
T_B:2	12.06	2 457	1 057	32.4	4.34	3.10	30.7	15.3	0.27	11 150
T_B:3	16.77	3 511	1 438	33.1	4.42	3.18	23.0	20.0	0.48	15 200
T_B:4	17.40	3 628	1 477	32.8	4.40	3.17	22.2	21.1	0.51	15 900
T_B:5	20.05	4 079	1 619	31.7	4.27	3.09	19.6	24.0	0.66	19 000
T_B:6	28.07	5 451	2 132	30.7	4.04	2.95	14.4	32.7	1.22	27 500
T_B:7	29.97	5 855	2 323	31.4	4.05	2.97	13.5	34.7	1.38	28 600
T_B:8	40.16	7 561	2 934	30.3	3.86	2.86	10.3	45.5	2.37	39 800
T_C:1	12.04	2 532	1 105	33.7	4.45	3.17	30.5	15.4	0.27	16 100
T_C:2	16.67	3 551	1 478	33.9	4.47	3.21	22.9	20.5	0.48	22 150
T_C:3	17.13	3 640	1 497	33.5	4.45	3.20	22.4	21.0	0.50	23 000

TABLE 3. Experimental parameters for present hot-wire experiments. Explanation of column headings and abbreviations is given in section 4.

5. Results

5.1. *Skin friction determination*

The primary need for the oil-film interferometry technique was to provide a direct and independent (of any assumption regarding the scaling behaviour of the mean velocity profile) measure of the skin friction, in order to provide the friction velocity needed to scale the data as well as to obtain the skin friction relation for the present turbulent boundary layer needed to assess its quality and equilibrium state.

Following the outlined procedure in section 3.1 the skin friction and thereby the friction velocity was determined. In the following the individual results are expressed through a continuous relation so that the correct friction velocity is provided for the concrete profile measurement. Figure 10 depicts the individually obtained friction velocities, which were measured between 10 and 30 m/s at the exact same downstream position and on the same glass plug used during the hot-wire measurements.

Three to six runs were performed at each free stream velocity depicted in figure 10, but only those values are shown and finally used, which had sufficient convergence of the results, i.e. long enough sampling time in terms of taken pictures after reaching a steady state in terms of the free stream velocity and the temperature, and where the images showed no strong deformation of the fringes due to dust deposition. The results are shown in physical units and scaled by the free stream velocity against the free stream velocity itself and the unit Reynolds number, $Re_m = U_\infty/\nu$, respectively. The latter takes the ambient conditions, expressed in the free stream velocity and the kinematic

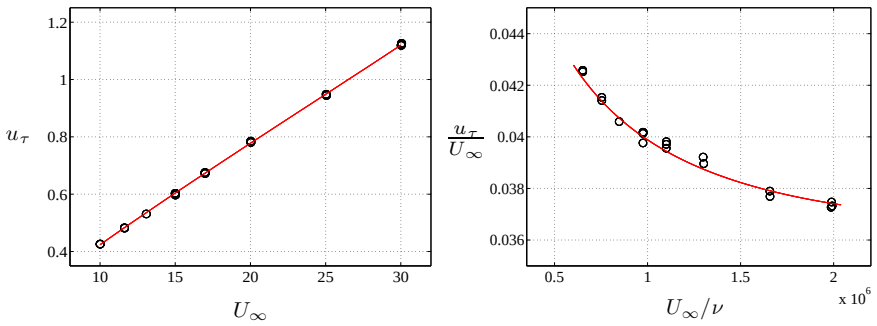

FIGURE 10. Friction velocity, u_τ, and skin friction coefficient, $u_\tau/U_\infty = \sqrt{c_f}/2$, obtained from the oil-film interferometry technique vs. the free stream velocity and unit Reynolds number, $Re_m = U_\infty/\nu$, respectively. ○: results obtained from each individual run, —: fit of equations (9) and (10) through the data.

eq.	c_1	c_2	c_3
(9)	5.94755e-02	3.71448e-02	-6.08526e-05
(10)	4.44913e-01	5.38322e-02	1.77447e-03

TABLE 4. Coefficients for equation (9) and (10) for the friction velocity obtained by oil film interferometry.

viscosity, into account and is the relation used to extract the friction velocity at the desired experimental condition. The data points are fitted through equations (9) and (10) and their constants are given in table 4.

$$u_\tau = c_1 + c_2 U_\infty + c_3 U_\infty^2. \tag{9}$$

$$\frac{u_\tau}{U_\infty} = c_1 + c_2 \ln\left(\frac{U_\infty}{\nu}\right) + c_3 \ln\left(\frac{U_\infty}{\nu}\right)^2. \tag{10}$$

The skin friction coefficient,

$$c_f = 2\left(\frac{u_\tau}{U_\infty}\right)^2, \tag{11}$$

as function of the Reynolds number based on the momentum thickness is shown in figure 11 together with a least squares fit through the Coles-Fernholz relation,

$$c_f = 2\left(\frac{1}{\kappa}\ln(Re_\theta) + C\right)^{-2}. \tag{12}$$

The number of points as well as the Reynolds number range for which the skin friction is determined may not be sufficient to compute the fitting parameters, i.e. the von Kármán constant as well as the additive constant, to the accuracy needed. However, they are found to be very close to the values proposed by Österlund (1999) and Nagib *et al.* (2007) as apparent from the dashed line indicating the Coles-Fernholz relation with the values put forward by the latter authors. The values proposed by the mentioned authors are given in the caption of the figure and were obtained by means of the direct and independent oil-film measurements over a wide range conducted in the MTL and NDF (National Diagnostic Facility, IIT Chicago) wind tunnels. The same relation with the classical parameters is shown through the dotted line, and indicates the clear disparity with the newly established and current values. Another way of presenting the skin friction is in terms of the free stream velocity in viscous units in a similar fashion as the previous relation,

$$U_\infty^+ = \frac{1}{\kappa}\ln(Re_\theta) + C\,, \tag{13}$$

given in figure 12. Here the same notation as in the previous figure is used and the constants are again given in the caption. It is important to note that the last two data points in both figures are not computed from the oil-film measurements, due to the limit in Reynolds number the study was focussed on, and are therefore not accounted for in the fit. The values were found by fitting the velocity profile to the composite profile by Chauhan *et al.* (2009) according to their suggested procedure.

5.2. *Near-wall and blockage effects and the diagnostic plot*

Before the integral turbulent boundary layer quantities and profiles obtained by means of hot-wire anemometry are evaluated and presented it is important to ensure that the measured velocity fluctuations near the wall are not influenced by the presence of the wall or by aerodynamic blockage due to interference between the probe and the wall. Having mentioned that the wall position is not known *a priori* another way of assessing the points which are affected may be helpful. Recalling that deflections of the probe position of a few wall units can easily occur and that the friction velocity is often not measured directly, the classical way to plot the mean velocity in inner scaling is highly dependent on both axes of the U^+ vs. y^+ plot. Hence inaccuracies in both coordinate

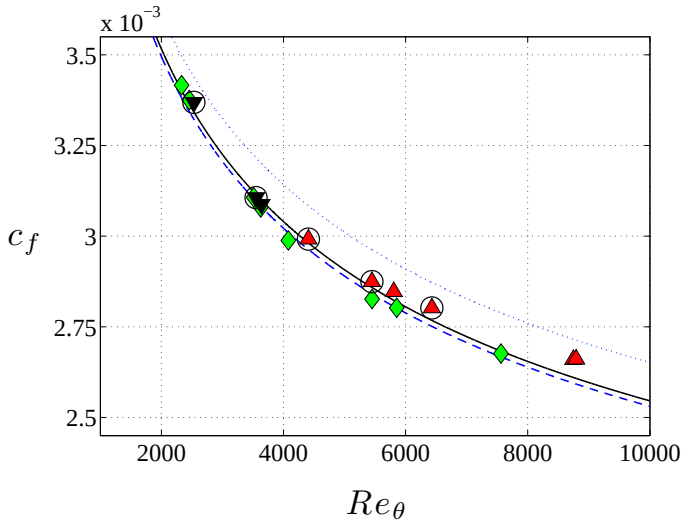

FIGURE 11. Skin friction coefficient, c_f, vs. Re_θ. Tripping configuration A: ▲, B: ♦ and C: ▼. Coles-Fernholz relation fitted through the present data (κ= 0.385 & C= 4.093): —, with coefficients determined by Nagib *et al.* (2007) (κ= 0.384 & C= 4.127): - -, and with classical values (κ= 0.41 & C= 5.0): · · · . For the encircled cases see section 5.4.

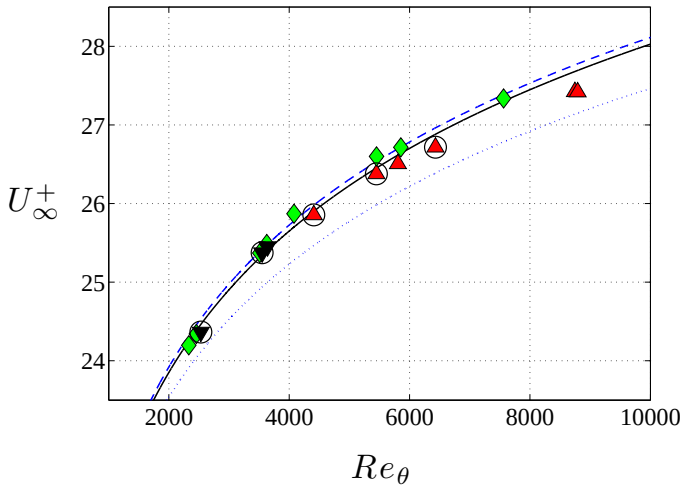

FIGURE 12. U_∞^+ vs. Re_θ. Tripping configuration A: ▲, B: ♦ and C: ▼. Coles-Fernholz relation fitted through the present data (κ= 0.382 & C= 3.958): —, with coefficients determined by Nagib *et al.* (2007) (κ= 0.384 & C= 4.127): - -, and with classical values (κ= 0.41 & C= 5.0): ···. For the encircled cases see section 5.4.

axes will affect the measured points. It would therefore be desirable to be free of both inaccuracies when selecting the points in which one can trust in.

One possible way is to plot the measured rms values against their local mean velocities where both are scaled by the free stream velocity. The so formed *diagnosic plot*, depicted in figure 13, was introduced by Alfredsson *et al.* (2009) and shows some interesting features. For wall bounded turbulent flows it is known that the rms of the fluctuating wall shear stress and hence the velocity fluctuations is a constant when scaled with its local mean value when approaching the wall (Alfredsson *et al.* 1988). Experiments, underpinned by DNS (Schlatter *et al.* 2009*b*), indicate that this constant ratio prevails also away from the wall for several wall units. Consequently, profiles of U/U_∞ vs. u'/U_∞ for different Reynolds numbers should fall on top of each other when approaching the wall as long as the measured values are not affected by the presence of the wall or spatial resolution issues, and the Reynolds numbers are high enough to establish an overlap region.[16]

[16]Comparing available DNS (Tsukahara *et al.* 2005; Hoyas & Jiménez 2006; Schlatter *et al.* 2009*b*) and LES (Schlatter *et al.* 2009*a*) data sets, it can be inferred, that the increase in the slope value is substantially weaker for ZPG TBL flows, than for internal flows. So, for instance, increases u'/U in the limit of $y^+ \to 0$ for channel flows from 0.32 to 0.43 and for ZPG TBL flows from 0.39 to 0.43 when Re_τ increases from 100 to 2000, respectively.

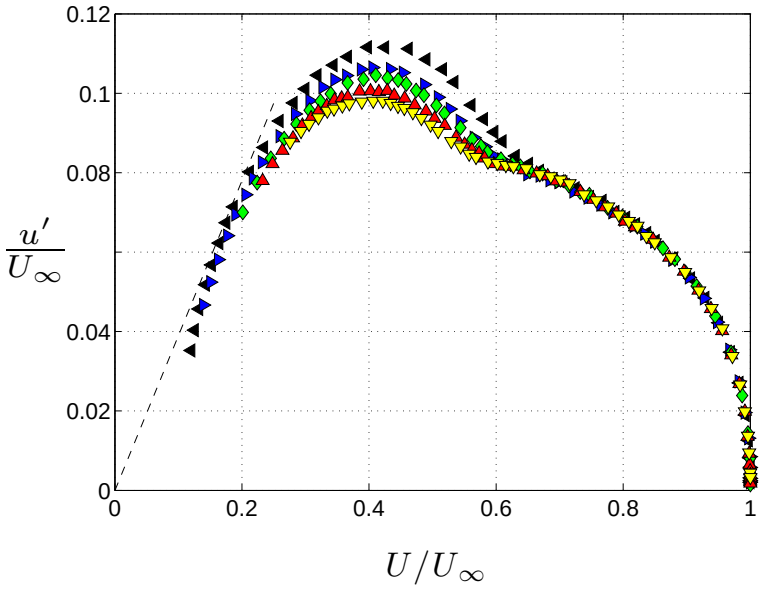

FIGURE 13. Mean streamwise velocity and streamwise turbulence intensity shown in the diagnostic plot for Re_θ= 2532 (◀), 3551 (▶), 4408 (♦), 5449 (▲) and 6429 (▼). - - -: tangent to the near-wall data with a slope of 0.39. The measured points below this line for $U/U_\infty \lesssim 0.15$ are clearly effected by the wall.

A tangent to the near wall data points in figure 13 with the slope of 0.39 indicates, that the data points below the tangent are increasingly affected due to the presence of the wall. As expected the mean velocity is shifted towards higher values, whereas the rms value, due to the changed velocity sensitivity at the new higher mean velocity, is increasingly reduced. Note that spatial resolution for these points is not the cause for the reduced rms values, due to the sufficiently short wire length for these lower Reynolds numbers. Instead the profiles for higher Reynolds numbers, which do not come as close to the wall as their low Reynolds number counterparts, have spatial attenuation problems, which is apparent due to their reduced values at around $U/U_\infty = 0.2$. Such problems do not appear as clearly in the conventional mean or rms plots, due to their dependence on the friction velocity and absolute wall position.

Another interesting feature of the diagnostic plot is the collapse of the profiles for $U/U_\infty > 0.6$, which exposes the fully developed nature of the various profiles and that the free stream velocity is an appropriate velocity scale for the outer region of turbulent boundary layers, at least for the Reynolds numbers considered here. In turn the diagnostic plot can be used to collapse data in the

viscous sublayer and outer region in the same plot for diagnostic purposes. Only within the buffer and overlap region a Reynolds number trend (its quantivative trend is here amplified due to spatial resolution effects) is apparent, as may be expected due to the scaling of the streamwise rms profile.

5.3. *Quality assessment of ZPG TBL*

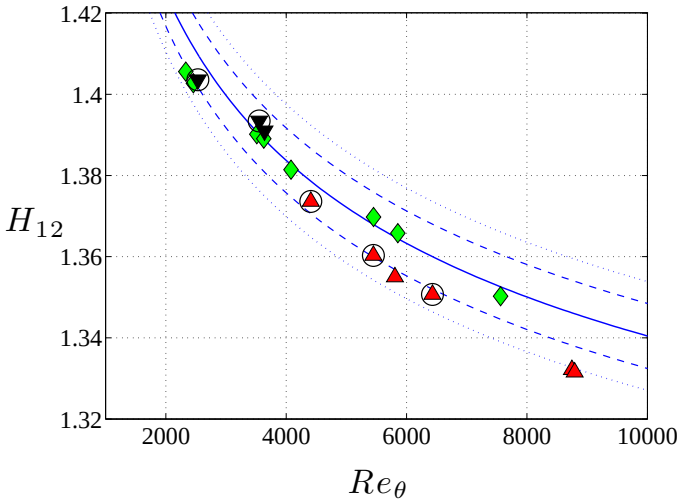

FIGURE 14. Shape factor, H_{12}, vs. Re_θ. Tripping configuration A: ▲, B: ♦ and C: ▼. Integration of composite profile (Chauhan *et al.* 2009), H_{num},: —, $H_{num} \pm 0.008$: - -, $H_{num} \pm 1\ \%\ H_{num}$: ·.

The importance of the skin friction coefficient as one of the criteria to judge the equilibrium state of the flow has already been shown. What remains is the shape factor and wake parameter, which are given in the following. Especially the shape factor has been used as an indicator and shown to be a sensitive parameter which at the same time is considered a robust indicator of the state of the flow. Since it is computed from the dimensional mean streamwise velocity profile, it does not involve the skin friction coefficient. Therefore the scatter between various experiments in equlibrium state can not be related to the uncertainties emerging from the determination of the skin friction, which makes the shape factor to a fairly unbiased parameter, compared to the skin friction or wake parameter. Nevertheless also here different ways exist to compute the shape factor, some of which have been mentioned in section 4.

The shape factor is the ratio of the displacement to momentum thickness, computed as indicated in section 4, and is given in figure 14 together with the analytical function based on the integration of the composite profile by

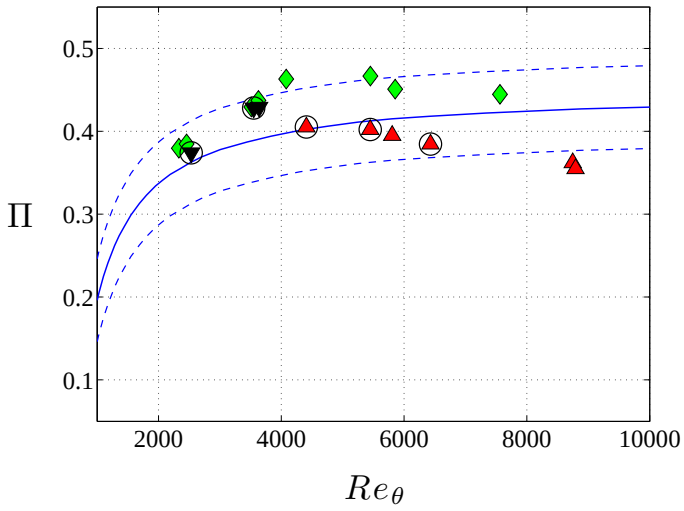

FIGURE 15. Wake parameter, Π, vs. Re_θ obtained using the composite profile (Chauhan *et al.* 2009). Tripping configuration A: ▲, B: ♦ and C: ▼. Integration of composite profile (Chauhan *et al.* 2009), Π_{num},: —, $\Pi_{num} \pm 0.05$: - -.

Chauhan *et al.* (2009). Also given are the tolerances defined in the same paper believed to distinguish between equilibrium and non equilibrium flows. The wake parameter computed by fitting the data to the composite profile and shown in figure 15 was obtained together with the boundary layer thickness from the composite profile and is given together with the analytical curve based on the same analytical expression.

The independent and direct measured skin friction as well as the shape factor and wake parameter have shown that most of the obtained profiles fulfill all equilibrium criteria for zero pressure-gradient turbulent boundary layers as defined by Chauhan *et al.* (2009). Only few cases fulfill them partially with a very weak deviation from the allowable tolerances. Note, however, that these deviations are comparably small when compared to other equilibrium data sets.

5.4. *Statistical quantities*

In what follows five selected turbulent boundary layer profiles will be presented and discussed, ranging from $Re_\theta = 2500$ to 6500. These profiles have been selected in such a way that they were taken at a free stream velocity and with a tripping configuration that has been found to give nominally zero pressure-gradient and fulfills in the same time the shape factor and wake parameter critieria, so that they faithfully represent equilibrium zero pressure-gradient

turbulent boundary layers (see the encircled cases in figures 11, 12, 14, and 15).

5.4a. *Streamwise mean velocity profiles.* The most studied quantity of turbulent boundary layers, and in the same time the most controversial one, is without doubt the streamwise mean velocity profile. Figure 16 shows this distribution for the five selected Reynolds number cases in classical inner-law scaling together with the law of the wall and the log law with the newly established Reynolds number independent constants under zero pressure-gradient conditions (Nagib *et al.* 2007). The inner-law scaling makes the data points within the viscous sublayer, buffer layer and overlap or logarithmic region for all Reynolds number cases as expected fall onto a single line. The classical log law constants could as well be used and they would produce the same seemingly well description of the data points in the log region. The reason for this is twofold. Although the Reynolds numbers discussed here are high to start a scale separation of inner and outer scales, they are not sufficiently high to establish a long enough overlap region in order to favour one mean velocity description (including its constants or variables) above another one. Furthermore, also the region in which the overlap is situated, and hence where the mean velocity

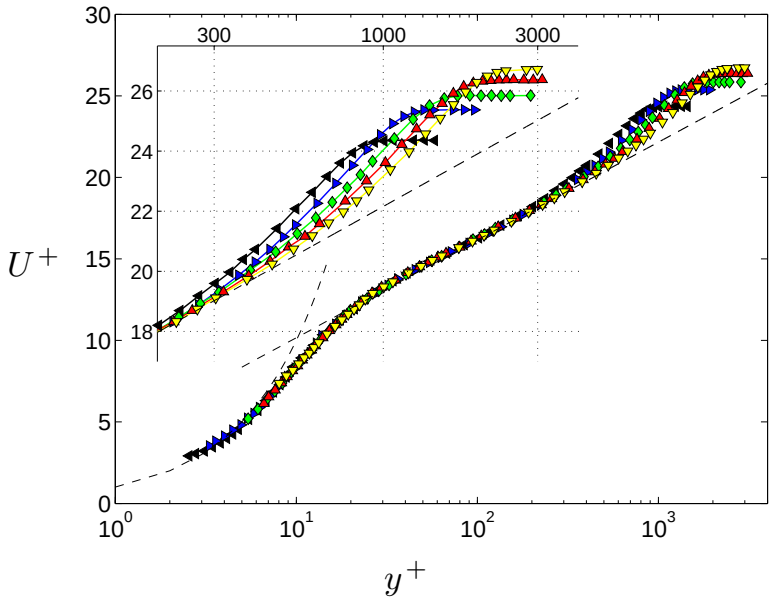

FIGURE 16. Profiles of the mean streamwise velocity in inner-law scaling for the same data and symbols as in figure 13. **- -**: $U^+=y^+$ and $U^+=1/\kappa \ln y^+ + B$, with $\kappa=0.384$ and $B=4.17$.

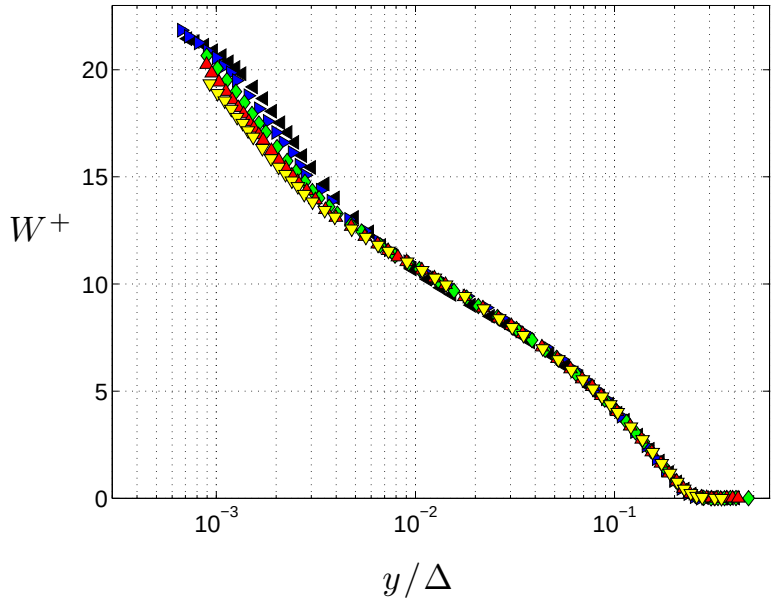

FIGURE 17. Profiles of the mean streamwise velocity in outer-law scaling for the same data and symbols as in figure 13.

description is sought for is not trivial. The classical overlap region starts quite early, viz. around $y^+ = 30$–50 (Pope 2000) and utilising the classical values for the slope would lead to a seemingly longer overlap region incorporating the observed overshoot centred around 50 wall units in our presented data. This overshoot is much more enhanced for high Reynolds number experiments, as in those presented by Hites (1997) or Österlund (1999), due to the "valley" relative to the log law between the overshoot and the beginning of the wake region. This explains why different Kármán constants can easily be obtained depending on the limits of the overlap region.

Another important effect of the chosen (the term "determined" can hardly be used at such small extents of the overlap region) log law constants is apparent from the insert in the same figure, where the wake region is enlarged. As can be anticipated the log law constants exert a strong effect on the strength of the wake and thereby the wake parameter itself, which in turn is one criterion used to assess equilibrium conditions.[17] The lower the Reynolds number becomes, the smaller the overlap region and the larger the uncertainty in the determined

[17]This was already observed by Spalart (1988), who states: "Very accurate measurements or simulations over a wide Reynolds-number range, as well as a strong consensus on the value of κ (at least two significant digits), will be needed before definitive results are obtained for [Π]."

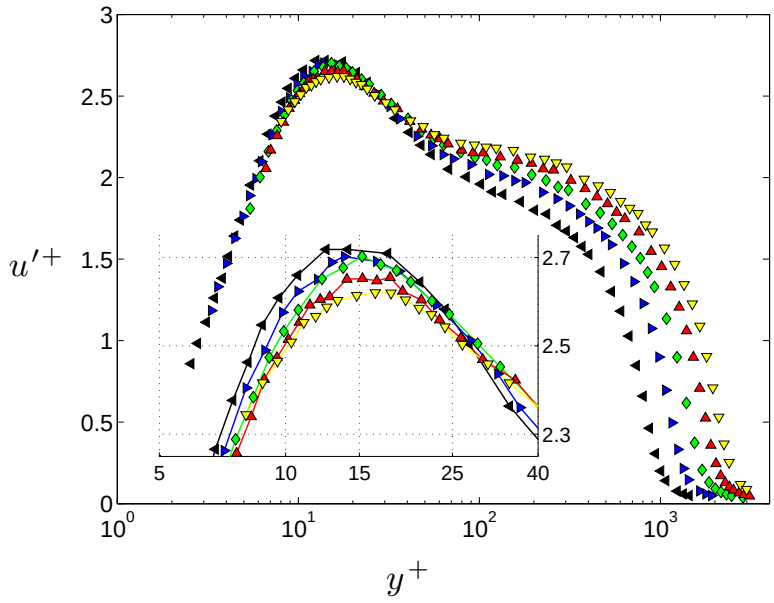

FIGURE 18. Profiles of the streamwise turbulence instensity in inner-law scaling for the same data and symbols as in figure 13.

wake parameter becomes. For the sake of consistency the newly established log law constant (Österlund *et al.* 2000; Nagib *et al.* 2007) were used, which agree fairly well with the values extracted from the direct and independent oil film interferometry measurements presented in section 5.1.

Carrying forward the classical understanding, figure 17 depicts the mean streamwise velocity deficit, $W^+ = U^+_\infty - U^+$, profile in outer-law scaling, i.e. scaled by the Rotta-Clauser length-scale, $\Delta = U^+_\infty \delta^*$. As expected, the various profiles collapse nicely on a single line for the outer region. It is worth noting that although a perfect overlap is not as often observed in the literature as for the inner-scaled mean profiles, here the agreement between various profiles is seemingly as good as the inner-scaled profile. One possible explanation for this is, that only profiles, fulfilling all equilibrium criteria, are shown. It was demonstrated by Chauhan *et al.* (2009) that only when (their) equilibrium criteria were fulfilled an acceptable similarity in the outer region appeared. Hence the equilibrium state of the presented data is once more demonstrated.

5.4b. *Streamwise turbulence intensity plots.* A simple inner and outer scaling as in the case for the mean velocity profile, is generally not believed to work for the streamwise turbulence intensity. Although here a mixed scaling, i.e. the geometrical mean of the friction and free stream velocity, has been favoured by

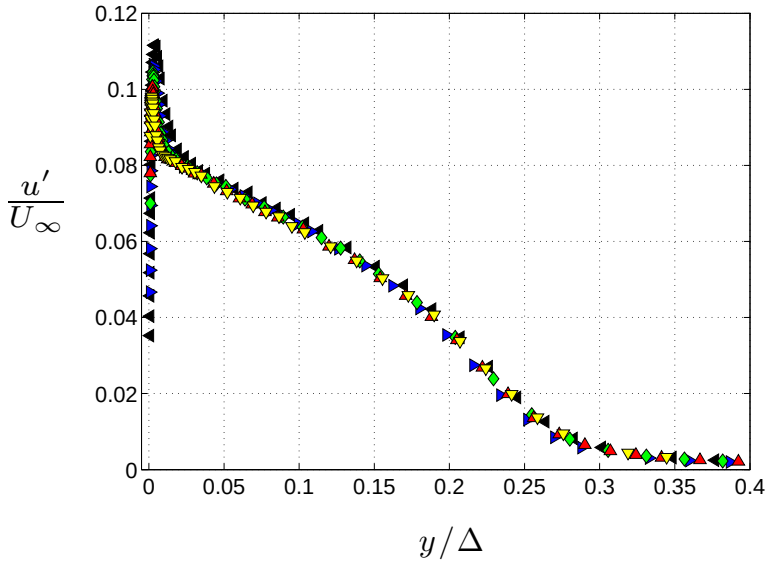

FIGURE 19. Profiles of the streamwise turbulence instensity in outer-law scaling for the same data and symbols as in figure 13.

DeGraaff & Eaton (2000) and shown to be able to describe the near-wall region up to $y^+ = 30$ (Marusic & Kunkel 2003), figure 18 shows the traditional (inner-scaled) streamwise turbulence intensity profile. The buffer region is enlarged in the insert, which emphasises that spatial resolution is a problem, at least around the near-wall peak. For a more thorough investigation regarding spatial resolution effects the reader is referred to Örlü (2009*a*). The outer-scaled turbulence intensity, shown in figure 19, is less controversial and shows a better collaps of the data, albeit of smaller extent and of less quality than for its mean quantity. It is important to note that the outer-scaled profiles for the mean and streamwise turbulence intensity as well as the coming higher moments can also be plotted against y/δ. Here however, for the limited Reynolds number range, qualitative differences were hardly encounterable between the scaling by δ or Δ.

One difference between free shear flows and wall-bounded flows is that for the former it is quite natural to expect self-similarity for increasing order of the moments with increasing development lengths, i.e. while the mean streamwise velocity profile is found to be self-similar at a certain downstream location, the turbulence intensity reaches a self-similar state at considerably larger downstream locations. For wall-bounded flows on the other hand, such a distinctions is hardly encountered when reviewing the literature. Nevertheless it may serve

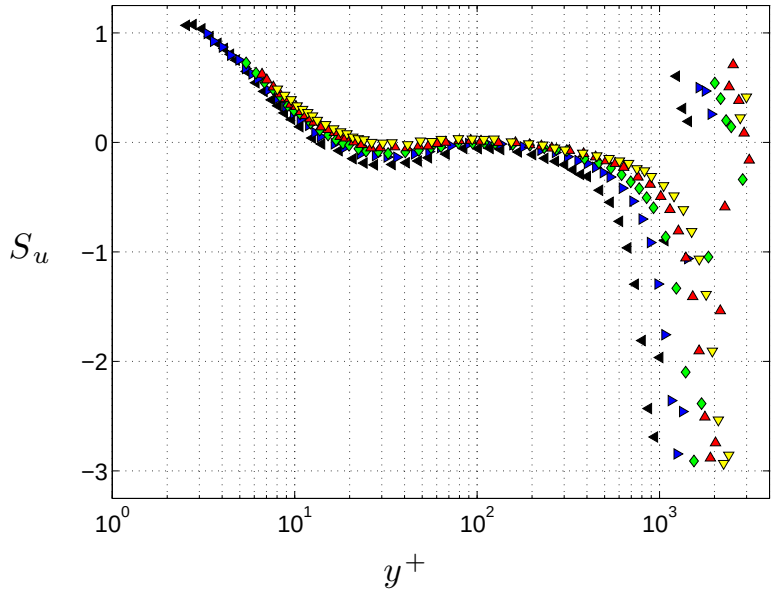

FIGURE 20. Profiles of the streamwise fluctuations skewness factor in inner-law scaling for the same data and symbols as in figure 13.

as an explanation why, despite excellent collapse in mean profiles, the higher order moments show a less convincing collapse of the data. This view can further be reasoned when noting that the collaps of the data in the outer region is improved when neglecting the two lowest Reynolds numbers shown in figure 19.

5.4c. *Higher order moments.* In the following the skewness and flatness factors in inner and outer-law scaling are shown in figures 20–23, clearly demonstrating the non-Gaussian character of the turbulent boundary layer. Especially in the near-wall region and the highly intermittent region the skewness and flatness factor strongly deviates from a Gaussian value. Whereas the region between the wall and the near-wall peak in the streamwise turbulence intensity is characterised by a positive skewness, the region close but below the mean boundary layer thickness highly negative. While the former implies that large positive velocity fluctuations are more frequent than low ones, due to the presence of the wall, the latter encounters more frequent low speed fluctuations associated with the sharp intermittent interface between the rotational boundary layer and the irrotational free stream. Analogous to the streamwise turbulence intensity distribution the outer-law scaled skewness factor distribution exhibits overlap of the profiles to an extent that is even slightly better. This may, however, be an

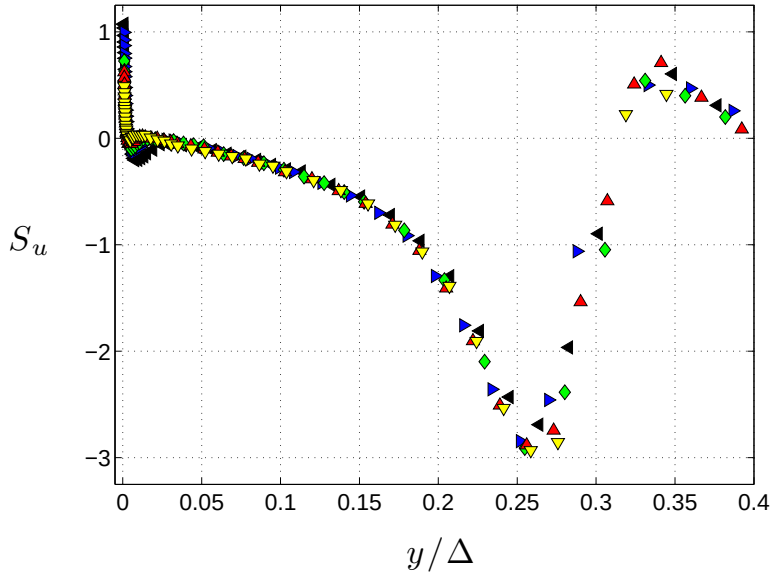

FIGURE 21. Profiles of the streamwise fluctuations skewness factor in outer-law scaling for the same data and symbols as in figure 13.

artifact of spatial resolution, because both quantities are affected by it in different directions and the skewness factor is formed as their quotient. This also inhibits the study of Reynolds number dependencies in the near-wall region, where high turbulence intensities are encountered, because spatial attenuation is known to mask, but also "masquerade", Reynolds number effects, as for instance demonstrated by Johansson & Alfredsson (1983) and further discussed in Örlü (2009*a*). The smoothness of the higher order profiles indicates also that the sampling time, shown in table 3, is sufficient to obtain converged statistics.

6. Summary

A review on available low Reynolds number turbulent boundary layer experiments has revealed that there is a scarcity of data fulfilling equilibrium zero pressure-gradient conditions. Furthermore the skin friction is in most of the reported cases been found to be determined from the mean velocity profile and the assumption on the validity of certain "universal" log law constants, which are not self-consistent, i.e. they do not agree with the momentum equation in pipe flows, nor with direct and independent measured values. Since direct numerical simulations are reaching for Reynolds numbers at which a scale

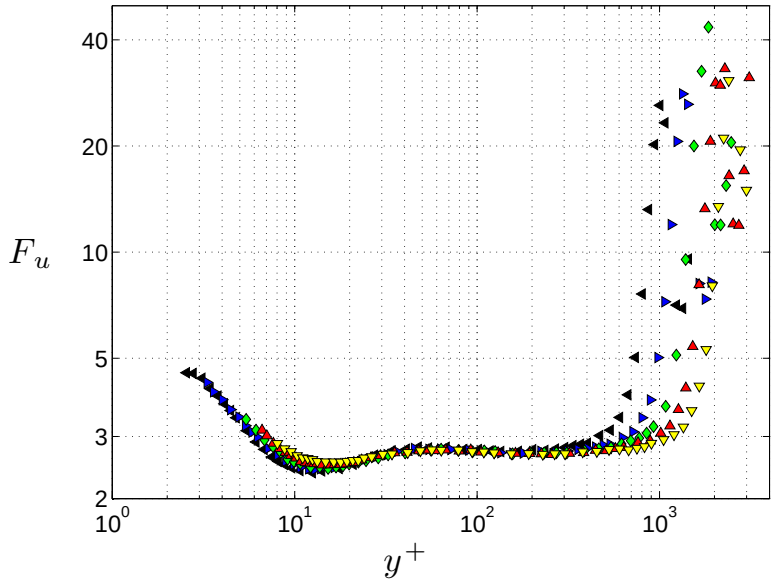

FIGURE 22. Profiles of the streamwise fluctuations flatness factor in inner-law scaling for the same data and symbols as in figure 13.

separation starts to occur, the need for quality zero pressure-gradient equilibrium turbulent boundary layer experiments with directly and independently obtained friction velocities emerge.

The present paper reports on a new set of experiments, which fulfill the above requirements and document the experimental set-up, measurement technique, as well as the methods employed to extract the statistical and integral quantities. The presented quantities therefore enable an independent and objective assessment of the quality of the zero pressure-gradient equilibrium turbulent boundary layer conditions.

Acknowledgment

The present work was conducted under the supervision of Dr. Jens H. M. Fransson and Prof. P. Henrik Alfredsson, and the complementary measurements at the 3.625 m station were performed together with Thomas Kurian. The author expresses his gratitude to all of them.

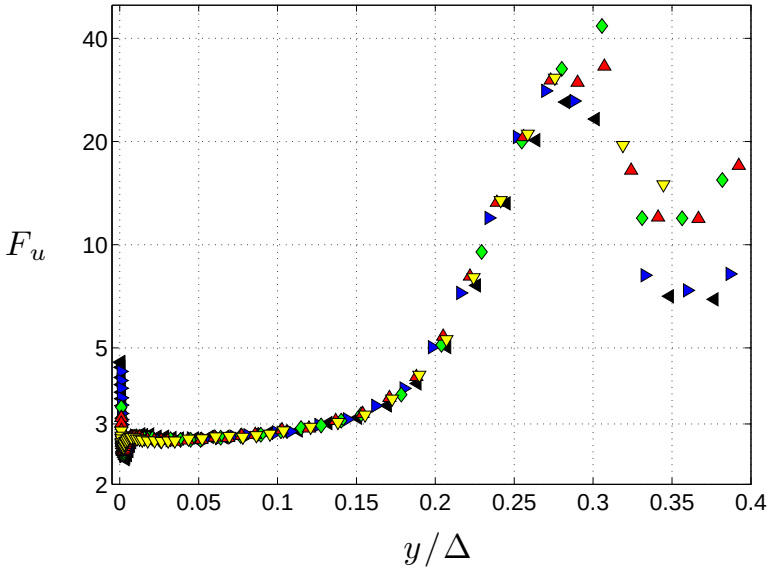

FIGURE 23. Profiles of the streamwise fluctuations flatness factor in outer-law scaling for the same data and symbols as in figure 13.

References

Ahn, S. 1986 Some unsteady features of turbulent boundary layers. *M. Sc. Thesis, Dept. of Aerospace and Ocean Engrg. Virginia Tech., USA*.

Alfredsson, P. H., Johansson, A. V., Haritonidis, J. & Eckelmann, H. 1988 The fluctuating wall-shear stress and the velocity field in the viscous sublayer. *Phys. Fluids* **31**, 1026–1033.

Alfredsson, P. H., Örlü, R., Kurian, T., Fransson, J. H. M., Segalini, A., Rüedi, J.-D. & Talamelli, A. 2009 The diagnostic plot - a new way to appraise turbulent boundary layer data. *Proc. 12th European Turbulence Conference, Marburg, Germany*.

Andreopoulos, J., Durst, F., Zaric, Z. & Jovanovic, J. 1984 Influence of Reynolds number on characteristics of turbulent wall boundary layers. *Exp. Fluids* **2**, 7–16.

Barenblatt, G. I. & Chorin, A. 1998 Scaling of the intermediate region in wall-bounded turbulence: The power law. *Phys. Fluids* **10**, 1043–1044.

Barr, G. 1931 A monograph of viscometry. *Oxford University Press*.

Brown, J. & Naughton, J. 1999 The thin-oil-film equation. *NASA TM-1999-208767*.

Bruun, H. H. 1995 Hot-wire anemometry: Principles and signal analysis. *Oxford University Press Inc., New York, USA*.

Buschmann, M. H. 2000 Power law or logarithmic law?–A data analysis for zero pressure gradient turbulent boundary layers with low Re. *J. Therm. Sci.* **9**, 23–29.

Buschmann, M. H. & Gad-el-Hak, M. 2006 Recent developments in scaling of wall-bounded flows. *Prog. Aero. Sci.* **42**, 419–467.

Chauhan, K. A., Monkewitz, P. A. & Nagib, H. M. 2009 Criteria for assessing experiments in zero pressure gradient boundary layers. *Fluid Dyn. Res.* **41**, 021404.

Coles, D. E. 1962 The turbulent boundary layer in a compressible fluid. *Rand. Rep. R-403-PR*.

Comte-Bellot, G., Strohl, A. & Alcaraz, E. 1971 On aerodynamic disturbances caused by single hot-wire probes. *J. Appl. Mech.* **93**, 767–774.

DeGraaff, D. B. 1999 Reynolds number scaling of the turbulent boundary layer on

a flat plate and on swept and unswept bumps. *Ph. D. thesis, Stanford University, USA*.

DeGraaff, D. B. & Eaton, J. 2000 Reynolds-number scaling of the flat-plate turbulent boundary layer. *J. Fluid Mech.* **422**, 319–346.

Djenidi, L. & Antonia, R. A. 1993 LDA measurements in low Reynolds number turbulent boundary layer. *Exp. Fluids* **14**, 280–288.

Erm, L. P. 1988 Low-Reynolds-number turbulent boundary layers. *Ph. D. thesis, University of Melbourne, Australia*.

Erm, L. P. & Joubert, P. 1991 Low-Reynolds-number turbulent boundary layers. *J. Fluid Mech.* **230**, 1–44.

Fernholz, H. H. & Finley, P. 1996 The incompressible zero-pressure-gradient turbulent boundary layer: An assessment of the data. *Prog. Aero. Sci.* **32**, 245–311.

Fernholz, H. H., Janke, G., Schober, M. & Wagner, P. 1996 New developments and applications of skin-friction measuring techniques. *Meas. Sci. Tech.* **7**, 1396–1409.

Ferrante, A. & Elghobashi, S. E. 2005 Reynolds number effect on drag reduction in a microbubble-laden spatially developing turbulent boundary layer. *J. Fluid Mech.* **543**, 93–106.

Goya, P. & Roman, P. 2005 Wolfram vs. tungsten. *Chemistry international* **27**, 26–28.

Head, M. & Bandyopadhyay, P. 1981 New aspects of turbulent boundary-layer structure. *J. Fluid Mech.* **107**, 297–338.

Hites, M. H. 1997 Scaling of high-Reynolds number turbulent boundary layers in the National Diagnostic Facility. *Ph. D. thesis, Illinois Institute of Technology, USA*.

Hoyas, S. & Jiménez, J. 2006 Scaling of the velocity fluctuations in turbulent channels up to Re=2003. *Phys. Fluids* **18**, 011702.

Hutchins, N. & Marusic, I. 2007 Large-scale influences in near-wall turbulence. *Phil. Trans. R. Soc. A* **365**, 647–664.

Janke, G. 1993 Über die Grundlagen und einige Anwendungen der Ölfilm-Interferometrie zur Messung von Wandreibungsfeldern in Luftströmungen. *Ph. D. thesis, Technical University Berlin, Germany*.

Johansson, A. V. & Alfredsson, P. H. 1983 Effects of imperfect spatial resolution on measurements of wall-bounded turbulent shear flows. *J. Fluid Mech.* **137**, 409–421.

Karlsson, R. I. 1980 Studies of skin friction in turbulent boundary layers on smooth and rough walls. *Ph. D. thesis, Chalmers University of Technology, Göteborg, Sweden*.

Karlsson, R. I. & Ramnefors, M. 1978 Streamwise turbulence structure in a flat-plate turbulent boundary layer. *Internal Rep. 78/14, Chalmers University of Technology, Göteborg, Sweden*.

Khujadze, G. 2005 DNS and Lie group analysis of zero pressure gradient turbulent boundary layer flow. *Ph. D. thesis, Technical University Darmstadt, Germany*.

Khujadze, G. & Oberlack, M. 2004 DNS and scaling laws from new symmetry

groups of ZPG turbulent boundary layer flow. *Theoret. Comput. Fluid Dynamics* **18**, 391–411.

Klebanoff, P. S. & Diehl, Z. 1954 Some features of artificially thickened fully developed turbulent boundary layers with zero pressure gradient. *NACA Tech. Rep. 1110*.

Klewicki, J. C. & Falco, R. 1990 On accurately measuring statistics associated with small-scale structure in turbulent boundary layers using hot-wire probes. *J. Fluid Mech.* **219**, 119–142.

Knobloch, K. 2008 Skalierungen und Zweipunkt-Geschwindigkeitskorrelationen in turbulenten Grenzschichten bei großen Reynoldszahlen. *Ph. D. thesis, Technical University Berlin, Germany*.

Knobloch, K. & Fernholz, H. H. 2004 Statistics, correlations, and scaling in a turbulent boundary layer at $\mathrm{Re}_{\delta_2} \leqslant 1.15 \times 10^5$. *IUTAM Symposium on Reynolds Number Scaling in Turbulent Flow. A. J. Smiths (Ed.), Kluwer Academic Publisher*, pp. 11–16.

Li, J. D., McKeon, B., Jiang, W., Morrison, J. F. & Smits, A. J. 2004 The response of hot wires in high Reynolds-number turbulent pipe flow. *Meas. Sci. Tech.* **15**, 789–798.

Ligrani, P. & Bradshaw, P. 1987 Spatial resolution and measurement of turbulence in the viscous sublayer using subminiature hot-wire probes. *Exp. Fluids* **5**, 407–417.

Lindgren, B. & Johansson, A. V. 2002 Evaluation of the flow quality in the MTL wind-tunnel. *Tech. Rep. TRITA-MEK 2002:13, Royal Institute of Technology, Stockholm, Sweden*.

Lomas, C. G. 1986 Fundamentals of hot wire anemometry. *Cambridge University Press*.

Marusic, I. & Kunkel, G. J. 2003 Streamwise turbulence intensity formulation for flat-plate boundary layers. *Phys. Fluids* **15**, 2461–2464.

Mochizuki, S. & Nieuwstadt, F. T. M. 1996 Reynolds-number-dependence of the maximum in the streamwise velocity fluctuations in wall turbulence. *Exp. Fluids* **21**, 218–226.

Monkewitz, P. A., Chauhan, K. A. & Nagib, H. M. 2008 Comparison of mean flow similarity laws in zero pressure gradient turbulent boundary layers. *Phys. Fluids* **20**, 105102.

Murlis, J., Tsai, H. & Bradshaw, P. 1982 The structure of turbulent boundary layers at low Reynolds numbers. *J. Fluid Mech.* **122**, 13–56.

Nagib, H. M. & Chauhan, K. A. 2008 Variations of von Kármán coefficient in canonical flows. *Phys. Fluids* **20**, 101518.

Nagib, H. M., Chauhan, K. A. & Monkewitz, P. A. 2005 Scaling of high Reynolds number turbulent boundary layers revisited. *AIAA Paper 2005-4810*.

Nagib, H. M., Chauhan, K. A. & Monkewitz, P. A. 2007 Approach to an asymptotic state for zero pressure gradient turbulent boundary layers. *Phil. Trans. R. Soc. A* **365**, 755–770.

Nagib, H. M., Christophorou, C. & Monkewitz, P. A. 2004*a* High Reynolds

number turbulent boundary layers subjected to various pressure-gradient conditions. *IUTAM Symposium on one hundred years of boundary layer research, G. E. A. Meier and K. R. Sreenivasan (Eds.), Göttingen, Germany*, pp. 383–394.

Nagib, H. M., Christophorou, C., Rüedi, J.-D., Monkewitz, P. A. & Österlund, J. M. 2004*b* Can we ever rely on results from wall-bounded turbulent flows without direct measurements of wall shear stress? *AIAA Paper 2004-2392*.

Naguib, A. N. 1992 Inner- and outer-layer effects on the dynamics of a turbulent boundary layer. *Ph. D. thesis, Illinois Institute of Technology, USA*.

Naughton, J. & Sheplak, M. 2002 Modern developments in shear-stress measurement. *Prog. Aero. Sci.* **38**, 515–570.

Ng, H., Marusic, I., Monty, J. P., Hutchins, N. & Chong, M. S. 2007 Oil film interferometry in high Reynolds number turbulent boundary layers. *16th Australian Fluid Mechanics Conference*.

Örlü, R. 2006 Experimental study of passive scalar mixing in swirling jet flows. *TeknL thesis, Royal Institute of Technology, Stockholm, Sweden, TRITA-MEK 2006:11*.

Örlü, R. 2009*a* On spatial resolution issues on mean quantities using hot-wire anemometry. *Ph. D. thesis, Royal Institute of Technology, Stockholm, Paper 6*.

Örlü, R. 2009*b* On the determination of the wall position in wall-bounded turbulent flows. *Ph. D. thesis, Royal Institute of Technology, Stockholm, Paper 5*.

Osaka, H., Kameda, T. & Mochizuki, S. 1998 Re-examination of the Reynolds-number-effect on the mean flow quantities in a smooth wall turbulent turbulent boundary layer. *JSME International Journal Series B* **41**, 123–129.

Österlund, J. M. 1999 Experimental studies of zero pressure-gradient turbulent boundary layer flow. *Ph. D. thesis, Royal Institute of Technology, Stockholm, Sweden*.

Österlund, J. M., Johansson, A. V., Nagib, H. M. & Hites, M. H. 2000 A note on the overlap region in turbulent boundary layers. *Phys. Fluids* **12**, 1–4.

Perry, A. E. & Li, J. D. 1990 Experimental support for the attached-eddy hypothesis in zero-pressure-gradient turbulent boundary layers. *J. Fluid Mech.* **218**, 405–438.

Pope, S. 2000 Turbulent flows. *Cambridge University Press*.

Purtell, L., Klebanoff, P. S. & Buckley, F. 1981 Turbulent boundary layer at low Reynolds number. *Phys. Fluids* **25**, 802–811.

Rotta, J. C. 1950 Über die Theorie der turbulenten Grenzschichten. *Mitteilungen aus dem Max-Planck-Instritut für Strömungsforschung (Göttingen)* **1**.

Rüedi, J.-D. 2009 (personal communication).

Rüedi, J.-D., Nagib, H. M., Österlund, J. M. & Monkewitz, P. A. 2003 Evaluation of three techniques for wall-shear measurements in three-dimensional flows. *Exp. Fluids* **35**, 389–396.

Sandborn, V. 1972 Resistance temperature transducers. *Metrology Press*.

Schlatter, P., Li, Q., Brethouwer, G., Johansson, A. V. & Henningson, D. S. 2009*a* Towards large-eddy simulations of high-Reynolds number turbulent

boundary layers. *Proc. 6th Int. Symp. on Turbulence and Shear Flow Phenomena, Seoul, Korea*.

Schlatter, P., Örlü, R., Li, Q., Brethouwer, G., Fransson, J. H. M., Johansson, A. V., Alfredsson, P. H. & Henningson, D. S. 2009*b* Turbulent boundary layers up to $Re_\theta = 2500$ studied through simulation and experiment. *Phys. Fluids*, (accepted).

Simpson, R. 1970 Characteristics of turbulent boundary layers at low Reynolds numbers with and without transpiration. *J. Fluid Mech.* **42**, 769–802.

Smith, D. & Walker, J. H. 1959 Skin-friction measurements in incompressible flow. *NACA Tech. Rep. R-26*.

Smith, R. 1994 Effect of Reynolds number on the structure of turbulent boundary layers. *Ph. D. thesis Princeton University, USA*.

Smits, A. J., Matheson, N. & Joubert, P. 1983 Low-Reynolds-number turbulent boundary layers in zero and favorable pressure gradients. *J. Ship Res.* **27**, 147–157.

Spalart, P. 1988 Direct simulation of a turbulent boundary layer up to $R_\theta = 1410$. *J. Fluid Mech.* **187**, 61–98.

Squire, L. 1961 The motion of a thin oil sheet under the steady boundary layer on a body. *J. Fluid Mech.* **11**, 161–179.

Squire, L. 1962 The motion of a thin oil sheet under the boundary layer on a body. *Flow visualization in wind tunnels using indicators. AGARDograph* **70**.

Strickert, H. 1974 Hitzdraht- und Hitzfilmanemometrie. *VEB Verlag Technik*.

Tanner, L. & Blows, L. 1976 A study of the motion of oil films on surfaces in air flow, with application to the measurement of skin friction. *J. Phys. E* **9**, 194–202.

Tropea, C., Yarin, A. & Foss, J. 2007 Springer Handbook of Experimental Fluid Mechanics. *Springer-Verlag Berlin Heidelberg*.

Tsukahara, T., Seki, Y., Kawamura, H. & Tochio, D. 2005 DNS of turbulent channel flow at very low Reynolds numbers. *Proc. 4th Intl Symp. on Turbulence and Shear Flow Phenomena, Williamsburg, USA,* pp. 935–940.

Tsuji, Y. 1999 Peak position of dissipation spectrum in turbulent boundary layers. *Phys. Rev. E* **59**, 7235–7238.

Tsuji, Y. & Nakamura, I. 1999 Probability density function in the log-law region of low Reynolds number turbulent boundary layer. *Phys. Fluids* **11**, 647–658.

Viswanath, D. S., Ghosh, T., Prasad, D. H. L., Dutt, N. V. K. & Rani, K. Y. 2006 Viscosity of liquids: Theory, estimation, experiment, and data. *Springer*.

Wark, C. 1988 Experimental investigation of coherent structures in turbulent boundary layers. *Ph. D. thesis, Illinois Institute of Technology, USA*.

Wark, C. & Nagib, H. M. 1991 Experimental investigation of coherent structures in turbulent boundary layers. *J. Fluid Mech.* **230**, 183–206.

Warnack, D. 1996 Eine experimentelle Untersuchung beschleunigter turbulenter Wandgrenz-schichten. *Ph. D. thesis, Technical University Berlin, Germany*.

Wieghardt, K. & Tillmann, W. 1951 On the turbulent friction layer for rising

pressure. *NACA Tech. Rep. 1314, Translation of "Zur turbulenten Reibungsschicht bei Druckanstieg", ZWB Untersuchungen und Mitteilungen, Nr. 6617, 1944*.

Wu, X. & Moin, P. 2008 Direct numerical simulation of turbulence in a nominally-zero-pressure-gradient flat-plate boundary layer. *CTR Manuscript 193*.

Appendix: Complementary measurements

In addition to the measurements discussed in the main part of this paper a number of complementary measurements were conducted. One set of these measurements was taken with the main traversing system of the MTL wind-tunnel, in order to provide turbulent boundary layer profiles at the same free stream velocity at different downstream positions, which in turn would give the opportunity to keep an equally long wire in viscous units for different Reynolds numbers. However, as mentioned in section 2.2, the main traversing arm was found to alter the flow when approaching the wall due to its large blockage downstream of the probe. Nevertheless similar measurements can be found in the literature and when neglecting the measurements in the near-wall region, the remaining part can still be used for other purposes. Figure 24 shows selected mean and rms data from these measurements in the diagnostic plot. Here, contrary to the measurements with the wall traversing system (cf. figure 13), the near-wall data collapses on a somewhat smaller slope, viz. $u'/U \approx 0.34$–0.35, indicating that the near wall region is influenced by the presence of the traversing arm. The points falling under the tangent (below $U/U_\infty \approx 0.2$) are affected by the presence of the wall, which acts as a heat sink. The slight deviation in the outer region for the lowest Reynolds number, on the other hand, may be an indication for a not fully developed turbulent flow behaviour, as will shown in the next paragraphs. However all other profiles collapse nicely within the outer region, indicating that the development length is sufficient.

Another set of measurements was performed at a further downstream position in order to provide higher Reynolds numbers at matched viscous wire length as well as a different wire length at a matched Reynolds number. This set was taken by means of the wall traversing system and shows therefore no traces of blockage on the overall statistics. It is however important to note that both of these sets of measurements are not supplemented by independent and direct measured skin friction measurements and will therefore employ the composite fit by Chauhan *et al.* (2009), to extract this quantity and to correct for the wall position. This method was shown to give the best overall performance in comparison with our oil film measurements (cf. Örlü 2009*b*, for a more detailed investigation). It is also important to note that the aerodynamic interference of the traversing arm could have easily been ignored, when utilising the traditional U^+ vs. y^+ and u'^+ vs. y^+ plots. Örlü (2009*b*) have shown, that common methods to extract the friction velocity and to correct for wall positions, can mask these non-equilibrium conditions. Therefore figure 24, with its invariance to the friction velocity and wall position, serves as a independent and objective tool to diagnose which measurement points can be trusted in. This emphasises also the need to measure and evaluate higher order moments in order to ensure that the mean value is correctly measured (cf. Örlü 2009*a*).

Table 5 gives the experimental parameters for these additional measurements. The skin friction coefficient obtained from the composite fit is shown in figure 25 and has per definition to follow the Coles-Fernholz relation with the given coefficients, which is inherent in the composite profile description by Chauhan *et al.* (2009). Alternatively it could also been obtained directly though equation (12). It should be noted that the skin friciton relation can hence not been utilised to judge the quality of the data. Instead the shape factor and wake parameter, shown in figures 26 and 27, clearly indicate that especially the data taken with the main traversing system exhibit a clear deviation from an equilibrium state. The measurements taken with the wall traversing system, however, show acceptable trends. It is interesting to note that the zero pressure-gradient and the tripping for the latter case were adjusted for free stream velocities of 20–40 m/s and that exactly these data points are those fulfilling the equilibrium criteria. The trend in the wake parameter is symptomatic for high Reynolds number experiments, where a high Reynolds number is achieved by a high free stream velocity and a too short development length. Here, as for instance reported in DeGraaff & Eaton (2000) or Knobloch (2008), the wake parameter exhibits a maximum and decays with increasing Reynolds numbers. Such a trend was first believed to characterise an equilibrium state, however as noted in Nagib *et al.* (2007), it is instead an indication of an underdeveloped turbulent boundary layer.

Case	x_{pos} [m]	U_∞ [ms^{-1}]	Re_θ [-]	Re_τ [-]	δ [mm]	δ^* [mm]	θ [mm]	ℓ_* [μm]	L^+ [-]	Δt^+ [-]	TU_∞/δ [-]
T$_A$:7	3.625	20.06	8 105	3 105	65.3	8.35	6.18	21.0	26.1	0.58	9 200
T$_A$:8	3.625	30.45	11 772	4 578	65.2	7.85	5.90	14.3	38.6	1.25	14 000
T$_A$:9	3.625	39.97	14 959	6 114	67.5	7.52	5.73	11.0	49.8	2.09	17 750
T$_A$:10	3.625	49.70	18 661	7 762	70.2	7.48	5.76	9.0	60.8	3.13	21 250
T$_C$:4	1.075	9.52	1 033	532	18.6	2.43	1.67	35.0	14.9	0.42	20 500
T$_C$:5	1.075	11.05	1 469	710	22.5	2.94	2.05	31.7	16.4	0.51	19 600
T$_C$:6	1.075	13.06	2 011	851	24.0	3.39	2.37	28.2	18.4	0.65	16 300
T$_C$:7	1.425	13.03	2 538	1 046	30.4	4.25	2.99	29.1	17.9	0.61	15 000
T$_C$:8	1.625	13.05	2 866	1 153	33.9	4.77	3.37	29.4	17.7	0.59	23 100
T$_C$:9	2.075	13.06	3 502	1 364	41.1	5.80	4.13	30.2	17.2	0.56	15 850
T$_C$:10	2.225	13.06	3 694	1 434	43.3	6.07	4.33	30.2	17.2	0.56	19 600
T$_C$:11	2.425	13.05	3 995	1 532	46.7	6.56	4.69	30.5	17.1	0.66	18 150
T$_C$:12	3.625	13.03	5 569	2 084	65.8	9.04	6.53	31.6	16.5	0.51	15 850

TABLE 5. Experimental parameters for complementary hot-wire experiments. Explanation of column headings and abbreviations is given in sections 4.

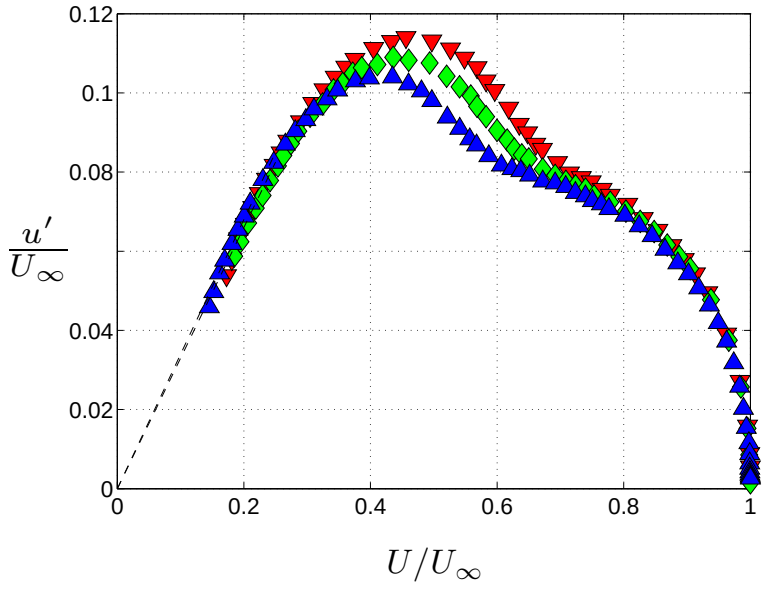

FIGURE 24. Mean streamwise velocity and streamwise turbulence intensity shown in the diagnostic plot for Re_θ= 1468 (▼) , 2010 (▲), 3994 (▲). - -: tangent to the near-wall data with a slope of 0.34 and 0.35.

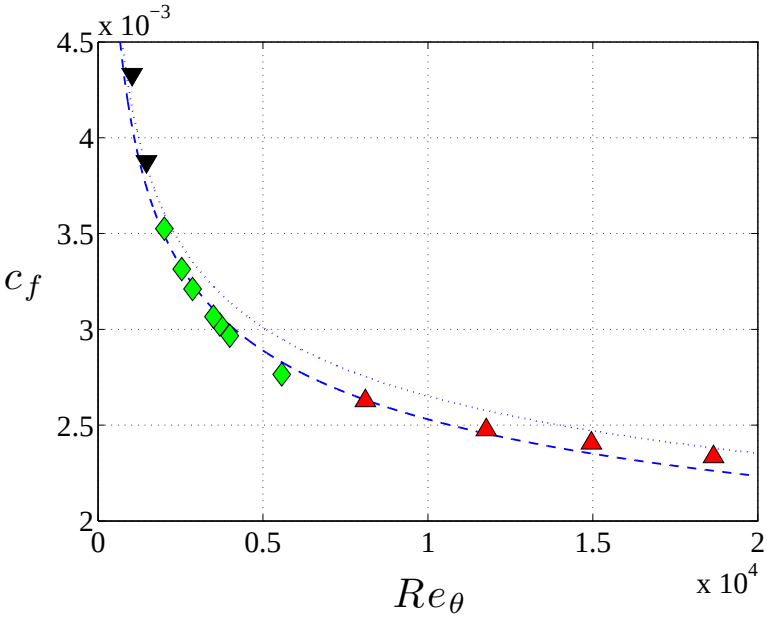

FIGURE 25. Skin friction coefficient, c_f, vs. Re_θ. Tripping configuration A: ▲, B: ♦ and C: ▼. Coles-Fernholz relation with coefficients determined by Nagib *et al.* (2007) (κ= 0.384 & C= 4.127): - -, and with classical values (κ= 0.41 & C= 5.0): · · · .

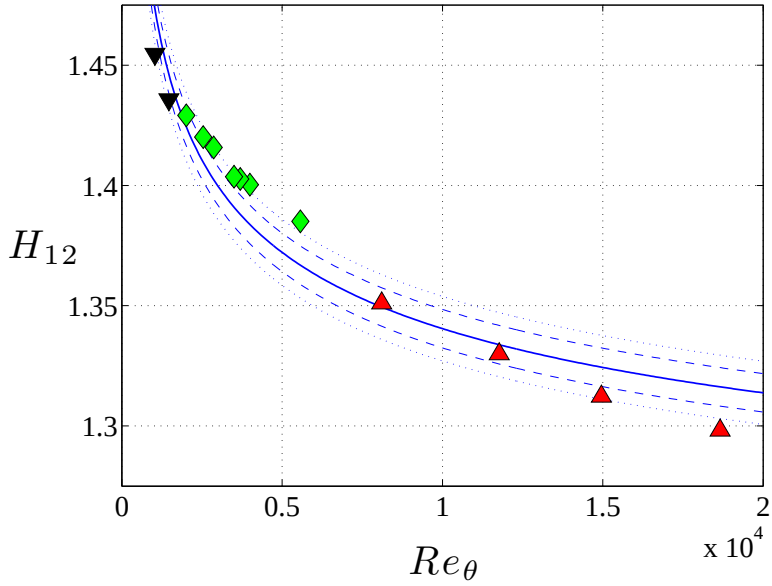

FIGURE 26. Shape factor, H_{12}, vs. Re_θ. Tripping configuration A: ▲, B: ♦ and C: ▼. Integration of composite profile, H_{num},: —, $H_{num} \pm 0.008$: - - -, $H_{num} \pm 1$ % H_{num}: ·.

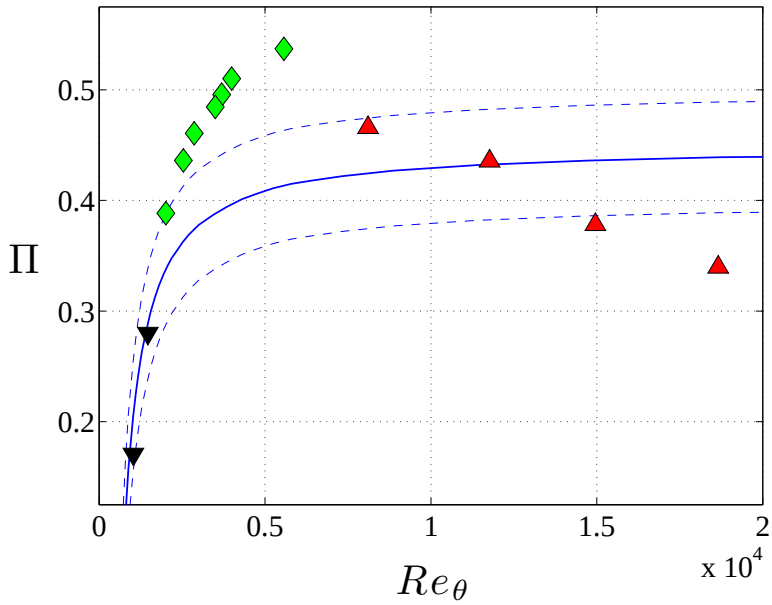

FIGURE 27. Wake parameter, Π, vs. Re_θ obtained using the composite profile. Tripping configuration A: ▲, B: ♦ and C: ▼. Integration of composite profile, Π_{num},: —, $\Pi_{num} \pm 0.05$: - - -.

Paper 5

"Measure what is measurable,
and make measurable what is not so."

Galileo Galilei (1564 – 1642)

5

On the determination of the wall position in wall-bounded turbulent flows

By Ramis Örlü

Linné Flow Centre, KTH Mechanics, SE-100 44 Stockholm, Sweden

The present investigation is an account on the wall position determination in wall-bounded turbulent flow studies. A thorough review on common measurement techniques as well as correction methods reveals, that there are a number of pitfalls, that—when not accounted for—can lead to wrong conclusions about the wall position and thereby also on the near-wall behaviour of mean and turbulence quantities. It is also demonstrated, that accurate measurements reaching into the viscous sublayer are necessary in order to ensure a correctly deduced wall position.

1. Introduction

Wall-bounded turbulent flows are classically divided into two regions (Pope 2000; Schlichting & Gersten 2006), one being the inner region close to the wall, where the flow is independent of the Reynolds number and outer constraints, and the other being the wake or core region governed by the large scales dictated by the geometry of the flow and the Reynolds number. Using dimensional analysis the inner region in the case of hydrodynamically smooth walls can be shown to be a function of the wall distance in inner (viscous scaled) variables, y^+, only.[1] Hence, the wall distance can be interpreted as a local Reynolds number, whereas the outer region is governed by the global (friction) Reynolds number, $Re_\tau = u_\tau \delta/\nu$, where δ denotes the outer length scale, be it the boundary layer thickness, channel half-width or pipe radius in the case of turbulent boundary layers, channel and pipe flows, respectively. A region in which both descriptions are valid in their asymptotic limits is the overlap region, derived by matching both descriptions (Millikan 1938). Despite an advanced understanding in wall-bounded turbulence the description of even the simplest quantity, the streamwise mean velocity component, brings along controversial and "hot" debates. Depending on the scaling of the outer region, either by the friction or free stream velocity, the overlap region is described by

[1] Inner or viscous scaling is here denoted with +, and indicates non-dimensionalisation with the viscous length scale, $\ell_* = \nu/u_\tau$, or the friction velocity, $u_\tau = \sqrt{\tau_w/\rho}$. Hereby ν, ρ and τ_w denote the the kinematic viscosity, density and skin friction at the wall, respectively.

a logarithmic (Österlund *et al.* 2000) or power law (George & Castillo 1997), respectively. While the logarithmic description is classically favoured, not only due to its assumed Reynolds number independent and universal constants, the power law description needs to be Reynolds number dependent, in order to be representative for a wide range of Reynolds numbers.

While both descriptions are legitimate based on asymptotic matching, the reasoning for or against one of them is entirely based on experimental evidence (Panton 2005; Buschmann & Gad-el-Hak 2006). Only recently, have direct numerical simulations (DNS) in canonical wall-bounded turbulent flows become available exceeding Reynolds numbers where a scale separation of inner and outer scales starts to emerge (cf. Hoyas & Jiménez 2006; Wu & Moin 2008; Schlatter *et al.* 2009*b*, representative for channel, pipe and zero-pressure gradient turbulent boundary layer flows). However, the overlap region is still far from being established, so that the debate, logarithmic versus power law, is for the time being dependent on quality experiments in canonical wall-bounded flows.

Recalling that the inner region, comprehending the viscous, buffer and overlap regions, scales on y^+, it becomes apparent that despite high quality turbulent boundary layers and accurate measurements of the velocity fluctuations, also the friction velocity and the absolute and relative wall positions have to be known to high accuracy. Reviewing a number of well-known turbulent boundary layer experiments (cf. references in Fernholz & Finley 1996; Chauhan *et al.* 2009), it can easily be recognised that the friction velocity is in most cases determined from a fit of the experimental data in the overlap region to the log law with prescribed universal constants, the so-called Clauser chart method (Clauser 1954). It may be surprising, but even where the friction velocity could have easily been computed independent of the velocity profile, like in pipe flows (Abell 1974) or where high quality measurements in the viscous sublayer by means of laser Doppler velocimetry (LDV) were available (DeGraaff 1999), the friction velocity was extracted from the Clauser chart.[2] Where the skin friction was determined directly, as for instance by means of floating elements (Smith & Walker 1959; Karlsson 1980), any deviation from the values deduced from the log law with classical universal constants has usually been attributed to measurement uncertainties (Coles 1956, 1968), rather than to question the universality of the log law constants or the log law itself. Hence, having assumed what was set out to be proven, it is of no surprise that the log law with its universal constants for canonical wall-bounded flows (but also for turbulent boundary layers with pressure gradients), has been treated as "one of the cornerstorns of fluid dynamics" (Bradshaw & Huang 1995).

[2]The skin friction or friction velocity extracted from the Clauser chart/plot/method is an extracted and not measured value, no matter how often the opposite has been stated in the literature, so for instance by Willmarth & Lu (1972): "The wall shear stress was measured using the Clauser plot".

The renaissance of the power law, advocated among others by George & Castillo (1997) and Barenblatt & Chorin (1998), has lead to a refinement of the constants of the log law and the region where it is supposed to be valid (Österlund *et al.* 2000; Monkewitz *et al.* 2008). Over the last years further support has been reported for the refined log law constants (Perry *et al.* 2001; Zanoun *et al.* 2003), underpinned by independent measurements of the skin friction, either by means of the pressure drop in pipe flows or directly through oil-film interferometry in turbulent boundary layer and channel flows. The lesson to be learnt is, that an independent and/or direct measure of the skin friction is a crucial supplement to be provided in order not to be dependent on prejudgment (Nagib *et al.* 2004*b*).

Keeping in mind that the inner scaled mean velocity profile is dependent on accurate velocity measurements, an independent and/or direct measurement of the friction velocity as well as an accurately determined wall position, it may come as a surprise that, despite the mentioned fallacy, the latter has—to our knowledge—not been treated with the same care.

As simple and trivial the task of determining the absolute wall position may sound, it remains an important and difficult task in laboratory experiments with consequences not directly obvious. Most of the early studies in wall-bounded turbulent flows employed Pitot tubes and were therefore not able to resolve the sublayer, whereas some of those reaching into the buffer region or even sublayer displayed (with todays knowledge) an erroneous behaviour, as for instance evident in the data provided by Patel (1965). Similar problems can also be found in hot-wire measurements, as for instance those presented by Blackwelder & Haritonidis (1983). While most of the observed trends were attributed to measurement uncertainties or inaccuracies in the determined friction velocity, the possibility of an inaccurate determination of the wall position has—to our knowledge—not been considered.

Figure 1 illustrates the effect of uncertainties in the friction velocity as well as inaccuracies in the absolute wall position. The mean streamwise profile for a turbulent boundary layer was generated by means of a composite profile description by Chauhan *et al.* (2009) with a nominal friction Reynolds number, or so-called Kármán number, of $Re_\tau = \delta^+ = u_\tau \delta/\nu = 5000$, and a viscous length scale of $\ell_* = 15$ micron. While figures 1*(a)* and *(b)* depict the effect of wrongly deduced friction velocities for correctly and wrongly deduced wall positions, respectively, *(c)* and *(d)* give the effect of inaccuracies in the wall position for a correctly and wrongly deduced friction velocity, respectively. It is apparent that the semilogarithmic plot of the mean streamwise velocity component in inner scaling, $U^+ = U/u_\tau$ against y^+ emphasises deviations in the friction velocity and the wall position differently. While the former is more apparent in the overlap and outer region, the effect of the latter is more pronounced in the viscous and buffer region.

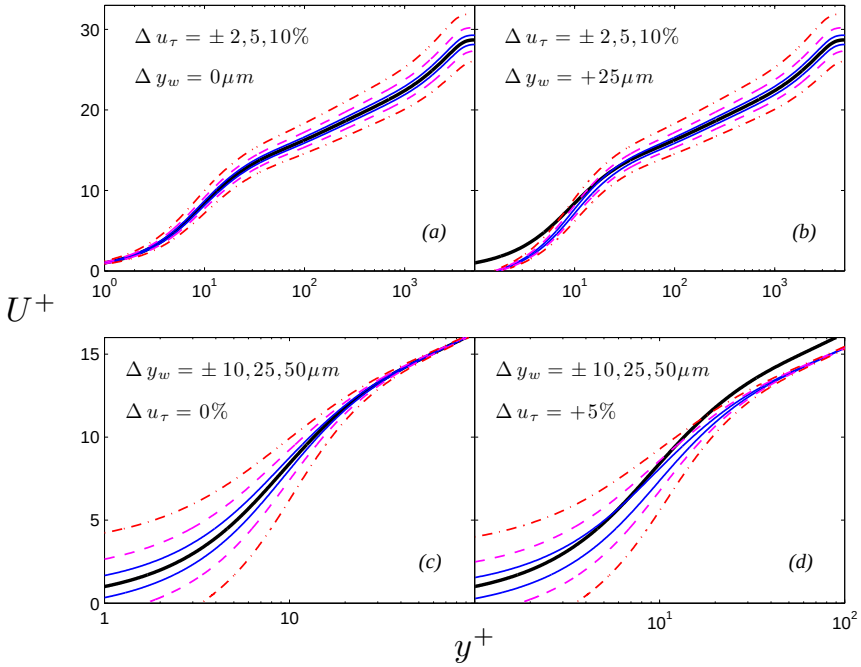

FIGURE 1. Effect of errors in the determined friction velocity and absolute wall distance in inner-scaled coordinates. Effect of inaccuracies in the determined friction velocity for a correct *(a)* and erroneous *(b)* absolute wall position, as well as the effect of inaccuracies in the determined absolute wall position for a correct *(c)* and errornous *(d)* computed friction velocity. The turbulent boundary layer profile was generated by means of the composite profile by Chauhan *et al.* (2009) for a nominal Re_τ of 5000 and a viscous length scale of $\ell_* = 15$ micron.

A number of controversies associated with the study of wall-bounded turbulent flows, among others the proper scaling of the mean velocity profile, the scaling of the bursting frequency or the quantitative value and location of the streamwise rms near-wall peak, has partially been masked due to the overhasty acceptance of universal log law constants and a varying range of validity and the resulting value of the friction velocity. Only recently has it become generally accepted that the skin friction needs to be measured independently of any relation which is set out to be proven (Nagib *et al.* 2004*b*). The above said suggests that the same caution regarding the absolute wall position may contribute to some of the controversies in concurrent wall-bounded turbulent flows studies.

Having reasoned for the need of reviewing the ways in which the absolute wall distance of the measurement location have and can be deduced the remainder of the paper will first review the common measurement techniques for the determination of the wall position as well as their shortcomings and associated problems, and then review and assess correction methods based on the velocity measurements. Finally the results will be summarised and possible issues in the current debate will be approached based on the current findings. Hence, the present work attempts to explain some of the observed peculiarities and controversies in the experimental study of wall-bounded turbulent flows.

2. An overview on measurement techniques

A number of techniques and methods have been utilised to measure or estimate the distance between the sensing probe, be it a hot-wire or a Pitot tube, and the wall. However, only few of these have been mentioned in reference textbooks, as, for instance, those by Sandborn (1972), Lomas (1986), or Bruun (1995). While the utilisation of a simple ruler may suffice for measurements in the outer/core region of wall-bounded flows (Lomas 1986) as well as rough walls (Benson & Eaton 2003), more sophisticated methods are needed for measurements in the inner and overlap region, but also for quantitative contributions to the scaling of the outer region. Microscopes (Wills 1962; Bhatia *et al.* 1982), theodolites (Antonia *et al.* 1990; Krishnamoorthy *et al.* 1985) and cathetometers (Klewicki & Falco 1990; Priyadarshana & Klewicki 2004) are among the more frequent used devices, and have indicated accuracies between 1 and 25 micron. While microscopes coupled with a micrometer gauge focus on the wire and wall separately in order to determine the distance between them, the distance in the case of theodolites and cathetometers is extracted as half the distance from the wire to its image in the polished wall surface, as long as the viewing angle is perpendicular to the distance between the sensor and the wall. With the advances in digital photography the latter techniques are often replaced or supplemented by photographs taken with digital cameras with telephoto zoom lenses. Such methods are depicted in figure 2, where the absolute distance is measured both in regards to a precision gauge block and a vernier height gauge, as well as the aforementioned reflection method. For cases where the measurement location is transparent laser distance meters can be used as well (Österlund 1999).

The mentioned techniques all presume that optical access is available. However, this is not always given, as for instance in many internal flows. Here instead, the electrical contact between the wall and the probe can be exploited to find the position of the probe, as for instance employed by Azad & Burhanuddin (1983) and McKeon *et al.* (2004) in the case of hot-wire probes and Pitot tubes, respectively. While this method is quite common for Pitot tubes and accuracies between 5–100 micron have been reported, it is rather delicate to put the hot-wire in "danger" in order to determine its absolute wall position.

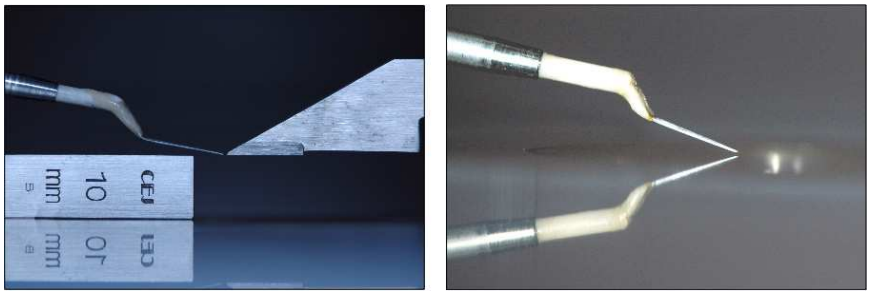

FIGURE 2. Photograph showing a boundary layer type probe during the wall position determination using physical methods, viz. by means of *(a)* a precision gauge block and a vernier height gauge and *(b)* the mirrored image.

One way of avoiding the direct contact with the wall is to attach a third prongs or a needle, a so-called wall stop, to the hot-wire probe facing the surface with a predetermined distance to the hot-wire. Achieved accuracies given in the literature vary substantially and are usually around 25 micron, whereas errors up to 200 micron were reported by Monty (2005).

Pitot tubes and hot-wire probes, due to their intrusive nature, will once they are exposed to a force deflect and thereby falsify the measured distance. Hites (1997) for instance observed deflections of the used hot-wire probes of up to 100 microns at a free stream velocity of 40 m/s. Additionally the traversing arm may deflect as well and depending on the individual configuration the probe position may move towards or away from the wall. For the case of flat plate boundary layers, the surface on which the boundary layer is to be measured, may experience a lift or down force, depending on the pressure distribution underneath and on the flat plate. Consequently, a system with a few degrees of freedom is at hand depending on how the plate, the traversing arm, the probe and the measuring device used to determine the distance between the sensor and the wall is fixed in the tunnel and relative to each other. It is hence important to ensure that the deflections are not dependent on the (wall normal) traversing position. Free stream velocity dependent deflections on the other hand, are probable to be expected and encountered, and need to be corrected for. Cathotemeters, theodolites as well as digital cameras with telephoto zoom lenses can, for instance, be used to detect these deflections and to locate the source and dependencies of these deflections.

Regarding the mentioned non-optical methods a number of problems can arise. While for instance electrically conducting surfaces are needed for the methods utilising the electrical contact methods, non-conducting surfaces may be desirable for hot-wire measurements in the near-wall region, in order to limit the effect of additional heat losses towards the wall (Bhatia *et al.* 1982).

Another problem mentioned by Hutchins & Choi (2002) regarding both electrical contacts as well as wall stops is that "electrical contact is rarely made at a clearly defined and repeatable point. This, along with slight probe deformations caused when the contact is made, can limit the accuracy of these methods."

Another technique to deduce the wall position, described in Durst *et al.* (1987, 1988) and employed among others by Durst *et al.* (2001) and Zanoun (2003), is based on the finding that the mean velocity read by a hot-wire increases when the wire is in close vicinity to a heat-conducting wall. Since, for a given hot-wire, the measured voltage in quiescent air, is dependent on the hot-wire probe, its operating parameters as well as the distance to the wall, a suitable calibration enables the determination of the wall position. Reported accuracies, lie within ± 10 micron (Durst *et al.* 1988, 2001). However, since the wall position is deduced under no flow conditions, the given accuracy can not be transferred to situations under flow conditions.

Keeping in mind that most laboratory experiments in wall-bounded turbulent flows have momentum thicknesses of the order of millimeters and viscous length scales of the order of 10 microns, it becomes apparent (cf. figure 1) that in most practical cases the determined absolute wall position serves rather as an initial guess, than an ultimately determined quantity. Although this has not been reported as openly in the literature as the problems encountered when determining the friction velocity, a number of post-processing procedures can be found in the literature, which will be reviewed or introduced in the following.

3. An overview on correction methods

A glimpse at the literature reveals that most of the measurements in wall-bounded turbulent flows are not supplemented by independent and/or direct skin friction measurements. Therefore, a number of methods have been reported in order to estimate the friction velocity. Among these are the already mentioned Clauser chart method, the utilisation of the linear profile in the viscous sublayer as well as the employment of analytical descriptions for the law of the wake and so-called composite profiles. Since the friction velocity is deduced by employing a pair of velocity and wall positions, all methods to deduce the friction velocity can in principal also be utilised to extract a corrected absolute wall position. Although both quantities could be determined simultaneously in the same manner, we will in the following focus on the correction of the absolute wall position only, and assume that the friction velocity has been determined prior to the correction of the wall position determination. The reason for this is that the skin friction, besides its practical importance, is a quality criterium to be assessed in order to ensure canonical flow behaviour (Chauhan *et al.* 2009), and should therefore not be computed based on the assumption that a certain flow state has already been established. Nevertheless, the following methods can easily be extended to determine the friction velocity

besides the corrected absolute wall position or both. In the following some of the descriptions for the mean streamwise velocity profiles will be summarisied in order of their theoretical completeness together with a discussion on its advantages and disadvantages in respect to their potential use to determine the absolute wall position.

3.1. *The sublayer*

The linear law of the wall can be derived from the integration of the streamwise momentum equation and evaluating it with a Taylor series expansion at the wall. It is commonly given as a first order approximation (Pope 2000; Bernard & Wallace 2002),

$$U^+(y^+) = y^+ \,, \tag{1}$$

together with its range of validity, viz. $y^+ < 5$, and can be traced back to Prandtl (1925). While internal flows are driven by a streamwise pressure gradient, which expresses itself as a second order correction to the linear law of the wall, the next terms in the Taylor series expansion are of forth and fifth order (Monin & Yaglom 1971; Townsend 1976),

$$U^+(y^+) = y^+ - \frac{y^{+2}}{2Re_\tau} - \frac{\sigma_1}{4}y^{+4} + \frac{\sigma_2}{5}y^{+5} + \cdots \,. \tag{2}$$

The second order term asymptotes against zero in the limit of infinite Reynolds numbers, but becomes practically negligible already for $Re_\tau > 300$. In the case of zero pressure-gradient turbulent boundary layers (ZPG TBL), it diminishes exactly, since its appearance in equation (2) is solely due to the streamwise pressure gradient.[3]

3.1a. *The linear velocity profile.* While the linear law of the wall, be it with or without higher order terms, is an explicit and simple expression, the estimated wall position (as well as the obtained friction velocity when used for that purpose) is solely dependent on the accuracy of the measured near-wall data as well as the reliability of the traversing system and encoder used to measure the relative distance between the measurement points. Hot-wire readings are known to be affected by the presence of the wall. Not only does the hot-wire "sense" the additional heat loss towards the wall, which acts as a heat sink, when being closer than approximately 3.5 wall units (Janke 1987; Hutchins & Choi 2002), but—depending on the geometrical constellation—it may also distort or alter the flow field in the proximity of the probe, due to aerodynamic blockage (Comte-Bellot *et al.* 1971). Whereas the effect of the first error source

[3]While a more thorough derivation of equation (2) can be found in Cenedese *et al.* (1998), the relative importance of the higher order terms as a function of Reynolds number and wall distance is presented in appendix A.

is quite well understood and the effect of the seemingly increasing mean velocity with decreasing wall distance is well documented[4], the effect of the probe (body) in the near-wall region on the flow field and thereby the relation of the measured velocity to the velocity which would be present in the absence of the probe is not well understood. It is also dependent on the exact probe-body geometry and dimension, and therefore general relations can not be expected. Consequently, the use of the law of the wall for $y^+ < 3.5$ to determine the wall position (or the friction velocity) is not advisable, unless near-wall effects on the measurement technique can be excluded. Furthermore it should be ensured that the deduced mean velocity readings are evaluated from velocity signals, which are calibrated for, and are free from increased heat-conduction effects. The latter calls therefore for an optimised selection of wire diameter, operational temperature, i.e. overheat ratio, and wall material, since they all may effect the deduced velocity readings within the viscous sublayer.

The selected calibration relation can alter the time-averaged velocity readings as well, especially at low velocities (Örlü 2009*a*), which calls for special attention when using solely these near-wall measurements to deduce the wall position. For measurements in the viscous sublayer the hot-wire has to be calibrated from around 20 % of the lowest mean velocity on, due to the high skewness and flatness factors as well as the high local rms values present within the viscosity dominated region (Örlü 2009*a*). This calls for special attention regarding the choice of the calibration relation. The non-linear relation between the velocity and the hot-wire anemometer signals contribute as well towards an increased mean velocity reading. Contrary, in the case of Pitot tubes, the non-linearity tends to decrease the deduced velocity reading. However, in the latter case, other corrections, e.g. for displacement, turbulence and shear (see e.g. Tropea *et al.* 2007, chap. 5), may dictate whether the readings are under or overcorrected. Hence it is advisable to neglect the "wall-effect region" denoted with **I** in figure 3. Doing so, will not leave more than 1–1.5 wall units in region **II** for the fitting of the near wall data to the linear profile.

Keeping the above said in mind, the linear profile should be used with caution when used for the wall determination or the friction velocity. In order to ensure correclty deduced quantities within the small range an unusual high number of measurement points is needed. The experimental investigation by Hutchins & Choi (2002), for instance, "indicates that over 80 individual velocity measurements [...] are required to characterise the velocity gradient and obtain the wall skin friction to a standard error of ± 1.8 %." Instead they

[4]Literature on parametric studies and numerical analysis on, for instance, the dependence on wall and wire materials, wire length and diameter or the overheat ratio is rich (see for instance Bhatia *et al.* 1982; Chew *et al.* 1995, and references therein) and is even exploited to calibrate hot-wires at extremely low velocities, viz. down to 0.03 m/s (Janke 1987), or to deduce the absolute wall position under no flow conditions (Durst *et al.* 1988; Hutchins & Choi 2002).

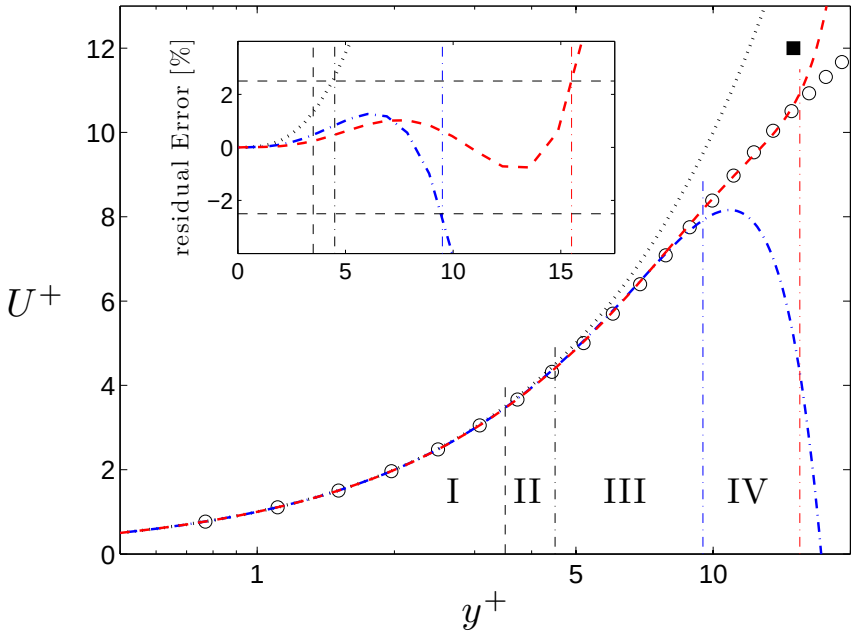

FIGURE 3. Mean streamwise velocity profile within the sublayer and buffer region for a zero pressure-gradient turbulent boundary layer in inner scaling. ○: DNS by Schlatter *et al.* (2009*b*) at $Re_\theta = 2500$, law of the wall to first (· · ·), forth (– · –) and fifth (– – –) order. The residual percentage error between the law of the wall and the DNS data is depicted in the insert. **I** Wall-effect region, **II** usable linear region for hot-wire measurements, **III**+**IV** region described by including the forth and fifth order terms in equation (2). ■: Indicative point $(y^+, U^+)=(15, 12)$ used by Blackwelder & Haritonidis (1983) for a correctly measured profile.

suggest one quality measurement at the end of the linear region and an absolute wall position determination with an accuracy better than ± 0.02 viscous units (usually $< 1\ \mu m$), which in their view provides a more accurate friction velocity. This would, however, presume that the determined wall position is accurate also under flow conditions.

The full linear profile seems therefore merely useful for LDV measurements, that are both non-intrusive and free from heat-conduction effects as well as hot-film measurements in water or oil.[5] While the former procedure

[5]Note, however, that LDV is not immune against near-wall effects. Reflections at the surface, can cause the mean velocity readings to increase artificially, similiar to near-wall effects in

was for instance used by Ching *et al.* (1995) and Durst *et al.* (1995), where the friction velocity was in both studies determined from the linear profile by using only measurement points below $y^+ = 2.5$. An example for the latter, utilising the entire linear profile, are for example the works by Alfredsson & Johansson (1984) and Eckelmann (1974), respectively. Although there is theoretically no difference whether the skin friction or the wall position is determined through a fit of the data to the linear profile, the literature is scarce when it comes to the determination of the absolute wall position. On the contrary, the friction velocity is quite often determined from a fit to the linear profile, the so-called viscous layer or wall-slope method, (cf. references given in Mochizuki & Nieuwstadt 1996; Fernholz & Finley 1996). By doing so, values of the von Kármán constant, κ, have occasionally been found to be lower than the classically accepted ones (van Manen *et al.* 1993). While the linear profile is commonly employed in laminar flows to correct for wall positions (White & Ergin 2004), it is not as easy to find any reference where it has been used to correct for the absolute wall position in wall-bounded turbulent flows. An exception is for instance the work by Ching *et al.* (1995), where its use revealed differences up to 150 microns corresponding to 3 wall units compared to the initially measured distance.

The reason for this may be the fact, that the linear profile covers a much wider range in physical units for laminar boundary layers than for its turbulent counterpart, and that it is therefore too trivial to be even mentioned. On the other hand the viscous sublayer is not often accurately resolved in turbulent wall-bounded flows, explaining why it can hardly be used for the purpose of finding the wall position. Recalling figure 1, it appears, however, as if the fit to the linear profile is much more sensitive to variations in the wall position than the friction velocity, and is therefore, at least from a theoretical point of view, much more suited to extract the physical wall position.[6]

On the other hand, the viscous layer method is a rather common practise in rough wall experiments, where no clear aerodynamic origin for the mean profile can be defined. Here, y^+ is substituted with $y^+ + \Delta y^+$ and solved together with the other unknowns (Acharya & Escudier 1983; van Manen *et al.* 1993).

3.1b. *The expanded linear velocity profile.* Having mentioned the problems to be taken into account when utilising the linear profile, it is obviously desirable

hot-wire measurements as observed by van Manen *et al.* (1993). The seeding of the wall is another problem. Similar problems are also encountered in particle image velocimetry (PIV) measurements close to solid walls, due to the relatively thick laser sheet and the problem to associate the velocity field with an exact wall position. An alternative way would be particle-tracking velocimetry (PTV), where the position of the particles can accurately be monitored. Such an approach for the purpose of wall shear stress measurements is for instance employed in the mirror PTV technique (Kunze *et al.* 2008; Große 2008).

[6]This is of course also an artifact of the commonly found logarithmic spacing of the measurement points.

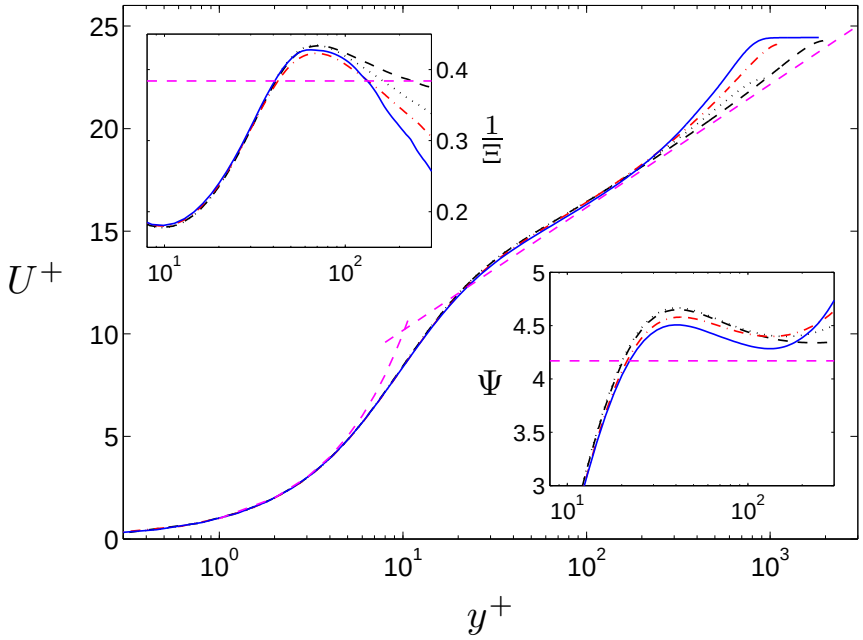

FIGURE 4. Mean streamwise velocity profile in inner scaling for channel (del Álamo *et al.* 2004; Hoyas & Jiménez 2006), pipe (Wu & Moin 2008) and ZPG TBL (Schlatter *et al.* 2009*b*) flows. The linear and log law profiles with $\kappa = 0.384$ and an additive constant of 4.17 is indicated through the dashed lines. The deviation from the log law, Ψ, is given in the lower insert, whereas the indicator function for the log law is depicted in the upper insert.

to extend the range of the law of the wall in order to have a wider range to which data points can be fitted. Additionally, the confidence in the mean streamwise velocity measurements is much higher above the viscous sublayer. The next higher order term for internal flows is of second order in equation (2), whereas for ZPG TBL flows it is of forth order. Inclusion of the quadratic term does not significantly extend the useful range as shown by Cenedese *et al.* (1998), whereas the inclusion of the quartic term was found by the same authors and Park & Chung (2004) to represent the (channel flow DNS) data within 5 % up to $y^+ = 6$–8. These results are, however, mainly based on low Reynolds number channel flow DNS, where the pressure gradient remains important and expresses itself through the Reynolds number in the quadratic term. Depending on the deemed range to be represented by the Taylor series expansion of the

law of the wall as well as the data used to extract the coefficients, substantially different coefficients and ranges of applicability can be determined.[7]

Available higher Reynolds number DNS of canonical wall-bounded turbulent flows (Hoyas & Jiménez 2006; Wu & Moin 2008; Schlatter *et al.* 2009*b*) can be utilised to find the optimal range within which the expansion of the linear profile including the forth and fifth order terms represent the data well. Assuming the commonly accepted limit for the linear profile of $y^+ = 4.5$, which gives an residual error of around 2.5 % in the velocity from the turbulent boundary layer DNS by Schlatter *et al.* (2009*b*), it can be shown that the forth and fifth order terms can be used to extend the valid range up around 9 and 15 wall units, respectively, as illustrated through regions **III** and **IV** in figure 3. It is important to note that DNS of the three canonical wall-bounded turbulent flows show no differences in the mean streamwise velocity for $y^+ < 10$, whereas small differences can be observed when considering the slope of the streamwise velocity component, in form of the so-called (logarithmic) indicator function, $\Xi = y^+ \partial U^+ / \partial y^+$, or the overshoot above the log law, $\Psi = U^+ - 1/\kappa \ln y^+$, depicted in figure 4. Comparing the channel flow DNS at $Re_\tau = 950$ (del Álamo *et al.* 2004) and 2000 (Hoyas & Jiménez 2006) with each other indicates that the observed differences between the different flows within the buffer region are unlikely to be Reynolds number effects. Utilising channel flow DNS at around the same friction Reynolds numbers from a number of authors (Moser *et al.* 1999; Hu & Sandham 2001; Abe *et al.* 2001; Iwamoto *et al.* 2002; del Álamo & Jiménez 2003), it can be deduced that the observed differences between the different flow cases are of the same order as those observed between different DNS results used by various groups for the same flow case at around the same Reynolds number.[8] Hence, it can not be ascertained whether the observed differences are flow dependent or whether they lie within the accuracy that different groups can reproduce their DNS.

In light of the above said, the extended *(linear) law of the wall* including the forth and fifth order terms could, without loss of generality, been utilised

[7]This explains why the range of usefulness of the quartic extension of the law of the wall varies in the literature from around 6 up to 20 wall units (see for instance Monin & Yaglom 1971; Sreenivasan 1989). It should however be noted that the values given by Sreenivasan (1989) are probably erronous, since they do not even describe the correct profile beyond the linear region, while it is claimed to represent the mean streamwise profile up to $y^+ = 20$. The same values were for instance adapted by Gad-el-Hak (2000).

[8]While the DNS results by Iwamoto *et al.* (2002) and del Álamo & Jiménez (2003) at Re_τ of 650 and 550, respectively, are in excellent agreement up to y^+ of around 80, where the wake region starts and hence Reynolds number effects become important, the data by Moser *et al.* (1999) and Abe *et al.* (2001) at $Re_\tau = 590$ and 640, respectively, displays differences over the entire buffer region, when compared to the other two simulations. Even stronger deviations (into the viscous layer), can be observed when considering the data by Hu & Sandham (2001) at $Re_\theta = 720$. For a qualitative assessment of the differences the reader is referred to appendix C.

to determine both the skin friction and the wall position for canonical wall-bounded flows. This has for instance been demonstrated by Durst *et al.* (1996) for turbulent pipe and channel flows, with the main emphasis on its advantage to determine the friction velocity within 1 % accuracy. The authors also assessed the possibility of utilising equation (2) to determine the friction velocity together with the corrected absolute wall position. When one of the mentioned values is given due to a direct measurement, the accuracy of the other determined quantity will improve. Even when the above mentioned extended law of the wall is used to shift the mean velocity profile so that it matches the analytical curve, the number of measurement points may still be small and it would be desirable to extend the range even further, in order to increase the accuracy of the determined quantity. This becomes even more of importance when considering high Reynolds number experiments measured in flows where the Reynolds number is increased by increasing the free stream velocity or the density. Similar problems can occur for low Reynolds number experiments with short development length. In both cases the viscous sublayer is barely measurable with conventional measurement techniques.

A number of analytical expressions have been derived more or less based on physical arguments and some curve fitting in order to transition from the viscous sublayer to the logarithmic (or the power) law. Since most of the descriptions asymptote to the logarithmic overlap mean velocity description, first the logaritmic law will be introduced and commented on, although on its own it has no potential to provide an accurate estimate of the absolute wall position.[9]

3.1c. *Pressure gradient and Reynolds number effects.* A further comment on equation (2) may be suited at this place. Also the derivation of equation (2) can be found in a number of textbooks and papers, there seems to be some confusion regarding the origin of the higher order terms as well as their relative importance, and consequently the range of validity. Since the Taylor-series expansion of the fluctuating velocity components is performed around $y^+ = 0$, the relative importance of the subsequently higher order terms becomes less important. However, this is only guaranteed as long as the assumption of being in the vicinity of $y^+ = 0$ is not violated vigorously. So, for instance, argues Große (2008) that the Taylor-series expansion up to the quadratic term is valid for $y^+ \leqslant 7$, and that the linear profile can be used within the same range with an error of less than 1 % (Große & Schröder 2008). Their given error is, however, solely based on the assumption, that the higher order terms are relatively small compared to the lower order counterparts. This is, however,

[9]Note, however, that where the absolute distance to the wall can not be defined conclusively as for instance in rough-wall flows, the logarithmic law can, nevertheless, serve as an "approximate method" to locate the virtual origin of the wall position and to extract the friction velocity (Perry *et al.* 1969). It was, however, already pointed out by Perry & Joubert (1963), that this turns out to be "the most difficult task".

only the case for $y^+ < 3$ at $Re_\tau \approx 300$, where the quartic term is already of the same order as the quadratic. With increasing Reynolds number and further away from the wall the error by utilising the linear profile can easily be an order of magnitude larger than indicated by the above authors. This can easily be demonstrated through available DNS data, as done in appendix A. Although their employed micro-pillar shear-stress sensors are a welcomed and promising alternative for the measurement of wall shear stresses, the above erroneous assumption may give masked Reynolds number effects. So for instance do their pillars range within the range of 3 to 10 viscous units depending on the Reynolds number ($Re_\tau = 170$ to 570). Since the Reynolds numbers are relatively low, they will have influence through the quadratic term, however in the wrong direction. While in reality, an increasing Reynolds number decreases the inner-scaled mean streamwise velocity away from the linear profile, the aforementioned authors assume that it increases towards the linear profile. The errors can therefore easily reach up to 15 % and introduce wrong qualitative trends (cf. figure 9 in appendix A). In their turbulent boundary layer experiments, the pillars reach even 15 viscous units (Große 2008), calling for systematic errors up to 40 %. [10]

3.2. *The log(arithmic) law*

Classical turbulence textbooks (Tennekes & Lumley 1972; Townsend 1976) give the impression as if the logarithmic law, has an accepted and indisputed status for wall-bounded turbulent flows. Nonetheless every new student of turbulence will at some point cross the debate "log versus power law" (George 2007; Monkewitz *et al.* 2008) which has been controversially debated over the last decade. However, for the purpose of the present investigation, where the primary goal is to utilise descriptions of the mean velocity profile in order to determine the wall position, a deepening on the arguments has no benefit.

The first derivation of the log law can be traced back to von Kármán (1930), who employed dimensional arguments, whereas Prandtl (1932) and Millikan (1938) made use of the mixing length concept and asymptotic matching, respectively (Buschmann & Gad-el-Hak 2006).[11] Following any of these routes leads to

$$U^+ = \frac{1}{\kappa} \ln y^+ + B, \tag{3}$$

[10] The authors refer to Bernard & Wallace (2002), for the Taylor-series expansion of the linear profile, and it seems that the confusion is partially explained through the misleading explanation given in that reference.

[11] The excitement and eagerness of von Kármán to present his findings in Stockholm at the 3$^{\text{rd}}$ International Congress for Applied Mechanics as well as to confirm his theory experimentally (prior to Prandtl) is best described in his own words (cf. von Kármán 1967, chap. 17).

which is the log law with the so-called Kármán constant, κ, and an additive constant, B. Both of these constants were assumed to be universial for all wall-bounded flows and thereby independent of the pressure gradient with $\kappa = 0.41$ and $B = 5.0$. Although a remarkable scatter for the experimentally deduced values of these constants has been collected until the late 1990 (Zanoun *et al.* 2003) the mentioned constants were generally assumed to be universal.[12] High Reynolds number experiments by Österlund *et al.* (2000) and Nagib *et al.* (2004*a*) employing hot-wire anemometry and independent skin friction determination by means of oil-film interferometry, however, established values of 0.384 and 4.17 for κ and B in equation (3) for ZPG TBLs. Similar values have been reproduced by Perry *et al.* (2001)[13] and Zanoun *et al.* (2003) in pipe and channel flows, respectively, whereas Monkewitz *et al.* (2008) and McKeon *et al.* (2004) give the classical or even higher values for the SuperPipe experiments, respectively. Keeping in mind that several skin friction determination methods are solely based on the log law and its "universal constants", like the Preston tube or Clauser-type methods, the scatter observed in skin friction relations or the amplitude and position of maxima in different Reynolds stresses is not surprising.

One issue has not been addressed so far, namely the extent of the wall distance in which the log law is believed to be valid, i.e. describes the mean velocity distribution the best. While classical theory gives $y^+ \geqslant 30$–70 as the lower and $\eta = y/\delta \approx 0.1$–$0.2$ as the upper limit (Sreenivasan 1989; Gersten & Herwig 1992; Piquet 1999), experiments by Österlund (1999) have, however, indicated an overshoot over the log law around $y^+ = 50$, which in turn shifts the lower limit to somewhat higher values, viz. $y^+ =$160–200 (Lindgren *et al.* 2004; Österlund *et al.* 2000), where according to Lindgren *et al.* the probability density distributions becomes universal (see discussion in Örlü 2009*b*). This overshoot is usually ignored, when utilising the classical log law constants, or exploited to support the need for a power law description. Additionally the amplitude of the overshoot seems to be affected by the applied correction methods in the case of Pitot tubes and by spatial resolution issues in the case of hot-wires. The former and latter effects are more thoroughly discussed in **?** and Örlü (2009*b*), respectively. Since, the overlap region, can be derived by matching an inner scaled and outer scaled velocity description in their high

[12]The dilemma is maybe best expressed in a statement by Bradshaw *et al.* (1992) regarding the log law and its universally accepted constants: "The actual range—ignoring a few outlying methods—implies a 10 % "uncertainty" in skin friction on a flat plate in a low-speed flow, the simplest of all test cases. We are trying to achieve a consensus!", Similarly Tennekes (1982) proposes, after reviewing the reported values for the Kármán constant, that "one should restrain the urge to expound on this issue, and state simply that $\kappa =$0.4±0.04 represents the state of the art".

[13]By re-analysing the SuperPipe data, they deduced $\kappa = 0.39$, instead of the claimed value of 0.436 found by Zagarola & Smits (1998). The difference was mainly caused, due to the applied turbulence correction.

Reynolds number limit, the bounds for the inner and outer limits have to be given in inner and outer scaling, respectively. Due to the Reynolds number indepence of the inner region, the limit for the beginning of the overlap region is fixed in inner scales, but moves closer to the wall in outer scales. On the other hand, the outer limit is defined as a fraction of the friction Reynolds number, and hence Reynolds number dependent in inner scaling. Nevertheless, the employment of the classical log law constants (Coles 1968) can give the wrong impression as if the log law has a fixed upper limit in inner-scaled coordinates, around $y^+ = 350$–1000, as for instance given in Kestin & Richardson (1963), Spurk (1996), Oertel *et al.* (2006) or Jirka (2007).

The issues touched upon the log law and its constants may seem artifically exaggerated, and of no particular importance for the purpose of the following paper, however a number of studies (among others Purtell *et al.* 1981; Klewicki & Falco 1990; Erm & Joubert 1991) have applied the Clauser chart method to relatively low Reynolds number flows (thereby violating the necessary condition for the overlap region and hence log law to emerge, not to mention its establishment). In consequence, the use of the deduced friction velocities may have influenced their results and conclusions. It has for instance, recently been shown by Wei *et al.* (2005), that "using the Clauser chart method can potentially mask subtle Reynolds-number-dependent behaviour". Nevertheless, experimental data employing the Clauser chart method at Reynolds numbers as low as $Re_\tau = 180$ (Roach & Brierly 1992), have for instance been used by Buschmann & Gad-el-Hak (2003*a*,*b*) to test scaling laws.

3.3. *Analytical descriptions for the inner region*

Although the classical view that the inner-scaled mean streamwise velocity component, U^+, within the inner (including the overlap) region is a function of the local Reynolds number, i.e. y^+, only, no analytical expression has been derived from first principles to describe the above relationship. Nevertheless the term "law of the wall" has loosely been used to account for relations of the form $U^+ = f(y^+)$, for $0 \leqslant y^+ \leqslant y^+_{\mathrm{crit}}$, with y^+_{crit} being the upper bound of the log-law. The need for a smooth junction between the "linear law of the wall" on one side and the "logarithmic law of the wall" on the other is not only obvious from the desire to describe the mean velocity profile, but also to extract integral quantities from it. Furthermore such relations can readily be used in heat-transfer problems, due to "the relation between the shearing stress at the wall [...] and the heat flux at the wall [...] known under the name of the Reynolds-Analogy" (Kestin & Richardson 1963). Some of the early relations are summarised in Kestin & Richardson (1963), Monin & Yaglom (1971) and Hinze (1975). Here, however, we consider only the more "prominent" descriptions, and assess both, how well they describe the transition region between its two limiting cases, i.e. the linear and logarithmic profile, and their potential for the purpose of determining the wall position.

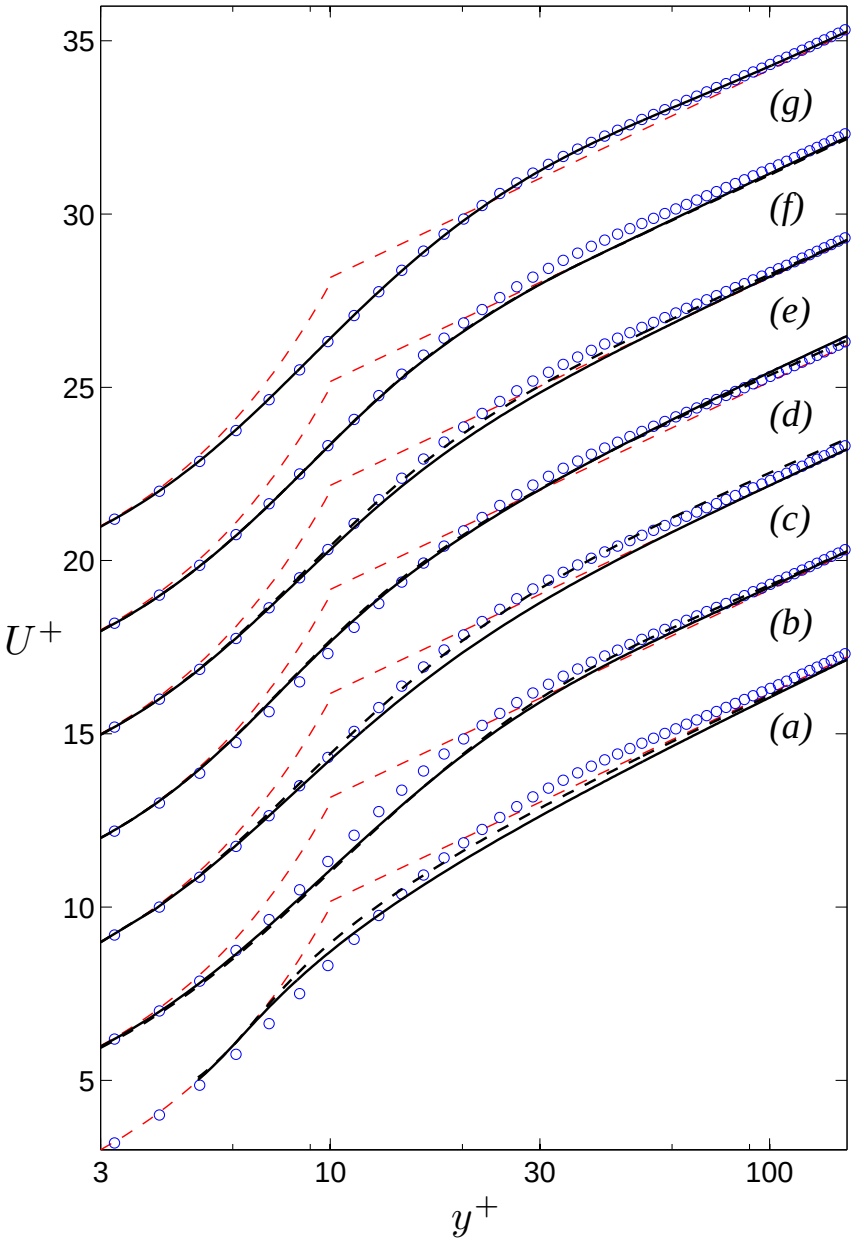

FIGURE 5. Comparison of analytical mean streamwise velocity profiles with the ZPG TBL DNS by Schlatter *et al.* (2009*b*) at $Re_\theta = 2500$ (○). The analytical expressions are computed with their constants given by the corresponding authors (—) and with $\kappa = 0.384$ and $B = 4.17$ (– –), respectively. Light dashed lines indicate the linear and logarithmic profiles (using the aforementioned constants). Analytical expressions after: *(a)* Rotta (1950), *(b)* Reichardt (1951), *(c)* van Driest (1956), *(d)* Spalding (1961), *(e)* Musker (1979), *(f)* Nickels (2004), and *(g)* Chauhan *et al.* (2009). The corresponding expressions can be found in appendix C.

Figure 5 depicts data from a zero pressure-gradient turbulent boundary layer from the DNS by Schlatter *et al.* (2009*b*) at $Re_\theta = 2500$ within the region $3 \leqslant y^+ \leqslant 150$. Overlaid are the analytical expression by *(a)* Rotta (1950), *(b)* Reichardt (1951), *(c)* van Driest (1956), *(d)* Spalding (1961), *(e)* Musker (1979), *(f)* Nickels (2004), and *(g)* Chauhan *et al.* (2009), with their constants given in the corresponding reference (– –) as well as with the log law constants used throughout this paper (—), viz. $\kappa = 0.384$ and $B = 4.17$. Also shown are the linear and log profiles (with the mentioned constants). As expected all of the descriptions asymptote towards the linear and log profile as y^+ tends to zero and infinity, respectively, whereas the upper limit seems already to be fulfilled around $y^+ \approx 150$. While marginally all of the descriptions can be used to describe the mean velocity profile in the inner region quite well, there are apparent differences. While, for instance, the descriptions denoted with *(a)*, *(c)* and *(f)* approach the logarithmic profile monotonically, *(b)* and *(g)* display an overshoot. It is also interesting to point out that neither of the descriptions, except the one by Chauhan *et al.* (2009), which is based on the one by Musker (1979), describes the buffer region represented by the DNS, correctly. Note that the results from the shown ZPG TBL DNS agree fairly well with the highest available Reynolds number DNS from pipe and channel flows (cf. figure 4).[14]

Besides the use of the above mentioned analytical expressions for comparisons with experiments, they have also been used to extend the range of applicability of Preston tubes (Nitsche *et al.* 1983) or to extract the wall skin friction (Szablewski 1954; Kendall & Koochesfahani 2008). Hafez *et al.* (2004), on the other hand, employed the formulation by Reichardt (1951), to determine the wall position. As can be seen from figure 5 the effect of the chosen log constants on the velocity distribution within the buffer region is of varying strength. Nevertheless it is generally assumed that the selected constants are fairly insensitive to the extracted skin friction values (Kendall & Koochesfahani 2008).[15] While the apparent differences are small and negligible in regards of their effect on the extracted friction velocity, it will be shown later on that the determined wall position, is dependent on the chosen relation and the log law constants. This becomes especially important when the measured velocity profiles do not reach into the viscous sublayer or even buffer region as is the

[14]Note that the pipe and channel flow DNS display an even higher overshoot over the log law (with the chosen constants). The description by Chauhan *et al.* (2009) was particularly designed to express this overshoot, based on the ZPG TBL experiments by Österlund (1999) and DNS in canonical wall-bounded flows (see also Monkewitz *et al.* (2007)).

[15]As can be inferred from the selected range of analytical expressions, this conclusion is rather biased by the choice of investigated relations. Kendall & Koochesfahani (2008), for instance, utilised the profiles given by Spalding (1961) and Musker (1979), which are indeed insensitive. The relation by van Driest (1956), on the other hand, shows a stronger influence on the log law constants, with differences into the logarithmic region. Note also, that the differences have not diminished for higher y^+ values; they will become apparent, once the logarithmic region extend over wider y^+ values.

case for most of the high Reynolds number experiments (as for instance those by McKeon 2003; Jones *et al.* 2004; Nagib *et al.* 2004*a*, to mention just a few).

In addition to the above functional forms for the law of the wall, a number of composite velocity profiles have been proposed valid for the entire flow region. Despite the fact, that some of the aforementioned descriptions were intended to describe the entire velocity profile for the case of internal flows, the need for more appropriate relations has been recognised from Rotta (1950) on. One of the first formal descriptions were for instance given by Coles (1956), based on his additional wake function. The composite velocity profile can thus be given as a superposition of the description for the (linear and logarithmic) law of the wall and an additive wake function

$$U^+_{\text{composite}} = U^+_{\text{inner}}(y^+) + \frac{2\Pi}{\kappa}\mathcal{W}\left(\frac{y^+}{\delta^+}\right), \quad 0 \leq y^+ \leq \delta^+, \tag{4}$$

where Π and $\mathcal{W}$ are the so-called wake parameter and wake function, respectively. A number of wake functions have been proposed, of which some have been discussed in Lewkowicz (1982) and Sandham (1991).

The analytical forms of the presented descriptions for the law of the wall is given in appendix E. The use of the mentioned composite mean streamwise velocity profiles is handy and self-consistent when used to extract boundary layer parameters, as for instance, done by Coles (1968) or Chauhan *et al.* (2009). Both authors utilised a composite profile description to extract the boundary layer thickness, δ, the wake parameter, Π, as well as the local skin friciton factor, c_f, from a huge number of experimental velocity profiles, thereby eliminating the subjectivety of the originally provided parameters. Furthermore, this enabled them to compare experimental results from surveys without near-wall data, or an insufficiently resolved wake region. Nevertheless, the success of composite velocity profiles should not overtone their inadequacies, namely that they are based on (advanced) curve fitting, especially in regards of the wake region, or the transition region between the viscous sublayer and the overlap region. Hence, if not sufficient data is available, the results are dictated by the predetermined shape of the velocity profile in the above mentioned regions.

Since, the composite descriptions employ one of the mentioned analytical descriptions for the inner region, they will not be treated separately in the following paper. For the case, that no data is available within the buffer region and the friction velocity is determined accurately prior to the wall position, the employment of a composite profile may serve as a additional restrictor when determining the wall position. However, in the absence of near-wall data, none of the velocity profile descriptions can provide an accurately determined wall position, as will be shown in the next section.[16]

[16]For the case, that no data are available within the buffer region, and the friction velocity as well as the wall position are unknown, the measured data points can be shifted along the log law towards higher U^+ and y^+ values without any physical bounds. Utilisation of

4. Results

4.1. *Employment of the expanded linear velocity profile*

For the following analysis, the expanded linear profile including the forth and fifth order terms in equation (2), as well as the modified Musker profile by Chauhan *et al.* (2009) and the description by Reichardt (1951) willl be used to assess their performance in determining the wall position. The choice for the selected mean velocity descriptions is given by the fact that the linear profile has been treated elsewhere (van Manen *et al.* 1993; Durst *et al.* 1996), and that for most moderate to high Reynolds number experimental investigations quality data is seldom available within the viscous sublayer. The choice for the analytical descriptions by Reichardt (1951) and Chauhan *et al.* (2009), on the other hand, is due to their apparent differences (cf. figure 5) within the buffer region.

Using the DNS by Schlatter *et al.* (2009*b*) for a ZPG TBL under equilibrium conditions, the coefficients as well as the range of validity of equation (2) were obtained by varying the upper limit. By doing so, the following (calibration) coefficients for equation (2) were obtained for the forth and fifth order description, respectively:[17] $\sigma_1 = 7.75 \times 10^{-4}$ as well as $\sigma_1 = 1.18 \times 10^{-3}$ and $\sigma_2 = 0.07 \times 10^{-3}$. Utilising these coefficients, the expanded linear profile can represent the results from the DNS up to $y^+ = 9$ and 15, respectively, within a maximum relative error of 2.5 %, as shown in the insert in figure 3. The mentioned error is deemed accebtable, when considering the widely accepted range for the linear profile, which is commonly believed to be valid up to $y^+ = 4.5$–5.

Figure 6 depicts the relative differences between the extracted wall positions by means of equation (2) with the above given constants and the originally given ones. Use was made of the DNS data sets by Schlatter *et al.* (2009*b*) at $Re_\theta = 2500$ (dash-dotted) and Ferrante & Elghobashi (2005) at $Re_\theta = 2900$ (dotted), as well as the experiments by Örlü (2009*a*) at $Re_\theta = 2532$ (solid) & 3640 (dashed). To test the sensibility of the procedure to the number of measured or simulated data points within the sublayer, the closest point to the wall (indicated through $y^+_{1^{\text{st}}}$) was successively removed. Additionally the 50 % confidence interval for the determined wall position is given, indicated by the shaded areas. The retrieved wall positions for the DNS data sets lie always within 0.1 wall units from the originally given ones. Hence the extended linear profile to forth or fifth order, figure 6 *(a)* and *(b)*, respectively, is capable of recovering the correct wall position. For the case of experimental data sets,

a least squares method, would in that case not guarantee that the friction velocity or wall position obtained from a best fit, would physically be meaningful. Only, in the case of a known friciton velocity, or available near wall data, would a least squares method be able to provide a "best fitted" solution, which is restricted by physical bounds.

[17] Although the given values are rounded, they were employed as given and not with their actual values.

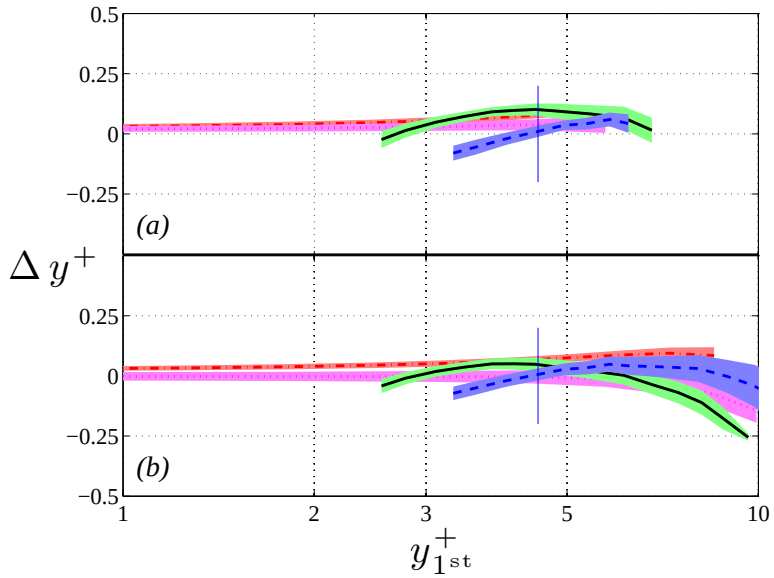

FIGURE 6. Obtained offset, Δy^+, in the wall position by employing equation (2) including the *(a)* 4th and *(b)* 5th order term as a function of the first utilised point, $y^+_{1\mathrm{st}}$, with fixed u_τ. DNS by Schlatter *et al.* (2009*b*) at $Re_\theta = 2500$ (dash-dotted) and Ferrante & Elghobashi (2005) at $Re_\theta = 2900$ (dashed). Experiments by Örlü (2009*a*) at $Re_\theta = 2532$ (solid) & 3640 (dashed) with $L^+ = 15$ & 21, respectively. Shaded areas indicate a 50 % confidence interval, and the vertical solid line indicate the position to which near-wall effects are detected by use of the diagnostic profile (Alfredsson *et al.* 2009).

where accurate data points within the viscous sublayer are scarce, the ability of the extended velocity profile descriptions is also demonstrated. The deviation from the given and retrieved wall positions is in the worst case still within 0.25 wall units, which corresponds to around 6 micron.[18] The vertical solid line indicates the position from where on the measurements are believed to be free of near-wall effects (e.g. additional heat losses to the wall or aerodynamic blockage) based on the mean and rms streamwise velocity readings from the hot-wire based on the diagnostic plot (Alfredsson *et al.* 2009). The indicated position is independent of the friction velocity and the wall position and gives a

[18]The wall positions given in Örlü (2009*a*) were corrected for by means of the composite velocity profile employing the modified Musker profile (Chauhan *et al.* 2009) for the inner region. Hereby all measurements points (reaching for most cases into the viscous sublayer) excluding those effected by near-wall effects, were employed.

quick (i.e. without having the need to ponder about the accuracy of the determined wall position or the friction velocity) indication, which near-wall points should be neglected when using near-wall data to compute the wall position.

Coming back to figure 3, it becomes apparent that a single indicative point within the transitional region (i.e. between the viscous sublayer and the overlap region) to ensure an accurately determined friction velocity and wall position is—to say the least—misleading. Not only are Reynolds number effects important at low Reynolds numbers (Wei *et al.* 2005), but also can a combination of a wrongly deduced friction velocity and wall position give a seemingly correct point in a U^+ vs. y^+ plot. In their well-known study regarding the scaling of the bursting frequency at $y^+ = 15$ Blackwelder & Haritonidis (1983) state regarding their deduced wall position, that from "the mean-velocity profiles [...] it is ascertained that the mean velocity at $y^+ = 15$ was 12 u_τ. This criterion was used for locating $y^+ = 15$ when recording the bursting-frequency data, giving a maximum error of $\Delta y^+ = \pm\ 2$ at all Reynolds numbers used in the investigation." In other words, $y^+ = 15$ is found by locating the position, were $U^+ = 12$.[19] Additionally they determined the friction velocity from a fit to the linear profile, which, in their case, extends up to around $y^+ = 11$. This also explains, why they obtained a Reynolds number dependent underestimation of the friction velocity between 10 and 25 % compared to those obtained from a fit to the logarithmic region. Note, that the application of the Clauser method with classical log law constants leads generally to an overestimation of the friction velocity (cf. Tropea *et al.* 2007, chap. 12), and that the accuracy improves with higher Reynolds number, due to the longer extent of the logarithmic region (Kendall & Koochesfahani 2008). However, the extracted values by Blackwelder & Haritonidis show consistently the opposite trend, i.e. the difference between the values obtained from both methods increase with increasing Reynolds number. Consequently, their conclusions regarding the scaling of the bursting frequency and their proposed frequency correction relation (used for instance by Wark & Nagib 1990) are to be considered with caution.

4.2. *Employment of analytical mean velocity descriptions for the "law of the wall"*

While it is advisable to utilise solely near wall data to extract the wall position, this is barely possible for most of the moderate to high Reynolds number experiments. Hence the need to employ data outside the viscous sublayer becomes necessary. Since the ZPG TBL database of Österlund (1999) is supplemented by direct and independent skin friction measurements, it has over the last decade extensively been used to test scaling laws as well as to test methods

[19] Although they contradict themselves in one of their footnotes, by stating, "that, at $y^+ = 15$, U/u_τ was typically 10.5 in agreement with previous results.", their shown figure reveals that U^+ at $y^+ = 15$ was for the entire range of Reynolds numbers investigated between 11.5 and 13.5.

to extract the friction velocity. In a recent work by Kendall & Koochesfahani (2008), the data has been used to illustrate that the employment of analytical descriptions for the law of the wall can "be estimated very accurately from mean velocity measurements over a large ra[n]ge of [...] cutoff values with a mean error that is better than 0.5 % in friction velocity (or 1 % in shear stress), an accuracy comparable to that from independent direct measurements of wall shear stress".[20] Although, their primary intention was to assess the accuracy of the estimated friction velocity, they also comment on the possibility to estimate the wall position. In this context they state: "The optimization routine was performed [...] on the entire Österlund database, allowing for (possible) non-zero y_0 [wall position] in the reported data. The mean wall location that was recovered was within the $\pm$ 5 μm reported accuracy of the actual wall location." This would correspond to a maximum accuracy of $\pm$ 0.15 to 0.7 wall units for the entire database of Österlund (1999) depending on the viscous length scale.

In the following, two selected velocity profiles from the database of Österlund (1999) at $Re_\theta = 6624$ and 27320 with a corresponding wire length of $L^+ = 13$ and 60, respectively, were selected to test the performance of the modified Musker profile by Chauhan *et al.* (2009) and the analytical profile by Reichardt (1951). The results with a predetermined or fixed u_τ are shown in figure 7, whereas those with a variable u_τ and wall position are given in figure 8.[21] Contrary to the results from the DNS presented in figure 6, where the wall position is given by definition, in the case of experimental data, this is not guaranteed. Therefore, the determined offset from the given wall position is rather an relative deviation from the original wall position, and not, as in the case of the DNS data sets, a relative error.

Based on the results from Kendall & Koochesfahani (2008) one would expect highly accurate estimates of the friction velocity independent of the number of measurement points available. Their mentioned possibility to extract the wall position as well to a high accuracy, is however not further investigated. Furthermore their result is biased, at least when it comes to the determination of the wall position, due to the fact that they assess the performance of their method as a function of excluded measurement points by keeping the points closest to the wall. A more representative procedure would be to keep the measurement points within the overlap region and skip data points from the wall on, since this would give an idea how close to the wall one has to measure in order to accurately determine the absolute wall position. This is the procedure

[20] The same authors, based on the identical presented results conclude in an earlier version of their paper (Kendall & Koochesfahani 2006): "We note the remarkable accuracy with which the friction factor is estimated over a large range [...], with a mean error that is better than 1 % (or 2 % for wall shear)."

[21] The determined u_τ values are given in appendix D.

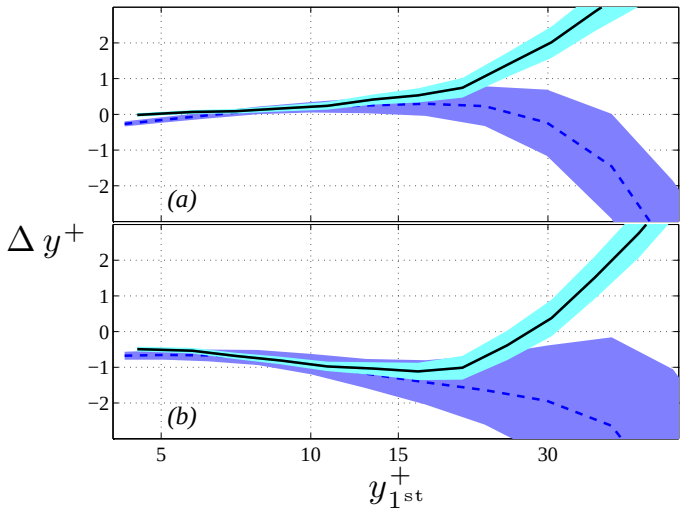

FIGURE 7. Obtained offset, Δy^+, in the wall position by employing the *(a)* modified Musker profile (Chauhan *et al.* 2009) and *(b)* the analytical profile by Reichardt (1951) as a function of the first utilised point, $y^+_{1\mathrm{st}}$, with fixed (original) u_τ. Experiments by Österlund (1999) at $Re_\theta = 6624$ (solid) & 27320 (dashed) with $L^+ = 13$ & 60, respectively. Shaded areas indicate a 50 % confidence interval.

adapted throughout the present paper and gives results in accordance with expectation, viz. the closer to the wall one is able to measure the more accurate becomes the extracted wall position. Figure 7 reveals that with measurement points as close as 10 wall units the determined wall position independent of the selected analytical description can be found within one wall unit.[22] For the case that no near-wall data within the sublayer are available the extracted wall position depends heavily on the selected analytical description as well as the accuracy of the mean velocity profile. Since it is unlikely that Reynolds number effects are causing the encountered differences within the buffer region, spatial resolution may explain the deviations within the buffer region as argued

[22]The chosen analytical profiles for the analysis presented here have been selected from the ones depicted in figure 5, and were found to display the largest differences (with the exception of the one by Rotta (1950). Hence the shown results can be considered to be representative for a wide range of analytical profiles.

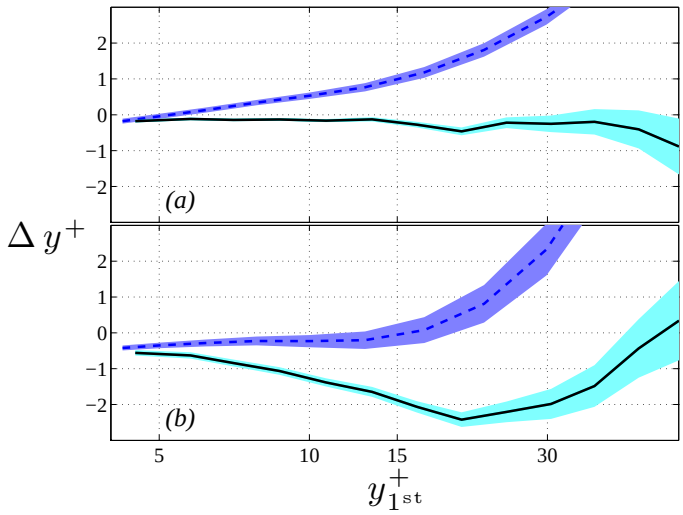

FIGURE 8. Same as figure 7, but Δy^+ obtained together with u_τ from the same least-squares fit.

by Örlü (2009*b*).[23] It can also be inferred that the profile with $L^+ = 60$ has a higher uncertainty in the determined wall position.

Since in most of the experimental investigations, especially in the case of ZPG TBLs, the friction velocity is neither determined independently, nor direct, hence it is important to check the influence of an undetermined friction velocity. Figure 8 shows therefore the same analysis, but this time with Δy^+ and u_τ being "fitting parameters". A gratifying result is, that as long as near-wall data reaching the viscous sublayer are available, the determined wall position for all four cases is within 0.5 wall units independent of the analytical description or the fact whether or not the friction velocity was measured or determined during post-processing of the data. It will, however, later on be shown, that this can unfortunately not be said for the determined friction velocity.

It is interesting to note that utilisation of the modified Musker profile on the profile with $L^+ = 13$ gives an unchanged wall position even when the first measured point is clearly within the buffer region. This may, however, be an artifact of the fact the the modified Musker profile was designed to represent DNS and the Österlund data. However, the same can not be said about the profile measured with the longer wire. Note also the opposing trends of the

[23] Note that Reynolds number effects are likely to occur at rather low Reynolds numbers. The shown region in figure 7 extends up to $y^+ = 55$, hence one would not expect the wake region to interfere for Re_τ >1000, for the shown profiles, nor for the entire database of Österlund (1999).

determined wall positions depending on whether or not the friction velocity was given or extracted from the fit. Hence it can be concluded, that only for profiles with measurement points within 10 wall units can the wall position be determined within an accuracy of one wall unit. This accuracy is not based on the absolute given position by Österlund (1999), but on the relative deviation of the determined positions, for all used analytical descriptions and regardless of how the friction velocity was determined. For the case, that no near-wall data are available, the extracted wall position is highly dependent on the chosen analytical function, the measured or determined friction velocity, as well as how close to the wall one measures or how many measurement points one includes in the fitting procedure.

Consequently, the possibility to determine the wall position accurately within $\pm$ 0.15 to 0.7 as claimed by Kendall & Koochesfahani (2008), is only true if, and only if, measurement points as close as 5 wall units are available.[24] This was not observed by Kendall & Koochesfahani (2008), since they assessed the performance of their method entirely on the fact that near-wall data reaching the viscous sublayer were available. This deficiency will also reflect itself on their conclusions for the determined friction velocity (see also appendix D, where the same procedure was performed on the extracted friction velocity).

5. Summary and Conclusions

It is widely accepted that mean quantities within the inner region of wall-bounded turbulent flows scale on viscous units. Having said that, it consequently follows, that the mean velocity has to be scaled by the friciton velocity and the wall-normal distance by the viscous length scale. While the importance of an independent and/or direct measure of the skin friction has recently widely been accepted, the possibility of a wrongly measured or deduced wall position has—to our knowledge—not been considered.

A review on commonly used measurement techniques to determine the wall position in experimental studies has shown, that the accuracies vary within an order of magnitude. Furthermore, the possibility of deflections of the measurement instruments have not always be considered. Despite a number of known post-processing methods to dedude (or correct for) the absolute wall position, a number of pecularities have been shown to exist. The linear velocity profile for the streamwise velocity component has, for instance, been applied for wall positions, where it does not even provide an engineering approximation. Similarly, the Taylor expanded linear profile has been calibrated against low Reynolds number DNS and applied to experiments to higher Reynolds numbers. The law of the wall as well as analytical descriptions from the wall to the overlap region or the entire profile have been utilised to determine the friction

[24] In fact, for all velocity profiles in the database of Österlund (1999), the first measured points was within 4 and 5.5 wall units.

velocity as well as wall position. A thorough review has been given to the above mentioned methods and attention has been drawn to a number of pitfalls.

The expanded law of the wall to forth and fifth order with calibration constants determined from recent high Reynolds number DNS has shown to be a promising post-processing tool to determine the wall position to a high accuracy. Accuracies of around 0.1 and 0.25 ℓ_* have been obtained for the latter method when accurately determined measurements reaching $y^+ = 5$ and 10, respectively, are available.

For the case that the viscous sublayer can not be accessed experimentally, a variety of analytical descriptions can be utilised to extract the wall position. However, the choice of the analytical function as well as its describing constants, has been found to effect the determined wall position to a high degree. Nevertheless, an accuracy independent of analytical description, of around one wall unit can be expected whenever measurement points as close as 10 wall units are available.

The state of the art understanding in wall-bounded turbulent flows, including recent DNS and quality experiments, is not in the position to declare a correct mean streamwise velocity profile within the buffer region. Reynolds number effects are present at low Reynolds numbers and make it therefore difficult to extrapolate DNS results to higher Reynolds numbers. Experiments on the other hand, suffer from spatial resolution issued, non-linearities, uncertainties in the wall position and the friction velocity, and are not conclusive regarding correction methods for Pitot tube measurements. Hence there is no ultimate profile valid for all experiments within the buffer region, to which experimental data can be fitted. Even if this would be the case and an universal profile could be defined, each measurement would be different from the universal one, due to its own shortcomings. Hence, one would again try to fit different profiles to each other. In the absence of any other alternative, near-wall measurements below $y^+ = 10$ or preferable 5 are essential in order to ensure a correct representation of the profiles.

In light of the above said, it is desirable that future studies consider to document the way in which the wall position was measured/deduced or corrected for, in a more thorough way. It may seem that some of the aspects of the present paper appear overemphasised. However, keeping in mind that Pitot tube corrections alter the log law constants by a few percent, and various methods to determine the friction velocity mask or introduce Reynolds number effects, there is no argument why a wrong wall position of a few wall units should not be considered. Furthermore the available literature gives the impression as if the determination of the wall position is free of any difficulty.[25] In the same time, hot-wire measurements by Morrison *et al.* (2004) with relatively

[25]So, for instance, gives Mochizuki & Nieuwstadt (1996), a value of 14.4+0.00017 Re_θ and 14.6+0.00020 Re_θ for the location of the near-wall peak in the streamwise rms distribution

short wires (for their lower Reynolds number range) show clear deviations from the generally accepted peak position of $y^+ \approx 15$.[26] Their rms near-wall peak is around 18.7 for $Re_\tau = 1500$, while it moves to around 16.1 for $Re_\tau = 1820$. The wire length in viscous units is around 12 in the former and 14 for the latter and should therefore not be effected by spatial resolution effects. While an overestimated friction velocity for the lower Reynolds number case may explain the observed peculiarity, another possibility could be a wrongly deduced wall position. Similarly high Reynolds number experiments in TBL flows at high free stream velocities, as those by Fernholz *et al.* (1995) and Knobloch & Fernholz (2004), depict a strong deviation from the log law, viz. they fall under the log law already a few hundred wall positions away from the wall.[27] Despite the proposed methods to correct for the wall position, the location of the near wall peak in the streamwise rms distributions, for measurements without spatial and temporal resolution issues, may serve as an additional indication for a correctly deduced wall position.

Another example, where a wrongly deduced wall position should be considered, is for instance the debate regarding an explicit turbulence correction for Pitot tubes. While McKeon *et al.* (2003) argues that there is no need for such a correction, based on a deviation of around a half wall unit, Monty (2005) notes that an error in the wall position "would completely account for the observed deviation in the viscous sublayer region".

While most of the mentioned peculiarities and controversies have previously not been associated with inaccuracies in the determined wall position, the present investigation shows that this may be a rather good candidate to explain the observed peculiarities.

Acknowledgement

The author has made use of the following databases: Data-Base of Turbulence and Heat Transfer (supported by the Ministry of Education Science and Culture in Japan), DNS Data Base for Wall Turbulence and Heat Transfer (Kawamura Lab, Laboratory of Thermo-fluid dynamics), Turbulence Database (AFM Research Group, School of Engineering Sciences, University of Southampton), the AGARD database for test-cases for LES, the DNS databases of Professors Wu and Moin (CTR, Stanford University) and Jiménez (E.T.S.I. Aeronáuticos,

for ZPG TBL and internal flows, respectively. Their results are based on 47 collected experiments. While the method with which the friction velocity was determined is given in their paper, the method or accuracy of the determined wall position is not considered at all.

[26] The DNS databases used in the present paper, albeit of low Reynolds number, indicate no conclusive Reynolds number trends. For $Re_\tau > 500$, the peak position resides within 14 and 15 wall units.

[27] Knobloch (2008) remarks, that an error of 20 wall units, corresponding to 0.1 mm, would account for the deviation in his highest Reynolds number case. Nevertheless, these data sets are often employed to test various scaling laws, be it for the mean velocity profile, or the Reynolds stresses (Buschmann *et al.* 2008).

Universidad Politécnica de Madrid). Dr. J. Österlund is thanked for making available his experimental data sets, and Doctors P. Ferrante and P. Schlatter for providing their DNS data through personal communication.

References

Abe, H., Kawamura, H. & Matsuo, Y. 2001 Direct numerical simulation of a fully developed turbulent channel flow with respect to the Reynolds number dependence. *J. Fluid Eng.* **123**, 382–393.

Abe, H., Kawamura, H. & Matsuo, Y. 2004 Surface heat-flux fluctuations in a turbulent channel flow up to $Re_\tau = 1020$ with $Pr = 0.025$ and 0.71. *Int. J. Heat Fluid Flow* **25**, 404–419.

Abell, C. J. 1974 Scaling laws for pipe flow turbulence. *Ph. D. thesis, University of Melbourne, Australia*.

Acharya, M. & Escudier, M. 1983 Measurements of the wall shear stress in boundary-layer flows. *Proc. 4th Symp. Turbulent Shear Flows, Karlsruhe, West Germany*, pp. 277–286.

del Álamo, J. & Jiménez, J. 2003 Spectra of the very large anisotropic scales in turbulent channels. *Phys. Fluids* **15**, L41–L44.

del Álamo, J., Jiménez, J., Zandonade, P. & Moser, R. D. 2004 Scaling of the energy spectra of turbulent channels. *J. Fluid Mech.* **500**, 135–144.

Alfredsson, P. H. & Johansson, A. V. 1984 On the detection of turbulence-generating events. *J. Fluid Mech.* **139**, 325–345.

Alfredsson, P. H., Johansson, A. V., Haritonidis, J. H. & Eckelmann, H. 1988 The fluctuating wall?shear stress and the velocity field in the viscous sublayer. *Phys. Fluids.* **31**, 1026–1033.

Alfredsson, P. H., Örlü, R., Kurian, T., Fransson, J. H. M., Segalini, A., Rüedi, J.-D. & Talamelli, A. 2009 The diagnostic plot - a new way to appraise turbulent boundary layer data. *Proc. 12th European Turbulence Conference, Marburg, Germany*.

Antonia, R. A., Bisset, D. & Browne, L. 1990 Effect of Reynolds number on the topology of the organized motion in a turbulent boundary layer. *J. Fluid Mech.* **213**, 267–286.

Azad, R. & Burhanuddin, S. 1983 Measurements of some features of turbulence in wall-proximity. *Exp. Fluids* **1**, 149–160.

Barenblatt, G. I. & Chorin, A. 1998 New perspectives in turbulence: Scaling laws, asymptotics, and intermittency. *SIAM Review* **40**, 265–291.

Benson, M. J. & Eaton, J. 2003 The effects of wall roughness on the particle

velocity field in a fully developed channel flow. *Stanford University, Report No. TSD-150*.

Bernard, P. & Wallace, J. 2002 Turbulent flow: Analysis, measurement, and prediction. *Wiley*.

Bhatia, J., Durst, F. & Jovanovic, J. 1982 Corrections of hot-wire anemometer measurements near walls. *J. Fluid Mech.* **123**, 411–431.

Blackwelder, R. & Haritonidis, J. 1983 Scaling of the bursting frequency in turbulent boundary layers. *J. Fluid Mech.* **132**, 87–103.

Bradshaw, P. & Huang, G. 1995 The law of the wall in turbulent flow. *Proc. Math. Phys. Sci.* **451**, 165–188.

Bradshaw, P., Launder, B. E. & Lumley, J. L. 1992 Collaborative testing of turbulence models. *AIAA 1991-0215*.

Brücker, C., Spatz, J. & Schröder, W. 2005 Feasability study of wall shear stress imaging using microstructured surfaces with flexible micropillars. *Exp. Fluids.* **39**, 464–474.

Bruun, H. H. 1995 Hot-wire anemometry: Principles and signal analysis. *Oxford University Press Inc., New York, USA*.

Buschmann, M. H. & Gad-el-Hak, M. 2003*a* Debate concerning the mean-velocity profile of a turbulent boundary layer. *AIAA J.* **41**, 656–572.

Buschmann, M. H. & Gad-el-Hak, M. 2003*b* Generalized logarithmic law and its consequences. *AIAA J.* **41**, 40–48.

Buschmann, M. H. & Gad-el-Hak, M. 2006 Recent developments in scaling of wall-bounded flows. *Prog. Aero. Sci.* **42**, 419–467.

Buschmann, M. H., Indinger, T. & Gad-el-Hak, M. 2008 Near-wall behaviour of turbulent wall-bounded flows *AIAA 2008-4236*.

Cenedese, A., Romano, G. P. & Antonia, R. A. 1998 A comment on the "linear" law of the wall for fully developed turbulent channel flow. *Exp. Fluids* **25**, 165–170.

Chauhan, K. A., Monkewitz, P. A. & Nagib, H. M. 2009 Criteria for assessing experiments in zero pressure gradient boundary layers. *Fluid Dyn. Res.* **41**, 021404.

Chew, Y., Shi, S. & Khoo, B. 1995 On the numerical near-wall corrections of single hot-wire measurements. *Int. J. Heat Fluid Flow* **16**, 471–476.

Ching, C., Djenidi, L. & Antonia, R. A. 1995 Low-Reynolds-number effects in a turbulent boundary layer. *Exp. Fluids* **19**, 61–68.

Clauser, F. H. 1954 Turbulent boundary layers in adverse pressure gradients. *J. Aero. Sci.* **21**, 91–108.

Coles, D. E. 1956 The law of the wake in the turbulent boundary layer. *J. Fluid Mech.* **1**, 191–226.

Coles, D. E. 1968 The young person's guide to the data. *AFOSR-IFP-Stanford Conf. on Computation of turbulent boundary layers, D. E. Coles and E. A. Hirst (Eds.)*, pp. 1–45.

Comte-Bellot, G., Strohl, A. & Alcaraz, E. 1971 On aerodynamic disturbances caused by single hot-wire probes. *J. Appl. Mech.* **93**, 767–774.

DeGraaff, D. B. 1999 Reynolds number scaling of the turbulent boundary layer on

a flat plate and on swept and unswept bumps. *Ph. D. thesis, Stanford University, USA*.

van Driest, E. 1956 On turbulent flow near a wall. *J. Aero. Sci.* **23**, 1007–1011.

Durst, F., Jovanovic, J. & Kanevce, L. 1987 Probability density Distribution in turbulent wall boundary-layer flows. *Turbulent Shear Flows 5, F. Durst et al. (Eds.), Springer-Verlag*, pp. 197–220.

Durst, F., Jovanovic, J. & Sender, J. 1995 LDA measurements in the near-wall region of a turbulent pipe flow. *J. Fluid Mech.* **295**, 305–335.

Durst, F., Kikura, H., Lekakis, I., Jovanovic, J. & Ye, Q. 1996 Wall shear stress determination from near-wall mean velocity data in turbulent pipe and channel flows. *Exp. Fluids* **20**, 417–428.

Durst, F., Müller, R. & Jovanovic, J. 1988 Determination of the measuring position in laser-Doppler anemometry. *Exps. Fluids* **6**, 105–110.

Durst, F., Zanoun, E. S. & Pashtrapanska, M. 2001 In situ calibration of hot wires close to highly heat-conducting walls. *Exps. Fluids* **31**, 103–110.

Eckelmann, H. 1974 The structure of the viscous sublayer and the adjacent wall region in a turbulent channel flow. *J. Fluid Mech.* **65**, 439–459.

Erm, L. P. & Joubert, P. 1991 Low-Reynolds-number turbulent boundary layers. *J. Fluid Mech.* **230**, 1–44.

Fage, A. & Townend, H. 1932 An examination of turbulent flow with an ultramicroscope. *Proc. R. Soc. London, Ser. A* **135**, 656–677.

Fernholz, H. H., Krause, E., Nockemann, M. & Schober, M. 1995 Comparative measurements in the canonical boundary layer at $\mathrm{Re}_{\delta_2} \leqslant 6 \times 10^4$ on the wall of the German–Dutch windtunnel. *Phys. Fluids* **7**, 1275–1281.

Fernholz, H. H. & Finley, P. 1996 The incompressible zero-pressure-gradient turbulent boundary layer: An assessment of the data. *Prog. Aero. Sci.* **32**, 245–311.

Fernholz, H. H., Janke, G., Schober, M. & Wagner, P. 1996 New developments and applications of skin-friction measuring techniques. *Meas. Sci. Tech.* **7**, 1396–1409.

Ferrante, A. & Elghobashi, S. E. 2005 Reynolds number effect on drag reduction in a microbubble-laden spatially developing turbulent boundary layer. *J. Fluid Mech.* **543**, 93–106.

Gad-el-Hak, M. 2000 Flow control: passive, active, and reactive flow management. *Cambridge University Press.*

George, W. K. 2007 Is there a universal log law for turbulent wall-bounded flows? *Phil. Trans. R. Soc. A* **365**, 789–806.

George, W. K. & Castillo, L. 1997 Zero-pressure-gradient turbulent boundary layer. *Appl. Mech. Rev.* **50**, 689–730.

Gersten, K. & Herwig, H. 1992 Strömungsmechanik: Grundlagen der Impuls-, Wärme- und Stoffübertragung aus asymptotischer Sicht. *Vieweg Verlag.*

Grosse, S. 2008 Development of the micro-pillar shear-stress sensor MPS3 for turbulent flows. *Ph. D. thesis, RWTH Aachen, Germany*.

Grosse, S. & Schröder, W. 2008 Mean wall-shear stress measurements using the micro-pillar shear-stress sensor MPS3. *Meas. Sci. Tech.* **19**, 015403.

Hafez, S., Chong, M. S., Marusic, I. & Jones, M. B. 2004 Observations on high Reynolds number turbulent boundary layer measurements. *Proc. 15th Australasian Fluid Mech. Conf., Sydney, Australia*.

Hinze, J. O. 1975 Turbulence. *McGraw-Hill, 2nd. Ed.*

Hites, M. H. 1997 Scaling of high-Reynolds number turbulent boundary layers in the National Diagnostic Facility. *Ph. D. thesis, Illinois Institute of Technology, USA*.

Hoyas, S. & Jiménez, J. 2006 Scaling of the velocity fluctuations in turbulent channels up to Re=2003. *Phys. Fluids* **18**, 011702.

Hu, Z. W. & Sandham, N. D. 2001 DNS databases for turbulent Couette and Poiseuille flow. *Report AFM-01/04, Aerodynamics and Flight Mechanics Group, School of Engineering Sciences, University of Southampton, UK*.

Hutchins, N. & Choi, K. 2002 Accurate measurements of local skin friction coefficient using hot-wire anemometry. *Prog. Aero. Sci.* **38**, 421–446.

Iwamoto, K., Suzuki, Y. & Kasagi, N. 2002 Reynolds number effect on wall turbulence: toward effective feedback control. *Int. J. Heat Fluid Flow* **23**, 678–689.

Janke, G. 1987 Hot wire in wall proximity. *Advances in Turbulence, Vol. I, Springer* pp. 488–498.

Jirka, G. 2007 Einführung in die Hydromechanik. *Universitätsverlag Karlsruhe*.

Jones, M. B., Nishizawa, N., Chong, M. S. & Marusic, I. 2004 Scaling of the turbulent boundary layer at high reynolds numbers. *IUTAM Symposium on Reynolds Number Scaling in Turbulent Flow. A. J. Smiths (Ed.), Kluwer Academic Publisher* pp. 271–278.

Karlsson, R. I. 1980 Studies of skin friction in turbulent boundary layers on smooth and rough walls. *Ph. D. thesis, Chalmers University of Technology, Göteborg, Sweden*.

von Kármán, T. 1930 Mechanische Ähnlichkeit und Turbulenz. *Proc. Proc. 3rd International Congress on Applied Mechanics, Stockholm, Sweden*, pp. 85–93.

von Kármán, T. 1967 The wind and beyond: Theodore von Kármán. Pioneer in aviation and pathfinder in space. *Little, Brown and Company, Canada*.

Kawamura, H., Abe, H. & Matsuo, Y. 1999 DNS of turbulent heat transfer in channel flow with respect to Reynolds and Prandtl number effects. *Int. J. Heat Fluid Flow* **20**, 196–207.

Kendall, A. & Koochesfahani, M. 2006 A method for estimating wall friction in turbulent boundary layers. *AIAA 2006-3834*.

Kendall, A. & Koochesfahani, M. 2008 A method for estimating wall friction in turbulent wall-bounded flows. *Exp. Fluids* **44**, 773–780.

Kestin, J. & Richardson, P. D. 1963 Heat transfer across turbulent, incompressible boundary layers. *Int. J. Heat Mass Transfer* **6**, 1–43.

Khujadze, G. & Oberlack, M. 2007 New scaling laws in ZPG turbulent boundary layer flow. *Proc. 5th Int. Symp. on Turbulence and Shear Flow Phenomena, München, Germany*.

Klewicki, J. C. & Falco, R. 1990 On accurately measuring statistics associated

with small-scale structure in turbulent boundary layers using hot-wire probes. *J. Fluid Mech.* **219**, 119–142.

Knobloch, K. 2008 Skalierungen und Zweipunkt-Geschwindigkeitskorrelationen in turbulenten Grenzschichten bei großen Reynoldszahlen. *Ph. D. thesis, Technical University Berlin, Germany*.

Knobloch, K. & Fernholz, H. H. 2004 Statistics, correlations, and scaling in a turbulent boundary layer at Re 115000. *IUTAM Symposium on Reynolds Number Scaling in Turbulent Flow. A. J. Smiths (Ed.), Kluwer Academic Publisher*, pp. 11–16.

Krishnamoorthy, L., Wood, D. & Antonia, R. A. 1985 Effect of wire diameter and overheat ratio near a conducting wall. *Exp. Fluids* **3**, 121–127.

Kunze, S., Chaves, H. & Brücker, C. 2008 Mirror particle-tracking-velocimetry in a strip-coded light-sheet: a new method to determine the wall-shear-stress field. *Exp. Fluids* **45**, 573–581.

Lanspeary, P. V. 1988 HEstablishing very low speed, disturbance-free flow for anemometry in turbulent boundary layers. *Ph. D. thesis, University of Adelaide, Australia*.

Lewkowicz, A. K. 1982 An improved universal wake function for turbulent boundary layers and some of its consequences. *Z. Flugwiss. Weltraumforsch.* **6**, 261–266.

Lindgren, B., Johansson, A. V. & Tsuji, Y. 2004 Universality of probability density distributions in the overlap region in high Reynolds number turbulent boundary layers. *Phys. Fluids* **16**, 2587–2591.

Lomas, C. G. 1986 Fundamentals of hot wire anemometry. *Cambridge University Press*.

van Manen, A. S., van Geloven, A., Nieuwenhuizen, J., Stouthart, J. C., Prasad, K. K. & Nieuwstadt, F. T. M. 1993 Friction velocity and virtual origin estimates for mean velocity profiles above smooth and triangular riblet surfaces. *Appl. Sci. Res.* **50**, 233–254.

McKeon, B. 2003 High Reynolds number turbulent pipe flow. *Ph. D. thesis, Princeton University, USA*.

McKeon, B., Li, J. D., Jiang, W., Morrison, J. F. & Smits, A. J. 2003 Pitot probe corrections in fully developed turbulent pipe flow. *Meas. Sci. Tech.* **14**, 1449–1458.

McKeon, B., Li, J. D., Jiang, W., Morrison, J. F. & Smits, A. J. 2004 Further observations on the mean velocity distribution in fully developed pipe flow. *J. Fluid Mech.* **501**, 135–147.

Millikan, C. B. 1938 A critical discussion of turbulent flows in channels and circular tubes. *Proc. 5th International Congress on Applied Mechanics, Cambridge, MA, USA* pp. 386–392.

Mochizuki, S. & Nieuwstadt, F. T. M. 1996 Reynolds-number-dependence of the maximum in the streamwise velocity fluctuations in wall turbulence. *Exp. Fluids* **21**, 218–226.

Monin, A. S. & Yaglom, A. M. 1971 Statistical fluid mechanics: Mechanics of turbulence. Vol. I. *MIT Press, Cambridge, Massachusetts*.

Monkewitz, P. A., Chauhan, K. A. & Nagib, H. M. 2007 Self-consistent high-Reynolds-number asymptotics for zero-pressure-gradient turbulent boundary layers. *Phys. Fluids* **19**, 115101.

Monkewitz, P. A., Chauhan, K. A. & Nagib, H. M. 2008 Comparison of mean flow similarity laws in zero pressure gradient turbulent boundary layers. *Phys. Fluids* **20**, 105102.

Monty, J. P. 2005 Developments in smooth wall turbulent duct flows. *Ph. D. thesis, University of Melbourne, Australia*.

Morrison, J. F., McKeon, B., Jiang, W. & Smits, A. J. 2004 Scaling of the streamwise velocity component in turbulent pipe flow. *J. Fluid Mech.* **508**, 99–131.

Moser, R. D., Kim, J. & Mansour, N. 1999 Direct numerical simulation of turbulent channel flow up to $Re_\tau = 590$. *Phys. Fluids* **11**, 943–945.

Musker, A. J. 1979 Explicit expression for the smooth wall velocity distribution in a turbulent boundary layer. *AIAA J.* **17**, 655–657.

Nagib, H. M. & Chauhan, K. A. 2008 Variations of von Kármán coefficient in canonical flows. *Phys. Fluids* **20**, 101518.

Nagib, H. M., Christophorou, C. & Monkewitz, P. A. 2004*a* High Reynolds number turbulent boundary layers subjected to various pressure-gradient conditions. *IUTAM Symposium on one hundred years of boundary layer research, G. E. A. Meier and K. R. Sreenivasan (Eds.), Göttingen, Germany,* pp. 383–394.

Nagib, H. M., Christophorou, C., Rüedi, J.-D., Monkewitz, P. A. & Österlund, J. M. 2004*b* Can we ever rely on results from wall-bounded turbulent flows without direct measurements of wall shear stress? *AIAA 2004-2392*.

Naughton, J. & Sheplak, M. 2002 Modern developments in shear-stress measurement. *Prog. Aero. Sci.* **38**, 515–570.

Nickels, T. B. 2004 Inner scaling for wall-bounded flows subject to large pressure gradients. *J. Fluid Mech.* **521**, 217–239.

Nitsche, W., Thünker, R. & Haberland, C. 1983 A computational Preston tube method. *Symposium on Turbulent Shear Flows, 4th, Karlsruhe, West Germany,* pp. 261–276.

Oertel, H., Böhle, M. & Dohrmann, U. 2006 Strömungsmechanik: Grundlagen, Grundgleichungen, Lösungsmethoden, Softwarebeispiele. *Viewig*.

Örlü, R. 2009*a* Low Reynolds number zero pressure-gradient equilibrium turbulent boundary-layer experiments. *Ph. D. thesis, Royal Institute of Technology, Stockholm, Paper 4* .

Örlü, R. 2009*b* On spatial resolution issues on mean quantities using hot-wire anemometry. *Ph. D. thesis, Royal Institute of Technology, Stockholm, Paper 6*.

Österlund, J. M. 1999 Experimental studies of zero pressure-gradient turbulent boundary layer flow. *Ph. D. thesis, Royal Institute of Technology, Stockholm, Sweden*.

Österlund, J. M., Johansson, A. V., Nagib, H. M. & Hites, M. H. 2000 A note on the overlap region in turbulent boundary layers. *Phys. Fluids* **12**, 1–4.

Panton, R. L. 2005 Review of wall turbulence as described by composite expansions. *Appl. Mech. Rev.* **58**, 1–36.

Park, J. Y. & Chung, M. K. 2004 Revisit of viscous sublayer scaling law. *Phys. Fluids* **16**, 478–481.

Patel, V. 1965 Calibration of the Preston tube and limitations on its use in pressure gradients. *J. Fluid Mech.* **23**, 185–208.

Perry, A. E., Hafez, S. & Chong, M. S. 2001 A possible reinterpretation of the Princeton superpipe data. *J. Fluid Mech.* **439**, 395–401.

Perry, A. E. & Joubert, P. 1963 Rough-wall boundary layers in adverse pressure gradients. *J. Fluid Mech.* **17**, 193–211.

Perry, A. E., Schofield, W. & Joubert, P. 1969 Rough wall turbulent boundary layers. *J. Fluid Mech.* **37**, 383–413.

Piquet, J. 1999 Turbulent flows: Models and physics. *Springer-Verlag*.

Pope, S. 2000 Turbulent flows. *Cambridge University Press*.

Prandtl, L. 1925 Bericht über Untersuchungen zur ausgebildeten Turbulenz. *ZAMM* **5**, 136–139.

Prandtl, L. 1932 Zur turbulenten Strömung in Rohren und längs Platten. *Ergebnisse der Aerodynamischen Versuchsanstalt zu Göttingen* **4**, 18–29.

Priyadarshana, P. J. A. & Klewicki, J. C. 2004 Study of the motions contributing to the Reynolds stress in high and low Reynolds number turbulent boundary layers. *Phys. Fluids* **16**, 4586–4600.

Purtell, L., Klebanoff, P. S. & Buckley, F. 1981 Turbulent boundary layer at low Reynolds number. *Phys. Fluids* **25**, 802–811.

Reichardt, H. 1951 Vollständige Darstellung der turbulenten Geschwindigkeitsverteilung in glatten Leitungen. *ZAMM* **31**, 208–219.

Roach, P. E. & Brierly, D.H. 1992 The influence of a turbulent free stream on zero pressure gradient transitional boundary layer development including the condition test cases T3A and T3B. *Numerical Simulation of Unsteady Flows and Transition to Turbulence. O. Pironneau and W. Rodi (Eds.), Cambidge University Press,* pp. 319–347.

Rotta, J. C. 1950 Das in Wandnähe gültige Geschwindigkeitsgesetz turbulenter Strömungen. *Ingenieur-Archiv* **18**, 277–280.

Sandborn, V. 1972 Resistance temperature transducers. *Metrology Press*.

Sandham, N. D. 1991 An alternative formulation of the outer law of the turbulent boundary layer. *Tech. Rep. No. DLR IB 221-91 A 10, DLR Göttingen*.

Schlatter, P. 2009 (personal communication).

Schlatter, P., Li, Q., Brethouwer, G., Johansson, A. V. & Henningson, D. S. 2009*a* Towards large-eddy simulations of high-Reynolds number turbulent boundary layers. *Proc. 6th Int. Symp. on Turbulence and Shear Flow Phenomena, Seoul, Korea*.

Schlatter, P., Örlü, R., Li, Q., Brethouwer, G., Fransson, J. H. M., Johansson, A. V., Alfredsson, P. H. & Henningson, D. S. 2009*b* Turbulent boundary layers up to $Re_\theta = 2500$ studied through simulation and experiment. *Phys. Fluids,* (accepted).

Schlichting, H. & Gersten, K. 2006 Grenzschicht-Theorie. *Springer-Verlag, 10th ed.*

Smith, D. & Walker, J. H. 1959 Skin-friction measurements in incompressible flow. *NACA Tech. Rep. R-26*.

Spalart, P. 1988 Direct simulation of a turbulent boundary layer up to $R_\theta = 1410$. *J. Fluid Mech.* **187**, 61–98.

Spalding, D. B. 1961 A single formula for the law of the wall. *J. Appl. Mech.* **28**, 455–458.

Spurk, J. H. 1996 Strömungslehre: Einführung in die Theorie der Strömungen. *Springer, 4th ed.*.

Sreenivasan, K. R. 1989 The turbulent boundary layer. *Frontiers in experimental fluid mechanics, M. Gad-El-Hak (Ed.), Springer-Verlag*.

Szablewski, W. 1954 Turbulente Strömungen in divergenten Kanälen. *Ingenieur-Archiv* **22**, 268–281.

Szablewski, W. 1960 Analyse von Messungen turbulenter Grenzschichten mittels der Wandgesetze. *Ingenieur-Archiv* **29**, 291–300.

Tennekes, H. 1982 Similarity relations, scaling laws and spectral dynamics. *Atmospheric Turbulence and Air Pollution Modelling. F.T.M. Nieuwstadt and H. Van Dop (Eds.)*, pp. 37–68.

Tennekes, H. & Lumley, J. L. 1972 A first course in turbulence. *MIT Press, Cambridge, Massachusetts*.

Townsend, A. A. 1976 The structure of turbulent shear flow. *Cambridge University Press, 2nd ed.*

Tropea, C., Yarin, A. & Foss, J. 2007 Springer Handbook of Experimental Fluid Mechanics. *Springer-Verlag Berlin Heidelberg*.

Tsukahara, T., Seki, Y., Kawamura, H. & Tochio, D. 2005 DNS of turbulent channel flow at very low Reynolds numbers. *Proc. 4th Intl Symp. on Turbulence and Shear Flow Phenomena, Williamsburg, USA*, pp. 935–940.

Wark, C. & Nagib, H. M. 1990 On the character of turbulence-producing events in near-wall turbulence. *Near-wall turbulence, New York, Hemisphere Publishing Corp.*, pp. 306–325.

Wei, T., Schmidt, R. & Mcmurtry, P. 2005 Comment on the Clauser chart method for determining the friction velocity. *Exp. Fluids* **38**, 695–699.

White, E. & Ergin, F. 2004 Using laminar-flow velocity profiles to locate the wall behind roughness elements. *Exp. Fluids* **36**, 805–812.

Wietrzak, A. & Lueptow, R. M. 1994 Wall shear stress and velocity in a turbulent axisymmetric boundary layer. *J. Fluid Mech.* **259**, 181–218.

Willmarth, W. & Lu, S. 1972 Structure of the Reynolds stress near the wall. *J. Fluid Mech.* **55**, 65–92.

Wills, J. 1962 The correction of hot-wire readings for proximity to a solid boundary. *J. Fluid Mech.* **12**, 388–396.

Wu, X. & Moin, P. 2008 A direct numerical simulation study on the mean velocity characteristics in turbulent pipe flow. *J. Fluid Mech.* **608**, 81–112.

Zagarola, M. V. & Smits, A. J. 1998 Mean-flow scaling of turbulent pipe flow. *J. Fluid Mech.* **373**, 33–79.

Zanoun, E. S. 2003 Answers to Some Open Questions in Wall Bounded Laminar and Turbulent Shear Flows. *Ph. D. thesis, University of Erlangen, Germany*.

Zanoun, E. S., Durst, F. & Nagib, H. M. 2003 Evaluating the law of the wall in two-dimensional fully developed turbulent channel flows. *Phys. Fluids* **15**, 3079–3089.

Appendix A: The extent of the linear velocity profile

The availability of DNS for wall-bounded turbulent flows up to Reynolds numbers, where Reynolds number effects diminish within the inner region, makes it possible to assess the errors associated when using the linear velocity profile. Since a number of studies have employed a linear velocity profile, irrespective of the Reynolds number, up to $y^+ = 7$, 11 or even 15 wall units (Große & Schröder 2008; Blackwelder & Haritonidis 1983; Große 2008), it is interesting to compute the errors to be expected. Therefore, the DNS Data Base for Wall Turbulence and Heat Transfer (Kawamura Lab, Laboratory of Thermo-fluid dynamics) has been utilised to compute the deviations of equation (2) to first and second order from the DNS results as a function of Re_τ and y^+.

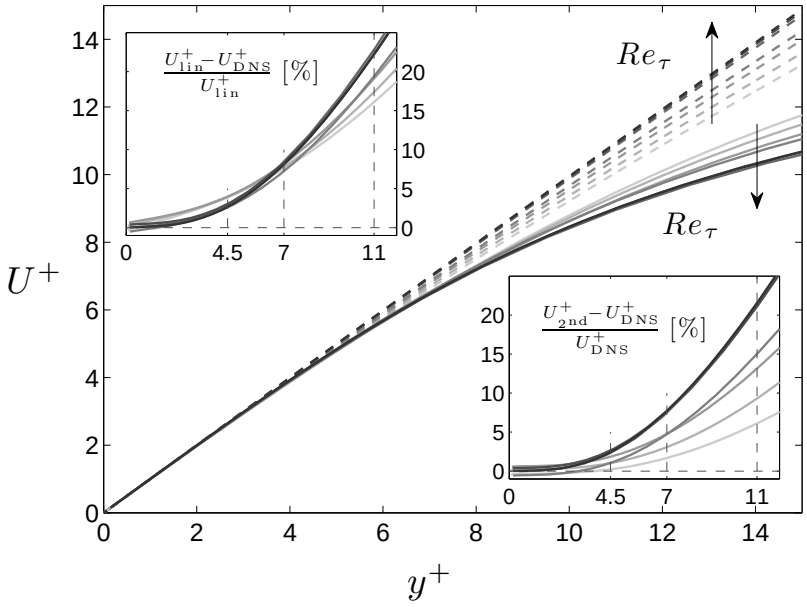

FIGURE 9. Mean streamwise velocity profile in inner scaling for channel flow with $Re_\tau = 64$, 80, 110, 150, 395, 640, and 1020 from DNS (—) (Tsukahara *et al.* 2005; Kawamura *et al.* 1999; Abe *et al.* 2004) and equation (2) to second order (- - -). The relative deviation of the linear profile without and with the second order term from the DNS is depicted in the upper and lower insert, respectively. Profiles and error curves with increasing Re_τ are shown in progressively darker shades of gray.

Figure 9 shows representative velocity profiles within the sublayer for $Re_\tau = 64$, 80, 110, 150, 395, 640, and 1020 and the corresponding profiles from the linear profile corrected with a second order term. The relative deviation of the linear profile without and with the second order term from the DNS is depicted in the upper and lower insert, respectively. As expected, the linear velocity profile overestimates the DNS results to around 2.5 % at $y^+ = 4.5$. The used results from the DNS also indicate that the employment of the linear profile for $Re_\tau > 300$ up to $y^+ = 7$, 11 or 15 overestimates the actual velocity to around 8, 20 and 40 %.

This is in contradiction to what is claimed by Große & Schröder (2008), where the error is given with 1 %. It is also interesting to note, that the addition of the second order term reduces the deviations from the DNS drastically, as long as $Re_\tau < 300$.

Figure 9 also explains why various coefficients for the Taylor expanded linear velocity profile have been reported over the years. The viscous region is strongly Reynolds number dependent, at least for $Re_\tau < 300$. This becomes further clear when utilising the shown DNS results to obtain the forth and fifth order terms in equation (2), as shown in table 1. The Reynolds number dependence seems to have levelled out for the highest three Reynolds number cases. Note also, that the values here are slightly below those given for the ZPG TBL flows mentioned in section 4, due to the missing second order term in the case of ZPG flows.[28]

[28]Omitting the second order term would increase both coefficients and thereby let the coefficients for the higher Reynolds number cases come closer to the values given in section 41 for the ZPG TBL flow.

Re_τ	incl. 4^{th} order	incl. 4^{th} & 5^{th} order	
	$\sigma_1 \times 10^4$	$\sigma_1 \times 10^4$	$\sigma_2 \times 10^4$
64	1.79	2.66	0.12
80	3.02	4.45	0.23
110	4.51	6.84	0.40
150	4.88	7.38	0.41
180	5.58	8.23	0.47
395	7.43	10.98	0.66
640	7.14	11.58	0.71
1020	7.34	11.26	0.67

TABLE 1. Coefficients for equation (2) for the DNS cases shown in figure 9 up to 4^{th} and 5^{th} order. Data points within $y^+ < 9$ and 15 were used to obtain the coefficients up to 4^{th} and 5^{th} order, respectively. Note that the number of decimal points does not indicate the accuracy of the obtained fitting parameters.

Appendix B: Pressure gradient and Reynolds number effects within the inner region

During the course of the following investigation, the commonly assumed universality of the inner region was assumed. One consequence of this assumption is that the buffer and overlap region (once established) are Reynolds number independent. Figure 9 anticipated already that for $Re_\tau > 300$ Reynolds number effects become negligible within the sublayer. To assess whether or not Reynolds number effects persist into the buffer region, figure 10 depicts DNS of channel flows with $Re_\tau = 180$, 550, 950 and 2000. In order to amplify the small differences in the U^+ vs. y^+ plot, the relative excess over the modified Musker profile, ΔU^+, is given as well in the insert. The rapid decrease of the Reynolds number effects indicates that the invariance to the Reynolds number

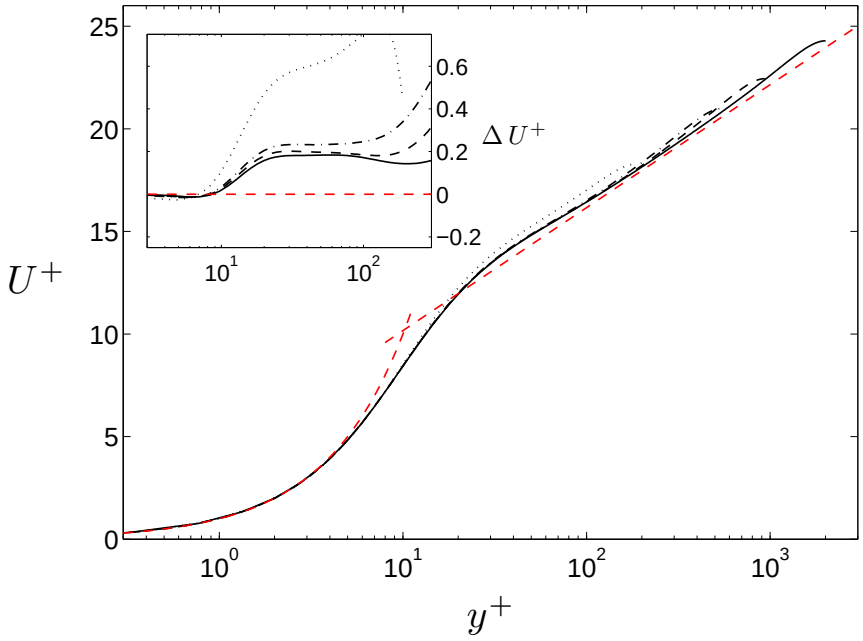

FIGURE 10. Mean streamwise velocity profile in inner scaling for channel (del Álamo *et al.* 2004; Hoyas & Jiménez 2006) flows with $Re_\tau = 180$ ($\cdots$), 550 ($-\ \cdots\ -$), 950 (- - -) and 2000 (—). The linear and log law profiles with $\kappa = 0.384$ and an additive constant of 4.17 are indicated through the dashed lines. The mean streamwise velocity relative to the "law of the wall" described through the "modified" Musker profile (Chauhan *et al.* 2009), ΔU^+, is given in the insert.

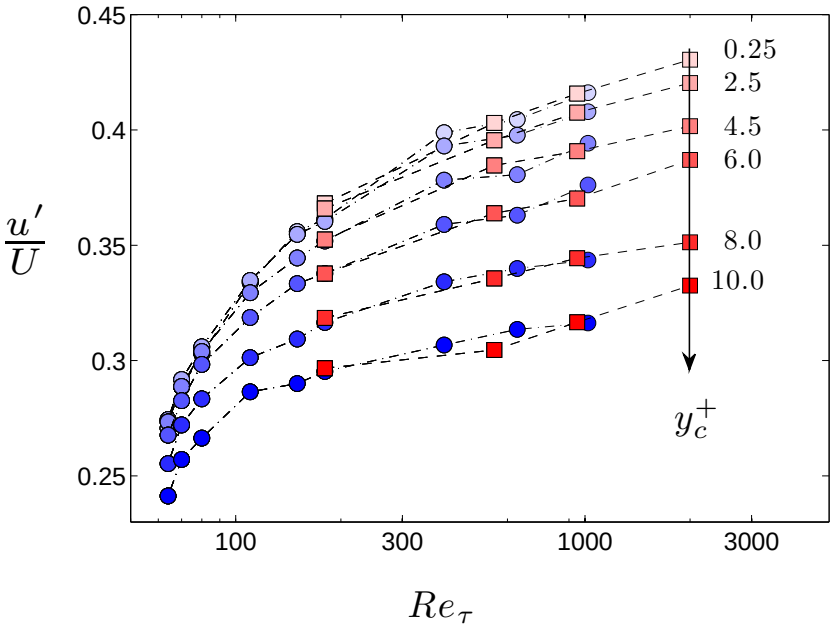

FIGURE 11. Relative turbulence intensity, u'/U, as function of the friction Reynolds number at different (approximate) wall positions, y_c^+, for channel flows: • (Tsukahara *et al.* 2005; Kawamura *et al.* 1999; Abe *et al.* 2004) and ■ (del Álamo & Jiménez 2003; del Álamo *et al.* 2004; Hoyas & Jiménez 2006).

is to a good degree given, once $Re_\tau > 500$. Note that the observed differences can not solely be explained by the protrusion of the wake region into the buffer region.

Although not directly related to the topic of this paper, it seems important to draw attention to the usage of DNS results from low Reynolds number simulations to check the accuracy of experimental results within the viscous sublayer. So, for instance, can it be found that the limiting behaviour of the relative streamwise turbulence intensity, i.e. $\lim_{y^+\to 0} u'/U = (u'/U)_{\rm lim}$, is employed to check the accuracy of (or correct for) the measured turbulence intensity within the viscous sublayer (Lanspeary 1988). While reported values for $(u'/U)_{\rm lim}$ varied in the range of 0.05–0.40 (see e.g. Alfredsson *et al.* 1988; Wietrzak & Lueptow 1994, for a summary of reported values), it was later on shown by Alfredsson *et al.* (1988), that most of the of the lower experimentally obtained values can be explained by the insufficiency of static calibrations for hot-films in order to measure fluctuations in air. The value deduced by them,

viz. 0.4, became an accepted value irrespective of Reynolds number and flow case (Bernard & Wallace 2002).

Figure 11 depicts the relative turbulence intensity from channel flow DNS as a function of the friction Reynolds number at different wall positions. The figure confirms, the results from the MPI oil channel measurements by Alfredsson *et al.* (1988), viz. that the limiting value is practically constant for $y^+ < 3$. However, it illustrates, that Reynolds number effects are substantial, particularly, for the lower Reynolds number range, and that the distance from the wall has to be accounted for when evaluating the fluctuating wall shear stress. While the results from the DNS depict clearly a decrease in the relative turbulence intensity with increasing wall distance and an increase with increasing Reynolds number, Bernard & Wallace (2002) give a relation, that increases with wall distance and decreases with increasing Reynolds number towards the value put forward by Alfredsson *et al.* (1988). New measurement techniques,

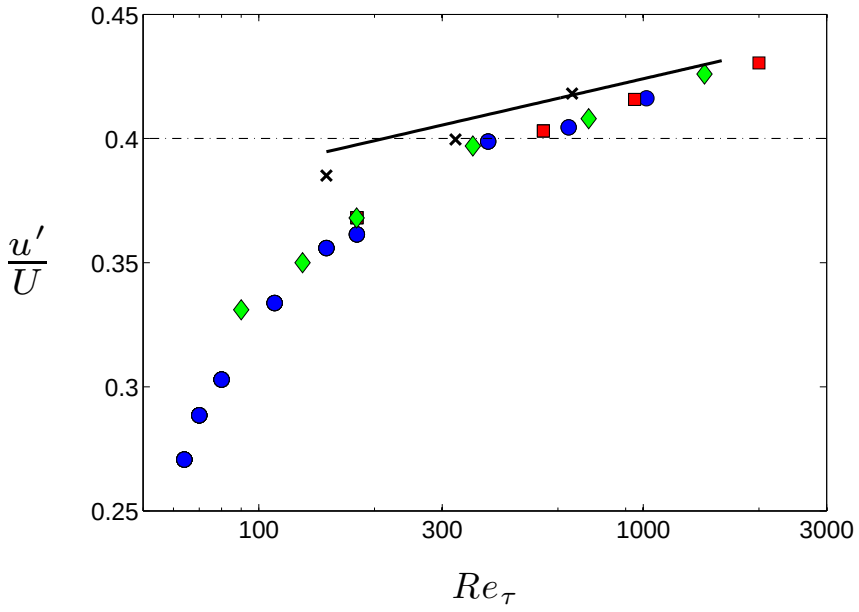

FIGURE 12. Limiting behaviour of $\lim_{y^+\to 0} u'/U$ as function of the friction Reynolds number for channel and ZPG TBL flows. Channel flows: • (Tsukahara *et al.* 2005; Kawamura *et al.* 1999; Abe *et al.* 2004), ♦ (Hu & Sandham 2001), ■ (del Álamo & Jiménez 2003; del Álamo *et al.* 2004; Hoyas & Jiménez 2006). ZPG TBL flows: × (Spalart 1988), — correlation based on the DNS (Schlatter *et al.* 2009*b*) and LES (Schlatter *et al.* 2009*a*) data (Schlatter 2009).

like the employment of micropillars for mean and fluctuating wall shear stress measurements (Große & Schröder 2008; Brücker *et al.* 2005), should therefore not be validated against one particular limiting value, when the experiments are performed over the Reynolds number range depicted in figure 11.

While classical textbooks make no distinction between channel, pipe and ZPG TBL flows regarding the turbulence intensity within the inner region, there seems to be compelling evidence, that—at least for low Reynolds numbers—these flows are different. That this is in fact the case, can be anticipated from the pressure gradient term in the Taylor expansion of the linear velocity profile, which diminishes for higher Reynolds numbers. Figure 12, compares the limiting value for the relative turbulence intensity from DNS of channel and ZPG TBL. The same strong Reynolds number trend can be observed for three independent channel flow simulations, while in the case of ZPG TBL flows, the Reynolds number effects, are weaker. The latter can be associated with the absence of pressure gradient effects. Similar trends have recently been noted by Buschmann *et al.* (2008) for all Reynolds stresses.

Appendix C: Differences between various DNS results for channels flows at around the same Reynolds number

In appendix B it was shown, that once Re_τ exceeds 500 the buffer region is Reynolds number independent. However, how small do the differences have to be in order to establish a Reynolds number independence, especially when utilising experimental data or DNS from various sources? To spread light on this question, a number of channel flow DNS results have been gathered for a suitable value of the Reynolds number. Suitable, in this case, means, that Re_τ is high enough, so that at least the buffer region is not influenced by the geometrical characteristics of the simulated channel, but still low enough to allow access to several independent DNS.

For the case of channel flows, $Re_\tau \approx 600$ seemed suitable. Figure 13 depicts five DNS results from various groups. Note, that although a small Reynolds number variation is present, figure 10 indicates that no discernable differences should emerge in the ΔU^+ plot. Here, however, differences of around 0.2 u_τ, are persistent over the entire buffer region and display trends, which are not explainable by Reynolds number effects. Even if the DNS by Hu & Sandham (2001) would be ignored[29], the differences are still around 0.1 u_τ, and thereby larger then those observed over a range of $Re_\tau = 550$–2000 (cf. figure 10). This emphasises, that even the mean streamwise velocity profile exhibits differences between various DNS, and should be kept in mind when utilising DNS results to extract u_τ or Δy^+.

Similar observations can be made when comparing DNS from ZPG TBL. Here the differences can be even larger, due the spatially developing character of the flow and its sensitivity to the computational domain, particularly when it comes to the wake part. But also within the buffer region, so for instance at $y^+ = 30$, can differences up to 0.5 u_τ be observed when comparing the highest Reynolds number cases of Ferrante & Elghobashi (2005) and Spalart (1988). This becomes especially of importance when utilising DNS from ZPG TBL flow to check scaling laws as, for instance, done by Khujadze & Oberlack (2007).

[29] There are a number of pecularities associated with this particular simulation. One is the clear deviation to all other DNS over the entire buffer region, but also viscous region. And the other is, that, Hu & Sandham (2001) provided data for the entire cross-section and not as commonly done only data covering the channel half-width. This enables one to check the symmetry of the flow, which in the present case is not given. In fact a clear offset over the entire inner region can be observed. The data shown here, display smaller differences to the other DNS results in figure 13. Utilising the data from the other half of the channel would increase the deviation from 0.2 to 0.5 u_τ.

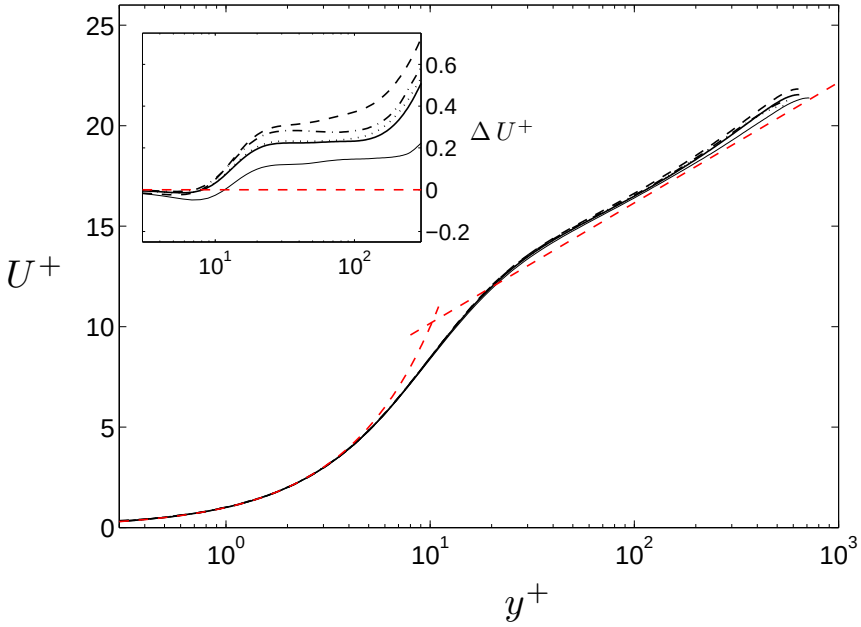

FIGURE 13. Mean streamwise velocity profile in inner scaling for channel flows from different sources. del Álamo *et al.* (2004): $Re_\tau = 550$ ($\cdots$), Moser *et al.* (1999): $Re_\tau = 590$ (- $\cdots$ -), Abe *et al.* (2001): $Re_\tau = 640$ (- - -), Iwamoto *et al.* (2002): $Re_\tau = 650$ (—) and Hu & Sandham (2001): Re_τ =720 (—). See caption of figure 10 for further details.

Appendix D: The use of the "law of the wall" to determine the friction velocity

Complementary notes to figures 7 and 8

In figure 14 and 15 the determined friction velocities for the cases shown in figures 7 and 8 are given. As anticipated through figure 1, (a reasonable) offset in the wall position can hardly be recognised, once y^+ is within the overlap region. This explains also, why an offset of a few wall units within the buffer region, as deduced from the results depicted in figures 7 and 8, do not alter the extracted u_τ value more than 1 %.

The choice of the appropriate "law" and method

Since the focus of the present paper is on the determination of the wall position, rather than the friciton velocity, the performance of the analytical descriptions for the law of the wall, to extract u_τ was left out so far. Analytical functions for the inner region or composite velocity profiles have been used since Szablewski (1954) and Coles (1968), respectively, to extract the skin friction from a fit of the data to the inner region or entire velocity profile, rather than only the overlap region (Clauser 1954). The investigation by Kendall & Koochesfahani

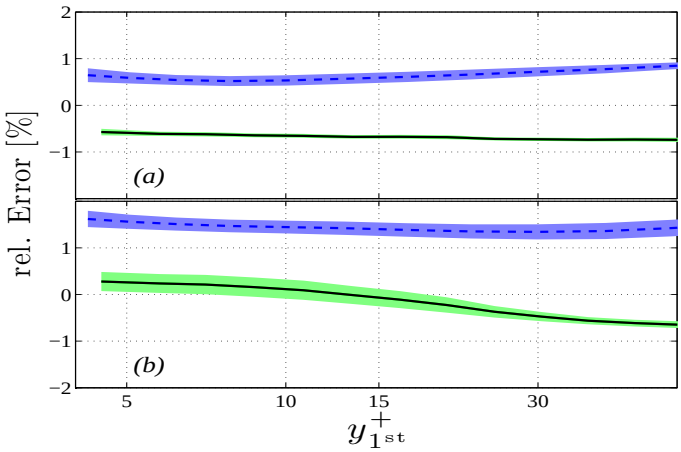

FIGURE 14. Obtained relative error in the friction velocity, u_τ, relative to its given value by employing the *(a)* modified Musker profile (Chauhan *et al.* 2009) and *(b)* the analytical profile by Reichardt (1951) as a function of the first utilised point, $y^+_{1^{st}}$, with fixed wall position, i.e. $\Delta y^+ = 0$. Experiments by Österlund (1999) at $Re_\theta = 6624$ (solid) & 27320 (dashed) with $L^+ = 13$ & 60, respectively. Shaded areas indicate a 50 % confidence interval.

(2008) concludes that the friction velocity can, for a wide range of Reynolds numbers, be determined with an accuracy of better than 0.5 %, which in their view is "comparable to that from independent direct measurements of the wall shear stress". However, their given accuracy is—to our knowledge—better than any (be it direct and/or independent) known method (Fernholz *et al.* 1996; Naughton & Sheplak 2002; Nagib *et al.* 2004*b*).

There are essentially two different approaches to compute u_τ from a fit to the "law of the wall". Either one starts from the near-wall data and successively adds points while advancing in y^+ as done by Kendall & Koochesfahani (2008), or one starts from the end of the overlap region and successively comes closer to the wall. While the former has the advantage of not having to determine the end of the overlap region, the latter is an extension of the Clauser chart method, and make it possible to assess the effect of missing near-wall measurements on the accuracy of the extracted quantities. Both approaches lead to the same result, when applied on artificially generated mean velocity profiles, as long as the analytical function used to generate the data is used to extract the friction velocity. When applied on "real" data, however, the results differ.

Kendall & Koochesfahani (2008) also conclude, that, since the accuracy of their method is already given as 0.5 %, "the use of refined values of boundary layer constants would not have a practical consequence for the reported results and would at best lead to an improvement of about 0.5 % in mean error for estimating the friction velocity." To check their statement, and the two aforementioned approaches, the friction velocity for one particular velocity profile by Österlund (1999) was computed. Figure 16*(a)* depicts the deviation of the selected profile by Österlund to the log law, Ψ. Additionally Ψ is given for the

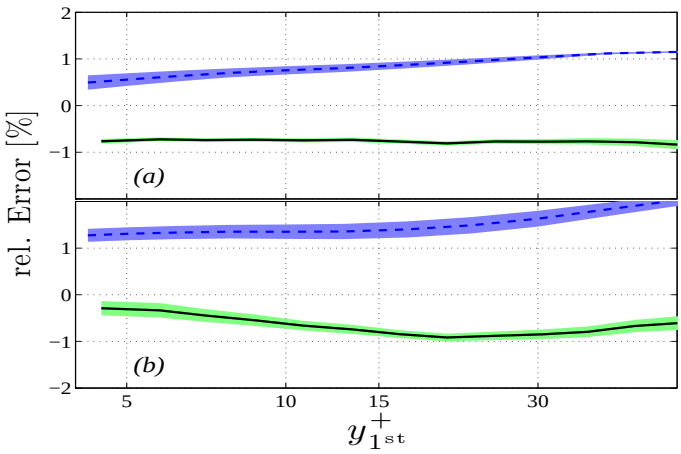

FIGURE 15. Same as figure 7, but u_τ obtained together with Δy^+ from the same least-squares fit.

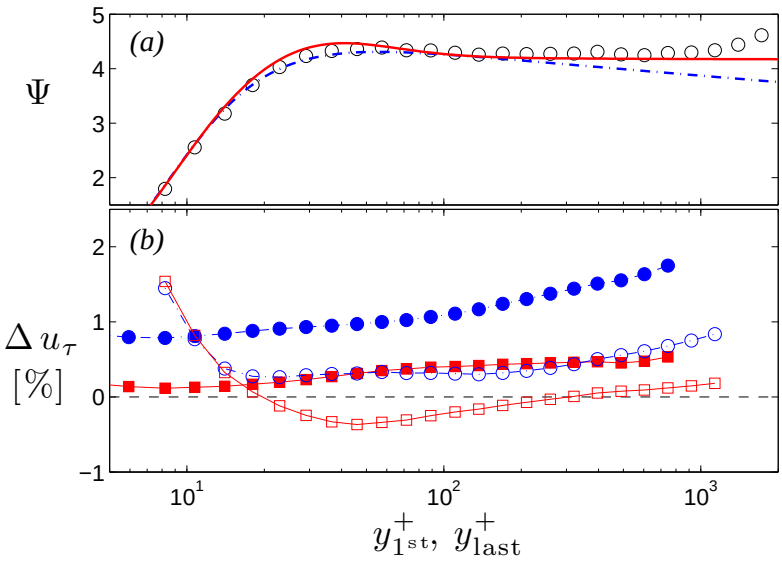

FIGURE 16. *(a)* Deviation from the log law (with $\kappa = 0.384$ and $B = 4.17$), Ψ, for a mean streamwise velocity profile of Österlund (1999) at $Re_\theta = 19235$ and the analytical description by Musker (1979) (· − ·) and Chauhan *et al.* (2009) (—). *(b)* Obtained relative deviations in u_τ compared to the given value, by utilisation of the approach proposed by Kendall & Koochesfahani (2008) (open symbols) and the once adapted here (solid symbols).

law of the wall expressed through the Musker profile (· − ·) and the modified Musker profile by Chauhan *et al.* (2009) (—). Since the latter utilises the same constants as the used log law the deviation from the log law asymptotes towards the used additive constants, B. Despite the apparent small differences between both profiles, the determined friction velocity by utilising one of the two shown analytical descriptions as well as the two aforementioned approaches give considerable larger deviations, than expected from the investigation by Kendall & Koochesfahani (2008). However, it is interesting to point out, that the method favoured by Kendall & Koochesfahani (2008) together with their favoured analytical description, viz. the one by Musker (1979), give surprisingly agreeing results with the approach adapted here by utilising the description by Chauhan *et al.* (2009). Hence, there is a certain degree of subjectivity. Nevertheless, an accuracy of 1.5 % in terms of u_τ seems to be more appropriate for the methods described here, when taking the effect of the chosen analytical functions, their constants, as well as the method used to extract the unknown(s) into account.

Recalling the accuracies of measurement techniques for u_τ, the observed inaccuracies are still acceptable and considerable better than those associated with the classical Clauser method or the employment of the linear profile outside its range of validity.

Appendix E: Analytical expressions for the law of the wall

Using Prandtl's mixing length hypothesis Rotta (1950) derived an expression for the inner region valid from the end of the so-called "laminar sublayer", from where on the linear profile was assumed to be valid. The "laminar sublayer" is the region in which the viscous friction dominates over the turbulent one, and is equivalent to the linear sublayer of the post-Fage & Townend (1932) era. Rotta also extended his formula to include roughness effects.

Based on the definition of the total shear stress, Prandtl's mixing length hypothesis and a damping factor accounting for the damping effect of the fluid on the wall, van Driest (1956), derives a relation for the shear stress, which upon integration gives a relation for the streamwise velocity in the following form

$$U^+ = \int_0^{y^+} \frac{2\,\mathrm{d}y^+}{1+\sqrt{1+(2\kappa y^+)^2[1-\exp(y^+/A)]^2}}\,, \tag{5}$$

whereas A denotes the damping factor and is given by van Driest for $\kappa = 0.4$ as 26. Using the log law with different constants a refined damping factor can be determined. The given relation was also extended to account for roughness effects. The expression has also been modified by Szablewski (1960) to account for various pressure gradients.

Using the mixing length hypothesis and the log law, Reichardt (1951), derives a single formula for the law of the wall and obtains the following relation

$$\begin{aligned} U^+ = \frac{1}{\kappa}\ln(1+\kappa y^+) + \left[B - \frac{\ln\kappa}{\kappa}\right] \\ \times\left[1-\exp\left(\frac{y^+}{\delta_l^+}\right) - \frac{y^+}{\delta_l^+}\exp(-0.33y^+)\right], \end{aligned} \tag{6}$$

where δ_l^+ denotes a measure for the strength of the region adjacent to the wall "in which the molecular friction exceeds the turbulent one". This is equivalent to the so-called "laminar sublayer" mentioned by Rotta. Reichardt (1951) gives a value of 11 for $\kappa = 0.4$ and an additive constant of 5.5. Hence δ_l^+ has to be adjusted, when used with different log law constants.

As Spalding (1961) notes, there is no need to express U^+ explicitely in terms of y^+, which lead him to establish a single formula for the law of the wall which, fulfils the no-slip condition, is tangential to the linear profile, asymptotes at large y^+ values into the logaritmic profile and fits the experimental data within the buffer region. By doing so he ends up with

$$y^+ = U^+ + \exp(-\kappa B)\left[\exp(\kappa U^+) - \sum_{n=0}^{4}\left(\frac{(\kappa U^+)^n}{n!}\right)\right]. \tag{7}$$

Another prominent relation, modified in a number of other mean velocity descriptions, is given by Musker (1979) and reads as follows

$$\frac{\mathrm{d}U^+}{\mathrm{d}y^+} = \frac{\kappa + Cy^{+2}}{\kappa + Cy^{+2} + C\kappa y^{+3}}\,. \tag{8}$$

where C is a constant of proportionality in $\nu_t/\nu \sim y^{+3}$, and ν_t denotes the eddy kinematic viscosity. An explicite form for U^+ can be found in Chauhan *et al.* (2009), whereas Musker obtains a explicit relation, after merging it with a wake function.

In addition to the above functional forms for the law of the wall, a number of composite velocity profiles have been proposed valid for the entire flow region. Despite the fact, that some of the aforementioned descriptions were intended to describe the entire velocity profile for internal flows, the need for more appropriate relations has been recognised from Rotta (1950) on. One of the first formal descriptions were for instance given by Coles (1956), based on his additional wake function. The composite velocity profile can thus be given as a superposition of the description for the (linear and logarithmic) law of the wall and an additive wake function

$$U^+_{\mathrm{composite}} = U^+_{\mathrm{inner}}(y^+) + \frac{2\Pi}{\kappa}\mathcal{W}\left(\frac{y^+}{\delta^+}\right), \quad 0 \leq y^+ \leq \delta^+\,, \tag{9}$$

where Π and $\mathcal{W}$ are known as the wake parameter and wake function, respectively. A number of wake functions have been developed, of which some have been discussed in Lewkowicz (1982) and Sandham (1991).

In the following two recent formulations for the complete velocity profile, shown in figure 5 will given. The composite velocity profile by Chauhan *et al.* (2009) utilises a modified version of the description by Musker, which is validated against the ZPG TBL measurements by Österlund (1999) and near-wall data of DNS, and accounts for the observed overshoot over the log law in the buffer region. Additionally a series of well-resolved measurements were performed in the outer region of ZPG TBL layers Nagib *et al.* (2004*a*), due to the usual habit to collect logaritmically spaced measurement points, leaving the wake region insufficiently resolved. Their composite description for turbulent boundary layer flows reads as follows

$$\begin{aligned} U^+ =& \frac{1}{\kappa}\ln\left(\frac{y^+ - a}{-a}\right)\left[(4\alpha + a)\ln\left(-\frac{a}{R}\frac{\sqrt{(y^+-\alpha)^2+\beta^2}}{y^+ - a}\right)\right. \\ &\left. + \frac{\alpha}{\beta}(4\alpha + 5a)\left(\arctan\left(\frac{y^+ - \alpha}{\beta}\right)\right) + \arctan\left(\frac{\alpha}{\beta}\right)\right] + U^+_{\mathrm{bump}} \\ \alpha =& (-1/\kappa - a)/2, \quad \beta = \sqrt{-2a\alpha - \alpha^2}, \quad R = \sqrt{\alpha^2 + \beta^2}, \quad s = aR^2\,. \end{aligned} \tag{10}$$

Hereby U^+_{bump} accounts for the overshoot in the mean velocity profile and undershoot in the indicator function within the buffer region and is given as follows

$$U^+_{\mathrm{bump}} = \frac{\exp[-\ln^2(y^+/M_1)]}{M_2}, \quad M_1 = 30, \quad M_2 = 2.85. \tag{11}$$

The value for a has to be obtained by fitting the expression for the inner region to the log law. For $\kappa = 0.384$ and $B = 4.17$ Chauhan *et al.* (2009) gives a value of -0.10361. Their wake function, on the other hand, is based on their measurements in the NDF and is of exponential form

$$\begin{aligned}\mathcal{W}_{\mathrm{exp}} =& \frac{1 - \exp\left[-\frac{1}{4}(5a_2 + 6a_3 + 7a_4)\eta^4 + a_2\eta^5 + a_3\eta^6 + a_4\eta^7 \right]}{1 - \exp[-(a_2 + 2a_3 + 3a_4)/4]} \\ &\times \left(1 - \frac{\ln\eta}{2\Pi}\right).\end{aligned} \tag{12}$$

Since the above composite profile has been explicitely designed for ZPG TBLs, modified versions for pipe and channel flows have been given by the authors (Nagib & Chauhan 2008).

Another composite profile description is the one by Nickels (2004), who gives an explicite profile, accounting for pressure gradient effects:

$$\begin{aligned}U^+ =& y_c^+ \left[1 - \left(1 + 2\frac{y^+}{y_c^+}\right) + \frac{1}{2}(3 - p_x^+ y_c^+)\left(\frac{y^+}{y_c^+}\right)^2 - \frac{3}{2}p_x^+ y_c^+ \left(\frac{y^+}{y_c^+}\right)^3\right] \exp\left(-3\frac{y^+}{y_c^+}\right) \\ &+ \frac{\sqrt{1 + p_x^+ y_c^+}}{6\kappa} \ln\left(\frac{1 + (0.6(y^+/y_c^+))^6}{1 + \eta^6}\right) + \frac{2\Pi}{\kappa}\left[1 - \exp\left(-\frac{5(\eta^4 + \eta^8)}{1 + 5\eta^3}\right)\right].\end{aligned} \tag{13}$$

Hereby

$$p_x^+ = \frac{\nu}{\rho u_\tau^3}\frac{\mathrm{d}p}{\mathrm{d}x}$$

and y_c^+ denote the inner-scaled pressure gradient coefficient and sublayer thickness, respectively. While the latter is a function of the former, a value of 12 is given by Nickels (2004) for ZPG conditions.

Paper 6

"The eye sees only what the mind is prepared to comprehend."

Henri-Louis Bergson (1859 – 1941)

6

On spatial resolution issues on mean quantities using hot-wire anemometry

By Ramis Örlü

Linné Flow Centre, KTH Mechanics, SE-100 44 Stockholm, Sweden

The effect of spatial resolution on streamwise velocity measurements with single hot-wires is targeted in the present study, where efforts have been made to distinguish between spatial resolution and Reynolds number effects. The basis for time resolved measurements to determine the mean velocity and higher moments accurately is that the probability density distribution is measured correctly. It is well known that the turbulence intensity is increasingly attenuated with increasing wire length. It is here also shown (probably for the first time), that even the mean velocity is affected as well, albeit to subtle extent, but with important consequences in studies of concurrent wall-bounded turbulence. The found results are finally used to illustrate that the controversy regarding the universality of the probability density distribution of the streamwise velocity fluctuations in the overlap region is to a large extend artificially generated, due to the fact that spatial resolution issues are not taken into account.

1. Introduction

Spatial averaging when measuring small (with respect to the measurement volume) scale turbulence is a well known problem when using hot-wire anemometry. However the literature—despite a few well known and often cited studies—is rather inconclusive and incomplete, since spatial resolution effects can also be obscured by Reynolds number effects. As long as the sensing part of the hot-wire is sufficiently small and can respond to the highest frequencies encountered in the flow, the measurements are believed to be free from spatial and temporal resolution issues. Since the employment of constant temperature anemometers for more than a half century ago, the latter has not presented major difficulties, i.e. the response of the hot-wire is well above the range of frequencies in which measurements are being performed (Smol'yakov & Tkachenko 1983). Spatial resolution effects, on the other hand, seem only adequately been studied in regards of multiple wire probes (Vukoslavčević *et al.* 2009, and references therein). For the (simple) single wire probe, however, the spatial attenuation of not resolved fluctuations remains a major problem in concurrent wall-bounded

turbulence studies. Similar issues, albeit of different nature and partially different consequences, have also been addressed with regard to laser-Doppler and particle image velocimetry, among others for instance, in Johnson & Barlow (1989) and Lavoie *et al.* (2007), respectively.

The problem of spatial resolution is simply the fact that the sensing element can not truly respond to scales smaller than its dimensions. For common hot-wire probes the diameter of the wire is usually much smaller than the smallest scales of turbulence, be it the Kolmogorov scale in general or the viscous scale in wall-bounded flows. What remains is the length of the wire, which in order to prevent end-conduction effects, i.e. to ensure a homogenous temperature profile along most of the wire has to be much larger than its diameter (at least 200 times), and hence usually exceeds the smallest scales (Bernard & Wallace 2002).

Recently, a great interest in high Reynolds number laboratory studies has emerged (Zagarola & Smits 1998; Österlund 1999; Nagib *et al.* 2004; Knobloch & Fernholz 2004; Hutchins & Marusic 2007, just to mention a few), due to the need to test asymptotic theories or scaling laws as well as to ensure that known phenomena at laboratory Reynolds numbers are representative for practical engineering situations (see e.g. Talamelli *et al.* 2009, for a more thorough pledge for the need of high Reynolds number experiments). The use of existing laboratory facilities to reach high Reynolds numbers (in air) by increasing the velocity or density, brings usually along a reduction of the viscous scale and hence lets the wire length to increase when compared to the smallest scales. The viscous length scale $\ell_* = \nu/u_\tau$, where u_τ denotes the friction velocity, and ν the kinematic viscosity, can easily be related to the Reynolds number. The definition of the friction Reynolds number (or Kármán number),

$$Re_\tau = \frac{u_\tau \delta}{\nu} = \frac{\delta}{\ell_*}\,, \tag{1}$$

where δ denotes the outer length scale, i.e. the boundary layer thickness, channel half-width or pipe radius, reveals that higher Reynolds numbers for a given outer scale bring a reduction of the viscous scale along. This limits the use of existing facilities, hence large scale facilities have been setup particularly for this purpose, i.e. in order to reach high Reynolds numbers and still ensure that the smallest length scales can be accessed with the available measurement techniques. Such an existing facility is the *High Reynolds Number Turbulent Boundary Layer Wind-Tunnel* (HRNBLWT) at the University of Melbourne (Nickels *et al.* 2007) and one under construction is the long pipe facility at the *Center for International Cooperation in Long Pipe Experiments* (CICLoPE) (Talamelli *et al.* 2009).

The present paper, after reviewing some previous studies, will reason that there is a need for systematic investigations to ensure that "spatial resolution [does not] mask the true Reynold number effects" (Metzger 2006). A recent

study by Hutchins *et al.* (2009) has found and described a number of common phenomena associated with Reynolds number effects and exposed them rather as a results of spatial (but to some extent also temporal) resolution issues. It will be shown that not only the measured spectra and hence the turbulence intensity are affected, as convincingly demonstrated by the above authors, but also other higher order moments. We also demonstrate that even the mean is found to be affected, which to our knowledge has not been reported so far. Although the effect of spatial resolution for the first order moment of the streamwise velocity component will be shown to be rather subtle, it still brings with it important consequences, especially in the context of the current debate regarding the appropriate scaling of the mean velocity distribution in wall-bounded turbulent flows.

2. Review of relevant studies

Early studies, as those by Dryden *et al.* (1937) and Corrsin & Kovasznay (1949) among others, focussed on temporal as well as spatial resolution issues with regard to the measured spectral distribution. Vorticity and temperature probes are restricted due to their size and thermal intertia, respectively, and have been studied extensively in the past. Some of these early studies are reviewed in Ligrani & Bradshaw (1987) and Vukoslavčević *et al.* (2009). Concerning higher order moments of the streamwise velocity fluctuation a number of studies have been published around 1983, whereas prior to that it was more or less assumed that the attenuation due to spatial resolution was negligible in terms of statistical quantities and is mainly restricted to measurements of the dissipative small-scales, as for instance concluded by Karlsson (1980).

Johansson & Alfredsson (1983) infer from their experiments in the buffer region of channel flows, that the *probability density function* (pdf), and hence the higher order moments are affected by spatial resolution effects. In particular they show that the near-wall peak in the streamwise turbulence intensity distribution is attenuated by around 10 % when measured with a sensing element of length 32 instead of 14 viscous length scales. They also note that the zero-crossing of the skewness factor shifts away from the wall when measured with their longer sensor. Especially the skewness factor of the streamwise velocity time-derivative was found to be reduced explaining their observed decrease in the number of events detected with the *variable-interval time average* (VITA) technique. The same observation was made by Blackwelder & Haritonidis (1983). In this context, they remark that the bursting frequency remained essentially constant when measured with hot-wires shorter than L^+ of 20, where $L^+ = L/\ell_*$, and L denotes the dimensional wire length and the superscript + indicates non-dimensionalisation by viscous scales. Both investigations connect their results to the presence of elongated structures in the buffer region, which are believed to have a spanwise extent of around 20 ℓ_* (cf. Blackwelder & Eckelmann 1979; Lin *et al.* 2008, regarding the width of the low

speed streaks), and conclude that the sensing length should be shorter than the width of these elongated structures in order to resolve the associated energy.

Contrary to the results of Johansson & Alfredsson (1983), Derksen & Azad (1983) found neither an effect of spatial resolution on the skewness nor on the flatness. However, they performed their measurements at one particular wall position, namely $y^+ = 150$, where y denotes the wall-normal coordinate. This is a location where both the skewness and flatness factors are hardly changing neither with Reynolds number nor with wire length as will be demonstrated in the present paper. Hence the selected position is not a suitable choice to detect Reynolds number or spatial resolution effects. Furthermore, no indication of the wire length in viscous units is given, which makes it rather unfeasible to detect trends in the data. Similarly Frenkiel & Klebanoff (1973) in their study in turbulent boundary layer flows exclude spatial and temporal resolution effects on the pdfs based on comparisons in the outer region.

An extensive experimental investigation at a Reynolds number of $Re_\theta = 2620$, where Re_θ denotes the Reynolds number based on the momentum-loss thickness and free stream velocity, U_∞, with 21 different hot-wire probes ranging from $L^+ = 1$–60 have been performed by Ligrani & Bradshaw (1987). The conclusions from their study remain until today accepted and are widely known as guidelines among hot-wire users, viz. that the length-to-diameter ratio, L/d, where d is the diameter of the sensing wire, of hot-wires should be greater than 200 in order to limit end-conduction effects, and that the wire be shorter than 20 viscous units to resolve the energy containing eddies.[1] An attenuation in the near-wall peak of the streamwise turbulence intensity in inner variables ($u'^+ = u'/u_\tau$, where u' denotes the the root mean square (rms) value of the streamwise velocity fluctuations) up to 30–40 % depending on L^+ and L/d could be observed and the level of reduction was shown (but not commented and also in no subsequent studies mentioned again) to be observable far out into the overlap region (up to around $y^+ = 300$).

Also a reduction in the u'^+-distribution over the whole buffer region was observed by all of the aforementioned investigators, its near-wall peak, u'^+_{max}, attracted most of the attention in the following studies. Klewicki & Falco (1990), for instance, quantified the competing effects of wire length and Reynolds number and observed a weak increase in u'^+_{max} for wires with matched L^+, whereas for matched Reynolds numbers the peak decreased stronger with increasing L^+, hence the attenuation effect is found to be stronger than the Reynolds number effect, as anticipated by the study of Johansson & Alfredsson

[1]It is worth noting that an L/d-ratio of 200 is usually given in the literature independent of material and geometrical properties of the wire (e.g. with and without stubs). Li *et al.* (2004), based on their numerical simulation, remark that the value of 200 is associated with Platinum wires and that the ratio has to be increased for Tungsten wires to 270 in order to reduce end-conduction effects to the corresponding level.

(1983). This explains partially why Fernholz & Finley (1996) in their extensive review of turbulent boundary layer data, came to the conclusion that the near-wall peak of the inner-scaled streamwise turbulence intensity is a function of L^+ only and hence Reynolds number independent, viz. due to its observed constancy with increasing Reynolds number. Mochizuki & Nieuwstadt (1996) collected data from 47 different experiments in pipe, channel and turbulent boundary layer flows and came to the same conclusion, viz, that u'^+_{max} is independent of the Reynolds number.[2] Their comparative study lead them to the conclusion that $L^+ \leqslant 30$ is sufficient to ensure resolved measurements of the skewness factor at $y^+ = 15$. Based on the conclusions from Fernholz & Finley (1996) and Mochizuki & Nieuwstadt (1996) a number of studies have used the criterion of a Reynolds number independent u'^+_{max}-value to check whether or not their data is affected by spatial resolution effects, by ensuring that the peak value did not decrease with increasing Reynolds number (whereas in reality it is supposed to increase).[3] Purtell *et al.* (1981), in their turbulent boundary layer experiments, observe an initial increase in u'^+_{max}, followed by a decrease with Reynolds number. This brought them to speculate, that with higher Reynolds number, all but the largest scales are suppressed. Only where sufficient resolution is ensured will u'^+_{max} keep increasing with Reynolds number, as for instance observed by DeGraaff & Eaton (2000).[4]

Recalling that the previous studies focussed mainly on the effect of spatial resolution on the near-wall streamwise turbulence intensity peak, Khoo *et al.* (1997) continued these studies with the focus on the linear sublayer. They extended the conclusions of Johansson & Alfredsson (1983) and Ligrani & Bradshaw (1987) to the sublayer and found that higher order moments are attenuated. They also found, that for wires with $L^+ < 22$ measurements within the linear sublayer will be fully resolved.

The near-wall peak in the streamwise rms distribution has recently systematically been investigated by Hutchins *et al.* (2009) and an empirical expression has been given to account for spatial resolution effects. In their experimental investigation, at a fixed Reynolds number, Re_θ, of around 20000, with wires varying in L^+ from 11 to 116 they also associate the appearence of a second

[2]They admit, however, a very weak increase in the peak value with increasing Reynolds number, but conclude that $u'/u_\tau = 2.71 \pm 0.13$ for a range of Reynolds numbers between $Re_\theta = 300$–20920 in turbulent boundary layer flows.

[3]It is interesting to note, that early hot-wire measurements in Göttingen around the late 30's indicate an increase in u'^+_{max} with increasing Reynolds number (cf. Dryden 1938, where Prandtl mentions the measurements in the *discussion* section, but also suggests a division of the velocity fluctuations into a viscosity dependent and independent part, where the former and latter are denoted as "*Wirbelfabrik*" and "*passiv*", respectively.).

[4]It is interesting to note that the data of Purtell *et al.* (1981) displays a steady increase in u'^+_{max} for the measurements at the same free stream velocity with increasing downstream location (their figure 11). However, the authors, associate the trend with boundary layer development obscurities and do not mention this further.

peak in the rms distribution further away from the wall to the attenuation of small scales. This peak was noted in Fernholz & Finley (1996) and appeared for their higher Reynolds numbers, especially in the data obtained in the *German-Dutch windtunnel* (DNW: Deutsch-Niederländischer Windkanal) with wire length of $L^+ = 70$ (Fernholz *et al.* 1995).[5] As observed by Hutchins *et al.* (2009), the second peak in the u'^+ distribution starts to emerge around L^+ of 50–60, and with further increase in the viscous scaled wire length the near-wall peak becomes lower than the outer peak and ultimately vanishes. Interestingly, they also note that for matched L^+ and Reynolds number a higher free stream velocity attenuated u'^+ even further. Experiments by Hites (1997) with different wire length and Reynolds number show a second peak for measurements with $L^+ = 69$, whereas it is absent for $L^+ = 6$ and 31, even when doubling the Reynolds number. Nonetheless, this outer peak is not commented by Hites, nor by Karlsson (1980), whose data presents a similar trend at even lower Reynolds numbers due to larger L^+ values. Similar observations can be made in the hot-wire measurements by Zanoun (2003), where such an outer peak is present for $Re_\tau > 2000$ and 4000 for experiments in channel and pipe flows, respectively.[6] This indicates that the second peak in the u'^+ distribution is strongly coupled to spatial resolution effects rather than the Reynolds number *per se*.

The *Princeton/DARPA-ONR SuperPipe Facility* (Zagarola 1996) has enabled studies exceeding all previous pipe flow studies in Reynolds number, but at the same time ℓ_* has reduced tremendously, due to the reduction in the kinematic viscosity letting common hot-wires (but also Pitot tubes) appear much larger than in other laboratory studies. Hot-wire measurements in the SuperPipe by Morrison *et al.* (2004) and Zhao & Smits (2007) with wire lengths varying from L^+ in the range of 12–385 and 20–1226, respectively, are clearly an order of magnitude larger than the length of the hot-wires employed in all aforementioned studies, but so are even more the Reynolds numbers. Both of the mentioned investigations encounter the second peak in the u'^+ distribution for $Re^+ > 5000$, and provide an empirical relation for its wall normal position. They speculate that the observed peak may be brought about due to structural changes in the flow anticipating Reynolds number effects way into the overlap region.[7] Furthermore, their interpretation of the observed phenomenon would

[5] Complementary measurements by the same group in the DNW tunnel extended the range of Reynolds numbers up to $Re_\theta = 115000$, obviously with even higher L^+ values, and observe an even more pronounced outer peak (Knobloch & Fernholz 2004; Knobloch 2008).

[6] The author associates the found similarity (the plateau in the u'^+ distribution) around $y^+ = 150$ to the beginning of the logarithmic region.

[7] It is interesting to note that the appearance of a second peak in previous studies performed in the Superpipe have not lead to the same conclusion. At that time, the phenomenon was rather associated with "[t]wo sources of possible error []: the spatial resolution of the probes (which would tend to reduce the measured turbulence intensity) and the fact that the flow may not be fully-developed [] at the highest Reynolds numbers." (Smits & Marusic 1999).

reason the need for a mesolayer description, as introduced by Long & Chen (1981). DeGraaff (1999), on the other hand, employing LDV and hot-wire anemometry in a turbulent boundary layer, observes the outer peak only in the hot-wire measurements with L^+ varying from 4 to 45 in a Reynolds number range of $1500 < Re_\theta < 15000$ (DeGraaff *et al.* 1999), but not in the LDV measurements (DeGraaff & Eaton 2000).

The above review has pointed out that spatial resolution and Reynolds number effects on u' counteract. This shows that conclusions based on data from both a varying Reynolds number and L^+ value will make it difficult to attribute observed phenomena solely to Reynolds number effects, unless spatial resolution effects can explicitly be excluded and *vice versa*. It hence becomes clear, that with the need for high Reynolds number experiments, spatial resolution becomes an even more important issue and the available literature on it is clearly neither conclusive nor complete. This problem has only recently been investigated systematically in the light of the ongoing debate in wall-bounded turbulence by Hutchins *et al.* (2009). However, the authors focussed their attention on the streamwise turbulence intensity distribution and elucidate the debate regarding the trends in the near-wall peak as well as the emergence of a second peak further away from the wall. Furthermore they show the effect on the spectral distribution and its scaling and conclude, that besides $L^+ \leq 20$ and $L/d \geq 200$, also $t^+ \leq 3$ or $f^+ \geq 1/3$, where t^+ and f^+ denote the sample intervall and sampling frequency in viscous time units, respectively, has to be guaranteed for spatially and temporally resolved measurements in wall-bounded flows.

The effect of spatial resolution on the probability density function and hence the skewness and flatness factors are barely studied so far, despite the results in the mentioned early investigations. Surprisingly, the question whether or not the mean velocity is affected by spatial resolution, has to our knowledge not been raised. These points will in the following be discussed and investigated by utilising experimental data for low to moderate Reynolds numbers and varying L^+ values. Although high Reynolds number data was not employed in the following study, the observed trends will be shown to be clearly above measurement uncertainties.

3. Preliminaries

In the statistical approach, random variables are characterised by probability density functions/distributions. Also the pdf is an important quantity in turbulence research, its central moments, as defined through,

$$u_n = \int_{-\infty}^{\infty} (u - U)^n \, p(u) \, \mathrm{d}u \,, \tag{2}$$

are usually given of most studies. Here u denotes the instantaneous streamwise velocity and U its time-averaged mean value, whereas $p(u)$ is the pdf of u. The

rms value, the square root of the second central moment, $u' = \sqrt{u_2}$, has already been discussed in Ligrani & Bradshaw (1987) as well as Hutchins *et al.* (2009), and hence, here we will focus primarily on the third and fourth order central moments, i.e. the skewness and flatness factors, S_u and F_u,

$$S_u = \frac{u_3}{u_2^{3/2}}, \quad F_u = \frac{u_4}{u_2^2}, \tag{3}$$

of the pdf. That these moments are affected by spatial resolution has already been pointed out by Johansson & Alfredsson (1983), but due to the active debate regarding the appropriate scaling of the mean (Österlund *et al.* 2000; Buschmann & Gad-el-Hak 2006; Nagib & Chauhan 2008), rms and spectra (Marusic & Kunkel 2003; Zhao & Smits 2007) in wall-bounded flows these moments had to take a back seat.

A truncated skewed pdf distribution alters the area under the pdf. Recalling that the first moment, the mean, is nothing else than the centre of gravity of the area under the pdf, this raises legitimately the question, whether or not the mean is affected if spatial resolution affects the pdf and if so to what extent. The answer to this question is, in consideration of the current debate regarding the scaling of the mean velocity distribution in the overlap region, and the universality of the inner region of canonical wall-bounded turbulent flows, of utmost importance. It remains therefore puzzling (at least to the author) why the question has not been raised and studied before.

4. Methodology and Experimental data

In the following, recently obtained measurements from zero pressure-gradient turbulent boundary layer experiments, reported in Örlü (2009*a*), will be used in conjunction with other available data in order to extend the range of Reynolds numbers and wire lengths. Higher order moments as well as the pdfs itself will be investigated in terms of Reynolds number and wire length effects and a small, but nevertheless important, detected effect on the mean velocity will be discussed. The outcome of the present study will finally be utilised to comment, but also query some conclusions of previous studies.

The experimental data of Örlü (2009*a*) was obtained in the MTL wind tunnel at KTH by means of hot-wire anemometry. Additionally oil-film interferometry measurements were performed in order to provide an independent and direct measure of the wall shear stress and thereby friction velocity. The details of the experimental set up, the measurement technique as well as the quality assessment of the zero pressure-gradient equilibrium turbulent boundary layer is documented in Örlü (2009*a*), to which the reader is referred to for further details.

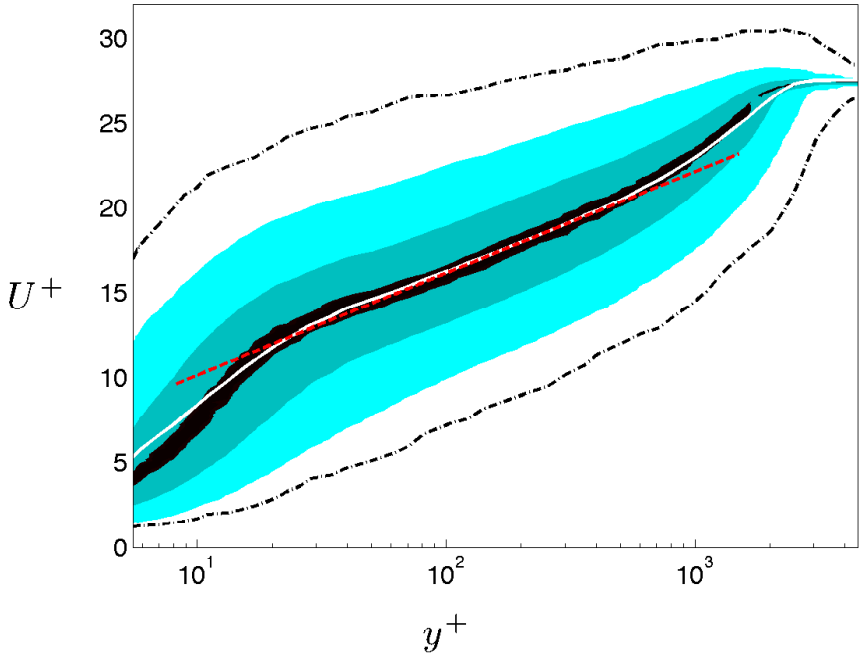

FIGURE 1. Mean streamwise velocity scaled in inner variables (white line) plotted above its pdf distribution for $Re_\theta = 8105$ and $L^+ = 61$. The three shaded areas indicate the confidence intervals for 3, 50 and 98.5 %, whereas the dash-dotted lines include all sampled velocity signals, i.e. the extreme values of the pdf. The log law with $\kappa = 0.384$ and $B = 4.17$ is shown through the dashed line.

5. Results

The moments of the fluctuating velocity are by definition inherently connected to their pdf and hence it is natural to explore prior to any investigation the pdf of the streamwise velocity fluctuations in conjunction with its mean value. Figure 1 shows the mean streamwise velocity component in inner scaled variables plotted on top of its pdf distribution for $Re_\theta = 8105$ measured with a hot-wire of length $L^+ = 61$. Additionally, the log law with $\kappa = 0.384$ and $B = 4.17$ (Österlund 1999; Nagib *et al.* 2004) is shown through the dashed line. Although, these constants differ from the classical ones, they are close to those obtained by means of oil-film interferometry for the present measurements (Örlü 2009*a*), and are adapted throughout the present paper. Nevertheless, the used constants will not alter the results presented here, but serve mainly as a reference line.

Figure 1 illustrates that in order to ensure correctly measured mean quantities within the viscous sublayer the hot-wire has to be calibrated for values down to at least 80 % below its average value[8], which demands special requirements for the calibration flow, the transducers involved as well as the calibration procedure. Furthermore one can observe that the effect of the wall on the hot-wire readings starts to influence the low speed fluctuations much earlier than usually assumed for its mean value. It is generally accepted that the mean streamwise velocity readings from hot-wires in air are affected by the presence of walls when they penetrate into the viscous sublayer. More specifically, Hutchins & Choi (2002) and Durst & Zanoun (2002) among others, give values between $y^+ = 3.5$–4 for the upper limit until which the mean velocity readings are affected by the presence of the wall. Considering figure 1 it can, however, be stated, that the low speed fluctuations are affected beyond the linear sublayer. With this in mind care should be paid on the absolute mean velocity reading even for points slightly above the linear sublayer when utilising it to determine the friction velocity or correct the wall position as for instance described in Hutchins & Choi (2002) or Örlü & Fransson (2009).

Focussing on the peak value of the pdf relative to its centre of gravity (depicted by its mean value) a region starting from around 150–200 wall units and extending up to around 500 wall units (corresponding to $y^+ = 0.15$–$0.2\,\delta^+$, where δ^+ is the Kármán number equivalent to the friction Reynolds number) can be detected in which the mean value is situated in the centre of the pdf. This region corresponds to the overlap region in which the log law with its newly established constants for zero pressure-gradient turbulent boundary layers of $\kappa = 0.384$ and $B = 4.17$ (Österlund *et al.* 2000) collapses with the mean velocity profile. Keeping the upper boundary of the log law the same and decreasing the slope (and thereby increasing κ and B) would give a wider range in which the log law would seemingly represent the mean profile well, due to the inclusion of the overshoot over the log law situated at the end of the buffer region. Although such a procedure is commonly observed in the literature, due to the acceptance of the classical log law constants and the thereby much lower beginning of it (see e.g. Tennekes & Lumley (1972) and Pope (2000), who give values around $y^+ = 30$–50), this would include a varying skewness of the pdf (to say the least) within the log law region, which in turn would exclude a scaling of (at least) the skewness factor. This demonstrates the importance of the log law limits, which determine the value of the extracted log law constants. But a more far reaching insight is that the choice of the limits will ultimatively establish whether or not a scaling of the skewness factor and thereby the pdf is possible or not. The vagueness of the limits of the log law will prevail, until well resolved high Reynolds number experiments are available, so that the overlap region and its scaling law can with certainty be established by different approaches.

[8]Even in the buffer region at $y^+ = 15$ the lowest velocities encountered in the probability density function are approximately 2 u_τ.

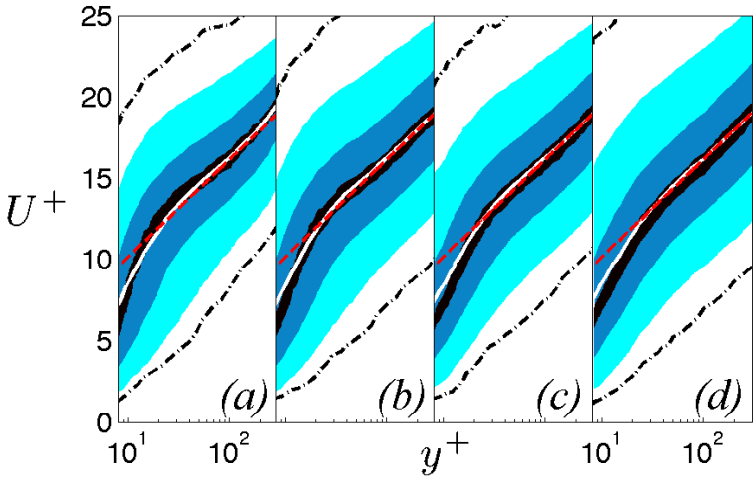

FIGURE 2. Same as figure 1, but restricted to $8 \leq y^+ \leq 300$, for (a) $L^+ = 15$ and $Re_\theta = 2532$, (b) $L^+ = 26$ and $Re_\theta = 8105$ (c) $L^+ = 46$ and $Re_\theta = 7561$, and (d) $L^+ = 61$ and $Re_\theta = 18661$.

Whereas the outer and overlap region is characterised by subtle and slow changes in the pdf compared to its centre of gravity, the inner region displays drastic changes. The data in the depicted figure is from a moderate Reynolds number of $Re_\theta = 8105$ measured with a single hot-wire with $L^+ = 26$, which is slightly above the requirements mentioned by Ligrani & Bradshaw (1987). Recalling the findings of Johansson & Alfredsson (1983) and Khoo *et al.* (1997) for the buffer region and linear sublayer, respectively, a different picture should be expected with a change in L^+, whereas the picture should be rather invariant to Reynolds number effects.

To illuminate this effect further the same kind of plot for a variety of Reynolds numbers and L^+ values is depicted in figure 2. The classical view of wall-bounded turbulent flows (Wieghardt & Tillmann 1951; Clauser 1954) considers pipe and channel flows as well as zero and non-zero pressure-gradient turbulent boundary layers similar, when scaled in inner variables within the inner and overlap region. This means, that any Reynolds number dependence is entirely limited to the outer, or wake, region. Only recently, has this view been challenged, due to the insight that the von Kármán constant was found to be different for different pressure gradients (Nagib *et al.* 2004) and hence the above mentioned similarity for pipe, channel and turbulent boundary layer flows was restricted to the viscous and buffer region, and would not extend to the overlap region. Whether or not the von Kármán constant and thereby

the overlap region for the three aforementioned canonical flow cases is identital is still under debate (Nagib & Chauhan 2008). Minor differences are also encountered when comparing DNS of the three canonical wall-bounded flow cases, which were believed to be universal, i.e. channel (Hoyas & Jiménez 2006), pipe (Wu & Moin 2008) and zero pressure-gradient turbulent boundary layer flows (Schlatter *et al.* 2009).[9] However, the Reynolds numbers reached are still low and make any conclusive statement impossible, due to the difficulty to define the bounds of the overlap region, provided that it is present at such low Reynolds numbers. The state of the art seems to suggest that the viscous and buffer region are universal for the above cases and that the debate regarding the appropriate description of the mean velocity concerns mainly the overlap region. Note, however, that some studies have raised concerns regarding the Reynolds number independence of the buffer region, e.g. Park & Chung (2004) in their study regarding fully developed turbulent channel flow.

Here, we compare zero-pressure gradient turbulent boundary layer data and therefore a universal mean velocity profile should be expected all the way up to the end of the overlap region for various Reynolds numbers. However the presented pdfs in figure 2 display a different scenario. While a clear deviation from a Gaussian pdf distribution is present in (a) below $y^+ = 100$, the deviation becomes smaller when successively moving to higher L^+ and Reynolds number cases, i.e. to (b), (c) and (d). For (a) the mean velocity profile in the overlap region does not even extend to $y^+ = 300$, due to the low Reynolds number of $Re_\theta = 2532$, whereas a successively longer part in inner-law scaling is covered for (b)–(d) and agrees nicely with the log law with its newly established constants. The reason for the apparent differences can be sought within Reynolds number and/or spatial resolution effects. Both are interrelated, at least for experiments, where higher Reynolds numbers are obtained by increasing the free stream velocity or the density, and therefore make it difficult to extract which of the two variables are actually dominating. Note, however that the subplots are sorted in order of increasing L^+, and connote a dependence on spatial resulution effects. Particularly the plot in (b) is from a slightly higher Reynolds number than the one shown in (c), but was measured with a wire with a nearly half as large L^+ value. The comparison of both subplots therefore supports the view put forward by Johansson & Alfredsson (1983), viz. that spatial resolution effects are stronger than Reynolds number effects, when measurements are made with a wire at constant physical length. Regardless of which of the two reasons is the main cause, a subtle difference in the mean quantity compared to the log law is discernable.

The observed bump or overshoot over the log law, was first mentioned by Österlund *et al.* (2000). The authors emphasised that the inclusion of the region where the bump resides, viz. $30 \leqslant y^+ \leqslant 150$, into the definition of the

[9] Such differences in DNS data of canonical wall-bounded turbulent flows are, for instance, presented in Örlü & Fransson (2009).

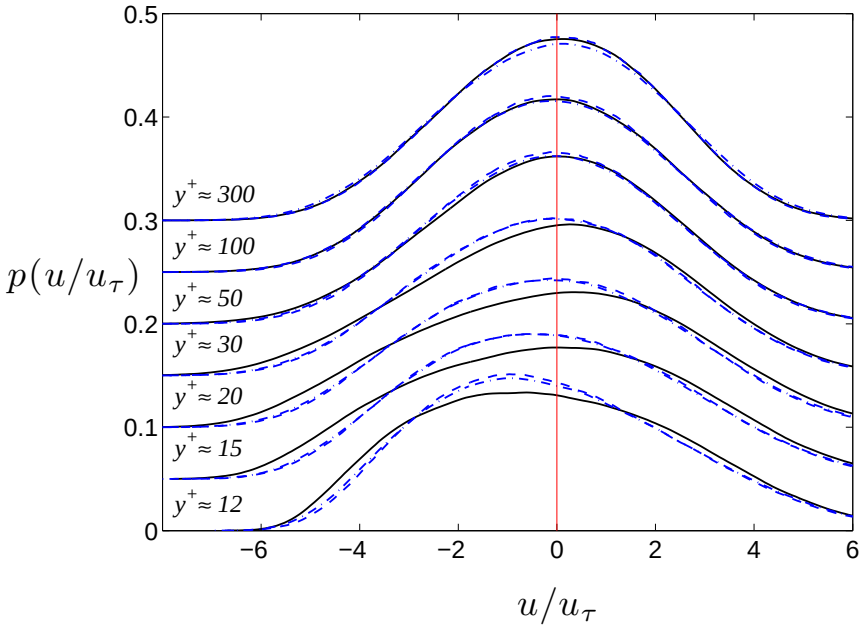

FIGURE 3. Probability density distribution of the streamwise velocity fluctuations scaled by u_τ: solid ($L^+ = 26$, $Re_\theta = 8105$), dashed ($L^+ = 46$, $Re_\theta = 7561$), and dash-dotted ($L^+ = 46$, $Re_\theta = 8792$) line for different y^+ positions, each y-position is shifted for visual aid by 0.05.

overlap region would give rise to different log law constant or make (at least for the low Reynolds number region) a power law fit the data apparently better.[10]

So far only results from a limited range of L^+ values have been presented for changing Reynolds numbers. Therefore figure 3 focusses on a matched Reynolds number case, measured with wires of different L^+. Here the pdf is presented above the mean and scaled by the friction velocity, rather than u'. Scaling of the pdf is necessary in order to compare the results from experiments taken at different free stream velocities, however the usual scaling with u' in the present context is misleading. As mentioned in section 1 the near-wall peak in the u'-distribution has been found to reduce substantially with increasing wire length and will consequently mask spatial resolution effects on higher order moments, and in turn the pdf distribution itself, when scaled with

[10] Buschmann & Gad-el-Hak (2006) refers to Buschmann & Gad-el-Hak (2003) for noting the bump, however, no indication can be found in the given reference. Instead, it was already mentioned and described in Österlund *et al.* (2000). Note also that the term "bump" is loosely used in the literature to indicate an overshoot or an undershoot compared to the log law, respectively, depending on the chosen log law constants.

the same quantity. The friction velocity on the other hand is a global constant for one velocity profile and is therefore not affected by spatial resolution effects. The pdfs for the two matched L^+ (= 46) cases, with Reynolds numbers below and above the case with smaller L^+, agree nicely with each other and depict a clear deviation from the pdf measured with an nearly half as long hot-wire ($L^+ = 26$). The tails of the pdfs illustrate that the longer wires are not able to detect the low-speed fluctuations with high amplitude and thereby smooth out the highly non-Gaussian features of the pdf within the buffer region. This trend is clearly observable, particularly where the overshoot in the mean velocity profile was encountered and where it was found to be reduced with increasing wire length and/or Reynolds number. Figure 3 demonstrates that mainly spatial resolution is responsible for smearing out extremal events and hence a reduction in the mean velocity, especially there where a high deviation from a Gaussian distribution is found, but does not conclusively exclude Reynolds number effects.

Further support for the above can be gained from figure 4, where the 2^{nd}, 3^{rd} and 4^{th} order central moments are presented from various sources for a Reynolds number of around 5000. Additional to the measurements of Örlü (2009*a*) results from DeGraaff & Eaton (2000) and Smith (1994) are shown in order to expand the range of L^+ values. The former employed LDV and has therefore no problem with spanwise averaging (note however the order of magnitude increase in the wall normal direction when compared to hot-wires), whereas the latter doubles the longest wire length of Örlü (2009*a*).

The streamwise turbulence intensity in inner-scaled variables, u'^+, illustrates what Ligrani & Bradshaw (1987) and Hutchins *et al.* (2009) have already demonstrated, namely that most of the attenuation is observed at the location of the near-wall peak, however, spatial attenuation persists over the entire buffer region and beyond (depending on its assumed upper limits). The reason for the observed different rms values within the overlap region may be twofold, viz. a Reynolds number effect or it could be caused by the scaling with the friction velocity, which in the case of Smith (1994) and DeGraaff & Eaton (2000) was deduced from a fit to the log law with classical values. The latter is probable to give higher values friction velocities and hence shifts the profiles towards smaller values (Karlsson 1980; Murlis *et al.* 1982).[11]

The skewness and flatness factors, S_u and F_u, respectively, emphasise what Johansson & Alfredsson (1983) pointed out, namely that the zero-crossing of the skewness factor is shifted further away from the wall with increasing L^+. It is interesting to note, that the Smith (1994) data with $L^+ = 62$ does not

[11] The profiles can be made to collapse in the overlap region by utilising the newly established log law constants, which were confirmed to be representative also for low Reynolds numbers as shown by Örlü (2009*a*), who employed oil-film interferometry to determine the friction velocity. Nevertheless we will use the data of Smith (1994) and DeGraaff & Eaton (2000) as originally provided.

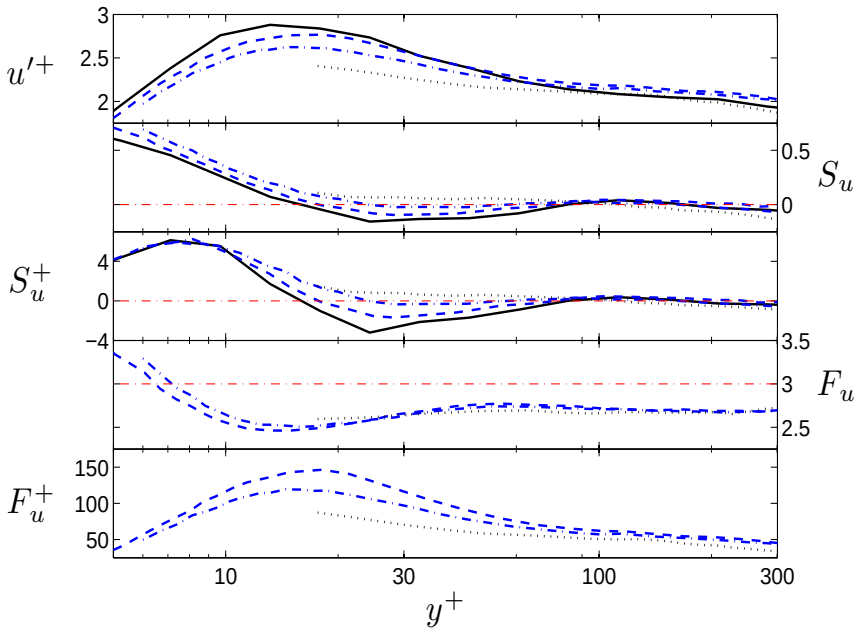

FIGURE 4. Inner-scaled rms value, u'^+, skewness and flatness factors, S_u and F_u, respectively, as well as the skewness and flatness scaled in viscous units, S_u^+ and F_u^+, for varying L^+ values around a nearly constant Reynolds number. LDV data by DeGraaff & Eaton (2000) for $Re_\theta = 5160$ & $L^+ =$ x: (solid), HWA data by Örlü (2009*a*) for $Re_\theta = 5569/5451$ & $L^+ = 17/33$: (dashed/dash-dotted) and Smith (1994) for $Re_\theta = 5021$ & $L^+ = 62$: (dotted). Gaussian values are indicated through the light dash-dotted lines. Note that the fourth order moment was not provided by DeGraaff & Eaton (2000).

display a zero crossing anymore and prevails positive for the entire buffer region. The negative values of S_u within the buffer region indicate that large negative fluctuations of u' are more probable than large positive values, as also evident from the pdfs shown in figure 3. As speculated by Smith (1994), these small scale, low speed events are likely ejections associated with the bursting process. These are probably the structures which are not resolved when measured with longer wires.

Also the flatness factor displays a trend towards a more homogenous distribution when measured with wires of increasing L^+. Note also, that only with a short enough wire ($L^+ \lesssim 20$) the zero-crossing of the skewness (and the minimum in the flatness) factor corresponds to the location of the near-wall

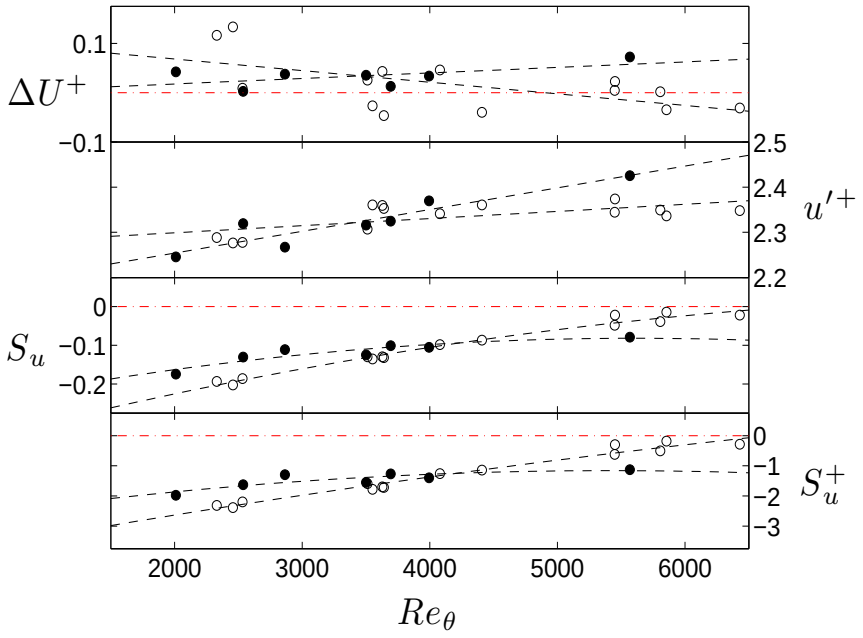

FIGURE 5. The mean velocity relative to the "law of the wall" described through the analytical expression given by Musker (1979), ΔU^+, the inner-scaled rms and skewness, u'^+ and S_u^+, as well as the skewness factor, S_u, against Reynolds number are given for matched and varying L^+ values at $y^+ \approx 40$. Measurements at the same downstream location and varying free stream velocity with increasing L^+ values from 15 to 35 (open circles) are compared to those from measurements with varying downstream locations with fairly constant L^+ ($\approx$ 17–18) values (filled circles). Dashed lines are for visual aid only.

streamwise turbulence intensity peak, contrary to the results of Mochizuki & Nieuwstadt (1996). The latter concluded that the skewness factor remained around zero at $y^+ = 15$ for $L^+ \leqslant 30$.

Johansson & Alfredsson (1983) anticipated that S_u and F_u may mask spatial resolution effects due to its scaling with u'. This becomes clear when considering S_u^+ and F_u^+,

$$S_u^+ = \frac{u_3}{u_\tau^3}, \quad F_u^+ = \frac{u_4}{u_\tau^4}, \tag{4}$$

which instead is non-dimensionaled by means of the friction velocity. In this way, the effect on u' will be separated from the skewness and flatness. Here,

the effect of L^+ is more clearly apparent. Similar trends are observed when comparing the data from the above sources around Re_θ of 13000 (not shown here). Reviewing the shown figures 1–4 it becomes clear that spatial resolution is an issue not only within the buffer region (within its classical bounds), but is—for the range of L^+ values investigated here—apparent up to at least $y^+ = 100$. It has also been shown, that the depicted clear trend on the pdf and hence its higher moments with increasing L^+ have a detectable effect on the mean value. However, these can hardly be appreciated in the form shown so far.

To further access the effect of Reynolds number and L^+ on the moments of the pdf separately, use is made of a second set of data by Örlü (2009*a*), that were collected at a constant free stream velocity. Hereby the Reynolds numbers were increased by advancing in the downstream direction. This gives access to a Reynolds number range with fairly constant L^+ values. Figure 5 compares the rms and skewness in form of S_u and S_u^+ at $y^+ \approx 40$ plotted against the Reynolds number. Additionally the mean velocity is given relative to the "law of the wall" expressed through the analytical expression given by Musker (1979)[12], $\Delta U^+ = U^+ - U^+_{Musker}$. This procedure avoids any effects of the small deviations of the measurement locations from the nominal wall distance of $y^+ = 40$.

The presented trends of both representations of the skewness confirm that spatial resolution has a stronger impact on the statistics than Reynolds number effects. Despite the limited Reynolds number range and the scatter in the data, the trends are apparent. The trends in the rms support the conclusions of previous studies by showing the increased attenuation with increasing L^+ values. It also becomes clear that conclusions from comparative studies, as those by Fernholz & Finley (1996) or Mochizuki & Nieuwstadt (1996), which employ data from various sources with coupled and uncoupled L^+ and Reynolds number values are highly dependent on the selected data (despite the fact that the friction velocity is usually extracted by various indirect methods, which add significantly and systematically to the scatter). The shown trends, visualised through the dashed lines, are more enhanced when considering wall distances closer to the near-wall peak in the rms. However $y^+ = 40$ was selected here, in order to check whether trends in the mean velocity would be present. The trends in the mean velocity were instead found to be more pronounced when moving further away from the near-wall peak. There are apparently different trends for matched and increasing L^+ cases, which go along with the observations made so far.

Also the effect of spatial resolution could be shown to be stronger than Reynolds number effects on the higher order moments, the effect on the mean

[12]Instead of the classical constants for the log law, which are originally used in this expression, here the newly established values from Österlund *et al.* (2000) were employed.

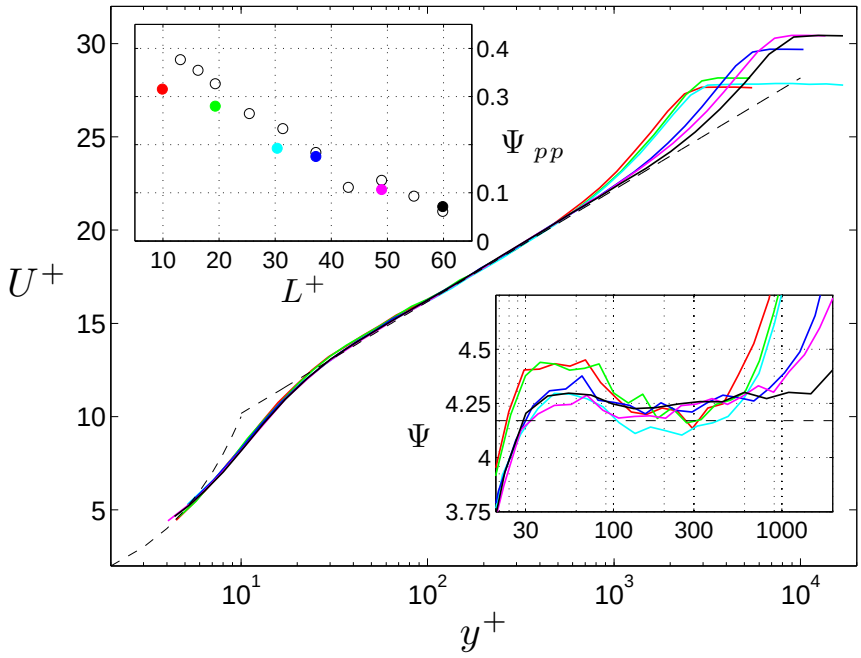

FIGURE 6. Mean velocity profiles in inner-scaling, U^+ vs. y^+, for a range of Reynolds numbers and wire length obtained by Österlund (1999) with the linear and log law profiles indicated through the dashed line. The deviation from the log law, Ψ, is given in the lower insert, whereas the upper one depicts the peak-to-peak value in the Ψ vs. y^+ plot as a function of L^+. Empty circles in the latter show results from all 2.54 micron wires deduced from the original data and are not shown in the other plots for clarity.

velocity was found to be rather subtle, albeit detectable. To ensure that the observed trends on the mean velocity are real the range of Reynolds numbers needs to be extended.

Therefore, use is made of the database of Österlund (1999), which provides mean velocity profiles over a wider Reynolds number and L^+ range. Figure 6 shows selected mean velocity profiles for various L^+ values between 10–60 at different Reynolds numbers. Note, that both quantities are interrelated for most of the shown data points, i.e. a high Reynolds number corresponds to a high L^+ value and *vice versa*. To detect effects on the mean velocity, the overshoot above the log law, $\Psi = U^+ - 1/\kappa \ln y^+$, can be employed, shown in the lower insert. The overlap region is clearly apparent for $y^+ > 150$, and

the overshoot over the log law is emphasised through the bump in the buffer region. Note that the log law constants are extracted from a huge number of measurement sets and present an average value. This explains the observed small offset seen in such a sensitive quantity as Ψ, which are not recognisable in the conventional U^+ vs. y^+ plot.

There is a clear difference between the profiles. The difference between the maximum and minimum values relative to the log law seems to diminish with increasing Reynolds number (and hence L^+ value). This is further illustrated in the upper insert, where the peak-to-peak value is plotted against L^+. Additionally to the selected mean profiles all extracted peak-to-peak values from nominal 2.54 micron hot-wires are indicated through open circles.[13] As pointed out by Österlund *et al.* (2000) and documented by Buschmann & Gad-el-Hak (2006) the additive constant, depicted through the dashed line in the lower insert, is Reynolds number dependent for low Reynolds numbers and decreases towards an asymptotic value for increasing Reynolds numbers. Keeping this in mind, one would expect an asymptotic increase in the peak-to-peak value, Ψ_{pp}, with increasing Reynolds number[14], however, the opposite trend is present, and emphasises the strength of the effect of spatial resolution on the mean quantity. These subtle difference may become more important, when considering the lower end of the classical overlap region, when obtained from hot-wires with even larger L^+ values. Small differences may in this case lead to a log law with different constants or a shift in the origin.[15] Additionally the mean streamwise velocity within the buffer region is frequently used to determine the friction velocity (Gibbings 1996) or correct for a wrong wall position (Hafez *et al.* 2004). When measurements are not available within the sublayer, the accuracy of the determined quantity relies entirely on the accuracy of the measured mean velocity within the buffer region and the employed method (see also the discussion in Örlü & Fransson 2009).

Contrary to the relative mean velocity, ΔU^+, depicted in figure 5, the peak-to-peak value, Ψ_{pp}, is a more reliable quantity. Whereas the former compares a single absolute value above an analytical expression for the "law of the wall", the latter employs the difference between two points of the same profile from the

[13] Note that while the open circles were extracted from the original data, the shown data in the figure were re-evaluated, in order to fit the data better to the shown log law, in order to ease comparison. Hence, some of the open circles are extracted from the same profiles as those represented by the solid symbols.

[14] Utilising the modified Musker profile by Chauhan *et al.* (2009), which incorporates the correct overshoot over the log law, one can employ the same procedure used to generate the upper insert in figure 6. Doing so it can be found that Ψ_{pp} increases asymptotically to a value of 0.28 at the higher end of Reynolds numbers measured by Österlund *et al.* (2000), giving an approximate increase of around 0.1 u_τ from his lowest Reynolds number on.

[15] A log law with a shifted origin, as for instance derived by Oberlack (2001), was shown to represent DNS data from an Ekman boundary layer (Spalart *et al.* 2008) over a larger extent then the usual log law.

buffer and overlap region. Hence, Ψ_{pp} is less sensitive to how the measurements were post-processed (scaling with the friction velocity or the determination of the wall position). Due to the low Reynolds numbers for the data in figure 5 and the consequently not fully established overlap region, ΔU^+ had to be used instead of Ψ_{pp}.

6. Conclusions

Reviewing the shown results, it has been demonstrated that for the same Reynolds number the viscous scaled hot-wire length, L^+, has a strong impact on the pdf and hence its higher order moments over a range where the pdf displays a strong deviation from a symmetric pdf. This range extends up to around y^+ of 150 for the range of parameters investigated here. For varying Reynolds numbers spatial resolution effects act against the trends imposed by Reynolds number effects. It is even found that spatial resolution imposes its trend above those given by the Reynolds number. This may, however, vary depending on the viscous scaled wall distance, due to the changing pdf within $y^+ \leqslant 150$.

Most surprisingly, spatial resolution effects were found to systematically reduce the mean velocity beyond the near-wall peak in the rms distribution over the entire buffer region. As apparent from figure 6 a reduction of around 0.3 u_τ was found when utilising a wire with $L^+ = 60$ instead of 15, whereas a weak increase would have been expected due to low Reynolds number effects. These subtle differences should be considered in the light of the current debate, particularly, when based on hot-wire results where the wire length is an order of magnitude larger than those employed here. Two mention just two, the proper scaling of the mean streamwise velocity distribution as well as the influence of viscosity and hence Reynolds number on the region beyond the classical buffer region, i.e. $y^+ > 30$, can be highly biased due to the effect of spatial resolution effects. The observed changes in the pdf also support the view put forward by Österlund *et al.* (2000), that the overlap region should be defined to start beyond $y^+ \geqslant 150$, so that the bump in the mean velocity as well as the varying pdf are excluded. Keeping in mind the much longer L^+ values in high Reynolds number experiments, mentioned in section 2, some of the controversies in the debate regarding the mean velocity scaling as well as the universality of the pdf in the overlap region (in its classical bounds, i.e. starting from around $y^+ = 30$–50), may clearly be associated to spatial resolution effects. Whether or not the Reynolds number has an effect on the mean velocity within the buffer region could not be satisfactorily answered in the present study, due to the limited Reynolds number range and its interrelation to L^+ values. Hence, there is a need for further experiments over a wider Reynolds number range with matched L^+ values. Based on the results presented here, there is no argument to exclude Reynolds number effects *a priori* within the buffer region, just because it has been common practice in the community.

Based on the presented results, it can also be questioned whether Pitot tube measurements within a region characterised by highly non-Gaussian pdfs are accurate and unbiased. Additionally the turbulence structure in wall-bounded turbulent flows is inhomogeneous, anisotropic and, particularly, the pdf is skewed in different directions depending on the wall-normal distance (Karlsson 1980). Besides a number of open issues, as for instance the controversy regarding the need for explicit turbulence corrections (Perry *et al.* 2001; McKeon *et al.* 2003), the effect of a non-Gaussian pdf is not accounted for by any correction method.

7. Impact on results from previous studies

Based on the presented results it seems reasonable to review a few controversial conclusions from previous studies, and check whether the controversy or disagreement among them may be explainable by spatial resolution effects. One of the topics which has attracted considerable attention is the question whether or not the pdf of the streamwise velocity fluctuations within the overlap region is universal, i.e. invariant to the distance from the wall as well as the Reynolds number. The answer to this question is not only important from a philosophical standpoint, but is rather of quite practical substance. Since most of our understanding of wall-bounded turbulence is based on low to moderate Reynolds numbers, it becomes clear that, the "key question in [...] high Reynolds number modeling as well as in devising novel flow control strategies is: what are the Reynolds number effects on the mean and statistical turbulence quantities [...]?" (Gad-el-Hak & Bandyopadhyay 1994). Furthermore Tsuji & Nakamura (1999) have shown that the log law can be derived from the pdf equations, and they suggest that the description of the mean velocity profile in wall-bounded turbulent flows by means of the log law should go along with a similar universality in the pdfs.

Using DNS of channel flow Dinavahi *et al.* (1995) conclude that the pdf of the fluctuating components above the buffer layer are independent of y^+, and the Reynolds number.[16] However, their results are limited due to the fact that their highest Reynolds number was $R^+ = 395$, where the Reynolds number is based on the outer length scale and the friction velocity. LDV measurements in a turbulent pipe flow by denToonder & Nieuwstadt (1997) extend the Reynolds number further, $338 \leqslant Re_\tau \leqslant 1380$, and find no clear Reynolds number dependence for the higher order moments of the streamwise velocity fluctuations. However, their data displays some peculiarities. Their near-wall peak value of the rms appears to be Reynolds number independent, whereas their mean velocity profile displays Reynolds number trends into the buffer region. Both effects can be explained by wrongly deduced friction velocities. Tsuji &

[16] Note in this context, that the wake region in channel flows is comparable small compared to its counterparts in canonical wall-bounded flows, as illustrated through their wake parameters (Nagib & Chauhan 2008).

Nakamura (1999), using hot-wire data from zero pressure-gradient turbulent boundary layer experiments in the range $1320 \leqslant Re_\theta \leqslant 3788$ (which overlaps with the Reynolds number range of denToonder & Nieuwstadt (1997)), employed the Kullback Leibler (KL) divergences to study the differences in the pdfs quantitatively and conclude that an universal region exists for $y^+ \geqslant 30$. Recalling our results, that the pdf is negatively skewed in the buffer region and approaches a Gaussian value with increasing wall distance, but also with higher L^+ value, their lower limit for the log region may be an artifact of spatial resolution caused by their employed X-wire probe, which despite varying L^+ values (from around 13 to 40) will also be effected by the velocity gradient in the inner layer.

To test the idea of universal pdfs proposed by Tsuji & Nakamura (1999) at higher Reynolds numbers the experimental data from Tsuji (1999) and Österlund (1999) was employed in Lindgren *et al.* (2004) and Tsuji *et al.* (2005). In the latter study a range of $1300 \leqslant Re_\theta \leqslant 13000$ was covered and only hot-wire data satisfying the condition $L^+ \leqslant 15$ were used. Adapting the KL divergence they found that the log law region starts around $y^+ = 180$ and extends to about 0.15–0.2 δ^+, whereas the pdfs display universality starting at the same lower end, but extend to a somewhat lower position. Experiments by Andreopoulos *et al.* (1984) in a turbulent boundary layer ranging over a similar Reynolds number range, $3624 \leqslant Re_\theta \leqslant 15406$, display variations in the skewness and flatness factor for the buffer and overlap regions. However their rms profiles displays clear evidence of effects from spatial averaging, that lead the authors to conclude: "in the buffer region the rms-longitudinal velocity fluctuations decrease with Reynolds number up to $Re_\theta \approx 10^4$." And, that "for higher Reynolds numbers, a universal distribution appears to be reached which extends into the log-law region of the flow".

From the conclusions of the presented studies so far it becomes clear, that the "issue of sufficient probe resolution is particularly acute when studying Reynolds number effects" (Gad-el-Hak & Bandyopadhyay 1994). These authors, in their review paper on Reynolds number effects in wall-bounded turbulent flows, impose that L^+ should not be much larger than 5, in order to be able to associate observed trends with Reynolds number effects. Comparing a large amount of data, they come to the same conclusions as Andreopoulos *et al.* (1984), namely that u'^+_{max} increases with Reynolds number only for low Reynolds numbers, and that the higher order moments depict clear Reynolds number effects. Their conclusions are, however, at odds with their own advice that spatial resolution effects can be interpreted as Reynolds number effects. The reason for this is that they obtained, estimated or calculated L^+ an order of magnitude too small, at least for the experiments by Purtell *et al.* (1981),

Andreopoulos *et al.* (1984), and Erm & Joubert (1991), on which their conclucions on the rms, skewness and flatness factors are primarily based.[17]

Morrison *et al.* (2004) examined the pdf and higher order statistics of the streamwise velocity component in the SuperPipe for a Reynolds numbers, Re^+, ranging from 1.50×10^3–1.01×10^5, thereby exceeding the highest Reynolds number of Andreopoulos *et al.* (1984) around 20 times. As mentioned in section 2 their data showed clear evidence of spatial resolution, with L^+ varying from 12 to 385.[18] Nevertheless, they use their data from $y^+ \geqslant 60$, and assume that "the data can be expected to be substantially free of resolution effects", which lead them to state: "It is clear that the pdfs are neither constant with y^+ at a given Reynolds number [...] nor constant at a given y^+ for a range of Reynolds numbers [...]". However, there are a number of peculiarities in their line of reasoning. The question is not whether the pdfs are universal over the entire flow, i.e. all y^+ positions, but rather whether universality can be found within the overlap region regardless of how its bounds are defined or which law describes its mean profile. Morrison *et al.* (2004), on the other hand, compares for instance the pdfs at $y^+ = 60$, 255, 598, 2653 and 8559 for $R^+ = 8560$. Here the last location is approximately at the centreline and 2653 corresponds to 0.3 R^+ and is clearly within the wake (core) region of the pipe.[19] Similarly they examine the pdfs at $y^+ \approx 600$ between $1500 \leqslant Re^+ \leqslant 101000$, where 3–5 of their 8 pdfs lie again within the core region. Recalling the results present here and those from Hutchins *et al.* (2009), viz. that spatial resolution can severely effect higher order statistics also beyond the buffer region, their conclusions are—to say the least—doubtful.[20]

[17] While Gad-el-Hak & Bandyopadhyay (1994) state $0.8 \leqslant L^+ \leqslant 3$, $1.7 \leqslant L^+ \leqslant 6.4$ and $L^+ \leqslant 5$ for for the experiments by Purtell *et al.* (1981), Andreopoulos *et al.* (1984), and Erm & Joubert (1991), respectively, the values given or estimated from the original sources (cf. values given by Mochizuki & Nieuwstadt (1996) or Fernholz & Finley (1996)) indicate $8 \leqslant L^+ \leqslant 30$, $17 \leqslant L^+ \leqslant 66$ and $21 \leqslant L^+ \leqslant 30$, respectively. The order of magnitude error seems to stem from an earlier paper (Bandyopadhyay 1991), on which the review article is based on.

[18] Morrison *et al.* (2004) cite Marusic & Kunkel (2003) to support the view "that the magnitude of the second maximum increases indefinitely with Reynolds number", and also state, that its "position [...] also increases with Reynolds number". However, neither does Marusic & Kunkel (2003) mention the second, outer peak in their work, nor does the atmospheric surface layer (ASL) data confirm this trend conclusively. Contrary, the cited paper utilises the ASL data to state that u'^+ increases with Reynolds number over the whole boundary layer.

[19] Pitot tube measurements in the SuperPipe indicate that the overlap region, comprising an initial Reynolds number dependent power law region and a Reynolds number independent log-law region starting from $y^+ = 600$ is found to exist up to 0.07 (Zagarola & Smits 1998) or 0.12 R^+ (McKeon *et al.* 2004).

[20] Although they summoned denToonder & Nieuwstadt (1997) to underpin their conclusions in regards of the higher order statistics by stating: "As denToonder & Nieuwstadt (1997)

Summarising it can be said that DNS studies are still not able to address whether universality exist within the overlap region, due to their limited Reynolds number range, and most experimental studies have not considered that spatial resolution may affect their results. An exception is the study by Lindgren *et al.* (2004) and Tsuji *et al.* (2005), that employed only hot-wire data satisfying $L^+ < 15$ from the data provided by Österlund (1999), one where also the friction velocity was directly measured. Whether or not universality in the pdfs and hence higher order statistics exist within the overlap region of wall-bounded flows will remain an open question, until new high Reynolds number experiments are available, that provide both, sufficient spatial resolution of the probes and a direct and/or independent measure of the friction velocity (the latter is not a necessity for this particular reason, but for almost all other open questions).

Acknowledgement

The author has made use of experimental data of Doctors D. B. DeGraaf, J. Österlund and R. W. Smith and expresses his thanks for making these data sets publicly available. Prof. P. H. Alfredsson is acknowledged for initiating the study and comments on the manuscript.

suggests, these statistics are Reynolds-number dependent even though the changes are modest." However, the cited source contradicts them by summarising their study with: "The higher-order turbulence statistics show no clear dependence on the Reynolds number [...]."

References

Andreopoulos, J., Durst, F., Zaric, Z. & Jovanovic, J. 1984 Influence of Reynolds number on characteristics of turbulent wall boundary layers. *Exp. Fluids* **2**, 7–16.

Bandyopadhyay, P. 1991 Comments on Reynolds number effects in wall-bounded shear layers. *AIAA Paper 1991–0231*.

Bernard, P. & Wallace, J. 2002 Turbulent flow: Analysis, measurement, and prediction. *Wiley*.

Blackwelder, R. & Eckelmann, H. 1979 Streamwise vortices associated with the bursting phenomenon. *J. Fluid Mech.* **94**, 577–594.

Blackwelder, R. & Haritonidis, J. 1983 Scaling of the bursting frequency in turbulent boundary layers. *J. Fluid Mech.* **132**, 87–103.

Buschmann, M. H. & Gad-el-Hak, M. 2003 Generalized logarithmic law and its consequences. *AIAA J.* **41**, 40–48.

Buschmann, M. H. & Gad-el-Hak, M. 2006 Recent developments in scaling of wall-bounded flows. *Prog. Aero. Sci.* **42**, 419–467.

Chauhan, K. A., Monkewitz, P. A. & Nagib, H. M. 2009 Criteria for assessing experiments in zero pressure gradient boundary layers. *Fluid Dyn. Res.* **41**, 021404.

Clauser, F. H. 1954 Turbulent boundary layers in adverse pressure gradients. *J. Aero. Sci.* **21**, 91–108.

Corrsin, S. & Kovasznay, L. 1949 On the hot-wire length correction. *Phys. Rev.* **76**, 999.

DeGraaff, D. B. 1999 Reynolds number scaling of the turbulent boundary layer on a flat plate and on swept and unswept bumps. *Ph. D. thesis, Stanford University, USA*.

DeGraaff, D. B. & Eaton, J. 2000 Reynolds-number scaling of the flat-plate turbulent boundary layer. *J. Fluid Mech.* **422**, 319–346.

DeGraaff, D. B., Webster, D. R. & Eaton, J. 1999 The effect of Reynolds number on boundary layer turbulence. *Exp. Thermal Fluid Sci.* **18**, 341–346.

denToonder, J. & Nieuwstadt, F. T. M. 1997 Reynolds number effects in a turbulent pipe flow for low to moderate Re. *Phys. Fluids* **9**, 3398–3409.

Derksen, R. & Azad, R. 1983 An examination of hot-wire length corrections. *Phys. Fluids* **26**, 1751–1754.

Dinavahi, S., Breuer, K. S. & Sirovich, L. 1995 Universality of probability density functions in turbulent channel flow. *Phys. Fluids* **7**, 1122–1129.

Dryden, H. L. 1938 Turbulence investigations at the National Bureau of Standards. *Proc. 5th International Congress on Applied Mechanics, MIT, Cambridge, Massachusetts, USA*, pp. 362–368.

Dryden, H. L., Schubauer, G. B., Mock, W. C. & Skramstad, H. K. 1937 Measurements of intensity and scale of wind-tunnel turbulence and their relation to the critical Reynolds number of spheres. *NACA Tech. Rep. 581*.

Durst, F. & Zanoun, E. 2002 Experimental investigation of near-wall effects on hot-wire measurements. *Exp. Fluids* **33**, 210–218.

Erm, L. P. & Joubert, P. 1991 Low-Reynolds-number turbulent boundary layers. *J. Fluid Mech.* **230**, 1–44.

Fernholz, H. H. & Finley, P. 1996 The incompressible zero-pressure-gradient turbulent boundary layer: An assessment of the data. *Prog. Aero. Sci.* **32**, 245–311.

Fernholz, H. H., Krause, E., Nockemann, M. & Schober, M. 1995 Comparative measurements in the canonical boundary layer at $\mathrm{Re}_{\delta_2} \leqslant 6 \times 10^4$ on the wall of the German–Dutch windtunnel. *Phys. Fluids* **7**, 1275–1281.

Frenkiel, F. & Klebanoff, P. S. 1973 Probability distributions and correlations in a turbulent boundary layer. *Phys. Fluids* **16**, 725–737.

Gad-el-Hak, M. & Bandyopadhyay, P. 1994 Reynolds number effects in wall-bounded turbulent flows. *Appl. Mech. Rev.* **47**, 307–365.

Gibbings, J. 1996 On the measurement of skin friction from the turbulent velocity profile. *Flow. Meas. Instrum.* **7**, 99–107.

Hafez, S., Chong, M. S., Marusic, I. & Jones, M. B. 2004 Observations on high Reynolds number turbulent boundary layer measurements. *Proc. 15th Australasian Fluid Mech. Conf., Sydney, Australia*.

Hites, M. H. 1997 Scaling of high-Reynolds number turbulent boundary layers in the National Diagnostic Facility. *Ph. D. thesis, Illinois Institute of Technology, USA*.

Hoyas, S. & Jiménez, J. 2006 Scaling of the velocity fluctuations in turbulent channels up to $Re_\tau = 2003$. *Phys. Fluids* **18**, 011702.

Hutchins, N. & Choi, K. 2002 Accurate measurements of local skin friction coefficient using hot-wire anemometry. *Prog. Aero. Sci.* **38**, 421–446.

Hutchins, N. & Marusic, I. 2007 Large-scale influences in near-wall turbulence. *Phil. Trans. R. Soc. A* **365**, 647–664.

Hutchins, N., Nickels, T. B., Marusic, I. & Chong, M. S. 2009 Hot-wire spatial resolution issues in wall-bounded turbulence. *J. Fluid Mech.*, (accepted).

Johansson, A. V. & Alfredsson, P. H. 1983 Effects of imperfect spatial resolution on measurements of wall-bounded turbulent shear flows. *J. Fluid Mech.* **137**, 409–421.

Johnson, P. & Barlow, R. 1989 Effect of measuring volume length on two-component laser velocimeter measurements in a turbulent boundary layer. *Exp. Fluids* **8**, 137–144.

Karlsson, R. I. 1980 Studies of skin friction in turbulent boundary layers on smooth and rough walls. *Ph. D. thesis, Chalmers University of Technology, Göteborg, Sweden*.

Khoo, B., Chew, Y. & Li, G. 1997 Effects of imperfect spatial resolution on turbulence measurements in the very near-wall viscous sublayer region. *Exp. Fluids* **22**, 327–335.

Klewicki, J. C. & Falco, R. 1990 On accurately measuring statistics associated with small-scale structure in turbulent boundary layers using hot-wire probes. *J. Fluid Mech.* **219**, 119–142.

Knobloch, K. 2008 Skalierungen und Zweipunkt-Geschwindigkeitskorrelationen in turbulenten Grenzschichten bei großen Reynoldszahlen. *Ph. D. thesis, Technical University Berlin, Germany*.

Knobloch, K. & Fernholz, H. H. 2004 Statistics, correlations, and scaling in a turbulent boundary layer at $\mathrm{Re}_{\delta_2} \leqslant 1.15 \times 10^5$. *IUTAM Symposium on Reynolds Number Scaling in Turbulent Flow. A. J. Smiths (Ed.), Kluwer Academic Publisher*, pp. 11–16.

Lavoie, P., Avallone, G., Gregorio, F. D. & Romano, G. P. 2007 Spatial resolution of PIV for the measurement of turbulence. *Exp. Fluids* **43**, 39–51.

Li, J. D., McKeon, B., Jiang, W., Morrison, J. F. & Smits, A. J. 2004 The response of hot wires in high Reynolds-number turbulent pipe flow. *Meas. Sci. Tech.* **15**, 789–798.

Ligrani, P. & Bradshaw, P. 1987 Spatial resolution and measurement of turbulence in the viscous sublayer using subminiature hot-wire probes. *Exp. Fluids* **5**, 407–417.

Lin, J., Laval, J. P., Foucaut, J. M. & Stanislas, M. 2008 Quantitative characterization of coherent structures in the buffer layer of near-wall turbulence. Part 1: Streaks. *Exp. Fluids* **45**, 999–1013.

Lindgren, B., Johansson, A. V. & Tsuji, Y. 2004 Universality of probability density distributions in the overlap region in high Reynolds number turbulent boundary layers. *Phys. Fluids* **16**, 2587–2591.

Long, R. & Chen, T. 1981 Experimental evidence for the existence of the 'mesolayer' in turbulent systems. *J. Fluid Mech.* **105**, 19–59.

Marusic, I. & Kunkel, G. J. 2003 Streamwise turbulence intensity formulation for flat-plate boundary layers. *Phys. Fluids* **15**, 2461–2464.

McKeon, B., Li, J. D., Jiang, W., Morrison, J. F. & Smits, A. J. 2003 Pitot probe corrections in fully developed turbulent pipe flow. *Meas. Sci. Tech.* **14**, 1449–1458.

McKeon, B., Li, J. D., Jiang, W., Morrison, J. F. & Smits, A. J. 2004 Further observations on the mean velocity distribution in fully developed pipe flow. *J. Fluid Mech.* **501**, 135–147.

Metzger, M. 2006 Length and time scales of the near-surface axial velocity in a high Reynolds number turbulent boundary layer. *Int. J. Heat Fluid Flow* **27**, 534–541.

Mochizuki, S. & Nieuwstadt, F. T. M. 1996 Reynolds-number-dependence of the maximum in the streamwise velocity fluctuations in wall turbulence. *Exp. Fluids* **21**, 218–226.

Morrison, J. F., McKeon, B., Jiang, W. & Smits, A. J. 2004 Scaling of the streamwise velocity component in turbulent pipe flow. *J. Fluid Mech.* **508**, 99–131.

Murlis, J., Tsai, H. & Bradshaw, P. 1982 The structure of turbulent boundary layers at low Reynolds numbers. *J. Fluid Mech.* **122**, 13–56.

Musker, A. J. 1979 Explicit expression for the smooth wall velocity distribution in a turbulent boundary layer. *AIAA J.* **17**, 655–657.

Nagib, H. M. & Chauhan, K. A. 2008 Variations of von Kármán coefficient in canonical flows. *Phys. Fluids* **20**, 101518.

Nagib, H. M., Christophorou, C. & Monkewitz, P. A. 2004 High Reynolds number turbulent boundary layers subjected to various pressure-gradient conditions. *IUTAM Symposium on one hundred years of boundary layer research, G. E. A. Meier and K. R. Sreenivasan (Eds.), Göttingen, Germany*, pp. 383–394.

Nickels, T. B., Marusic, I., Hafez, S. & Hutchins, N. 2007 Some predictions of the attached eddy model for a high Reynolds number boundary layer. *Phil. Trans. R. Soc. A* **365**, 807–822.

Oberlack, M. 2001 A unified approach for symmetries in plane parallel turbulent shear flows. *J. Fluid Mech.* **427**, 299–328.

Örlü, R. 2009*a* Low Reynolds number zero pressure-gradient equilibrium turbulent boundary-layer experiments. *Ph. D. thesis, Royal Institute of Technology, Stockholm, Paper 4*.

Örlü, R. & Fransson, J. H. M. 2009 On the determination of the wall position in wall-bounded turbulent flows. *Ph. D. thesis, Royal Institute of Technology, Stockholm, Paper 5*.

Österlund, J. M. 1999 Experimental studies of zero pressure-gradient turbulent boundary layer flow. *Ph. D. thesis, Royal Institute of Technology, Stockholm, Sweden*.

Österlund, J. M., Johansson, A. V., Nagib, H. M. & Hites, M. H. 2000 A note on the overlap region in turbulent boundary layers. *Phys. Fluids* **12**, 1–4.

Park, J. Y. & Chung, M. K. 2004 Revisit of viscous sublayer scaling law. *Phys. Fluids* **16**, 478–481.

Perry, A. E., Hafez, S. & Chong, M. S. 2001 A possible reinterpretation of the Princeton superpipe data. *J. Fluid Mech.* **439**, 395–401.

Pope, S. 2000 Turbulent flows. *Cambridge University Press*.

Purtell, L., Klebanoff, P. S. & Buckley, F. 1981 Turbulent boundary layer at low Reynolds number. *Phys. Fluids* **25**, 802–811.

Schlatter, P., Örlü, R., Li, Q., Brethouwer, G., Fransson, J. H. M., Johansson, A. V., Alfredsson, P. H. & Henningson, D. S. 2009 Turbulent boundary layers up to $Re_\theta = 2500$ studied through simulation and experiment. *Phys. Fluids*, (accepted).

Smith, R. 1994 Effect of Reynolds number on the structure of turbulent boundary layers. *Ph. D. thesis, Princeton University, USA*.

Smits, A. J. & Marusic, I. 1999 High Reynolds number flows–A challenge for experiment and simulation. *AIAA Paper 1999–3530*.

Smol'yakov, A. V. & Tkachenko, V. M. 1983 The measurement of turbulent fluctuations: An introduction to hot-wire anemometry and related transducers. *Springer*.

Spalart, P., Coleman, G. & Johnstone, R. 2008 Direct numerical simulation of the Ekman layer: A step in Reynolds number, and cautious support for a log law with a shifted origin. *Phys. Fluids* **20**, 101507.

Talamelli, A., Persiani, F., Fransson, J. H. M., Alfredsson, P. H., Johansson, A. V., Nagib, H. M., Rüedi, J.-D., Sreenivasan, K. R. & Monkewitz, P. A. 2009 CICLoPE - a response to the need for high Reynolds number experiments. *Fluid Dyn. Res.* **41**, 021407.

Tennekes, H. & Lumley, J. L. 1972 A first course in turbulence. *MIT Press, Cambridge, Massachusetts*.

Tsuji, Y. 1999 Peak position of dissipation spectrum in turbulent boundary layers. *Phys. Rev. E* **59**, 7235–7238.

Tsuji, Y., Lindgren, B. & Johansson, A. V. 2005 Self-similar profile of probability density functions in zero-pressure gradient turbulent boundary layers. *Fluid Dyn. Res.* **37**, 293–316.

Tsuji, Y. & Nakamura, I. 1999 Probability density function in the log-law region of low Reynolds number turbulent boundary layer. *Phys. Fluids* **11**, 647–658.

Vukoslavčević, P. V., Beratlis, N., Balaras, E., Wallace, J. & Sun, O. 2009 On the spatial resolution of velocity and velocity gradient-based turbulence statistics measured with multi-sensor hot-wire probes. *Exp. Fluids* **46**, 109–119.

Wieghardt, K. & Tillmann, W. 1951 On the turbulent friction layer for rising pressure. *NACA Tech. Rep. 1314, Translation of "Zur turbulenten Reibungsschicht bei Druckanstieg", ZWB Untersuchungen und Mitteilungen, Nr. 6617, 1944*.

Wu, X. & Moin, P. 2008 A direct numerical simulation study on the mean velocity characteristics in turbulent pipe flow. *J. Fluid Mech.* **608**, 81–112.

Zagarola, M. V. 1996 Mean flow scaling of turbulent pipe flow. *Ph. D. thesis, Princeton University, USA*.

Zagarola, M. V. & Smits, A. J. 1998 Mean-flow scaling of turbulent pipe flow. *J. Fluid Mech.* **373**, 33–79.

Zanoun, E. S. 2003 Answers to Some Open Questions in Wall Bounded Laminar and Turbulent Shear Flows. *Ph. D. thesis, University of Erlangen, Germany*.

Zhao, R. & Smits, A. J. 2007 Scaling of the wall-normal turbulence component in high-Reynolds-number pipe flow. *J. Fluid Mech.* **576**, 457–473.